Surface Water Photochemistry

Surface Water Photochemistry

Chapter 1

Introduction

Davide Vione* and Paola Calza

Department of Chemistry
University of Torino
Via P. Giuria 5 10125 Torino
Italy

davide.vione@unito.it

1. Introduction

In the following sections of this introductory chapter, some basic pieces of information are provided that will be useful for the understanding of the chapters that follow.

1.1. Basic principles of photophysics and environmental photochemistry [1,2]

In the natural environment sunlight is the source of radiation ($\lambda > 280$ nm) and, for photochemistry to be operational, one needs molecules that absorb radiation above 280 nm. When a molecule absorbs a photon, an electron is excited from the ground state (often it is the ground state from both an electronic and a vibrational point of view) to a vibrationally excited state of an electronically excited state. In the case of organic molecules, the ground electronic state is usually a singlet one (S_0), where the electrons are all paired in full orbitals with antiparallel spin. When the molecule absorbs radiation, it reaches an excited state that is also a singlet one. It could be the first (S_1), the second (S_2) or a higher excited singlet state depending on the energy of the photon and of the molecular states (see Figure 1). To begin with, assume that the electron reaches a vibrationally excited state of S_1. In some cases there might be an excess of vibrational energy, which may cause an excessive strain on the weakest molecular bond that is involved in the vibrational motions triggered by radiation absorption. In this case, bond breaking would take place: indeed, the very word *photolysis* suggests the occurrence of photoinduced bond breaking. As an alternative, the molecule can undergo fast vibrational deactivation to the S_1 ground state. From here, the molecule could take part in chemical reaction, thermal or photochemical deactivation to S_0, or inter-system crossing. Chemical reaction is quite rare in the case of the short-lived excited singlet states, but it accounts for instance for the photoisomerisation of 2-chlorophenol to 5-ring species.[3] Thermal deactivation (internal conversion) can be of some importance in the field of environmental photochemistry, because it would be enhanced by inter-molecular interactions that could for instance account for the limited photophysical activity and photochemical reactivity of high-molecular weight chromophoric dissolved organic matter (HMW CDOM).[4]

Place figure 1.1 near here

In some cases, the $S_1 \rightarrow S_0$ transition takes place by emission of a fluorescence photon. If this is the case, the electron reaches an excited vibrational state of S_0 and then the ground one by vibrational relaxation. The double loss of vibrational energy, in both S_1 and S_0, explains why the wavelength of the emitted (fluorescence) photon is higher (and, therefore, the associated energy is lower)

compared to the absorbed photon. Finally, the electron in the S_1 state can undergo inter-system crossing (ISC) to the first excited triplet state (T_1). The ISC implies spin inversion, and a further inversion would be required for the transition from T_1 to S_0. Such a transition is formally forbidden by the selection rules of quantum mechanics, which in practice means that its probability is low and that the T_1 state is longer-lived than S_1. The quite long lifetime means that T_1 can undergo chemical reactions, for instance with the solvent or with dissolved molecules, as well as intra-molecular rearrangements. A common energy-transfer reaction takes place with dissolved O_2, which is favoured by the fact that the O_2 ground state is a triplet one. The reaction yields singlet oxygen ($^1O_2$), while the molecule usually reaches the S_0 state. Internal conversion from T_1 to S_0 is also possible, in which case the energy is thermally lost through *e.g.* collisions with the solvent. In some rare cases, the transition from T_1 to S_0 can take place by emission of a phosphorescence photon. Similarly to the case of fluorescence emission, in the case of phosphorescence the molecule reaches a vibrationally excited state of S_0 from which a further vibrational loss of energy takes place.

Upon radiation absorption, other excited states different from S_1 may be reached. If the energy is high enough (which is more common in the case of the environmentally non-relevant UVC radiation, $\lambda < 280$ nm), the electron may be abstracted from the molecule to produce its photoionisation.[5] Interestingly, the irradiation of CDOM is well known to yield aquated electrons.[3,4] If the photon energy is not high enough to cause photoionisation, higher excited states than S_1 may be reached (S_2, S_3 and so on). In the case of most organic molecules, the electron reaches a vibrationally excited state of the singlet state S_n ($n > 1$), from which it undergoes vibrational deactivation to the ground vibrational level of S_1. This is quite important for photochemistry and photophysics because, independently of the excitation wavelength, the molecule always reaches the ground state of S_1, from which its further evolution will be the same independently of the details of the excitation process. It is the so-called Kasha's rule, according to which for instance the fluorescence emission wavelength is always the same (following the $S_1 \rightarrow S_0$ transition) independently of the excitation wavelength (which may cause transitions of the kind $S_0 \rightarrow S_1$, $S_0 \rightarrow S_2$ and so on, depending on the photon energy).

An interesting application of the Kasha's rule can be seen in the case of the irradiation of anthraquinone-2-sulphonate (AQ2S). This molecule is not fluorescent (its ISC is much more efficient than the energy deactivation by fluorescence emission), but upon irradiation AQ2S forms fluorescent hydroxyderivatives.[6] The fluorescence excitation-emission matrix spectrum of irradiated AQ2S is reported in Figure 2, showing a single emission band (in the range of 550-600 nm) that, however, corresponds to several excitation bands at different wavelengths, ranging from 200 to 500 nm and suggesting various $S_0 \rightarrow S_n$ transitions.

In some cases, the Kasha's rule is apparently not followed. This is the case for instance of the fluorescence spectrum of 4-phenoxyphenol, which has four paired emission bands (see Figure 3). One pair has emission at 300-350 nm, which corresponds to two excitation bands at 200-250 and 250-300 nm. The second pair has emission at 350-425 nm, corresponding to two excitation bands around 250 and 300 nm. According to Kasha's rule one would expect a single emission wavelength

($S_1 \rightarrow S_0$ transition), linked to the occurrence of one pair only or to four bands that should be vertically placed as in the case of Figure 2. However, 4-phenoxyphenol exists in aqueous solution in three different rotational conformations that undergo very slow inter-conversion (compared to the typical fluorescence lifetimes). It has been shown that a conformer accounts for the bands with emission at 300-350 nm, the other two for the bands with emission at 350-425 nm.[7]

Place figure 1.2. near here

Place figure 1.3. near here

1.2. Photosensitisers and photoinduced transients in surface waters

Several photochemical processes can take place in sunlit surface waters. Some of them involve the absorption of sunlight by the molecule(s) that are transformed, following reaction pathways that have been partly described in section 1.2 and that will be more extensively dealt with in Chapter 4.[3,8,9] However, additional reactions are triggered by the absorption of sunlight photons by naturally occurring photoreactive species called photosensitisers. Among these naturally compounds there are chromophoric dissolved organic matter (CDOM), nitrate, nitrite, Fe species and H_2O_2.[10] The (photo)chemistry of Fe, which also partially involves that of H_2O_2, is quite complex and will be the subject of a separate chapter. The present introduction will provide a general overview of the photochemistry of CDOM, nitrate and nitrite, to be further elucidated later on in this book.

CDOM is, almost beyond any doubt, the single most important photosensitiser (or better, class of sensitisers) that occurs in natural waters. Its complex and not yet completely elucidated molecular structure has been the subject of intense debate. Today, many scientists accept that it could be a supra-molecular (rather than a macromolecular) combination of smaller compounds, which form aggregates that vary for the apparent molecular size.[4,11,12] The most important photoactive moieties of CDOM are its humic and fulvic parts, which are responsible for an important fraction of sunlight absorption by CDOM itself.[13,14]

The absorption of sunlight by CDOM causes the excitation of its photoactive moieties to produce the excited singlet states (^{1}CDOM*). In the case of aromatic aldehydes, benzophenones, quinones and other chromophores, the singlet excited states tend to undergo an efficient inter-system crossing (ISC) to produce the longer-lived triplets (^{3}CDOM*),[4,8,9] which are often involved in chemical reactions that cause the transformation of other dissolved molecules including dissolved pollutants.

Despite the importance of triplet-sensitised transformation for the removal of many pollutants from surface-water environments,[8-10] the main ^{3}CDOM* sink is actually the reaction with O_2 to produce singlet oxygen ($^1O_2$). The latter is also an important transient that might be involved in the

indirect photochemistry of dissolved compounds (*e.g.* chlorophenolates and aromatic amino acids such as tryptophan and tyrosine) [15-17] or that, as an alternative, may undergo deactivation upon collision with water. On top of all this, irradiated CDOM can also induce the photochemical production of $^{\bullet}OH$, of which it is actually the main source in most surface waters.[10,18-21] Although several details are still missing, it is now generally acknowledged that part of the $^{\bullet}OH$ photoproduction by irradiated CDOM involves the photochemical generation of H_2O_2.[22,23] The latter probably takes place upon dismutation of $HO_2^{\bullet}/O_2^{-\bullet}$, produced upon scavenging by oxygen of the reduced radical transients that are formed by reaction between ^{3}CDOM* and dissolved compounds. Once photochemically generated, H_2O_2 can yield $^{\bullet}OH$ through direct photolysis or (more probably) the Fenton reaction with H_2O_2.[24] The Fenton process is actually much less "clean" than it may be suggested by its traditional stoichiometric notation, because super-oxidised Fe species (*e.g.* ferryl) may be formed in competition with $^{\bullet}OH$. The actual $^{\bullet}OH$ yield reaches ~60% under the most favourable conditions (pH 2-3) [25] and it decreases with increasing pH.[26] The reactions described so far are reported below, where S-H is a generic dissolved molecule that undergoes oxidation by reaction with ^{3}CDOM*.

$$\text{CDOM} \xrightarrow{h\nu} {}^1\text{CDOM}^* \xrightarrow{ISC} {}^3\text{CDOM}^* \quad (1)$$

$$^3\text{CDOM}^* + O_2 \rightarrow \text{CDOM} + {}^1O_2 \quad (2)$$

$$^1O_2 \xrightarrow{H_2O} O_2 \quad (3)$$

$$^3\text{CDOM}^* + \text{S-H} \rightarrow \text{CDOM-H}^{\bullet} + \text{S}^{\bullet} \quad (4)$$

$$^3\text{CDOM}^* + \text{S-H} \rightarrow \text{CDOM}^{-\bullet} + \text{S-H}^{+\bullet} \quad (5)$$

$$\text{CDOM-H}^{\bullet} + O_2 \rightarrow \text{CDOM} + HO_2^{\bullet} \quad (6)$$

$$\text{CDOM}^{-\bullet} + O_2 \rightarrow \text{CDOM} + O_2^{-\bullet} \quad (7)$$

$$HO_2^{\bullet} + O_2^{-\bullet} + H^+ \rightarrow H_2O_2 + O_2 \quad (8)$$

$$H_2O_2 \xrightarrow{h\nu} 2\,{}^{\bullet}OH \quad (9)$$

$$Fe^{2+} + H_2O_2 \rightarrow FeOH^{2+} + {}^{\bullet}OH \quad (10)$$

However, the photochemical production of $^{\bullet}OH$ by irradiated CDOM is also known to follow an additional, $^{\bullet}OH$–independent pathway. It is possible that this pathway does not only yield genuine $^{\bullet}OH$, because so-called low-level hydroxylating species are certainly formed in the process. However, a certain amount of $^{\bullet}OH$ is also produced.[22] To get an idea of what the additional hydroxylating species may be, one can consider the photochemistry of anthraquinone-2-sulphonate, the triplet state of which (^{3}AQ2S*) is certainly unable to produce $^{\bullet}OH$ upon water oxidation.[27] However, ^{3}AQ2S* quickly reacts with water to produce an adduct that may either evolve into AQ2S hydroxyderivatives or transfer the OH group to other molecules.[6,27,28] The reaction products are not different from those expected upon reaction with $^{\bullet}OH$, but the AQ2S-H_2O adduct is a much less powerful oxidant compared to $^{\bullet}OH$.

The H_2O_2-independent pathway to $^{\bullet}OH$ in the presence of irradiated CDOM might involve water oxidation by ^{3}CDOM* (which is still controversial, as some triplet states can oxidise H_2O but

others cannot),[27,29] or a preliminary CDOM oxygenation followed by *e.g.* $^{\bullet}OH$ production upon photochemical excitation of some oxygen-containing groups. Anyway, many details of the process are missing at the moment.

An interesting issue is the detection of very high concentration levels of $^1O_2$ in the inner hydrophobic cores of high-molecular weight CDOM (HMW CDOM). This concentrated $^1O_2$ seems to have few chances of escaping into the solution bulk, because hydrophobic $^1O_2$ probes (undergoing preferential partitioning into the waterless core environment) are needed to highlight it. However, it could play an important role in the degradation of hydrophobic pollutants that are partitioned inside CDOM cores.[30,31] The occurrence of elevated $^1O_2$ in HMW CDOM cores might be due to elevated photochemical formation or to longer lifetimes than in solution. Presently, little to no evidence is available to support the former hypothesis,[32,33] while there is evidence for the latter.[34]

Nitrate yields $^{\bullet}OH$ upon absorption of UVB and (to a lesser extent) UVA radiation. A major process is generally agreed to be the following:[35]

$$NO_3^- \xrightarrow{h\nu} {}^{\bullet}NO_2 + O^{-\bullet} \xrightarrow{H^+} {}^{\bullet}NO_2 + {}^{\bullet}OH \qquad (11)$$

The quantum yield of this reaction is independent of the wavelength and it is around 0.01.[36] The involvement of H^+ in the $^{\bullet}OH$ production might suggest that the process could depend on pH, which is not exactly the case (at least as far as reaction 11 is concerned). Indeed, $^{\bullet}OH$ has pKa ~ 12 and the acid-base equilibrium $^{\bullet}OH \leftrightarrows O^{-\bullet} + H^+$ can, therefore, only be of importance around pH 12. At the typical pH values of surface waters, the equilibrium is totally shifted toward $^{\bullet}OH$.[35]

Still, the photogeneration of $^{\bullet}OH$ by irradiated nitrate depends on pH in the ~neutral range,[37] which warrants a different explanation. A possibility is the contemporary photoisomerisation of nitrate to peroxynitrite, $ONOO^-$, taking place along with reaction (11). The $ONOO^-$ is the conjugated base of peroxynitrous acid, HOONO, a weak acid with pKa ~ 7. HOONO and $ONOO^-$ strongly differ for the inactivation pathways because, in addition to the common back-isomerisation to nitrate, HOONO decomposes into $^{\bullet}OH$ + $^{\bullet}NO_2$ while $ONOO^-$ reacts with dissolved CO_2.[38,39] Therefore, the prevalence of HOONO at pH < 7 and of $ONOO^-$ at pH > 7 could explain why the photogeneration of $^{\bullet}OH$ by nitrate decreases with pH in the ~neutral range.[37]

$$NO_3^- \xrightarrow{h\nu} ONOO^- \qquad (12)$$

$$ONOO^- + H^+ \leftrightarrows HOONO \qquad (13)$$

$$HOONO \rightarrow NO_3^- + H^+ \qquad (14)$$

$$HOONO \rightarrow {}^{\bullet}NO_2 + {}^{\bullet}OH \qquad (15)$$

$$ONOO^- \rightarrow NO_3^- \qquad (16)$$

$$ONOO^- + CO_2 \rightarrow ONOOCO_2^- \rightarrow \text{Other products (no } {}^{\bullet}OH) \qquad (17)$$

Nitrite mostly absorbs sunlight in the UVA region, with minor absorptions in the UVB and visible. Its $^{\bullet}OH$–producing photoreaction has the peculiarity of a wavelength-dependent quantum yield, from 0.065 at 300 nm to 0.025 at 360 nm and beyond.[40] The reason could be the fact that different bands of nitrite, with different quantum yields and different roles depending on the wavelength, are involved into sunlight absorption.

One should not forget that, in addition to photochemical production, the photogenerated transients undergo very fast inactivation ($^1O_2$, ^{3}CDOM*) or scavenging processes ($^{\bullet}OH$, $CO_3^{-\bullet}$, ^{3}CDOM*) in surface waters (in the case of ^{3}CDOM*, the main scavenger is O_2). The combination of production and very fast decay accounts for the fact that the transients reach relatively low (always < 10^{-12} M) steady-state concentrations in surface waters.[10]

Concerning $^{\bullet}OH$ one should not forget that, in addition to photochemical production, it also undergoes important scavenging in natural waters. The main $^{\bullet}OH$ scavengers are dissolved organic matter (DOM, either chromophoric or not), inorganic carbon (HCO_3^- and CO_3^{2-}), nitrite and, in brackish or seawater, bromide.[9,10] The reaction between $^{\bullet}OH$ and inorganic carbon yields $CO_3^{-\bullet}$, which is also a significant reactive transient in surface waters and might be involved into the transformation of phenolates, aromatic amines and sulphur-containing compounds. The radical $CO_3^{-\bullet}$ can also produced upon CO_3^{2-} oxidation by ^{3}CDOM*.[41] The steady-state [$CO_3^{-\bullet}$] in sunlit waters is strongly anticorrelated with DOM, for two reasons. First of all, DOM is by far the main $CO_3^{-\bullet}$ scavenger in surface waters. Moreover, by consuming $^{\bullet}OH$, DOM is also able to inhibit the photogeneration of $CO_3^{-\bullet}$.[9,10]

$$^{\bullet}OH + HCO_3^- \rightarrow H_2O + CO_3^{-\bullet} \quad (18)$$

$$^{\bullet}OH + CO_3^{2-} \rightarrow OH^- + CO_3^{-\bullet} \quad (19)$$

$$^3CDOM^* + CO_3^{2-} \rightarrow CDOM^{-\bullet} + CO_3^{-\bullet} \quad (20)$$

The reaction between $^{\bullet}OH$ and bromide yields $Br_2^{-\bullet}$, which is an effective brominating agent for aromatic compounds including most notably phenols.[42] In this way, the photogeneration of $^{\bullet}OH$ in saltwater may induce the production of persistent and potentially toxic organohalogenated compounds.[43-46]

$$^{\bullet}OH + Br^- \rightarrow OH^- + Br^{\bullet} \quad (21)$$

$$Br^{\bullet} + Br^- \leftrightarrows Br_2^{-\bullet} \quad (22)$$

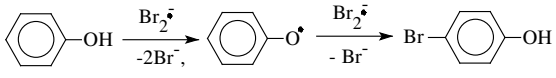

(23)

1.3. Seasonal and long-term variations of the main photosensitisers in lake water

In lake water, nitrate has often winter maxima and summer minima. In fact, during the warm season, inorganic nitrogen (including most notably nitrate) is largely consumed by micro-organisms to produce organic nitrogen. At the same time, the enhancement of photosynthesis during the summer season consumes dissolved CO_2 and causes an increase of the water pH. The combination of pH increase and higher water temperature often causes the precipitation of $CaCO_3$, which accounts for the summer minima of both alkalinity and inorganic carbon.[47]

The DOC may be quite variable during the different seasons. However, during summer, the combination of algal growth (where the necessary carbon is largely taken from the atmosphere) and death (which releases dissolved organic material into lake water) is usually associated with annual maxima of DOM.[48-50]

In alpine lakes, photochemistry may be strongly inhibited during winter and spring because of the ice cover and of the increased water turbidity soon after ice melting. In addition to photochemical issues, these phenomena are important for the protection of aquatic organisms from the harmful effects of the exposure to UVB radiation. In this context, climate warming could decrease the ice-cover period and indirectly cause an increased exposure of alpine plankton to UVB.[51-53]

In arid environments, the net water loss and subsequent decrease of the water column depth during the dry season can have important effects on photochemical reactions. If water is simply lost by outflow (to rivers draining a lake, or to the sediment), without significant changes of the concentration values of the dissolved species, the lower column depth would favour all photochemical reactions but, most notably, the processes induced by $^{\bullet}OH$ and $CO_3^{-\bullet}$. In contrast, water loss by evaporation causes a concentration of the non-volatile species that are dissolved in water. This phenomenon, while leaving almost unaltered the steady-state [$^{\bullet}OH$] and [$CO_3^{-\bullet}$], strongly enhances the processes induced by $^1O_2$ and ^{3}CDOM*.[54]

Eutrophication of lake water (*e.g.* because of inputs of nutrients from human waste) often leads to an increase in the levels of both nitrate and DOM, while the opposite is expected to happen in the case of recovery from eutrophication.[55-58] In nordic environments, climate change could give a contribution to eutrophication, with increasing levels of (most notably) DOM and CDOM. In contrast, in Mediterranean settings, climate change could induce desertification with loss of organic matter from soil that, after a first phase of organic carbon export to surface waters, would finally produce oligotrophication and very low DOM levels. Intermediate scenarios are of course highly likely, which makes it difficult to foresee in the general case the impact of climate change on DOM and CDOM.[59,60]

A more widely agreed effect that is connected with climate is the increase of lake water alkalinity. Actually, increasing temperature enhances the dissolution of minerals such as $CaSO_4$, producing in this case increased levels of both Ca^{2+} and sulphate. However, while Ca^{2+} is biologically stable, sulphate would be partially or largely converted into organic sulphur species (*e.g.* R-SH). The resulting imbalance of alkalinity is compensated for by increasing levels of inorganic carbon and pH.[61-63]

1.4. Photoinduced transformation of organic micropollutants

The presence of organic micropollutants may pose a potential threat to the aquatic environment. In particular, the occurrence of the so-called emerging contaminants (ECc) is receiving increasing attention nowadays. Biological processes usually lead to a limited transformation of micropollutants, but biotransformation is often the most important removal process for these compounds from water.[64] Additionally, photoinduced reactions involve the formation of radical species, able to almost completely abate micropollutants through non-specific reactions and to promote the formation of numerous transformation products (TPs). These TPs may possess diverse mobility, polarity and toxicity compared to the parent molecule and, therefore, the elucidation of transformation pathways followed by pollutants is crucial to evaluate their overall fate and the associated risks to the aquatic compartment.

There are several difficulties associated with degradation studies in environmental matrices, and most notably:

(1) the very low concentration of pollutants and, of course, of their TPs, thus very sensitive analytical instrumentation is required;

(2) the complexity of the matrices, which may affect the analytical performance.

Therefore, different strategies have been employed to generate and detect transformation products firstly at lab scale and then in natural systems, as described in chapters 12-14, where particular attention is devoted to the techniques that can be used in the field and in the laboratory for the detection of pollutants and of their transformation intermediates.

References

1. J. G. Calvert and J. N. Pitts, *Photochemistry*, Wiley, NY, 1966.
2. S. E. Braslavsky, *Pure Appl. Chem.*, 2007, **79**, 293–465.
3. P. Boule (ed.), *Environmental Photochemistry (The Handbook of Environmental Chemistry Vol. 2.L)*, Springer, Berlin, 1999.
4. C. M. Sharpless and N. V. Blough, *Environ. Sci.: Processes Impacts*, 2014, **16**, 654-671.
5. S. Rayne, K. Forest and K. J. Friesen, *Environment Int.*, 2009, **35**, 425-437.
6. A. Bedini, E. De Laurentiis, B. Sur, V. Maurino, C. Minero, M. Brigante, G. Mailhot and D. Vione, *Photochem. Photobiol. Sci.*, 2012, **11**, 1445-1453.
7. F. Barsotti, *Theoretical and experimental investigations on the fluorescence properties of humic substances.* M.Sc. Thesis, University of Torino, 2014.
8. P. Boule, D. W. Bahnemann and P. K. J. Robertson, *Environmental Photochemistry Part II (The Handbook of Environmental Chemistry Vol. 2.M)*, Springer, Berlin, 2005.

9. K. Mcneill (ed.), Themed issue on aquatic photochemistry, *Environ. Sci.: Processes Impacts*, 2014, **16**, 626-878.
10. D. Vione, M. Minella, V. Maurino and C. Minero, *Chemistry Eur. J.*, 2014, **20**, 10590-10606.
11. A. Piccolo, *Soil Sci.*, 2001, **166**, 810-832.
12. D. Smejkalova and A. Piccolo, *Environ. Sci. Technol.*, 2008, **42**, 699-706.
13. S. Halladja, A. Ter Halle, J. P. Aguer, A. Boulkamh and C. Richard, *Environ. Sci. Technol.*, 2007, **41**, 6066-6073.
14. L. Cavani, S. Halladja, A. Ter Halle, G. Guyot, G. Corrado, C. Ciavatta, A. Boulkamh and C. Richard, *Environ. Sci. Technol.*, 2009, **43**, 4348-4354.
15. M. Czaplicka, *J. Hazard. Mater.*, 2006, **B134**, 45-59.
16. A. L. Boreen, B. L. Edhlund, J. B. Cotner and K. McNeill, *Environ. Sci. Technol.*, 2008, **42**, 5492-5498.
17. E. M. L. Janssen, P. R. Erickson and K. McNeill, *Environ. Sci. Technol.*, 2014, **48**, 4916-4924.
18. D. Vione, G. Falletti, V. Maurino, C. Minero, E. Pelizzetti, M. Malandrino, R. Ajassa, R. I. Olariu and C. Arsene, *Environ. Sci. Technol.*, 2006, **40**, 3775-3781.
19. E. De Laurentiis, S. Buoso, V. Maurino, C. Minero and D. Vione, *Environ. Sci. Technol.*, 2013, **47**, 14089-14098.
20. S. E. Page, J. R. Logan, R. M. Cory and K. McNeill, *Environ. Sci.: Processes Impacts*, 2014, **16**, 807-822.
21. A. Marchisio, M. Minella, V. Maurino, C. Minero and D. Vione, *Water Res.*, 2015, **73**, 145-156.
22. S. E. Page, W. A. Arnold and K. McNeill, *Environ. Sci. Technol.*, 2011, **45**, 2818-2825.
23. G. McKay and F. L. Rosario-Ortiz, *Environ. Sci. Technol.*, 2015, **49**, 4147-4154.
24. M. Chiwa, N. Higashi, K. Otsuki, H. Kodama, T. Miyajima, K. Takeda and H. Sakugawa, *Chemosphere*, 2015, **119**, 1386-1390.
25. C. Minero, M. Lucchiari, V. Maurino and D. Vione, *RSC Adv.*, 2013, **3**, 26443-26450.
26. A. W. Vermilyea and B. M. Voelker, *Environ. Sci. Technol.*, 2009, **43**, 6927-6933.
27. P. R. Maddigapu, A. Bedini, C. Minero, V. Maurino, D. Vione, M. Brigante, G. Mailhot and M. Sarakha, *Photochem. Photobiol. Sci.*, 2010, **9**, 323-330.
28. D. Vione, M. Ponzo, D. Bagnus, V. Maurino, C. Minero and M. E. Carlotti, *Environ. Chem. Lett.*, 2010, **8**, 95-100.
29. B. Sur, M. Rolle, C. Minero, V. Maurino, D. Vione, M. Brigante and G. Mailhot, *Photochem. Photobiol. Sci.*, 2011, **10**, 1817-1824.
30. D. E. Latch and K. Mcneill, *Science*, 2006, **311**, 1743-1747.
31. M. Grandbois, D. E. Latch and K. Mcneill, *Environ. Sci. Technol.*, 2008, **42**, 9184-9190.
32. M. Minella, F. Romeo, D. Vione, V. Maurino and C. Minero, *Chemosphere*, 2011, **83**, 1480-1485.
33. M. Minella, M. P. Merlo, V. Maurino, C. Minero and D. Vione, *Chemosphere*, 2013, **90**, 306-311.
34. E. Appiani, and K. McNeill, *Environ. Sci. Technol.*, 2015, **49**, 3514-3522.

35. J. Mack and J. R. Bolton, *J. Photochem. Photobiol. A: Chem.*, 1999, **128**, 1-13.
36. P. Warneck and C. Wurzinger, *J. Phys. Chem.*, 1988, **92**, 6278-6283.
37. D. Vione, S. Khanra, S. Cucu Man, P. R. Maddigapu, R. Das, C. Arsene, R. I. Olariu, V. Maurino and C. Minero, *Water Res.*, 2009, **43**, 4718-4728.
38. J. W. Coddington, J. K. Hurst and S. V. Lymar, *J. Am. Chem. Soc.*, 1999, **121**, 2438-2443.
39. R. Meli, T. Nauser, P. Latal and W. H. Koppenol, *J. Biol. Inorg. Chem.*, 2002, **7**, 31-36.
40. M. Fischer and P. Warneck, *J. Phys. Chem.*, 1996, **100**, 18749-18756.
41. S. Canonica, T. Kohn, M. Mac, F. J. Real, J. Wirz and U. Von Gunten, *Environ. Sci. Technol.*, 2005, **39**, 9182-9188.
42. D. Vione, V. Maurino, S. Cucu Man, S. Khanra, C. Arsene, R. I. Olariu and C. Minero, *ChemSusChem*, 2008, **1**, 197-204.
43. P. Calza, C. Massolino, E. Pelizzetti and C. Minero, *Sci. Total Environ.*, 2008, **398**, 196-202.
44. P. Calza, D. Vione, A. Novelli, E. Pelizzetti and C. Minero, *Sci. Total Environ.*, 2012, **439**, 67-75.
45. E. De Laurentiis, M. Minella, V. Maurino, C. Minero, G. Mailhot, M. Sarakha, M. Brigante and D. Vione, *Sci. Total Environ.*, 2012, **439**, 299-306.
46. P. Calza, D. Vione and C. Minero, *Sci. Total Environ.*, 2014, **493**, 411-418.
47. R. G. Wetzel, *Limnology of Lake and River Ecosystems*, 3rd edn., Academic Press, NY, 2001.
48. T. Kusakabe, K. Ikeda, Y. Shimizu, S. Higashi, Y. Kawabata, T. Kitamura and Y. Suzuki, *Water Sci. Technol.*, 2008, **58**, 1609-1614.
49. P. Q. Fu, K. M. G. Mostofa, F. C. Wu, C. Q. Liu, W. Li, H. Q. Liao, L. Y. Wang, J. Wang and Y. Mei, *Geochem. J.*, 2010, **44**, 99-112.
50. M. T. Perez and R. Sommaruga, *Aquat. Microb. Ecol.*, 2011, **63**, 161-170.
51. M. Orfeo, M. Ventura, B. Tartarotti and R. Sommaruga, *J. Plankton Res.*, 2011, **33**, 1430-1444.
52. C. Ruiz-Gonzalez, R. Simo, R. Sommaruga and J. M. Gasol, *Frontiers Microbiol.*, 2013, **4**, 131.
53. B. Tartarotti, N. Saul, S. Chakrabarti, F. Trattner, C. E. W. Steinberg and R. Sommaruga, *J. Plankton Res.*, 2014, **36**, 557-566.
54. M. Minella, V. Maurino, C. Minero and Davide Vione, *Intern. J. Environ. Anal. Chem.*, 2013, **93**, 1698-1717.
55. B. L. Skjelkvåle, J. L. Stoddard, D. S. Jeffries, K. Tørseth, T. Høgåsen, J. Bowma, J. Mannio, D. T. Monteith, R. Mosello, M. Rogora, D. Rzychon, J. Vesely, J. Wieting, A. Wilander and A. Worsztynowicz, *Environ. Pollut.*, 2005, **137**, 165-176.
56. L. Camarero, M. Rogora, R. Mosello, N. J. Anderson, A. Barbieri, I. Botev, M. Kernan, J. Kopacek, A. Korhola, A. F. Lotter, G. Muri, C. Postolache, E. Stuchlik, H. Thies and R. F. Wright, *Freshwater Biol.*, 2009, **54**, 2452-2469.
57. M. Minella, M. Rogora, D. Vione, V. Maurino and C. Minero, *Sci. Total Environ.*, 2011, **409**, 3463-3471.
58. M. Minella, E. De Laurentiis, O. Buhvestova, M. Haldna, K. Kangur, V. Maurino, C. Minero and D. Vione, *Chemosphere*, 2013, **90**, 2589-2596.

59. P. Porcal, J. F. Koprivnjak, L. A. Molot and P. J. Dillon, *Environ. Sci. Pollut. Res*., 2009, **16**, 714-726.
60. C. Sucker and K. Krause, *Iforest - Biogeosciences and Forestry*, 2010, **3**, 106-108.
61. S. Sommaruga-Wögrath, K. A. Koinig, R. Schmidt, R. Sommaruga, R. Tessadri and R. Psenner, *Nature*, 1997, **387**, 64-67.
62. D. W. Schindler, *Hydrol. Proc*., 1997, **11**, 1043-1067.
63. C. E. Williamson, J. E. Saros and D. W. Schindler, *Science*, 2009, **323**, 887-888.
64. K. Fenner, S. Canonica, L. P. Wackett and M. Elsner, *Science*, 2013, **341**, 752-758.

Figure captions

Figure 1.1. Schematic of the processes that may follow radiation absorption by a water-dissolved organic compound. Solid horizontal lines represent ground vibrational states of electronic levels, excited vibrational states being dashed. Solid and straight vertical arrows represent radiation absorption processes (hν = photon), zigzag arrows are vibrational relaxation processes (including internal conversion), while dash-dotted arrows represent light emission (fluorescence or phosphorescence). ISC = inter-system crossing.

Figure 1.2. Fluorescence spectrum of irradiated AQ2S (Vione, unpublished data).

Figure 1.3. Fluorescence spectrum of 4-phenoxyphenol.[7]

Lakes ecology and chemistry

Marco Bartoli and Pierluigi Viaroli

Department of Environmental Sciences, Parma University, 43124 Parma, Italy

1. Introduction

1.1. Lakes as a research facility

Inland waters form the link between terrestrial and marine systems, being reactors of dissolved organic and inorganic matter along its path to the sea (Smith and Hollibaugh, 1993). Lakes have been a key subject of the ecological studies in the first half of the 20th century, when they were exploited as model ecosystems, thought to be fairly simple for testing the emerging ecological hypotheses. Later, they have revealed a much greater complexity, challenging modern studies on trophic interactions; ecosystem degradation and recovery, especially eutrophication and acidification; ecological succession and regime shift; biogeochemical processes (Connell 1975; Peters, 1991; Scheffer and Jeppesen, 2007, Nixon, 2009). Among others, the theoretical foundation of the trophic-dynamic model of energy flow (Lindeman, 1942) and the early key questions on biodiversity and its role (Hutchinson, 1959) were based on comprehensive studies of lake communities.

Lakes were also catalysts for the growth of research centres that achieved excellence and provided background for the new ecological science. Among others, the Italian Institute of Hydrobiology at Pallanza was an "heaven for ecologist" (Edmondson and Edmondson, 1990).

At present a large body of literature provides studies on causes, effects and processes of eutrophication; interactions among climate, in lake physical processes and community structure and processes; benthic metabolism and its effects on deoxygenation and solutes and dissolved gas (especially CO_2 and CH_4) exchanges at the water-sediment interface; the deep sediments as sinks or sources of biogenic elements, especially N, P and Si; the structuring role of the littoral macrophyte belt and the adjacent submerged vegetation in the photic shallow waters (Jeppesen, 1998; Bastviken et al., 2004; Nizzoli et al., 2010; Pinardi et al., 2011). Whole lakes are also used for the bio-manipulation experiments of the food webs in order to understand and manage trophic interactions and provide solutions for the recovery from deteriorated conditions (Shapiro et al., 1990).

1.2. Lakes as a resource: water, water scarcity and lakes' exploitation

More than 99% of the water present on Earth is in the oceans and in the polar ice caps: this immense quantity of water is not directly available for human use. Comparatively, surface freshwater environments have much smaller volumes, but are the only standing waters that can be exploited. Nonetheless, these valuable resources are threatened and degraded at the point that a freshwater crisis could potentially occur in the near future as a combination of increased

temperatures and changed precipitation patterns, increasing water demand, chemical and biological pollution (Yeston et al., 2006).

In Italy, approximately $170x10^9$ m^3 of freshwater are available in lakes, reservoirs and other lentic aquatic ecosystems, but nearly 120 $x10^9$ m^3 are stored in the four major sub-alpine lakes (Maggiore, Como, Iseo, Garda). These lakes are fed by glaciers, which are dramatically retreating with unpredictable future effects (Citterio et al., 2007). The large sud-alpine lakes are also man-regulated and used to store water in winter and spring, that is released through the emissary in summer for irrigation and industrial purposes. In parallel, lakes regulation allow the stabilization of hydrometric levels and the avoidance of their extreme fluctuations, keeping safe conditions for the human settlements along the coast (http://www.laghi.net/). Under these circumstances, contrasting and often conflicting targets by different stakeholders can establish for hydraulic safety, needs for touristic facilities, hydropower production and irrigation, and maintenance of the minimum environmental flow. The conflict extent can be amplified by climate changes especially in mid-summer of dry years, when the water demand exceeds its availability, with critical impacts especially on agriculture.

2. Physical factors structuring the lake ecosystem

The structure and functioning of a given lake cannot be fully understood without knowing its genesis, the watershed geology and hydrogeology, and climate-dependent physical processes (Wetzel, 2001).

2.1. Origin of lakes: an explanation of lakes diversity

The comprehension of lakes origin helps to understand their large variety of forms, depths and dynamics. Most natural lakes were formed by catastrophic events. *Tectonic lake basins* are depression formed by a displacement of the earth crust; *volcanic lakes* originate in volcanic cones or in partially emptied magmatic chambers; *kettle lakes* were formed from melted blocks of ice buried in moraine debris, during glacier retreat. Other natural lakes originate from gradual, less catastrophic events. *Solution lakes* result from sinks formed by the gradual dissolution of rocks along fissures and fractures; *oxbow lakes* result from erosional and depositional action of rivers, for example during flooding events; *dune lakes* form in sandy areas by erosion; they may contain water seasonally. *Reservoirs* and *quarry lakes* are very recent impoundments, created largely by man. They are generally short lived because of eutrophic conditions and high siltation rates.

2.2. Water quality as a result of watershed geology and lithology

Water quality depends on the interactions with the main lithological formations in the watershed. For example, the presence of limestone and marl is expected to naturally provide calcium and inorganic carbon ions; ophiolites can potentially leach magnesium, silica, alluminium and nichel and so forth (Table 1). Here, the inorganic carbon species are collectively represented by the total alkalinity (TA), that at the actual pH values is mainly accounted by HCO_3^- and to a much lesser extent by CO_3^{2-} and OH^-, this latter being nearly negligible. Lakes with carbonate poor lithology, namely with only traces of marl and limestone, have low Ca^2+Mg^{2+} and TA concentrations. The concentrations increase by approximately one order of magnitude in lakes with marl and limestone formations in the range 10-50% of the watershed surface. The presence of Triassic evaporites with gypsum outcrops accounts for significant increases of SO_4^{2-}, whilst in ophiolites-rich basins Mg^{2+} becomes dominant among cations.

Table 1. Major ions concentrations (μEq L^{-1}) in water of high altitude lakes in the Northern Apennines, Italy, with different surface lithology. N: number of data, CD: conductivity at 20 °C (μS cm^{-1}), TA: total alkalinity (μEq L^{-1}). SA: sandstone, ML: marl and limestone, MU: maphic and ultra-maphic (ophiolites), SG: sandstone and gypsum. Data from Viaroli et al. 1992; 1994.

lithology	N	pH	CD	TA	SO_4^{2-}	Cl^-	Na^+	K^+	Mg^{2+}	Ca^{2+}
SA	17	7,17±0,35	36±14	228±143	44±12	65±14	80±9	8±1	24±7	90±56
ML	9	8,00±0,18	164±48	1634±588	118±52	104±35	165±66	32±21	155±91	706±211
MU	6	7,67±0,39	82±29	793±385	52±15	77±18	89±21	12±15	290±162	165±91
SG	3	7,58±0,29	166±62	781±448	403±41	90±4	110±1	12±5	121±41	730±369

The ion budget of lake water is mainly accounted by bicarbonates and calcium, with exceptions due to the lithological features of the watershed. In the Northern Apennine lakes (Table 1), on average TA+ SO_4^{2-} accounts for 87% (70-95%) of the total anions and Mg^{2+} + Ca^{2+} represents 80% (50-93%) of the total cations (Figure 1a). Specifically, the ion composition of lake water is mainly determined by calcium and bicarbonates which are nearly equivalent (Figure 1b). Synthetically, the ionic strength of the water can be represented with the electric conductivity (Figure 1c).

The total alkalinity is almost completely due to the inorganic carbon equilibria that, under the pH and conductivity of the natural lake waters, are mainly driven by bicarbonates:

$$CO_2 + H_2O \leftrightarrow H_2CO_3$$

$$H_2CO_3\ H_2O \leftrightarrow HCO_3^- + H_3O^+ \ (pK_{a1}=6.35)$$

$$HCO_3^- + H_2O \leftrightarrow CO_3^{2-} + H_3O^+ \ (pK_{a2}=10.33)$$

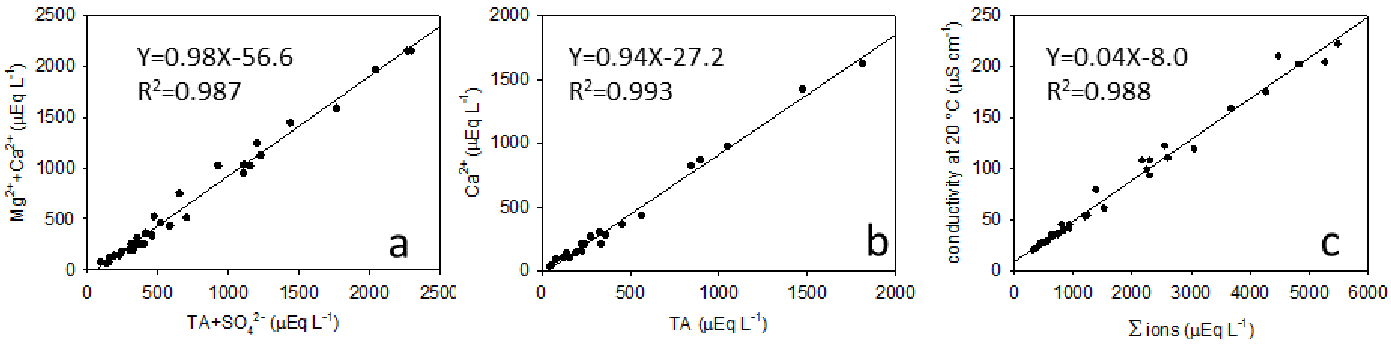

Figure 1. Relationships between (a) the main ionic components, (b) calcium and total alkalinity and (c) conductivity and total ion concentrations in the water of the Northern Apennines lakes.

Under these circumstances, increases of water acidity can be buffered by carbonates and bicarbonates that are converted into carbonic acid, finally releasing carbon dioxide in the atmosphere. The TA is operationally called Acid Neutralizing Capacity (ANC), which is equivalent to the acid quantity that is required to titrate a given water volume to pH 4.2, coinciding with the exhaustion of bicarbonates. To sum up, the sensitivity of lakes to acidification can be assessed with simple measures of pH, conductivity and, especially, ANC (Table 2).

Table 2. Simple criteria for assessing the lake sensitivity to acidification (modified from Mosello et al., 1993; Krzyzanowski and Inne, 2010).

	Very high	High	Moderate	Low
ANC ($\mu Eq L^{-1}$)	<50	50-200	200-400	>400
pH	<5.6	5.6-6.5	6.6-7.0	>7.0
CD ($\mu S\ cm^{-1}$)	<20	20-35	35-78	>60

The literature on lake acidification is particularly rich of studies on causes and effects of acid depositions and their effects in lakes' districts with very different lithology. Based on the knowledge of deterioration processes and possible remedial, restoration programs have been successfully applied at different spatial scales. However, one of the most famous example of successful management of lake acidification deals with the Lake Orta, that was recovered from heavy industrial acidification. The knowledge of inlake biogeochemical processes was a powerful support for designing the lake liming to buffer acidity, along with a cost-benefit analysis (Calderoni and Tartari, 2000).

2.3. Heat budget, density dependent processes and their effects on water chemistry

The seasonal dynamic of lakes is to a large extent regulated by physical processes which depends on the heat budget of the water mass and hydrodynamics. Heating and cooling have a profound effect on water temperature, which in turn is related to water density. At 1 atm pressure, the density peak of freshwater is attained at 3.98 °C. With water freezing, the water molecules become organized in the ice structure achieving the lowest density at 0 °C. For this reason, ice is floating on the underlying colder water masses. At high altitude and in the continental regions, the ice cap that progressively swell at the lake surface avoids the heat loss, thus preventing the water mass below to freeze. This way, the aquatic biota can survive albeit the atmospheric temperature is many degrees below zero.

The water density also progressively decreases when temperature increases from 3.98 °C up to ~30 °C. The energy required to change the water temperature by 1 °C depends upon the initial water temperature. For example, the energy required to rise the water temperature from 29 to 30 °C is nearly 40 times higher than the amount required to increase the temperature from 4 to 5 °C. Hence, the water mass tends to accumulate heat becoming less dense than the bottom waters. Under these conditions, lakes become stratified and the relative thermal resistance to mixing increases.

In stratified lakes, three main layers can be identified: the *epilimnion*, the surficial layer, uniformly warm and fairly turbulent; the *hypolimnion,* the deep and cooler layer, more dense and quiescent; these two layers are separated by the *metalimnion,* coinciding with the thermocline, the zone with the maximum rate of temperature decrease.

In the temperate regions, the sequence of water heating and cooling are clearly highlighted by vertical temperature profiles (Figure 2a). From spring to late summer the temperature of surface water mass increases, whilst in the deeper waters it remains nearly constant. At the end of summer, due to the atmosphere cooling, the net heat loss from the water mass progressively increases. The surface waters cool and when their temperature is closer or lower to that of the water mass below, the water turnover begins, the density being greater in the colder surface horizon which sink causing the bottom water up-welling. The water overturn also occurs at the end of winter when the surface waters attain the temperature of maximum density.

On the basis of the circulation patterns lakes are primarily classified into three groups: 1) amictic lakes, permanently stratified because of extreme environmental conditions, 2) holomictic lakes, showing at least one complete vertical mixing event: among them are dimictic lakes that mix twice a year, in spring and fall, 3) meromictic lakes, which circulate only partially, the bottom waters being permanently stratified. Their behavior is irregular and unpredictable being their stratification dependent also on chemical processes occurring in the hypolimnion and climate conditions.

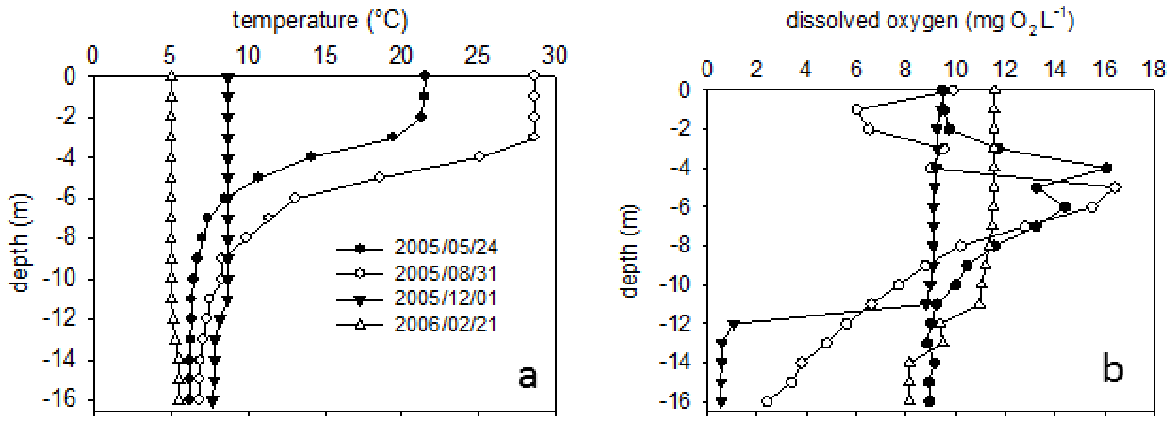

Figure 2. (a) Typical thermal stratification in a dimictic lake in the Po plain and (b) oxygen profiles along the maximum depth water column (modified from Nizzoli et al., 2010)

The thermal stratification has a number of implications for water chemistry. The photosynthetically active radiations (PAR) penetrates only in the upper water layer (euphotic zone) supporting the primary production by phytoplankton. Light penetration into the water mass is inversely related both to depth and turbidity (or water color). The phytoplankton itself can limit the radiation penetration, because during growth it increases the water turbidity. Thus in deep lakes, photosynthesis would be effective only in the uppermost part of the water column, where light intensity is high enough to support autotrophic activities. By contrast, during thermal stratification, the hypolimnion becomes a dark isolated subsystem.

Light penetration is one of the most constraints in the functioning of lake ecosystems. Dissolved oxygen is essential for the majority of aquatic organisms and its availability controls pathways and fate of other chemical elements. The concentration of oxygen in the water column depends on different abiotic (temperature, pressure, salinity, hydrodynamics) and biotic (photosynthesis, respiration and biologically mediated oxidations) factors. Oxygen has a low solubility in water and its concentration at the equilibrium is nearly 300 times lower than that in the atmosphere. The oxygen distribution along the water column is usually related with temperature profiles, according to the Henry law, but this seldom occurs due to the biological activity (Figure 2b).

Phytoplankton photosynthesis supplies oxygen to the water mass while opposite reactions (respirations and microbial and chemical oxidations) consume oxygen. If oxygen consumption prevails over oxygen production or diffusion, most aquatic organisms will suffer for oxygen deficiency. For this reason, in stratified lakes the oxygenation of deeper water layers and, in turn, the survival of benthic fauna, depends almost exclusively on water overturn.

The imbalance between primary production and respiration induced by stratification has major effects on lake metabolism. The epilimnetic waters are often O_2 enriched, and CO_2 and nutrient

depleted. By contrast, the oxygen shortage in the deeper hypolimnion may stimulate anaerobic mineralization which regenerates primarily inorganic carbon, ammonium, phosphates and reactive silicates (Figure 3). In meromictic lakes, due to the persistent stratification, bottom waters become anoxic with the onset of severe reducing conditions. Under these conditions, anaerobic microbial metabolism shift from denitrification or nitrate reduction to ammonium towards manganese, iron and sulphate reduction, and methanogenesis. The end products of these processes are detrimental for water quality, the hypolimnion becoming an highly reduced systems which accumulates soluble metals, toxic sulphides and supersaturated with methane (Cook, 1984; Liua et al., 1986; Nizzoli et al., 2010).

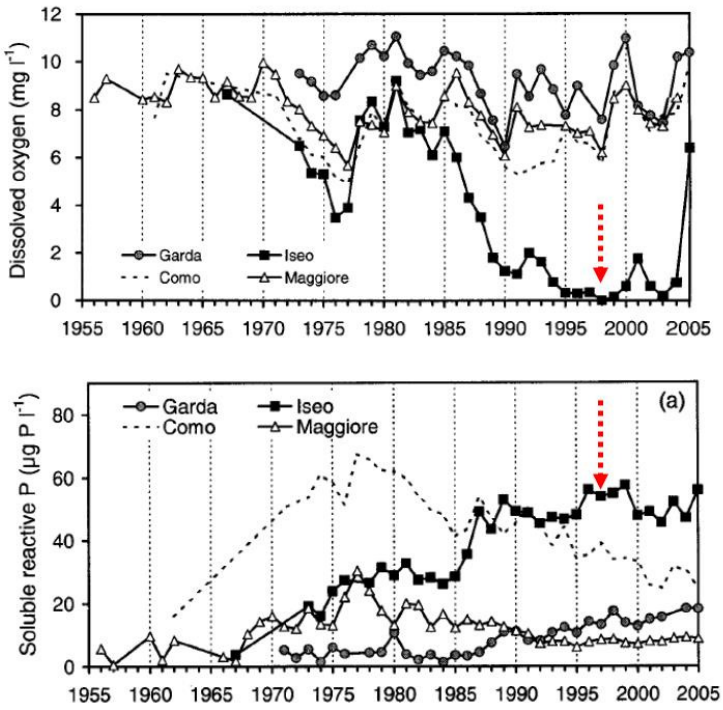

Figure 3. Examples of dissolved oxygen and inorganic dissolved phosphorus in the bottom waters of the main sud-alpine lakes. The arrows indicate the most critical conditions that established in Lake Iseo after approximately 20 years of thermal stratification (Salmaso et al., 2007).

3. Biotic structure and interactions, and processes of lake functioning

3.1. The lake "engine": the foodweb

The lake ecosystem is not homogeneous, but it composes of different subsystems whose biological components are constrained by morphology and physical factors (e.g. light penetration). One can distinguish three main components:

1) the pelagic environment, the deep open waters, whose community is based on the microscopic planktonic organisms (Figure 4);

2) the benthic subsystem, characterized by organisms living at the water-sediment interface and into the superficial sediments; in the deep waters it is aphotic and heterotrophic;

3) the littoral zone, with shallow waters, that composes of a mosaic of habitats mainly structured by macrophyte communities, with gradients from emergent to submerged macroscopic vegetation. Here, the benthic subsystem can receive solar radiation sufficient to support photosynthesis.

The primary production is based on the same process (photosynthesis) either for microalgae or macrophytes, but the fate of the photosynthetic products is quite different. Microalgae have an high probability to enter the grazing food web, while macrophyte tissues fuel mostly the detritus food web and often remains undecomposed due to the high content of refractory organic matter. For this reason, littoral sediments are often organic and characterized by high accretion rates.

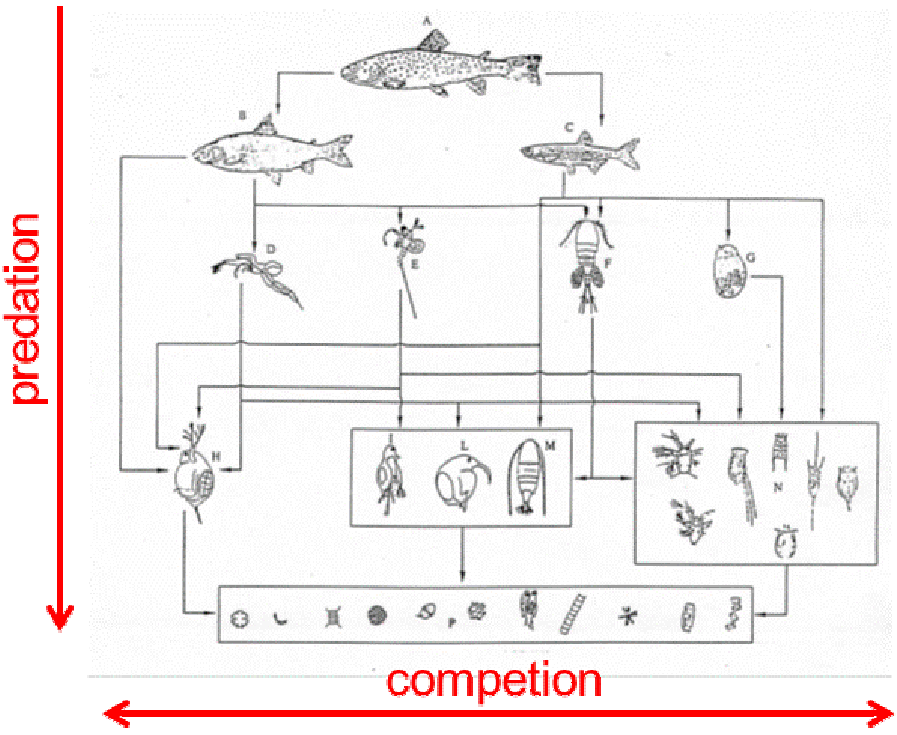

Figure 4. Representation of the pelagic food web of lake Maggiore (Giussani and De Bernardi, 2003). The main trophic interactions are shown by the arrows

Lake food web is fuelled by solar energy as well as by the organic matter entering the aquatic environment from the catchment area. Energy transformations within the food web are driven by trophic relationships, which are accounted mainly by predation and competition interactions,

(Figure 4). Solar energy is converted into chemical energy through photosynthesis by primary producers (i.e. microscopic microalgae suspended in the water mass as well as rooted plants attached to the sediments), then the vegetation biomass can enter the grazing or the detritus pathways. In the first case, herbivores feed on microalgae and carnivores feed on herbivores. In the second case, dead organic matter undergoes decomposition, first through the activity of bacteria and fungi, then through invertebrates feeding on the processed organic matter. Overall, inorganic compounds are assimilated by primary producers and converted into organic matter which is transferred across trophic layers and is then mineralized in the water column or in the sediments, thus releasing back its mineral components. Along the detrital path, detritus aggregates became richer in proteins edible for detritus feeder organisms, which in turn are preys of carnivore organisms. Such array of interactions results in what we see looking at the aquatic environment: plants growing around the shoreline, animals living within the coastal habitats, greenish water due to the growth of microalgae, small crustaceans and fishes feeding on them, and so on.

Surprisingly, the lake world composes mainly of very small living organisms, with a clear contrast with the common citizen perception. The contribution to the total biomass of organisms belonging to different class sizes is as it follows: 0.1% for size > 1 cm; 1.9% for size 100 μm - 1 cm; 39% for size 0.2 - 100 μm and 59% for size <0.2 μm. In other words, the lake ecosystems are dominated by microbes and virus.

Recent studies report also the relevance of dissolved organic matter (DOM) in the pelagic area as a trophic resource for bacteria, which is a potential food source for the food web. DOM may be produced in sediments due to incomplete mineralization, be released as by-products by phytoplankton during photosynthesis or imported from the watershed via runoff. DOM consists of a large pool of molecules which support the heterotrophic metabolism and the production of CO_2, which is usually supersaturated (Caraco and Cole, 1999). These issues are potentially relevant for lake functioning, but are still underestimated and understudied.

3.2. The "fuel" of lake engine: carbon cycle and organic matter

As introduced in the previous paragraph, energy transfers and transformations throughout lacustrine food webs are driven by the carbon cycle. As commonly thought, the photosynthesis acts as the critical step in energy flow. An high production of energy in the chemical form per unit of solar energy can be possible through the formation of carbon-carbon bond in carbohydrates molecules. Hence, carbohydrates act as "chemical trap" of energy making it available for the subsequent steps

of the food web. Therefore, such type of molecules, along with the derivative compounds (lipids, protein) become a sort of fuel which flows and is assimilated throughout the food chain.

In the lacustrine ecosystems carbohydrates are used via respiration as well as fermentation in a wide array of reactions that release and make available the energy step by step. Usually, inorganic carbon is supplied to the photosynthetic process as carbon dioxide. The majority of carbon in lakes is present in form of equilibrium products of carbonic acid. In the scheme reported in paragraph 2.2 are represented the main reactions of the equilibrium of carbonic acid which starts with the equilibrium between atmospheric and dissolved CO_2. These equilibria, not only supply inorganic carbon to the food web, but also constitute the buffering system that is able to oppose to pH variations due to photosynthesis, respiration, or acid deposition. Inorganic carbon is also supplied to the aquatic environment by the rocks belonging to the watershed. As a matter of fact carbonate rocks (marl, limestone) bring into solution carbonate and bicarbonate, maintaining operative all the reactions described above. Carbon, together with N and P, is a fundamental element for the photosynthetic metabolism, but contrarily to N and P, it is generally enough abundant and it seems never limiting the primary production.

The vast majority of the international literature dealing with limnological studies, and hydrochemistry in particular, focuses on the inorganic nutrients nitrogen and phosphorus, and more recently on dissolved silica. This is likely a consequence of those phenomena as water eutrophication that have strongly stimulated basic research in aquatic environments. Nutrient enrichment, in the form of reactive N and P and typically associated to the development of human activities and diffuse and point pollution of surface waters, has in the last decades enhanced primary production by autotrophs with detrimental consequences for water quality. Hypoxia, algal blooms, the disappearance of submersed macrophytes or of valuable fish species and their replacement by tolerant forms are relevant side effects of eutrophication. In many areas eutrophication phenomena were evident since the late 1960s and effective management strategies were performed in order to successfully reverse the trophic status of water bodies. With extremely detailed analysis of the multiple processes transforming N and P in the water and sediment compartments as well as in the food web the focus of limnologists is now on understudied pools of dissolved substances as DOM. There is a vast number of dissolved organic molecules in inland waters, forming a large pool which is poorly explored in terms of composition, reactivity, relevance for aquatic organisms and for whole system budgets. Previously considered scarcely reactive, and also due to analytical difficulties for routine measurements, the dissolved organic pools was neglected. Recent evidences on the contrary suggest the opposite, with relevant fluxes within aquatic ecosystems, for example from the roots to the pore water, from pelagic primary producers to the water column, from

sediments to the overlaying water and from the water back to micro- and macroorganisms. In some geographical areas, where the DOM is dominant if compared to the inorganic pool, DOM sustains entirely primary production and fuels a large microbial activity (Paeri, 1974; Wetzel, 1992; Amon and Benner, 1996). The microbial communities, through the utilization of the more labile fractions of the dissolved organic matter pool (DOM) determine the composition of DOM and in particular the accumulation of the refractory fraction (Hansell, 2013). However, the DOM pool is dynamically replenished with labile DOM from terrestrial runoff, inlake production by autotrophs and photolysis of refractory DOM (Nagata, 2000). The use of organic matter by heterotrophic bacteria in lakes displaces carbon to both the atmosphere and food webs (Del Giorgio and Cole, 1988). The bacterial growth efficiency (BGE) provides an indication on the use of DOM and its conversion into biomass. BGE depends upon temperature, the composition and lability of the DOM pool and the concentrations of inorganic nutrient; an increase in the availability of N and P makes the use of DOM more efficient (Del Giorgio and Cole, 1988; Asmala et al., 2013). The multiple biotic and abiotic processes and the fate of dissolved organic matter in lakes is an extremely stimulating subject for future research and open new and interesting windows on the pathways of energy and matter in aquatic water bodies.

3.3. Shallow lakes and littoral zone: neglected systems?

Shallow lakes are characterized by a low ratio between the water mass and the sediment surface and for this reason sedimentary processes may play a relevant role in water chemistry (Søndergaard et al., 2003). Benthic processes may recycle large amount of nutrients and promote eutrophic conditions and water turbidity but, simultaneously, shallowness may allow benthic primary production and the coupling between heterotrophic regeneration and autotrophic uptake (Pinardi et al., 2009; Nizzoli et al., 2014). Microbial respiration in organic sediments has also the potential to exhaust the small oxygen reserve of the water column and determine hypoxic or anoxic conditions, in particular during night hours (Bolpagni et al., 2007). However, even short periods of wind can mix the whole water mass promoting aeration and reoxidation of surface sediments. Different typologies of macrophytes may colonize shallow lakes, including emergent plants as the common reed, floating-leaved plants as the water lily or pleustonic communities as duckweeds. All these plants have photosynthetic apparatus outside the water column and therefore evolve oxygen and fix inorganic carbon to and from the atmosphere. They are also all characterized by elevated rates of production, resulting in accumulation of organic matter at the sediment level and determining rapid infilling of the water body. In shallow lakes photosynthesis may occur at the sediment-water interface, via benthic microalgae or rooted macrophytes. The latter may inject oxygen within

sediments via the roots, augmenting the volume where aerobic microbial processes as nitrification are confined (Soana and Bartoli, 2014). Such mechanism (ROL, radial oxygen loss), is an adaptation of plants to survive in otherwise anoxic sediments; oxygen penetration is in fact limited to a few millimeters. Despite thin, this horizon is characterized by an intense microbial activity and is fundamental for the reoxidation of the end-products of anaerobic metabolism as ferrous iron, manganous manganese, sulphide or methane (Ribaudo et al., 2009). The presence of oxygen within sediments indirectly buffers the release of P and promotes, via coupled nitrification and denitrification, the loss of nitrogen (Soana et al., 2015). Besides roots, the presence of bioturbating fauna as surface or deep burrowers (i.e. chironomids or oligochaetes) favors the oxygenation of sediments and the occurrence of aerobic microbial processes (Pelegrì and Blackburn, 1996; Svensson et al., 2001).

4. Eutrophication: an opportunity to study lacustrine food web and processes

Although the productivity is based on the carbon cycle, the magnitude of the production depends primarily on the availability of both P and N as well as minor elements (Si, Fe). The trophic status of a lake, i.e. its primary productivity level, has been assumed as a criterion to classify lakes. When nutrient availability exceeds certain thresholds, it triggers the onset of a degenerative process which is due to the excessive primary production, the so called eutrophication.

The term eutrophication derives from a Greek word that means good nutrition. The adjective eutrophic was used firstly in early 20th century by the German limnologist August Thienemann to indicate high lake productivity. He defined eutrophic the highly productive lakes and oligotrophic the low productive ones -oligo meaning poor-.

The modern definition was formerly proposed by Vollenweider (1968) as the water enrichment by phosphorus (P) and nitrogen (N) that stimulates primary production of phytoplankton up to levels that cannot be controlled by grazing. The excess biomass can thus settle and accumulate on the sediment surface, where its decomposition causes oxygen consumption till the complete depletion (see Figure 3). A special attention was devoted to P, that was assumed to be the main limiting factor for primary productivity. In this fashion, the cause-effect relationship appeared simple and was successfully applied in restoration programs since early 1970s. Further studies have demonstrated that eutrophication is also “an increase of the organic matter supply rates to aquatic ecosystems” (Nixon 1995). However, these definition of eutrophication disregarded the complexity of the involved processes, i.e. hydro-morphology, multiple element stoichiometry, biological and biogeochemical interactions (Cloern 2001; Duarte 2009; Nixon 2009; Howarth et al. 2011). In fact,

responses of phytoplankton communities are controlled not only by the bottom-up nutrient supply and stoichiometry, but also by top-down trophic interactions (Carpenter et al. 1985).

The long term data series from Lake Maggiore highlights how water contamination has changed in the last decades (Figure 5). From 1950s to late 1970s, P has been the most concern due to its exponential increase in the water column. The enforcement measures regarding wastewater controls and treatments (Law No 319/1976) and the reduction of P in detergents (Law No 82/1982 , Ministry Decree No 413/1988), along with protection measures of the coastal lake, allowed to reverse the trend, with a significant reduction of P concentration back to the levels detected in the 1950s.

A completely different trend is occurring for reactive inorganic nitrogen (N_{ir}), that is still increasing, albeit at much lower rates, it becoming a serious threat for most surface and groundwater.

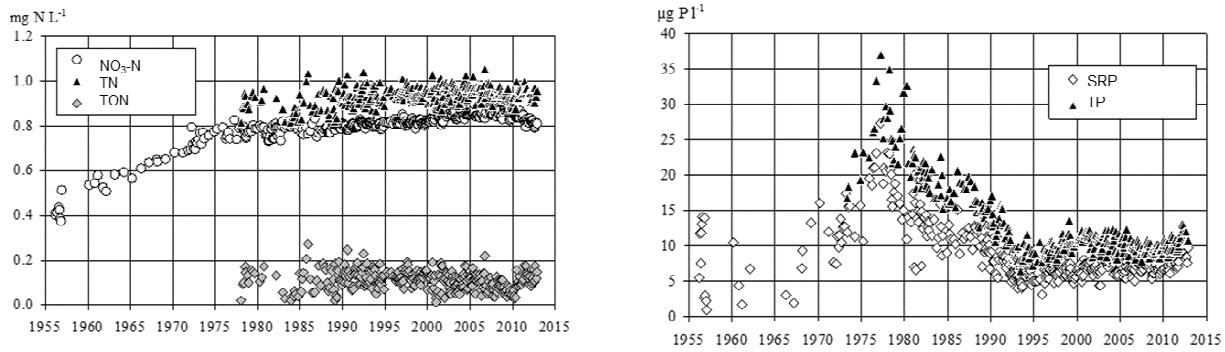

Figure 5. Long term evolution of nitrogen and phosphorus concentrations in the Lake Maggiore (Rogora et al., 2013). Legend: NO_3-N: nitrate nitrogen, TN: total nitrogen; TON: total organic nitrogen; SRP: soluble reactive phopshorus; TP: total phosphorus.

4.1. Nitrogen cycle

Nitrogen has an atmospheric storage which is accessible only to few taxa of both autotrophs (e.g. Cyanobacteria) and heterotrophs (e.g. *Rhizobium* sp.). The main pathways of the N cycle are mediated by bacteria, allowing different oxidation and reduction processes which are definitely responsible of N fate in the ecosystem (Figure 6). Among others, nitrogen fixation, and coupled nitrification and denitrification and anammox represent key processes regulating the inorganic reactive nitrogen input to and output from the ecosystem (Saunders and Kalff, 2001).

The industrial conversion of N_2 into NH_3, the so called Haber-Bosch process, has increased the availability of inorganic reactive nitrogen (N_{ir}) by 85 Tg N yr^{-1} since the last century. In parallel, the emission and deposition of nitrogen oxides (NO_x) from combustions has increased by 21 Tg N yr^{-1} (Galloway et al., 2003). A so great nitrogen availability, especially from industrial fixation, has had

relevant benefit for agricultural and livestock production, but in parallel the nitrogen contamination has increased two times in superficial waters and four times in the atmosphere.

In a lake nitrogen can be fixed either biologically or can reach the water body through runoff. Nitrogen salts (ammonium, nitrites and nitrates) are assimilated by aquatic plants and transformed into organic compounds: this happens in the water column throughout phytoplankton and floating macroalgae or in the sediment throughout rooted macrophytes (Pinardi et al., 2011; Nizzoli et al., 2014). Organic nitrogen is then recycled through benthic bacteria mostly as ammonium. In the recent past it was believed that the role of sediments in the nitrogen cycle was not relevant; however, with the problem of high nitrogen amounts reaching lakes it has been noted that an efficient way to lower nitrogen internal load is the coupling of nitrification and denitrification, bacterial processes occurring in the sediment which lead to the production of molecular nitrogen (Seitzinger et al., 2006).

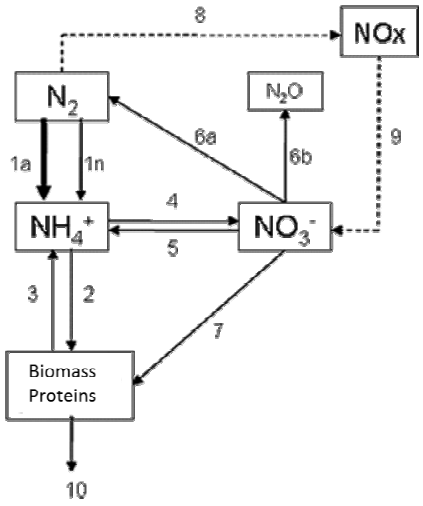

Figure 6. Main pathways of the nitrogen cycle.

1n: natural fixation
1a: industrial fixation (Haber-Bosch)
2: NH_4^+ assimilation
3: ammonification
4: nitrification
5: dissimilative reduction of nitrate to ammonium (DNRA)
6a,b: denitrification with molecular nitrogen and nitrous oxide as end products
7: assimilative NO_3^- reduction
8: atmospheric oxidation of N_2 to NO, N_2O and N_2O_5 (e.g. combustion)
9: reaction of NOx with rain to form HNO_3
10: export and burial

Unfortunately, the organic matter reaching the sediment of eutrophic water bodies usually exceeds the capacity of bacteria to degrade it and the consequent lack of oxygen on the bottom affects the process of nitrification carried out in the sediment by aerobic bacteria. So the coupling of nitrification and denitrification in eutrophic system is not working and this fact leads to an accumulation of ammonium in the water column. Furthermore, under reduced chemical conditions and organic enrichment, the dissimilative reduction of nitrate to ammonium may become a relevant process, replacing denitrification and resulting in further production of NH_4^+ (Fig. 7).

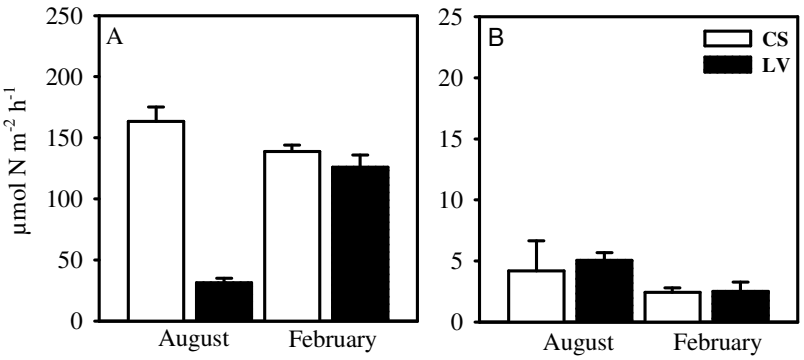

Figure 7. Total Denitrification (A) and total DNRA (B) rates in hypolimnetic sediment from two lakes with different trophic status: CS is mesotrophic and LV is eutrophic with an high organic load. Denitrification is lower in LV (older and more eutrophic) due to the reducing sedimentary conditions (Nizzoli et al., 2010)

4.2. Phosphorous cycle

The phosphorous cycle has a sedimentary pathway, with a negligible atmospheric reserve. Furthermore, contrarily to nitrogen, P does not undergo microbially-mediated redox processes. This peculiarity in any case does not simplify the study of P, as the geochemical transformations of this element and their regulation within sediments are directly affected by microbial activity (table 3)(Rigler, 1956). P enters all lake continuously in runoff water, mostly as inorganic P; it is assimilated by phytoplankton and plants, incorporated as organic P and recycled again by benthic bacteria as PO_4^{3-} (Dillon and Kirchner, 1975; Boström et al., 1988). A variable fraction of the regenerated inorganic P can also be trapped, complexed or fixed in many different ways by the sediments or by various compounds in unsoluble forms (Syers et al., 1973).

In oligotrophic condition, due to the low quantities of P that reach the lake and to the interactions of this element with the superficial oxic sediment, phosphorus is almost undetectable in the water column and often limits the primary production. In eutrophic conditions, P becomes abundant first of all due to the loads that enter the lake but also because of an elevated internal recycle linked to anaerobic bottom conditions that favor P release (Hupfer and Lewandowski, 2008).

In particular, it seems that P cycle in sediments is primarily regulated by iron and calcium availability (table 3). Ferric iron binds and precipitate phosphate in highly insoluble complex/forms. During the summer months, due to the lack of oxygen, specialized bacterial population use nitrates, sulphates or even ferric iron as electron acceptors. The produced ferrous iron is more soluble and releases PO_4^{3-} to the water column. Anoxia at the sediment level brings the regeneration of a large amount of P maybe stored for long periods in the mud, rendering it suddenly available for algal blooms.

Table 3. Principal Phosphorus species, with indicated the main features, reactivity and availability to primary producers.

P species	*Characteristics*	*Reactivity and availability to primary producers*
Organic P	Organic detritus	Not available. Mineralized by phosphatases
Ca≈PO_4 autigenic	Formed inlake due calcite precipitation, or biogenic processes (mollusc shells)	Not soluble. Extractable with strong acids
Ca≈PO_4 detrital	Originated from rocks and solid transport from watershed	Not soluble. Extractable with strong acids traibile con HCl 1 N
Fe≈PO_4	Ferric ($FePO_4$) and ferrous [Fe3(PO_4)] phosphates; complexes with iron hydro-oxides (FeOOH)	Low solubility. Redox sensitive.
Exchangeable P	Weak binding with exchange sites on clay, carbonates, etc.	Extractable with cation substitution at alkaline pH
Dissolved organic P	Organic metabolic by product	Readily available trough phosphatase activity
Dissolved inorganic P	Soluble mineral phosphates, that at 6.5<pH<8.5 are $H_2PO_4^-$ and $HPO4_2^-$	Readily available

4.3. Linking the water cycle with nutrient and catchment

The hydrological cycle is regulated by climate and its equilibrium depends upon two main processes: evaporation and precipitation, occurring both on the land and on the free water surface. Most evaporation occurs in the ocean surfaces and forms clouds that discharge on lands. Surface flow follows natural slopes and feed groundwater, rivers and lakes, transporting a variety of dissolved and particulate compounds. Weathering and solubilization of elements from rocks and soils link the hydrological and sedimentary cycles. Recent changes of climate, precipitation patterns and land use in watersheds have resulted in different timing and transport of the key nutrients N, Si and P to lakes, with relevant implications for the biological communities.

Agriculture and farming have simplified the landscape, removing natural elements as riparian corridors and wetlands and have enriched arable lands with large amounts of synthetic fertilizers and manure (Bartoli et al., 2012). A fraction of the nitrogen which is in excess to crop uptake is mobilized as nitrate via irrigation and precipitation waters and pollutes surficial water bodies and aquifers. Elevated nitrate concentrations are a major problem for inland and coastal areas, stimulating primary production, eutrophication phenomena and posing at risk water consumption by animals and humans.

In agricultural areas the hydrological cycle has been deeply altered by water abstraction for irrigation purposes; this has accelerated the pollutant transport to rivers and lakes.

The silica cycle has been altered as well due to progressive impoverishment of bioavailable silica in cultivated areas and to the river damming, which slows/hampers its solid transport (Carey and Fulweiler, 2007). Large and small artificial basins and hydropower plants allows to retain upstream freshwater, and to store it for the production of electricity and to feed the irrigation canal network. Minor transport of silica may unbalance the ecological stoichiometry of nutrients, favoring the appearance of potentially harmful algal blooms as flagellates and cyanobacteria, at the expense of diatom communities.

Lakes could become "probes" to track/detect relationships between humankind activities and water resources, to develop knowledge on ecosystem resilience and fragility, and to make clear the sustainable development concept. A number of lakes have undergone deep modifications of their chemical and biological quality, due to excess nutrient input and eutrophication phenomena, to acid rains, to unsustainable pressure on fish communities or to the introduction of alien species. There are also examples of successful interventions that have reversed such detrimental impacts towards the recovery of pristine conditions. A great effort has been also devoted to restore eutrophic lakes either with nutrient removal or with the mitigation of eutrophication effects (cit.). The lake oligotrophication is often apparent, since the recovery of the former chemical conditions is not followed by the restoration of the pristine biotic communities (Nixon 2009; Duarte et al 2009).

References

Amon, R.M.W. and R. Benner, 1996. Bacterial utilization of different size classes of dissolved organic matter. Limnol. Oceanogr., 41(1), 41-51.

Asmala, E., Autio, R., Kaartokallio, H., Pitkänen, L., Stedmon, C., & Thomas, D. N. (2013). Bioavailability of riverine dissolved organic matter in three Baltic Sea estuaries and the effect of catchment land use. Biogeosciences, 10(11), 6969-6986.

Bastviken, D., J. Cole, M. Pace, and L. Tranvik, 2004. Methane emissions from lakes: Dependence of lake characteristics, two regional assessments, and a global estimate, Global Biogeochem. Cycles, 18, GB4009, doi:10.1029/2004GB002238.

Bolpagni, R., Pierobon, E., Longhi, D., Nizzoli, D., Bartoli, M., Tomaselli, M., & Viaroli, P. (2007). Diurnal exchanges of CO 2 and CH 4 across the water–atmosphere interface in a water chestnut meadow (*Trapa natans* L.). Aquatic botany, 87(1), 43-48.

Boström, B., Andersen, J. M., Fleischer, S., & Jansson, M. (1988). Exchange of phosphorus across the sediment-water interface. In Phosphorus in Freshwater Ecosystems (pp. 229-244). Springer Netherlands.

Calderoni, A. and G.A.Tartari, 2000. Evolution of the water chemistry of Lake Orta after liming. J. Limnol., 60: 69-78, 2000.

Citterio, M., Diolaiuti, G., Smiraglia, C., D'Agata, C., Carnielli, T., Stella, G., Siletto, G.B., 2007. The fluctuations of Italian glaciers during the last century: A contribution to knowledge about alpine glacier changes. Geografiska Annaler, Series A: Physical Geography, 89 (3), pp. 167-184.

Connell, J. H. 1975. Some mechanisms producing structure in natural communities: a model and evidence from field experiments. Pages 460-490 in M. L. Cody and J. M. Diamond, editors. Ecology and evolution of communities. Harvard University Press, Cambridge.

Cook, R.B., 1984. Distributions of Ferrous Iron and Sulfide in an Anoxic Hypolimnion. Canadian Journal of Fisheries and Aquatic Sciences, 1984, 41(2): 286-293, 10.1139/f84-033

Del Giorgio, P.A., and J.J. Cole, 1998. Bacterial growth efficiency in natural aquatic systems. Annual Review of Ecology and Systematics: 503-541.

Dillon, P. J., & Kirchner, W. B. (1975). The effects of geology and land use on the export of phosphorus from watersheds. Water Research, 9(2), 135-148.

Duarte CM, Conley DJ, Carstensen J, Sanchez-Camacho M (2009) Return to *Neverland*: shifting baselines affect eutrophication restoration targets. Estuaries Coasts 32:29-36.

Edmondson, W.T. and Edmondson, Y.H. 1990. Pallanza as a haven for visiting limnologists. Mem. Ist. Ital. Idrobiol. 47: 47-55.

Galloway, J. N., Aber, J. D., Erisman, J. W., Seitzinger, S. P., Howarth, R. W., Cowling, E. B., & Cosby, B. J. (2003). The nitrogen cascade. Bioscience, 53(4), 341-356.

Giussani L., De Bernardi R., 2003. Conoscere un lago. Documenta Istituto Italiano Idrobiologia, Pallanza.

Hansell, D.A., 2013. Recalcitrant dissolved organic carbon fractions. Marine Science 5.

Hupfer, M., & Lewandowski, J. (2008). Oxygen Controls the Phosphorus Release from Lake

Sediments–a Long-Lasting Paradigm in Limnology. International Review of Hydrobiology,

93(4-5), 415-432.

Hutchinson, G.E., 1959. Homage to Santa Rosalia, or why are there so many kinds of animals? Am. Naturalist 93, 245-249.

Jeppesen, E., 1998. The structuring role of submerged macrophytes in lakes. New York: Springer.

Krzyzanowski J., Inne J.L., 2010. Back to the basic-Estimating the sensitivity of freshwater to acidification using traditional approches. Journal of Environmental management 91: 1227-1236.

Lindeman, R.L., 1942 The Trophic-Dynamic Aspect of Ecology. Ecology, 23, 399-417.

Liua, R., A. Hofmannb, F.O. Gülaçara, P. Favargerb, J. Dominik, 1996. Methane concentration profiles in a lake with a permanently anoxic hypolimnion (Lake Lugano, Switzerland-Italy) Chemical Geology, 133, 1–4: 201–209

Mosello R.barbieri A., Bendetta Gunther, Boggero A., Marchetto A., Psenner R., Tait D., Tartari G.A., 1993. Quantification of the susceptibility of alpine lakes to acidification. Mem. Ist. Ital.. Idrobiol., 52: 355-386.

Nagata, T., 2000. Production mechanisms of dissolved organic matter. Microbial ecology of the oceans: 121-152.

Nixon SW, 2009. Eutrophication and the macroscope. Hydrobiologia 629:5-19.

Nixon, S.W., 2009. Eutrophication and the macroscope. Hydrobiologia, 629 (1), pp. 5-19.

Nizzoli, D., Carraro, E., Nigro, V., Viaroli, P., 2010. Effect of organic enrichment and thermal regime on denitrification and dissimilatory nitrate reduction to ammonium (DNRA) in hypolimnetic sediments of two lowland lakes. Water Research, 44 (9), pp. 2715-2724.

Nizzoli, D., Welsh, D. T., Longhi, D., & Viaroli, P. (2014). Influence of Potamogeton pectinatus and microphytobenthos on benthic metabolism, nutrient fluxes and denitrification in a freshwater littoral sediment in an agricultural landscape: N assimilation versus N removal. Hydrobiologia, 737(1), 183-200.

Paeri Hans W. , (1974), Bacterial uptake of dissolved organic matter in relation to detrital aggregation in marine and freshwater systems, Limnology and Oceanography, 6: 966-972.

Pelegrí, S. P., & Blackburn, T. H. (1996). Nitrogen cycling in lake sediments bioturbated by Chironomus plumosus larvae, under different degrees of oxygenation. Hydrobiologia, 325(3), 231-238.

Peters, R. H., 1991. A critique for ecology. Cambridge University Press,369 pp.

Pinardi, M., Bartoli, M., Longhi, D., Marzocchi, U., Laini, A., Ribaudo, C., & Viaroli, P. (2009). Benthic metabolism and denitrification in a river reach: a comparison between vegetated and bare sediments. Journal of Limnology, 68(1), 133-145.

Pinardi, M., Bartoli, M., Longhi, D., Viaroli, P., 2011. Net autotrophy in a fluvial lake: The relative role of phytoplankton and floating-leaved macrophytes. Aquatic Sciences, 73 (3), pp. 389-403.

Ribaudo, C., Bartoli, M., Racchetti, E., Longhi, D., Viaroli, P. Seasonal fluxes of O2, DIC and CH4 in sediments with Vallisneria spiralis: Indications for radial oxygen loss (2011) Aquatic Botany, 94 (3), pp. 134-142.

Rigler, F. H. (1956). A tracer study of the phosphorus cycle in lake water. Ecology, 550-562.

Salmaso et al 2007, Fundamentals of Applied Limnology 170: 177-196.

Salmaso N., Morabito G., Garibaldi L., Mosello R., 2007. Trophic development of the deep lakes south of the Alps: a comparative analysis. Fundamental and Applied Limnology/Archiv für Hydrobiologie 170: 177-196.

Saunders, D. L., & Kalff, J. (2001). Nitrogen retention in wetlands, lakes and rivers. Hydrobiologia, 443(1-3), 205-212.

Rogora M, P Giacomotti, A. Orrù, A. Pranzo, G. A. Tartari. 2013. Considerazioni generali sull'evoluzione del chimismo delle acque lacustri e tributarie, con particolare riferimento al quinquennio 2008-2012 In R. Bertoni (ed), Ricerche sull'evoluzione del Lago Maggiore. Aspetti limnologici. Programma quinquennale 2008-2012. Commissione Internazionale per la protezione delle acque italo-svizzere. 119-130.

Scheffer, M. and E. Jeppesen, 2007. Regime Shifts in Shallow Lakes. Ecosystems, 10:1-3.

Seitzinger, S., Harrison, J. A., Böhlke, J. K., Bouwman, A. F., Lowrance, R., Peterson, B., ... & Drecht, G. V. (2006). Denitrification across landscapes and waterscapes: a synthesis. Ecological Applications, 16(6), 2064-2090.

Shapiro J. 1990. Biomanipulation: The Next Phase—Making It Stable. Hydrobiologia 200/201:13-27.

Smith, S.V. and Hollibaugh, J.T., 1993. Coastal metabolism and the oceanic organic carbon balance. Reviews of Geophysics 31, 1:75-89.

Soana, E., Naldi, M., Bonaglia, S., Racchetti, E., Castaldelli, G., Brüchert, V., Viaroli, P., Bartoli, M., 2015. Benthic nitrogen metabolism in a macrophyte meadow (Vallisneria spiralis L.) under increasing sedimentary organic matter loads Biogeochemistry, 124 (1-3), pp. 387-404.

Søndergaard, M., Jensen, J. P., & Jeppesen, E. (2003). Role of sediment and internal loading of phosphorus in shallow lakes. Hydrobiologia, 506(1-3), 135-145.

Svensson, J. M., Enrich-Prast, A., & Leonardson, L. (2001). Nitrification and denitrification in a eutrophic lake sediment bioturbated by oligochaetes. Aquatic Microbial Ecology, 23(2), 177-186.

Syers, J. K., Harris, R. F., & Armstrong, D. E. (1973). Phosphate chemistry in lake sediments. Journal of environmental Quality, 2(1), 1-14.

Viaroli, P., Ferrari, I., Mangia, A., Rossi, V., Menozzi, P., 1992. Sensitivity to acidification of northern Apennines lakes (Italy) in relation to watershed characteristics and wet deposition. Documenta Istituto Italiano di Idrobiologia, 32:, pp. 93-105.

Viaroli, P., Ferrari, I., Paris, G., Rossetti, G., Menozzi, P., 1994. Limnological research on northern Apennine lakes (Italy) in relation to eutrophication and acidification risk. Hydrobiologia, 274 (1-3), pp. 155-162.

Wetzel, R.G., 1992. Gradient-dominated ecosystems: sources and regulatory functions of dissolved organic matter in freshwater ecosystems. In: Dissolved Organic Matter in Lacustrine Ecosystems. Developments in Hydrobiology, Volume 73, pp 181-198.

Wetzel, R.G., 2001. Limnology: lake and river ecosystems. Gulf Professional Publishing, 985 pp.

Yeston J., Coontz R., Smith J., Ash C. (Eds), 2006. A Thirsty World – special section on Freshwater Resources. Science 313, 1068-1981

Book: Photochemical processes taking place in surface waters, role of natural organic matter in photochemical reactions and to recently developed tools, analytical techniques

Chapter 3. CHARACTERISTICS OF THE UNDERWATER LIGHT FIELD

Steven A. Loiselle[a], Hongtao Duan[b], Zhigang Cao[b]

a Environmental Spectroscopy Group, Dipartimento di Biotecnologie, Chimica e Farmacia, CSGI, Università degli Studi di Siena, 53100 Siena, Italy

b State Key Laboratory of Lake Science and Environment, Nanjing Institute of Geography and Limnology, Chinese Academy of Sciences, Nanjing 210008, China

Abstract

Photochemical processes are controlled by the characteristics of the underwater light field. These conditions will change over time and space, in relation to the position, concentration and properties of the optically active components in the water column as well as the direction and intensity of the incident solar radiation. This chapter will examine the underwater light field, the spectral properties of those components that influence this field and their estimation using appropriate modelling approaches as well as in situ and remote technologies.

Table of contents

Section 1.

Incident solar radiation

The total incident solar radiation (global solar radiation) on the surface of an aquatic ecosystem is the sum of the direct and indirect (diffuse) radiance on the water surface. Both the direct and indirect solar radiance depend on the total exo-atmospheric solar radiation, solar zenith angle and the resulting modifications that occur between the water surface and the top of the atmosphere, due to atmospheric absorption and scattering.

The sun emits similar to a blackbody at 5800K with a spectral distribution following Planck's law. The maximum emission is near 0.5 mm, with emission tails extending from the gamma region to infrared. The amount of solar radiation reaching the outer atmosphere depends on the distance (squared) of the Earth from the sun. The solar constant changes over the lifetime of the sun and is influenced by sun activity (in particular the number of sunspots), with 11, 22 and 80 year cycles. Typically, the solar constant of 1372 W m^{-2} varies less that 1% from year to year.[1] As the Earth orbits the sun in an elliptical manner (eccentricity of 0.0167 in 2006), the relative distance changes, with the smallest distance occurring in January and the largest in July (change in distance from the sun of 3.4% or 5.1 million km). The difference in exo-atmospheric radiation is 6.9%.

The seasonal cycle of solar radiation results from the tilt of the Earth's axis (obliquity of 23.5º) and influences the changes in the position of the sun in the sky (solar zenith angle) and the duration of the day with respect to the night. At the equator, the zenith angle reaches a maximum at noon during the vernal and autumnal equinox. At latitudes above 23º, the sun is never directly overhead.

The amount of solar energy incident on a horizontal surface at the top of the Earth's atmosphere is:

$$E_0 = S_0\left(\frac{r_0}{r}\right)^2 cos(\theta_z)$$

Where S_0 is the solar constant, r and r_0 are the instantaneous Earth-sun distance and its mean annual value and θ_z is the solar zenith angle. There are numerous online calculators to determine each one of these variables for different geo-locations and times (days and hours of the day).

The modification of the exo-atmospheric solar radiation through the atmosphere depends on the distance travelled to reach the surface of interest (optical pathway) as well as the characteristics of the intervening atmosphere. In a homogeneous medium, the intensity of monochromatic electromagnetic radiation will decrease in a logarithmic fashion following the Beer–Lambert–Bouguer law. The extinction of the incident radiation flux results from the capacity of the medium to absorb or scatter radiation at specific wavelengths. However, the atmosphere is not homogenous, as the position and concentration of its optically active components and their relative capacity to absorb and scatter in different wavelengths varies vertically, horizontally and temporally. It is possible to consider the atmosphere as a series of horizontal uniform layers, but temporal and geographical variations in the concentration of the

optically active components of each layer will influence the incident flux reaching the water surface.

In most cases, it is possible to estimate the atmospheric extinction of solar radiation by considering the total concentration and optical properties of the components in a standard cloud free homogeneous atmosphere. In the UV and short visible wavelengths, both scattering and absorption are important while at higher wavelengths, absorption dominates extinction of direct radiation (in a cloud free atmosphere). At sea level, the total solar irradiance on a surface, in clear sky conditions, has been modelled using estimates of the degree of scattering by molecules and aerosols and the absorption of water vapour and other gases, [2, 3, 4] including ozone. [5, 6] In general, UV radiation below 0.3µm is nearly completely absorbed due to oxygen (< 0.2 µm) and ozone (< 0.29 µm), while most of the UV-A and visible wavelengths are influenced by a few weak and narrow absorption bands of oxygen and ozone. Incident near infrared radiation (700 – 4000 nm) is attenuated by large absorption bands associated to water vapour, CO_2, CH_4 and N_2O, while the absorption of thermal infra-red radiation (4 – 22 µm) is dominated by CO_2, water vapour and ozone.
Molecular scattering is greater at low wavelengths (proportional to λ^{-4}, following the equation for elastic scattering of Rayleigh), meaning that scattering is 9 times stronger in the short visible (400 nm) with respect to long visible (700 nm) wavelengths. For aerosols and particles that have a similar dimension to the wavelengths of the incident radiation, the resultant scattering is less wavelength dependent. This latter type of scattering occurs mostly in the lower parts of the atmosphere.

Clouds have a strong influence on the incident solar irradiance. Because they contain droplets that are larger than aerosols and because the total mass of liquid water (or ice) can be significant, they can often completely block direct solar radiation. Spectrally, scattering from clouds dominates in the visible wavelengths, while absorption from clouds dominates in infrared. The transition from high scattering to high absorption varies between clouds types, and whether they consist of ice or liquid water. Most radiative transfer models include parameters for cloudy conditions. [6, 7, 8] In general, estimated cloud transmittance, derived by satellite measurements are sufficient to correct for the reduction of direct solar radiation on the surface of a water body.

Diffuse solar radiation (skylight) results from the elastic scattering by molecules and aerosols in the atmosphere. In a cloud free sky, the ratio of diffuse to direct radiation typically ranges from 15% at solar noon to 40% at small zenith angles, with the maximum intensity of diffuse radiation just below 500 nm. In conditions of high cloud cover, all of the available light is typically diffuse.

While most models consider the sum of direct and diffuse solar radiation on a horizontal surface at sea level, the incident radiation on inland water bodies depends on the altitude. Many of the world's largest lakes have altitudes near to and above 1000m (African Rift Valley Lakes, Lake Titicaca, Lake Sevan). Most models [9] use satellite estimated irradiances combined with a digital elevation model and consider the most important change with altitude to be the reduction of the optical pathlength (Δz). Broadly speaking, the increase in irradiance with altitude should be exponential, and follow $\Delta z \cos(\theta_z)$. There are a number of empirical and radiative transfer

models that can be used to estimate the change in total solar irradiance (global solar radiation) on a horizontal surface with altitude. [10,11,12,13] Most of these have been developed for use in renewable energy technologies. The increase in irradiance with altitude will be wavelength dependent and influenced by the atmospheric conditions relative to the area of study. This is particularly important for UV radiation where the "altitude effect" can result in a 20% increase in UV radiation for a 1000 m increase in altitude. [14] Dvorkin and Steinberger(1999) modelled changes in UV irradiance, direct and diffuse, with altitude using information about the vertical distribution of ozone concentration, aerosols, SO_2 and NO_2. [15]

Section 2.

Underwater light environment

Solar radiation incident on a water body can either be reflected from the surface (surface albedo) or enter the medium. Once solar radiation passes the air water interface, its spectral and spatial distributions in the water body depend on the concentrations and distribution of the optically active components (e.g. dissolved or particulate matter that absorbs or scatters in the visible or ultraviolet wavelengths) present.

Surface albedo is defined here as the surface reflection of direct and diffuse radiation (and does not include the volume scattering from within the water body) and follows Fresnel equations. For the direct component, surface albedo is influenced by the solar angle, wind speed (or surface roughness) and the relative refractive index of water and air. [16] Surface albedo increases to nearly 100% at high solar zenith angles (low solar elevation). Likewise, surface albedo is sensitive to the air-water refraction index. The refractive index of pure water is higher in the UVR with respect to the visible, ranging from 1.36 at 300 nm to 1.33 at 700 nm. Furthermore, the refractive index of water decreases with temperature. [17] Wind or wave action decrease surface albedo at high solar zenith angles but can increase albedo at lower solar zenith angles. [18] For diffuse radiation, surface albedo can be calculated by integrating the angular distribution of the incident diffuse radiation, or more simply by using empirical models based on surface roughness or wind speed. [19]

Once past the air-surface interface, the fate of solar radiation in the water column is controlled by the absorption and scattering characteristics of the optically active components of the water body. In clear water bodies, reflected radiation from the lake or ocean floor will also contribute to the available solar radiation within the water column.

Absorption occurs when photons of the incident solar radiation are removed by the incident flux by the presence of molecules in the aquatic medium. Photons that have sufficient energy bring about transitions from one electronic energy level to another in the receiving molecule. If that molecule is part of a photosynthetic system, its energy is transferred to a reaction centre for photosynthesis. For other molecules, the transition from a lower excited state to a higher occurs by interaction with a paramagnetic molecule such as oxygen. The excited molecule can return to its original state with dissipation as heat energy distributed amongst the molecules of the system or re-emission as fluorescence. In most aquatic ecosystems, the majority of the incoming photons are absorbed by four components: water, chromophoric dissolved organic matter (CDOM),

particulate organic matter (POM) including phytoplankton and particulate inorganic matter (PIM). This division can also be made on the basis of living and non-living matter as: water, CDOM, photosynthetic biota and tripton (inanimate particulate matter).

Scattering increases vertical attenuation by changing the direction of the downward directed photons as well as increasing their optical path length and therefore the probability of their absorption. The two kinds of scattering that occur in an aquatic environment are density fluctuation scattering and particle scattering. The former is caused by microscopic fluctuations in density which lead to changes in the dielectric constant of the aquatic medium. The interactions of the radiation field with these inhomogeneities lead to changes in angular distribution of the incident radiation, in relation to the wavelength. In the clearest waters, this "molecular" type scattering dominates. [20, 21] Particle scattering depends on the characteristics of the particulate matter present, following the theoretical basis developed by Mie (1908). Particle scattering results in an angular distribution that is different than that of density fluctuation scattering (increased forward direction) and is sensitive to the scattering cross section of the particle.[22] In general, particle scattering has a near linear relationship with the concentration of suspended inorganic or organic particulate matter present in the water body,[23,24] with differences in the constant of proportionality occurring with types of suspended matter. Spectrally, scattering decreases at higher wavelengths following a power function.[24] In recent years, significant efforts have been made to determine mass-specific coefficients for scattering in relation to the concentration of suspended particulate matter (SPM), or the individual contributions of organic (POM) and inorganic fractions (PIM). In some cases, a specific scattering function for individual phytoplankton groups can be determined.[25,26] In highly productive waters, phytoplankton cells make the most significant contribution to particle scattering while scattering in coastal and inland waters is often dominated by suspended organic (non-living) or inorganic matter. In general, the concentrations, size distribution and refractive index of the particulate matter will determine their influence on the scattering properties of a water body.

The spectral characteristics of the underwater light field are divided into optical water classes. Oceanic waters, where phytoplankton biomass dominates the underwater optical properties with its co-production of dissolved and particulate matter, are classified as Case 1 waters. [27] The apparent and inherent optical properties (sensu Preisendorfer, 1961)[28] of Case 1 waters are often associated to the concentration of chlorophyll a pigment, historically used as a proxy for phytoplankton biomass. Although put into a single class, there is a wide variability in the optical properties of Class 1 waters, in particular in the UVR.

In most coastal and inland water bodies, the inflow of terrestrial matter has significant direct and indirect impacts on the underwater optical field, through the increased absorption due to dissolved organic matter and the increased scattering due to suspended matter. These more optically complex ecosystems are classified as Case 2 waters. As both the inflow rate and in-lake processes (photobleaching, flocculation, and dilution) can change over space and time, variability in the underwater optical field is expected.[29,30,31] These variations can influence phytoplankton community structure and biodiversity,[32] as well as major biogeochemical processes and the radiative balance between absorbed and reflected solar irradiance. [22, 33]

In both Case 1 and Case 2 waters, the concentration of phytoplankton biomass strongly influences optical conditions, directly modulating the underwater light field and indirectly contributing to the optical characteristics of the dissolved and detrital matter present.[34, 35, 36] The resultant spectral characteristics of the underwater light field are strongly influenced by the concentration, ratio and state of photosynthetic pigments present in the phytoplankton community, including chlorophyll-a, chlorophyll-b and c, carotenoids and phycobiliproteins. As a whole, the absorption spectra due to phytoplankton have two peaks of maximum absorption in the blue and red wavelengths,[37, 38, 39, 40, 41] with the former higher than the latter due to the contribution of accessory pigments. The number and wavelength of absorption peaks is sensitive to the concentration and dominant algal group, with two peaks occurring in highly productive waters and a single peak in marine waters with lower biomass.[37,40,41]

While concentrations of phytoplankton play an important role in the spectral conditions of the underwater light field, attenuation in the short visible wavelengths and UVR in Case 2 waters is usually dominated by absorption by chromophoric dissolved organic matter (CDOM). CDOM is an important fraction of the dissolved organic matter in most aquatic ecosystems, representing up to 90% in some natural waters.[42] CDOM is operatively defined as the organic fraction that, after filtration at 0.2 μm, absorbs radiation in the ultraviolet and visible wavelength range.[43, 44, 45] CDOM absorption follows in a near exponential decrease from the UVR to the far visible wavelengths, declining to near zero at 700 nm (Figure 1). This shape has been associated to the charge transfer interactions between donor-acceptors formed by the oxidation of the aromatic polymers present in the natural sample,[43] as well as the superposition of independent chromophores. One of the most useful parameters in the characterization of CDOM absorption curve is based on the change in the slope of the exponential decrease in absorption. The absorption spectral slope (*S*) has most often been determined using a standard equation, $a(\lambda) = a_o e^{S(\lambda_0 - \lambda)}$, where a_o is the absorption coefficient at an initial wavelength λ_0 (eg. 270 nm).[46] Different wavelength intervals have been used to calculate spectral slope[47] (eg. 275-295 nm) which has allowed for some confusion, as the change in slope will vary significantly in different intervals. The distribution of spectral slope has been used to identify wavelength intervals related to specific CDOM origins and loss processes. [29, 48] The absorption spectral slope has been associated with aromaticity and average molecular weight of the CDOM compounds present.[49] Furthermore, the relationship between spectral slope and absorption over time or distance can be used to identify CDOM sources and sinks in estuaries, lakes and reservoirs.[50,51,52]

The influence of CDOM on the underwater light field depends on its optical characteristics, which reflect the temporal and spatial variations in CDOM sources and sinks.[29,53] In most aquatic ecosystems, autochthonous sources (generated from within the waterbody) and allochthonous sources (coming from the surrounding catchment) both contribute to the CDOM pool.[54,55,56] CDOM from terrestrial sources can dominate the optical conditions in lakes receiving waters from extensive wetlands or forested areas.[29] Phytoplankton related CDOM production, mediated by microbial activities, can make a significant contribution in water bodies with elevated primary productivity.[45,57,58] Protein-like CDOM from autochthonous sources (plankton exudates and

detrital material) is reported to be more resistant to photo-induced transformations, while indirect reactions of plankton derived organic matter have been reported where lignin-based CDOM is present.[59] In most lake environments, several sources may be present and the resulting CDOM optical properties will depend upon exposure history, mixing conditions and proximity to major sources or sinks. Another important factor in the optical properties associated to CDOM is the formation of Fe-CDOM complexes in hypoxic and anoxic water, when a buildup of nutrients and organic matter in the sediments and in the water column result in an accumulation of H_2S and Fe^{2+}. When the redox water conditions change, dissolved Fe^{2+} is oxidized to Fe^{3+} which may precipitate out of the water column into the sediment but may also remain in solution, binding to dissolved organic matter. The impact on CDOM absorption can be significant, with a clear increase in all wavelengths typically associated to CDOM.[60,61]

It is well noted that photochemical processes play an important role in altering CDOM optical properties. Changes in CDOM absorption characteristics occur directly from solar exposure and indirectly upon oxidation of the aromatic compounds,[33, 62] which cause losses in humification and aromaticity. In the ultraviolet B wavelengths (UVB, 280–315 nm), absorption losses of CDOM are related to the degradation of the olefinic components.[63] Exposure to UVA (315-400 nm) has been associated to modifications in the CDOM aromatic fraction. [64] Changes in absorption in the visible wavelengths have been associated to a disruption in the intramolecular charge transfer that is associated to the CDOM absorption spectrum.[65]

CDOM may be classified as refractory, semilabile and labile in relation to its availability to microbial consumption. By considering the refractory and semilabile portion of CDOM, Nelson et al. proposed that CDOM optical properties may be used as semi-conservative tracer of water masses. [45] Changes in CDOM absorption follow that of the concentration of dissolved organic carbon (DOC) in many ecosystems.[66,67] However, most inland ecosystems with multiple sources and sinks of organic carbon show significant variability in CDOM/DOC ratios (Figure 2).

Particulates can strongly influence the optical properties of water bodies due to their absorption as well as scattering properties. Particulate matter usually consists of both organic and inorganic fractions, the former including both inanimate organic matter and phytoplankton. The absorption spectra of the total particulate fraction will typically follow an exponential decay from the UV wavelengths with “shoulders” of absorption due to phytoplankton, most notably at 670nm (chlorophyll a). Absorption from the inanimate (organic and inorganic) fraction (tripton) has a similar spectrum as that of CDOM but often with a lower exponential slope (Figure 3). [68,69]

Scattering by particles varies little in the visible wavelengths, with a general increase at lower wavelengths. This is generally the case with phytoplankton related scattering as well.[22] Scattering by phytoplankton will vary depending on the dominant type of phytoplankton present; the composition of its cell walls, average cell size and the presence of gas vacuoles. A chlorophyll specific scattering coefficient is often used in modelling the impact of phytoplankton cells on the underwater light environment.[70, 71] For particulates in general and phytoplankton in particular, scattering increases in a near linear manner with concentration.

Water molecules absorb and scatter incident light. Absorption increases throughout the near infrared wavelengths with five prominent absorption bands at 760 nm (2.6 m^{-1}), 970 nm, 1190 nm, 1450 nm, and 1940 nm.[72] Studies of the absorption of pure water in the UVR shows a range of values, most showing an increase in absorption from 400 nm (~0.01 m^{-1}) to 300 nm (~0.1 m^{-1}) .[73] Scattering by water is largely elastic scattering (density fluctuation) and is highly wavelength dependent, with elevated scattering in the lower visible wavelengths and UVR; one has b=0.058 m^{-1} at 400nm and 0.1 m^{-1} at 350 nm. Raman (inelastic) scattering by water molecules plays a smaller role in modifying the underwater light field, but can have a significant influence on the remote estimation of optical properties. Inelastic scattering occurs when the photons interact with the water molecule, through the vibrational (O-H) energy transition. The scattered photons are red-shifted about 100 nm of the excitation wavelength. Raman scattering of water is highly wavelength dependent (λ^{-5}), with the highest scattering at the lowest wavelengths.[74]

Section 3. Measurement of underwater light field and Inherent Optical Properties

The measurement of the underwater light field is essential to understanding the dynamics of primary production, photodegradation of organic matter as well as photoinhibition of aquatic fauna and flora. Approaches to estimate the optical properties of marine and inland waters have been used since the early days of aquatic science and are now greatly facilitated by the availability of low cost underwater radiometers. The absorption and scattering properties of the medium (inherent optical properties) provide likewise fundamental information on the optical components that determine the characteristics of the underwater light field. Other properties such as remote sensing reflectance and upwelling radiance (apparent optical properties) can also provide fundamental optical information over large geographic areas, but remain sensitive to external environmental conditions such as sun location.

One of the oldest and most common measurement of the light environment is Secchi depth, measured using a Secchi disk or tube. Secchi depth has been shown to be inversely proportional to the sum of the beam attenuation coefficients (c = a + b, where a is the absorption and b is the scattering) and is most commonly used to estimate the diffuse attenuation coefficient ($K_{d\lambda}$),[22] when no irradiance meter is available.

The downward radiant flux per unit area in a single wavelength or larger waveband can be measured by means of a submersible radiometer. These collect all the photons that reach its collector, usually in a proportional manner to the cosine of the angle between the normal to the collector surface and the direction of the incident flux. Cosine collectors are usually located slightly above the radiometer casing and are calibrated in water to avoid the “immersion effect” related to the differences in the refraction index of air and water.[22] Below the sensor are photodetectors and a photomultiplier which produce a signal related to the incident irradiance. Synchronous measurements of irradiance and depth allow for the determination of a downward irradiance profile, which is used to measure the downward diffuse attenuation coefficient $K_{d\lambda}$. $K_{d\lambda}$ quantifies the rate of change of solar irradiance in a specific wavelength or waveband with increasing depth in the euphotic zone. It is defined as the exponential decrease with depth of the ambient downwelling irradiance $E_{d\lambda}$ (W m^{-2} nm^{-1}), which comprises all photons moving in a

downward direction (> 90° with respect to the vertical):

$$P_{d\lambda}(1\%\,;10\%) = E_{d\lambda}(z) = E_{o\lambda}\ e^{-K_{d\lambda}\,z} \quad (W\,m^{-2}\,nm^{-1})$$

where $K_{d,\lambda}$ is the diffuse attenuation coefficient (m^{-1}) at wavelength λ (nm), $E_{d\lambda}$ is the downward irradiance measured at depth z (m) in a homogeneous water column, while $E_{o\lambda}$ is the downward irradiance just below the water surface.[38] It should be noted that the estimation of $K_{d,\lambda}$ is sensitive to the method used to fit the profile of decreasing irradiance with depth.[75]

Measurements of $K_{d,\lambda}$ assume that the optical conditions to the depth z are consistent, which may often not be the case. Stratification may occur in relation to changes of density over depth (e.g. thermal stratification) or as the result of biological (e.g. chlorophyll maximum) or optical (epilimnal CDOM photodegradation) factors. The penetration depth $P_{d\lambda}$ for 1% (or 10%) of the sub-surface solar irradiance is determined using $K_{d\lambda}$ as:

$$P_{d\lambda}(1\%\,;10\%) = -\frac{1}{K_{d\lambda}} \cdot \ln\,(0.01\,;0.1)$$

Considerable research has been done to estimate $K_{d\lambda}$ for various types of water bodies using remote sensors. Remote sensing methods to estimate $K_{d\lambda}$, using empirical and semi-analytical approaches have proven very successful in Case 1 waters, but less successful in more optically complex waters. Standard $K_{d,490}$ algorithms are now available on most optical ocean colour systems (e.g. MODIS). Remote sensed spectral attenuation has been used successfully to identify the temporal and spatial variations of the biogeochemical processes in the world's oceans and lakes. By understanding the distribution of $K_{d\lambda}$, it is possible to estimate solar irradiance at different depths, thereby providing fundamental information for photo-limited processes such as lake productivity and photodegradation.

In addition to downwelling irradiance, upwelling irradiance also plays an important role in primary productivity and radiative transfer, as well as determining the appearance of the water body. In situ measurement of the upwelling irradiance can be made using a radiometer directed downward below the water surface. The upwelling irradiance is the sum of upward traveling photons (< 90^o with respect to the downward vertical direction). Typically, upwelling irradiance diminishes with depth in a similar manner to downwelling irradiance in a homogeneous medium (without optical stratification), following an exponential decay,

$$E_{u\lambda(z)} = E_{u\lambda(z=0)}\ e^{-K_{u\lambda}(z)} \quad (W\,m^{-2}\,nm^{-1}) \qquad (1)$$

where $E_{u\lambda(z)}$ is the upward spectral irradiance at depth z, $K_{u\lambda(z)}$ (m^{-1}) is the coefficient of exponential decay with depth and $E_{u\lambda(z=0)}$ is the upwelling irradiance just below the surface. The maximum depth of the water column that influences the water leaving radiance can be defined as the "effective upwelling depth",[75] below which the optical properties of the water body no longer influence the water leaving radiance. If, at a specific wavelength, the effective depth is greater than the lake depth, the upwelling irradiance will be influenced by the spectral reflectance properties of the lake bottom, mediated by the optical properties of the intervening water layers.

Upwelling irradiance plays a key role in primary productivity and radiative transfer, as well as determining the appearance of the water body. As the upwelling irradiance is influenced by the angular distribution of the downwelling radiance and the optical properties of the water body, it serves as the basis of remotely made observations of water quality in lakes, estuaries and the ocean.
Radiative-transfer models (e.g. Hydrolight) and semi-analytical models separate bottom and water column reflectance by using a typical particle phase function for specific water classes. If the water body is stratified and the effective depth is greater than the depth of the surface layer, upwelling irradiance will contain a depth-weighted exponential mean of the optical properties of the layers present.

Scalar irradiance is defined as the integral of radiance distribution at a point over all directions about the point. It is equivalent to the total radiant flux per m^2 from all directions at a given point in the medium.[22] The measurement of scalar irradiance is similar to that of irradiance with a spherical collector. Meters with all three collectors, downward, upward and spherical are now commonly used. The determination of the angular distribution of radiant flux, using for example a tube photometer containing a cylindrical tube to limit the acceptance angle, provide a more complete description of the radiance distribution.

Inherent Optical Properties (IOPs) are related to the optical properties and concentration of the particulate and dissolved substances present. They directly control the absorption and scattering properties of the water column but are not sensitive to changes in radiance distribution. Generally, the estimate of phytoplankton biomass, CDOM and particulate matter is made by sampling, storage in appropriate conditions and laboratory measurements. In situ measurements provide the most accurate method of estimation. However, they are limited to the temporal and spatial constraints of a field campaign.

The in situ concentrations of photosynthetic pigments and their degradation products are estimated using extraction in an organic solvent and quantification of one or more specific photosynthetic pigments by spectrophotometry, fluorometry or chromatography.[76] In situ estimates by fluorescence have also been used successfully to measure spatial (horizontal and vertical) and temporal changes in phytoplankton biomass, at a high resolution.[77,78] They include light emitting diodes for the excitation of specific pigments with sensors to measure the response in fluorescence, for example of chlorophyll a (excitation 440 nm, emission 680 nm) or phycocyanin of cyanobacteria (excitation 620 nm, emission 645 nm).

In recent decades the use of satellite based optical sensors has opened up new opportunities for extensive measurements of IOPs, with initial emphasis on phytoplankton biomass and their related pigments. Models were proposed to estimate the concentration of chlorophyll a based on absorption characteristics,[79, 80,81] and regression analysis using in situ data.[37, 41, 82] However, the absorption of phytoplankton is a combination of chlorophyll a as well as other accessory pigments. For this reason, the ratio of total absorption coefficient of phytoplankton and chlorophyll-a concentration is often used ($a^*_{ph}(\lambda)$):

$$a^*_{ph}(\lambda) = \frac{a_{ph}(\lambda)}{C_{CHL}}$$

The absorption efficiency of phytoplankton chloroplasts will decrease with higher algal density. This "package effect" is a main source of spectral absorption variability.[83] Pigment concentrations determine the absorption spectral shape, but the package effect can significantly influence on the absorption efficiency.[40] Several methods have been utilised to estimate Chla from remotely sensed data of reflected radiance; near-infrared/red band ratio empirical methods [84, 85], semi-analytical methods [84] and three-band empirical methods.[81, 86] Phycocyanin is a unique pigment in cyanobacteria, and thus provides a more useful indicator of cyanobacterial biomass [87, 88] and its measurement has often been based on the 620-nm absorption.[87-92]

The remote estimation of phytoplankton related absorption and scattering is hindered by the presence of detritus and cell constituents other than pigments. Band ratios are often used to remove the effects of absorption by other optically active components present.[38] One major drawback to remote estimation of phytoplankton is that direct measurements are limited to the upper layers of the water column. Thus indirect or secondary approaches are necessary to estimate a full profile of phytoplankton biomass and pigment compositions. However, remote sensing allows for regular and extensive estimates where in-situ measurements are insufficient to capture the spatial and temporal variability of this important optical component.[93]

The in situ measurement of the non-living particulate fraction, both organic and inorganic is usually carried out by sampling, filtering and quantification using gravimetric or combustion with infrared gas analysis. Remote measurements of the particulate fraction offer numerous advantages at the cost of a lower accuracy. In comparison to phytoplankton pigments, the estimate of the different particulate fractions, living and non-living, organic and inorganic presents a larger challenge, as their optical properties can vary significantly in relation to their sources and sinks. The particulate organic carbon (POC) pool, in particular, contains a wide variety of optically distinct components, from bacteria to macrophyte detritus.[94] In the first published algorithm for estimating POC from remote sensing, a two-step process was based on the dependence of the backscattering coefficient (b_{bp}) by particles suspended in seawater and the dependence of the spectral remote-sensing reflectance ($R_{rs}(\lambda)$) on b_{bp}.[95] More recently, reflectance ratios and multiple-spectral approaches (e.g. Normalized Difference Carbon Index) were used to estimate POC distribution in the open ocean by relying on the dominance of phytoplankton biomass in the total POC concentration. There are clear difficulties in applying this to turbid inland waters, where inorganic particles play a more important role in the optical backscattering properties of the water body. [96, 97] Duan et al. developed a power regression model of the direct empirical relationship between POC and atmospherically Rayleigh-corrected MODIS data for inland turbid waters.[52] Such approaches indicate that remote sensing of different particulate fractions, their concentrations and optical properties is feasible.

CDOM is typically measured using spectrophometric measurements of filtered water samples. The significant spatial variability of CDOM can be captured using an extensive sampling network. High frequency studies of CDOM variability are more rare. Hourly changes in CDOM in streams and rivers due to variability in runoff, autochthonous production, photobleaching and

interactions with sediment detritus are not uncommon.[98,99] Recently, deployable spectrophotometric probes have been used to acquire high frequency measurements.[100]

The remote estimation of CDOM and DOC presents an opportunity to examine spatial and temporal changes in this important optical and biological component (Figure 4). Spectral band ratios, linear band combinations and semi-analytical algorithms have been used to estimate CDOM dynamics using the remote sensing reflectance data.[101,102,103] While most of these are limited ecosystems where a single CDOM source undergoes dilution and conservative mixing, recent developments indicate that regional wide algorithms can also be used to examine CDOM in different inland water bodies (Figure 4).[104]

Conclusion

The spectral distribution of the underwater solar radiation field is both a function of as well as a driver of the biological, chemical and physical conditions at any particular depth. While the dissolved and suspended organic matter modify the penetration depth of UV radiation and visible solar radiation, their exposure to solar radiation modifies their optical and biological characteristics.[29] In lakes, rivers and wetland ecosystems, where the CDOM and POM levels can be elevated, the penetration of UV may only be few centimetres and products of photodegradation can strongly influence biological cycles.[51,105] Low molecular weight photoproducts of degraded CDOM are more edible to bacterial communities while solar UV radiation may increase the toxicity of natural and anthropogenic organic compounds leading to negative effects on biota .[106,107] The spectral distribution of light within the mixed portion of the water will modify the ability of phytoplankton to conduct photosynthesis. Phytoplankton, the first level of the aquatic food web, utilise various mechanisms of orientation and vertical migration to optimize their exposure to solar radiation.[108,109] While solar radiation provides the energetic basis for photosynthesis, high doses of UV radiation may cause chlorophyll photobleaching, modification of the DNA structure, cellular damages, inhibition of motility and orientation, as well as photoinhibition. [110,111,112,113]

Variations in the spectral intensity of solar radiation in the water column, in particular UVR, modify the aquatic cycles of carbon, nitrogen, sulphur, and metals.[114] Changes in the concentrations and optical characteristics of components of the water column (and atmosphere) will influence basic biogeochemical cycles of aquatic ecosystems. Long term monitoring and improved understanding of these transformations is fundamental to understanding the fate of organic matter in these ecosystems.

REFERENCES

1. R. B. Lee, M. A. Gibson, R. S. Wilson and S. Thomas, *J. Geophys. Res.: Space Phys.*, 1995, **100**, 1667-1675.
2. F. E. Lumb, *Q. J. R. Meteorol. Soc.*, 1964, **90**, 43-56.
3. M. A. Atwater and P. S. Brown, *J. Appl. Meteorol.* , 1974, **13**, 289-297.
4. J. A. Davies, W. Schertzer and M. Nunez, *Boundary Layer Meteorol.* , 1975, **9**, 33-52.
5. R. Frouin, D. W. Lingner, C. Gautier, K. S. Baker and R. C. Smith, *J. Geophys. Res.: Oceans*, 1989, **94**, 9731-9742.
6. G. Dedieu, P. Y. Deschamps and Y. H. Kerr, *J. Clim. Appl. Meteorol.*, 1987, **26**, 79-87.
7. M. A. Atwater and J. T. Ball, *Mon. Weather Rev.*, 1981, **109**, 878-888.
8. C. Gautier, G. Diak and S. Masse, *J. Appl. Meteorol.* , 1980, **19**, 1005-1012.
9. J. A. Ruiz-Arias, T. Cebecauer, J. Tovar-Pescador and M. Šúri, *Sol. Energy* 2010, **84**, 1644-1657.
10. C. Ertekin and O. Yaldiz, *Energy Convers. Manage.* , 2000, **41**, 311-330.
11. H. Duzen and H. Aydin, *Energy Convers. Manage.* , 2012, **58**, 35-46.
12. I. Korachagaon and V. N. Bapat, *J. Renewable Energy*, 2012, **41**, 394-400.
13. Q. Dai and X. Fang, *Adv. Space Res.* , 2014, **53**, 1239-1245.
14. M. Blumthaler, W. Ambach and R. Ellinger, *J. Photochem. Photobiol., B*, 1997, **39**, 130-134.
15. A. Y. Dvorkin and E. H. Steinberger, *Sol. Energy* 1999, **65**, 181-187.
16. Z. Jin, T. P. Charlock, K. Rutledge, K. Stamnes and Y. Wang, *Appl. Opt.* , 2006, **45**, 7443-7455.
17. M. Daimon and A. Masumura, *Appl. Opt.* , 2007, **46**, 3811-3820.
18. R. Frouin, M. Schwindling and P.-Y. Deschamps, *J. Geophys. Res.: Oceans*, 1996, **101**, 14361-14371.
19. Z. Jin, Y. Qiao, Y. Wang, Y. Fang and W. Yi, *Opt. Express* 2011, **19**, 26429-26443.
20. H. Buitevel, J. H. M. Hakvoort and M. Donze, *Proc. SPIE.*, 1994, **2258**, 174-183.
21. A. Morel, H. Claustre, D. Antoine and B. Gentili, *Biogeosciences*, 2007.
22. J. T. Kirk, *Light and photosynthesis in aquatic ecosystems*, 2nd Edition edn., Cambridge University Press, New York, 1994.
23. R. W. Sternberg, E. T. Baker, D. A. McManus, S. Smith and D. R. Morrison, *Deep-Sea Res. Oceanogr. Abstr.*, 1974, **21**, 887-892.
24. D. Blondeau-Patissier, V. E. Brando, K. Oubelkheir, A. G. Dekker, L. A. Clementson and P. Daniel, *J. Geophys. Res.: Oceans*, 2009, **114**, C05003.
25. Y. Huot, A. Morel, M. Twardowski, D. Stramski and R. Reynolds, *Biogeosciences*, 2008, **5**, 495-507.
26. V. Martinez-Vicente, P. E. Land, G. H. Tilstone, C. Widdicombe and J. R. Fishwick, *J. Plankton Res.*, 2010, **32**, 603-619.
27. A. Morel and L. Prieur, *Limnol. Oceanogr.*, 1977, **22**, 709-722.
28. R. W. Preisendorfer, *Application of radiative transfer theory to light measurements in the sea*, Institut géographique national, 1961.
29. S. A. Loiselle, L. Bracchini, A. Cózar, A. M. Dattilo, A. Tognazzi and C. Rossi, *J. Photochem. Photobiol., B*, 2009, **95**, 129-137.
30. D. W. Schindler, S. E. Bayley, B. R. Parker, K. G. Beaty, D. R. Cruikshank, E. J. Fee, E. U. Schindler and M. P. Stainton, *Limnol. Oceanogr.*, 1996, **41**, 1004-1017.
31. E. von Wachenfeldt and L. Tranvik, *Ecosystems*, 2008, **11**, 803-814.

32. M. Stomp, J. Huisman, L. J. Stal and H. C. Matthijs, *The ISME journal*, 2007, **1**, 271-282.
33. S. Loiselle, D. Vione, C. Minero, V. Maurino, A. Tognazzi, A. M. Dattilo, C. Rossi and L. Bracchini, *Water Res.* , 2012, **46**, 3197-3207.
34. H. R. Gordon, O. B. Brown, R. H. Evans, J. W. Brown, R. C. Smith, K. S. Baker and D. K. Clark, *J. Geophys. Res. : Atmos.*, 1988, **93**, 10909-10924.
35. A. Morel, *J. Geophys. Res.: Oceans*, 1988, **93**, 10749-10768.
36. T. Platt and S. Sathyendranath, *Science*, 1988, **241**, 1613-1620.
37. R. Ma, J. Tang, J. Dai, Y. Zhang and Q. Song, *Int. J. Remote Sens.* , 2006, **27**, 4277-4304.
38. C. D. Mobley and C. D. Mobley, *Light and water: Radiative transfer in natural waters*, Academic Press San Diego, 1994.
39. G. Pérez, C. Queimaliños, E. Balseiro and B. Modenutti, *Limnologica*, 2007, **37**, 3-16.
40. K. Suzuki, M. Kishino, K. Sasaoka, S.-I. Saitoh and T. Saino, *J. Oceanogr.* , 1998, **54**, 517-526.
41. G. Wu, L. Cui, H. Duan, T. Fei and Y. Liu, *Appl. Opt.* , 2011, **50**, 6358-6368.
42. E. M. Thurman, *Organic geochemistry of natural waters*, Springer, 1985.
43. R. Del Vecchio and N. V. Blough, *Mar. Chem.* , 2004, **89**, 169-187.
44. D. Siegel, S. Maritorena, N. Nelson, D. Hansell and M. Lorenzi‐Kayser, *J. Geophys. Res.: Oceans*, 2002, **107**, 21-21-21-14.
45. N. B. Nelson, D. A. Siegel, C. A. Carlson, C. Swan, W. M. Smethie Jr and S. Khatiwala, *Deep Sea Res. Part I* 2007, **54**, 710-731.
46. A. Bricaud, A. Morel and L. Prieur, *Limnol. Oceanogr*, 1981, **26**, 43-53.
47. J. R. Helms, A. Stubbins, J. D. Ritchie, E. C. Minor, D. J. Kieber and K. Mopper, *Limnol. Oceanogr.*, 2008, **53**, 955.
48. J. R. Helms, A. Stubbins, E. M. Perdue, N. W. Green, H. Chen and K. Mopper, *Mar. Chem.* , 2013, **155**, 81-91.
49. N. Blough and S. Green, *The Role of Non-living Organic Matter in the Earth's Carbon Cycle (RG Zepp and C. Sonntag, eds.)*, 1995, 23-45.
50. C. A. Stedmon, S. Markager and H. Kaas, *Estuarine Coastal Shelf Sci.* , 2000, **51**, 267-278.
51. L. Bracchini, S. Loiselle, A. M. Dattilo, S. Mazzuoli, A. Cózar and C. Rossi, *Photochem. Photobiol.* , 2004, **80**, 139-149.
52. H. Duan, R. Ma, S. A. Loiselle, Q. Shen, H. Yin and Y. Zhang, *Sci. Total Environ.* , 2014, **482–483**, 174-183.
53. McKnight, E. D. Andrews, S. S.A. and G. R. Aiken, *Limnol. Oceanogr*, 1994, **39**, 1972-1979.
54. N. B. Nelson, C. A. Carlson and D. K. Steinberg, *Mar. Chem.* , 2004, **89**, 273-287.
55. A. Vodacek, N. V. Blough, M. D. DeGrandpre, E. T. Peltzer and R. K. Nelson, *Limnol. Oceanogr.*, 1997, **42**, 674-686.
56. L. Bracchini, A. M. Dattilo, V. Hull, S. A. Loiselle, L. Nannicini, M. P. Picchi, M. Ricci, C. Santinelli, A. Seritti and A. Tognazzi, *Photochem. Photobiol. Sci.*, 2010, **9**, 304-314.
57. K. L. Carder, R. G. Steward, G. R. Harvey and P. B. Ortner, *Limnol. Oceanogr.*, 1989, **34**, 68-81.
58. E. Rochelle-Newall and T. Fisher, *Mar. Chem.* , 2002, **77**, 23-41.
59. L. Tranvik and S. Kokalj, *Aquat. Microb. Ecol.*, 1998, **14**, 301-307.
60. E. S. Kritzberg and S. M. Ekström, *Biogeosciences*, 2012, **9**, 1465-1478.
61. G. A. Weyhenmeyer, Y. T. Prairie and L. J. Tranvik, *PloS one*, 2014, **9**, e88104.
62. I. Reche, M. L. Pace and J. J. Cole, *Ecosystems*, 2000, **3**, 419-432.
63. S. A. Loiselle, L. Bracchini, A. M. Dattilo, M. Ricci, A. Tognazzi, A. Cózar and C. Rossi, *Limnol.*

Oceanogr., 2009, **54**, 590.
64. N. Corin, P. Backlund and M. Kulovaara, *Chemosphere*, 1996, **33**, 245-255.
65. C. L. Osburn, L. Retamal and W. F. Vincent, *Mar. Chem.* , 2009, **115**, 10-20.
66. M. Meili, in *Dissolved Organic Matter in Lacustrine Ecosystems*, eds. K. Salonen, T. Kairesalo and R. I. Jones, Springer Netherlands, 1992, vol. 73, pp. 23-41.
67. S. A. Green and N. V. Blough, *Limnol. Oceanogr.*, 1994, **39**, 1903-1916.
68. M. Babin, D. Stramski, G. M. Ferrari, H. Claustre, A. Bricaud, G. Obolensky and N. Hoepffner, *J. Geophys. Res.: Oceans*, 2003, **108**, 3211.
69. C. E. Binding, J. H. Jerome, R. P. Bukata and W. G. Booty, *Remote Sens. Environ.*, 2008, **112**, 1702-1711.
70. A. Ferreira, D. Stramski, C. A. E. Garcia, V. M. T. Garcia, Á. M. Ciotti and C. R. B. Mendes, *J. Geophys. Res.: Oceans*, 2013, **118**, 698-714.
71. F. M. Morel, *J. Phycol.*, 1987, **23**, 137-150.
72. J. A. Curcio and C. C. Petty, *JOSA*, 1951, **41**, 302-302.
73. E. S. Fry, *Appl. Opt.* , 2000, **39**, 2743-2744.
74. J. S. Bartlett, K. J. Voss, S. Sathyendranath and A. Vodacek, *Appl. Opt.* , 1998, **37**, 3324-3332.
75. R. Ma, G. Jiang, H. Duan, L. Bracchini and S. Loiselle, *Opt. Express* 2011, **19**, 7127-7138.
76. T. R. Jacobsen, *Mar. Sci. Commun.*, 1978, **4**, 33-47.
77. M. Beutler, K. H. Wiltshire, B. Meyer, C. Moldaenke, C. Lüring, M. Meyerhöfer, U. P. Hansen and H. Dau, *Photosynth. Res.* , 2002, **72**, 39-53.
78. C. Leboulanger, U. Dorigo, S. Jacquet, B. Le Berre, G. Paolini and J.-F. Humbert, *Aquat. Microb. Ecol.*, 2002, **30**, 83-89.
79. H. Duan, R. Ma and C. Hu, *Remote Sens. Environ.*, 2012, **126**, 126-135.
80. H. Duan, R. Ma, Y. Zhang and B. Zhang, *Limnology*, 2009, **10**, 135-141.
81. A. A. Gitelson, G. Dall'Olmo, W. Moses, D. C. Rundquist, T. Barrow, T. R. Fisher, D. Gurlin and J. Holz, *Remote Sens Environ*, 2008, **112**, 3582-3593.
82. V. Stuart, S. Sathyendranath, T. Platt, H. Maass and B. D. Irwin, *J. Plankton Res.*, 1998, **20**, 187-217.
83. A. Bricaud, H. Claustre, J. Ras and K. Oubelkheir, *J. Geophys. Res.: Oceans*, 2004, **109**, C11010.
84. H. J. Gons, *Environ Sci Technol*, 1999, **33**, 1127-1132.
85. S. G. H. Simis, A. Ruiz-Verdu, J. A. Dominguez-Gomez, R. Pena-Martinez, S. W. M. Peters and H. J. Gons, *Remote Sens Environ*, 2007, **106**, 414-427.
86. G. Dall'Olmo, A. A. Gitelson and D. C. Rundquist, *Geophys Res Lett*, 2003, **30**, 1938.
87. A. Ruiz-Verdu, S. G. H. Simis, C. de Hoyos, H. J. Gons and R. Pena-Martinez, *Remote Sens Environ*, 2008, **112**, 3996-4008.
88. S. G. H. Simis, S. W. M. Peters and H. J. Gons, *Limnol Oceanogr*, 2005, **50**, 237-245.
89. K. Randolph, J. Wilson, L. Tedesco, L. Li, D. L. Pascual and E. Soyeux, *Remote Sens Environ*, 2008, **112**, 4009-4019.
90. P. D. Hunter, A. N. Tyler, L. Carvalho, G. A. Codd and S. C. Maberly, *Remote Sens Environ*, 2010, **114**, 2705-2718.
91. A. G. Dekker, T. J. Malthus and E. Seyhan, *Ieee T Geosci Remote*, 1991, **29**, 89-95.
92. J. F. Schalles and Y. Z. Yacobi, *Ergebnisse der Limnologie*, 2000, **55**, 153-168.
93. H. Duan, R. Ma, J. Xu, Y. Zhang and B. Zhang, *Environ. Monit. Assess.* , 2010, **170**, 231-244.
94. A. Morel and Y.-H. Ahn, *J Mar Res*, 1990, **48**, 145-175.

95. D. Stramski, R. A. Reynolds, M. Kahru and B. G. Mitchell, *Science*, 1999, **285**, 239-242.
96. M. Tzortziou, A. Subramaniam, J. R. Herman, C. L. Gallegos, P. J. Neale and L. W. Harding, *Estuar Coast Shelf S*, 2007, **72**, 16-32.
97. R. H. Ma, D. L. Pan, H. T. Duan and Q. J. Song, *Int J Remote Sens*, 2009, **30**, 2321-2335.
98. L. Galgani, A. Tognazzi, C. Rossi, M. Ricci, J. Angel Galvez, A. M. Dattilo, A. Cozar, L. Bracchini and S. A. Loiselle, *J.Photochem. Photobiol., B*, 2011, **102**, 132-139.
99. J. A. Downing, J. J. Cole, J. J. Middelburg, R. G. Striegl, C. M. Duarte, P. Kortelainen, Y. T. Prairie and K. A. Laube, *Global Biogeochem. Cycles* 2008, **22**, GB1018.
100. R. A. Müller, D. N. Kothawala, E. Podgrajsek, E. Sahlée, B. Koehler, L. J. Tranvik and G. A. Weyhenmeyer, *Journal of Geophysical Research: Biogeosciences*, 2014, 2014JG002719.
101. T. Kutser, A. Herlevi, K. Kallio and H. Arst, *Sci. Total Environ.* , 2001, **268**, 47-58.
102. S. Maritorena, D. A. Siegel and A. R. Peterson, *Appl. Opt.* , 2002, **41**, 2705-2714.
103. E. Boss, R. Collier, W. S. Pegau, G. Larson and K. Fennel, in *Long-term Limnological Research and Monitoring at Crater Lake, Oregon*, eds. G. L. Larson, R. Collier and M. W. Buktenica, Springer Netherlands, 2007, vol. 191, pp. 149-159.
104. G. Jiang, R. Ma, S. A. Loiselle and H. Duan, *Environ. Res. Lett.* , 2012, **7**, 034014.
105. P. S. Huovinen, H. Penttilä and M. R. Soimasuo, *Chemosphere*, 2003, **51**, 205-214.
106. O. C. Zafiriou, *Limnol. Oceanogr. Bull*, 2002, **11**, 69-71.
107. S. A. Diamond, in *UV Effects in Aquatic Organisms and Ecosystems*, eds. E. W. Helbling and H. Zagarese, The Royal Society of Chemistry, Cambridge, UK, 2003, pp. 219-250.
108. D.-P. Häder, E. Rhiel and W. Wehrmeyer, *J. Photochem. Photobiol., B*, 1987, **1**, 115-122.
109. D.-P. Häder, in *Biophysics of Photoreceptors and Photomovements in Microorganisms*, eds. F. Lenci, F. Ghetti, G. Colombetti, D. P. Häder and P.-S. Song, Springer US, 1991, vol. 211, pp. 157-172.
110. D. M. Leech and S. Johnsen, in *UV effects in aquatic organisms and ecosystem*, eds. E. W. Helbling and H. Zagarese, The Royal Society of Chemistry, Cambridge, UK, 2003, pp. 455-481.
111. A. Dattilo, L. Bracchini, L. Carlini, S. Loiselle and C. Rossi, *Int. J. Biometeorol.* , 2005, **49**, 388-395.
112. R. C. Smith and K. S. Baker, *Photochem. Photobiol.* , 1979, **29**, 311-323.
113. P. J. Neale, *J.Photochem. Photobiol., B*, 2001, **62**, 1-8.
114. R. G. Zepp, T. V. Callaghan and D. J. Erickson Iii, *Photochem. Photobiol. Sci.*, 2003, **2**, 51-61.

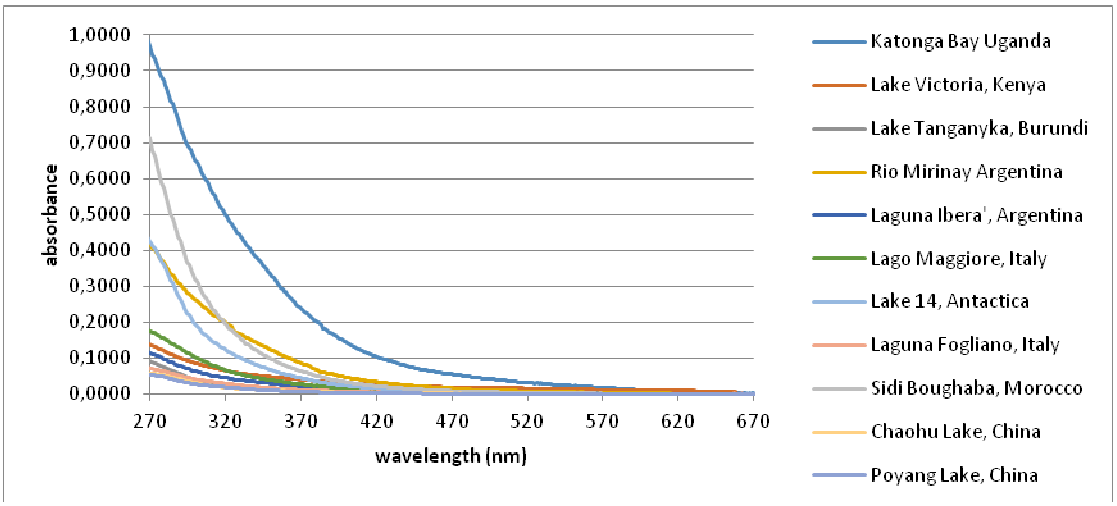

Figure 1. CDOM absorbance follows a near exponential decay with increasing wavelengths. Samples from freshwater lakes across different bio-regions.

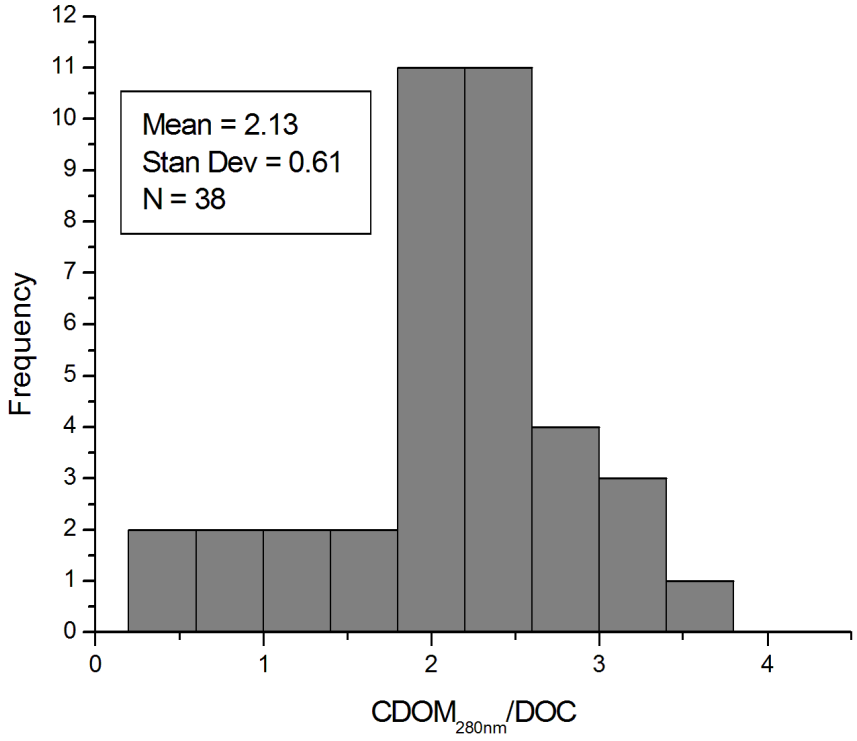

Figure 2. CDOM/DOC ratios from 38 lakes in southeast China sampled in April 2012. CDOM absorption measured at 280 nm.

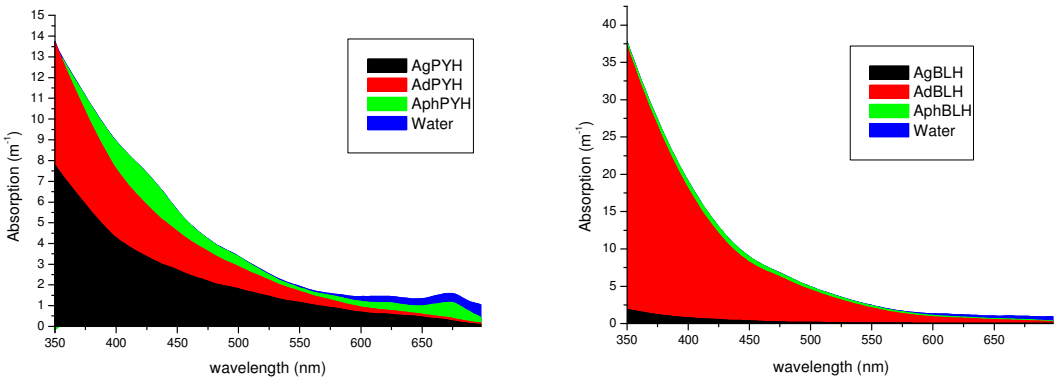

Figure 3. Total absorption with relative contributions from CDOM (a_g), nonliving particulate matter (a_p), phytoplankton (a_{ph}) and water in two Chinese lakes, Lake Poyang (PYH) and Lake Bali (BLH).

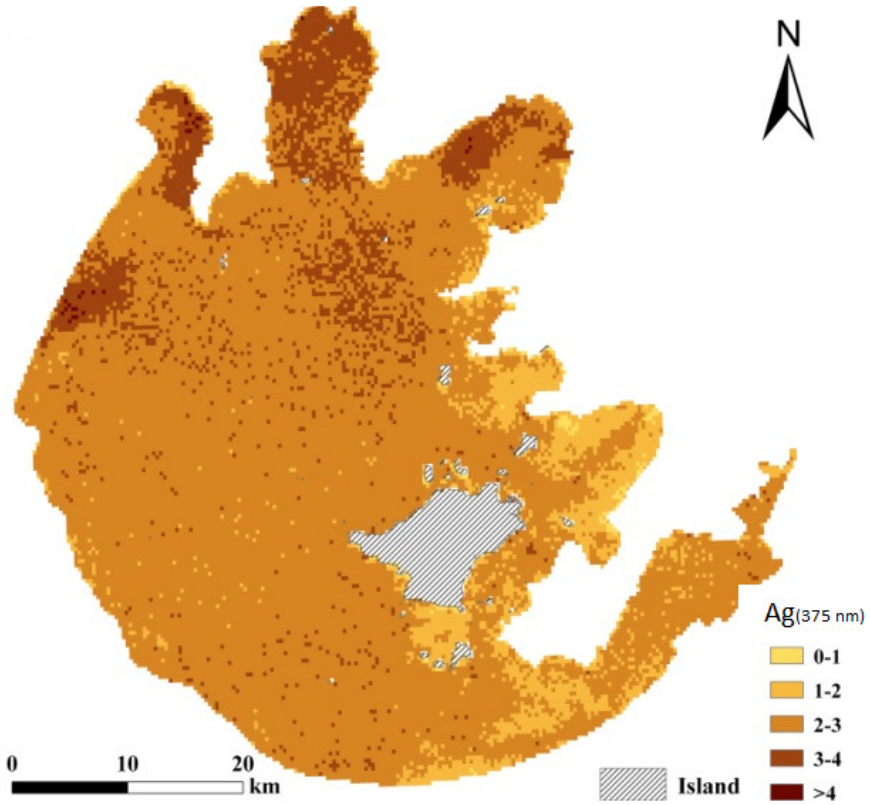

Figure 4. CDOM absorption $A_{g375\ nm}$ in Lake Taihu Lake in for March 2004 using a linear regression model.

Chapter 4: Direct photolysis processes

Claire Richard[1,2*], Norbert Hoffmann[3]

[1] Clermont Université, Institut de Chimie de Clermont-Ferrand, BP 10448, 63000 Clermont-Ferrand, France.

[2] Equipe Photochimie CNRS, UMR 6296, ICCF, 63171 Aubière, France.

[3] Institut de Chimie Moléculaire de Reims, UMR CNRS 7312, BP 1039, 51687 Reims, Cedex 2, France

*Corresponding author :

Claire.richard@univ-bpclermont.fr

Tel : +33 (0)4 73 40 71 42

Fax : +33 (0)4 73 40 77 00

Chapter 4. Abstract

Solar light is able to photoinduce the phototransformation of a lot of pesticides. In this chapter we describe some of the most important photochemical processes leading to the chemical transformation of pesticides, in particular photodehalogenation, photoisomerization, photo-fries and photo-claisen. In each case, theoretical considerations are given and illustrated by examples taken from the literature. This chapter provides useful data for the understanding of the photoreactivity of a wide range of molecules of environmental concern.

Table of contents

4.1 Introduction

Pesticides are intensively used to improve crop yields and meet the challenge of feeding an ever-increasing population. Yet, pesticides are biologically active molecules that may have a

toxic effect on non-target organisms, in particular human beings and fauna. Once they have been released to the environment pesticides can undergo transformation through biotic and abiotic processes leading to degradation products that may happen to be also toxic. This is therefore of importance to get insight into these reactions to evaluate the risk that may cause pesticides use. Solar light can induce chemical transformation of pesticides provided that these latter absorb radiations wavelength of which is longer than 290-295 nm. These photochemical reactions can take place in all the environmental compartments, surface waters, surface of leaves, surface of soils, atmosphere and whatever the state of the molecule, solid or dissolved.

When compared to chemical transformation at the ground state, photochemical reactions are characterized by electronic excitation and thus by the change of electronic configuration.[1-3] As the chemical reactivity of a molecule is determined by the electronic configuration, ground state reactions significantly differ from photochemical reactions. Most frequently, pesticides as many other organic compounds are synthesized using ground state reactions. They are stable under usual conditions but not necessarily when electronically excited. Since nowadays molecular structures in pesticides become more and more complex, the problem of photostability becomes more and more urgent. Complex molecules possess an increased number of photochemical degradation pathways. In principle, the ground electronic state of any compound can give rise to a number of different excited electronic states, singlet or triplet, each with its own electronic distribution and its own reactivity (Scheme 1). Since excited electronic states have a higher internal energy than ground states, many processes are possible.

[Scheme 1]

The photochemical transformation of pesticides has been intensively studied for decades and a lot of data can be found in the literature concerning the rates of pesticides photolysis and the nature of their photoproducts. The objective of this review is not to make an inventory of existing data, but to detail the mechanism of some types of reaction, in particular, photodehalogenation, photoisomerization, photo-fries, photo-claisen, that are observed for a lot of pesticides.

4.2 Photodehalogenation

Many pesticides are arylhalides or contain such moieties. Dehalogenation in these compounds is one of the most important photodecomposition modes. The arene halogen bond fragmentation may be induced mainly by four processes.[4,5] A homolytic cleavage leading to two radicals may occur (equation 1). A heterolytic cleavage of the arene halogen bond generally leads to the formation of the aryl cation and the release of the halide (equation 2).[6] Photochemical electron transfer form an external electron donor to the electronically excited aryl halide induces the release of the halide and the formation of an aryl radical (equation 3).[7,8] Less frequently, a direct nucleophilic substitution at an electronically excited aryl halide is observed (equation 4).

$Ar\text{-}X^* \rightarrow Ar^{\bullet} + X^{\bullet}$ (equation 1)

$Ar\text{-}X^* \rightarrow Ar^{+} + X^{-}$ (equation 2)

$Ar\text{-}X^* + \text{electron donor} \rightarrow (Ar\text{-}X)^{\bullet -} \rightarrow Ar^{\bullet} + X^{-}$ (equation 3)

$Ar\text{-}X^* + Nu^{-} \rightarrow Ar\text{-}Nu + X^{-}$ (equation 4)

In the context of photochemical degradation of pesticides, the resulting intermediates react either by addition of OH^- to give Ar-OH in the presence of water or by reduction to give Ar-H in the presence of a suitable hydrogen donor. The addition of water to a phenyl radical leading

to phenol was recently studied in detail.[9] Photocyclization may also take place in particular when the molecule carries a substituent with a more or less extended π-electron system.[10] Depending on the nature of such substituents, this transformation can involve a variety of mechanisms. Generally, HX is released.

4.2.1 Nucleophilic substitution

When the herbicide bromoxynil (3,5-dibromo-4-hydroxybenzonitrile) is irradiated in unbuffered water (pH=4.2) between 300 and 350 nm, 3-dibromo-4,5-hydroxybenzonitrile is produced with a chemical yield of 65 %.[11] This is fully consistent with the substitution of Br by OH (equation 2 or 4).

The herbicide 2,4-dichlorophenoxyacetic acid is slowly photodegraded in aqueous solution. Again, the photosubstitution of Cl by OH is observed at the two positions.[12] The ether bond being quite weak, 2,4-dichlorophenol is formed along with dechlorinated compounds (Scheme 2).

[Scheme 2]

4.2.2 Reductive dehalogenation

Chlorothalonil (1,3-dicyano-2,4,5,6-tetrachlorobenzene) is a broad spectrum foliar fungicide, very commonly used worldwide, absorbing solar light until 350 nm. Its photolysis was studied in various media (Scheme 3). When chlorothalonil is solubilized in n-heptane or deposited on paraffinic wax films surface, the mono, di and tridechlorinated derivatives are formed. In aqueous medium, photoproducts corresponding to the replacement of Cl by OH in position 2 and 4 in respect with CN are detected, but dechlorinated derivatives are again the main photoproducts.[13-15]

[Scheme 3]

A detailed investigation based on steady-state and laser flash photolysis experiments allowed to rationalize the mechanism of this photodehalogenation.[16] It was established that the photolysis of chlorothalonil involves the triplet excited state. This species could be successfully detected and its reactivity investigated. The triplet whose transient absorption spectrum shows two maxima at 320 and 580 nm is trapped by oxygen with a bimolecular rate constant of 7.8×10^{8} $M^{-1}s^{-1}$. The reaction with oxygen essentially consists in energy transfer from triplet chlorothalonil to triplet ground state oxygen yielding singlet oxygen. Quantification of the yield of singlet oxygen was done by measuring the IR emission of singlet oxygen at 1270 nm.[17] The yield is 0.88 in pure acetonitrile and falls to 0.48 in water:acetonitrile (95:5, v/v). Steady-state experiments showed that the quantum yield of chlorothalonil photolysis is enhanced when oxygen is removed from the solution is line with the triplet involvement or in the presence of H-donor molecules showing that chlorothalonil photodehalogenation is governed by the direct interaction between the triplet and H-donor molecules present in the medium.[16] The important consequence is that formulation components, that are potential H-donor molecules, are expected to increase the rate of chlorothalonil photolysis in the first stage of its life cycle, that is to say when it is at the surface of the leaf cuticle just after the spraying. The enhancing effect of formulation adjuvants was actually confirmed. The reaction of the triplet with the solvent or any H-donor molecule generates the reduced radical that could be produced by irradiating chlorothalonil in pure 2-propanol (Scheme 4).

[Scheme 4]

The change of photoproducts when passing from heptane to aqueous medium is explained by the possibility of nucleophilic substitution when water is present. But interestingly, 2-

hydroxychlorothalonil and 4-hydroxychlorothalonil are produced by different reactions. By comparing the data obtained in the presence and in the absence of oxygen it was concluded that 2-hydroxychlorothalonil is directly generated from the triplet by nucleophilic substitution of Cl by OH from water (equation 2 or 4) while formation of 4-hydroxychlorothalonil requires the presence of oxygen and the preliminary reduction of chlorothalonil triplet by the solvent (equation 3). Acetonitrile is often used as a co-solvent to improve the solubility of molecules. It must be kept in mind that even though this solvent is a poor H-donor, it can promote photoreduction in some cases.

4.2.3 Photocyclisation

Sulcotrione (2-(2-chloro-4-mesylbenzoyl)cyclohexane-1,3-dione) is a triketonic herbicide used in replacement of atrazine. It absorbs solar light with an absorption extending until 350 nm. In neutral water, the photolysis of sulcotrione is very slow with a reported half-live around 100 days, and the only described photoproduct in the registration report is 2-chloro-4-methylsulfonylbenzoic acid. When sulcotrione is as a solid on leaves or wax films, its photolysis is much faster with a half-life of several hours, and the main photoproduct is the xanthene depicted in Scheme 5.[18,19] This photocyclisation also occurs in acidic water when sulcotrione is in the molecular form (pKa = 3.1). Due to the weak photolytic quantum yields, it was not possible to detect any transient species and therefore clear up the reaction mechanism of the HCl elimination.

[Scheme 5]

Triclosan is another molecule whose photolysis also produces a cyclic compound.[20,21] When triclosan is irradiated in the anionic form (pKa = 8.1), four major photoproducts are identified among which 2,8-dichlorodibenzodioxin (Scheme 6).

[Scheme 6]

To investigate deeply the mechanism of photocyclisation, several experiments were conducted. Firstly, triclosan was irradiated in the presence of d_8-2-propanol. The substitution of Cl by a deuterium atom demonstrated that the biradical depicted in Scheme 7 is the key intermediate in the reaction.

[Scheme 7]

Secondly, the nature of the C-Cl cleavage was investigated. Laser flash photolysis of triclosan allowed to rule out the homolytic nature of the cleavage as in the presence of high amount of Cl^-, $Cl_2^{-\cdot}$ was not detected. Moreover, high amounts of NaCl or NaBr did not affect the photolysis of triclosan showing that carbocations are not formed and the cleavage of the C-Cl not heterolytic. Giving all these data, it was proposed that an intramolecular electron transfer occurs from the phenolic moiety to the chlorinated ring in the excited triclosan. The resulting biradical anion eliminates Cl^- to form the neutral biradical (Scheme 8). Density functional calculations supported this mechanism.

[Scheme 8]

Propiconazole ((+)-1-[2-(2,4-dichlorophenyl)-4-propyl-1,3-dioxolan-2-ylmethyl]-1*H*-1,2,4-triazole), a foliar fungicide, also undergoes photocyclization through elimination of Cl from the dichlorinated ring and H from the triazole (Scheme 9). The quantum yield of propiconazole photolysis is rather high (0.11 ± 0.01) but the photocyclisation product is only one of the main photoproducts.[22]

[Scheme 9]

In the case of itraconazole another fungicide showing a structure close to that of propiconazole the formation of an aryl radical was proposed.[23] Cyclisation is assumed to proceed by an intramolecular attack of the initially generated aryl radical towards the triazole ring in poorly H-donating solvents such as acetonitrile. In good H-donor solvents such as ethanol reductive dehalogenation takes place.

4.3 Photoisomerization

E/Z photoisomerization is a typical example of a photostationary equilibrium (Scheme 10).[24-27]

[Scheme 10]

In contrast to thermodynamic equilibria, photostationary equilibria do not depend on the thermodynamic stability of the constituents but on their ability to absorb light at a particular wavelength (equation 5). For example, when the *E*-isomer absorbs better than the *Z*-isomer (Absorption coefficients: $\varepsilon_E > \varepsilon_Z$), the *Z*-isomer is accumulated in the reaction medium (concentration of E (c(E)< concentration of Z (c(Z)) since the transformation $E \rightarrow Z$ is faster than the inversed reaction and *vice versa*. In many cases, the corresponding quantum yields ($\Phi_{E\rightarrow Z}$ and $\Phi_{Z\rightarrow E}$) are in the same order of magnitude.

$$\frac{c(E)}{c(Z)} = \frac{\varepsilon_Z(\lambda)\Phi_{Z\rightarrow E}}{\varepsilon_E(\lambda)\Phi_{E\rightarrow Z}} \qquad \text{(equation 5)}$$

Photochemical *E/Z* isomerization may be induced by photosensitization *via* energy triplet or singlet transfer. Reversible addition of a photochemically generated radical intermediate on a triplet excited species such as an aromatic ketone may also lead to such an isomerization.[30,31]

E/Z Photoisomerization is observed in compounds possessing a C=N, N=N or similar units as well.[32] Many pesticides contain such bonds. Often biological activity is only observed for one of these isomers since the structural change caused by such a transformation is considerable from the enzymatic reactivity point of view. For reasons just discussed, the photochemical intermediate significantly differs from the thermodynamic intermediate generated in the synthesis of these compounds using organic ground state reactions.

4.3.1 Ethylene bonds

Azoxystrobin is a systemic fungicide only active in the E form. Its photochemistry was investigated in solvents of low polarity (n-heptane and isopropanol) to mimic the fate of the fungicide at the surface of leaves cuticle and also in water to understand its fate once it is released in surface waters.[33,34] Based on analytical and kinetic data, it was demonstrated that in heptane isomer E undergoes efficient photoisomerization into the isomer Z with a quantum yield of 0.75±0.08 (Scheme 11). The isomer Z also undergoes photoisomerization into isomer E with a quantum yield close to 1. A pseudo photostationary equilibrium is therefore reached when the ratio [isomer E]/[isomer Z] is 2.0±0.1.[33] Photodegradation only takes place from E isomer (quantum yield = 0.073±0.008). In isopropanol, both photoisomerization and photodegradation are significantly slower.

[Scheme 11]

Theoretical calculations using a simplified molecule were performed to understand these results. They revealed that four conformers may participate in the isomerization mechanism (E_{cis}, E_{trans}, Z_{cis} and Z_{trans}). The E_{cis}/E_{trans} and Z_{cis}/Z_{trans} pairs of conformers have similar energies (0.0/0.6 kcal mol^{-1} and 4.0/3.5 kcal mol^{-1}) and are separated by low electronic energy activation barriers (6.7 and 2.1 kcal mol^{-1}, respectively). Ground state E and Z species

are thus an equimolar mixture of the respective two conformers. In addition, large activation barriers (above 45 kcal mol^{-1}) prevent isomerization in the ground state ($E_{trans} \rightarrow Z_{trans}$ or $E_{cis} \rightarrow Z_{cis}$). The excited state potential energy surface shows two avoided crossings. As the energy gap is much smaller for isomerization *via* the trans isomers at the first avoiding crossing than for isomerization *via* the cis isomers at the second avoiding crossing and as $E_{cis}(S_1)$ faces a large barrier toward $E_{trans}(S_1)$, isomerization is favored between E_{trans} and Z_{trans}. The dipole moments were also investigated to understand the effect of solvent polarity that is rationalized in terms of stabilization of ground and excited states at the avoided crossing. At the first avoided crossing, the ground state dipole moment is larger (8.3 D) than that of the excited state (1.8 D). Thus, in polar solvents, the excited state is less stabilized than the ground state potential energy. This leads to a larger S_0/S_1 gap in isopropanol, a lower transition probability in isopropanol than in heptane and finally a lower photoreactivity.

4.3.2 Oxime bonds

A lot of pesticides bear an oxime function. Oxamyl is active in the Z form. Under irradiation, it undergoes photoisomerization (Scheme 12) and is also converted in a nitrile after losses of the carbamate and CH_3S.[35] The oximino derivative obtained by hydrolysis in the dark only undergoes photoisomerization.

[Scheme 12]

Cyclohexanedione oximes are herbicides that bear two keto groups and an O-substituted oxime that can be in E or Z form (Scheme 13). Cyclohexanedione oximes are marketed in the active E form. Typically, cyclohexanedione oxime herbicides undergo photochemical transformation but dark chemical rearrangements are also possible in acidic medium (Scheme 12).[36] Isomerization of the E-isomer into the Z-isomer has been reported to take place in the

dark and under irradiation in water.[37,38] If the photochemical isomerization of oximes is a well-known reaction,[39] the dark isomerization is more surprising. It is explained by the acidic hydrolysis of the oxime which makes possible the rotation of the O-alkyl about the C-N bond. The formation of oxazole from cyclohexanedione oxime herbicides was also reported.[40] In the dark, this reaction starts by N protonation followed by cleavage of the N-O bond, loss of R_3OH, Beckmann type rearrangement and final cyclization. The photochemical production of oxazole is observed in various media such as water, methanol or soil surface. Last, the imine is the main photoproduct in solid and in solution while its formation is very minor in the dark. The oxime function is clearly at the core of the (photo)rearrangement.

[Scheme 13]

In the case of cycloxydim, the absence of photoisomerization in acetonitrile was demonstrated.[41] NMR and absorption data showed that in non-protic solvent such as acetonitrile, the enol form is stabilized by an intramolecular hydrogen bond with the oxime nitrogen. After the π/π^* oxime excitation, the C=N bond is weakened. This allows isomerization about the CN bond. In contrast, in water, where the keto form is favoured due to intermolecular hydrogen bonds between the carbonyl and solvent OH, internal rotation is free and isomer Z can be obtained. Such an inhibiting effect of intramolecular hydrogen bonds on photoisomerization has been reported in the literature.[42,43]

4.4 Photo-fries

In a classical Fries rearrangement, for example, a phenolester is transformed into a hydroxyacetophenone derivative by migration of an acyl group. At the ground state, this reaction occurs under Lewis acid catalysis. The same reaction also takes place without any chemical activation when it is carried out under UV irradiation.[44,45] Singlet and triplet excited states may be involved. It is generally admitted that arylester such as **1** undergo homolytic fragmentation which leads to the formation of a phenoxyl (**2**) and an acyl (**3**) radical (Scheme 14).[46] Radical combination leading to the formation of C-C bonds yields the regio isomers **4** and **5**. After tautomerisation which reestablishes aromaticity, the final products **6** and **7** are obtained. The regio selectivity depends on the nature of further substituents at the aromatic moiety. Furthermore, it can be affected by the reaction medium. For example, when carried out in solution the selectivity is often low while when the reaction is performed in a constrained environment such as zeolites, it may be increased.[47] The reaction is observed with a variety of functional groups such as amides, sulfonates and sulfonamides or aromatic lactones and lactams. Similar transformations have been observed with compounds carrying an alkene moiety instead of an aromatic group.[44,48] For example enolethers derived from cyclic 1,2-diketones or 1,3-diketones have been transformed.[49,50]

Phenylurea herbicides that do not bear halogens undergo photo-fries rearrangement upon excitation at $\lambda > 300$ nm.[51] On the other hand, photo-fries rearrangement is not observed in the case of 1-naphthyl methylcarbamate (carbaryl) that is photolyzed into 1-naphthol.[52] This behavior contrasts with that of other naphthyl esters.[53]

4.5 Photo-claisen

The Claisen rearrangement is a well known and widely used ground state reaction. Most frequently, this reaction occurs according to a concerted mechanism. A photochemically version of the reaction has also been reported.[54] Under these conditions, it is often performed with aromatic compounds. A classical example is that of the transformation of allyl phenyl ether.[55] As in the case of the photo Fries reaction and in contrast to the Claisen reaction at the ground state, there is formation of two radical species.[56] Most probably, the reaction occurs at the singlet state. A $^1\pi\sigma^*$ (S_2) state is involved in the fragmentation. Radical combination then leads to two regioisomeric adducts. And again, tautomerization generates the final products. The regioselectivity is highly affected by the environment. For example, when corresponding phenol derivatives form inclusion complexes with cyclodextrines, the formation of *para* products is stronger favored as in the case of a homogeneous medium like a solution.[57] Such studies are also useful to discuss photochemical degradation of pesticides which often occurs in heterogeneous media.

The herbicide napropamide (*N,N*-diethyl-2-(1-naphthyloxy)propionamide) undergoes photo-claisen reaction in aqueous medium and on solid supports such as cellulose and silica.[58,59] This shows that radicals are sufficiently mobile on solid supports to generate the keto tautomers. The cage escape product, 1-naphthol, is also produced in water as on solid supports.

References

[1] P. Klán, J. Wirz, *Photochemistry of Organic Compounds*; Wiley: Chichester, 2009

[2] N. J.Turro, V.Ramam[urthy], J. C. Scaiano, *Modern Molecular Photochemistry of Organic Molecules*; University Science Books: Sausalito, 2010

[3] N. Hoffmann, *Chem. Rev.,* 2008, **108**, 1052.

[4] L. Pretali, A. Albini, In *Organic Photochemistry and Photobiology, 3rd Edition, Vol. 1* (A. Griesbeck, M. Oelgemöller, F. Ghetti, eds.), CRC Press, Boca Raton, 2012, pp. 369-391.

[5] L. Schutt, N. J. Bunce, In *Organic Photochemistry and Photobiology, 2nd Edition* (W. Horspool, F. Lenci, eds.), CRC Press, Boca Raton, 2004, pp. 38/1-38/18.

[6] V. Dechiarante, M. Fagnoni, *Synlett*, 2008, 787.

[7] J. Grimshaw, A. P. de Silva, Chem. Soc. Rev., 1981, **10**, 181.

[8] R. A. Rossi, A. B. Pierini, A. S. Santiago, *Org. React.,* 1999, **54**, 1.

[9] A. Mardyukov, R. Crespo-Otero, E. Sanchez-Garcia, W. Sander, *Chem. Eur. J.,* 2010, **16**, 8679.

[10] J. Grimshaw, A. Prasanna de Silva, *Can. J. Chem*., 1980, **58**, 1880.

[11] F. Machado, L. Collin, P. Boule, *Pestic. Sci.*, 1995, **45**, 107.

[12] R. Zepp, N. Wolfe, J. Gordon, G. Baughman, *Environ. Sci. Technol*., 1975, **9**, 1144.

[13] G. A. Penuela, D. Barcelo, *J. Chromatogr. A*, 1998, **823**, 81.

[14] V. A. Sakkas, D. A. Lambropoulou, T. A. Albanis, *Chemosphere*, 2002, **48**, 939.

[15] A. G. Giumanini, G. Verardo, P. Strazzolini, *J. Photochem. Photobiol. A*, 1989, **48**, 129.

[16] S. Monadjemi, M. el Roz, C. Richard, A. ter Halle, *Environ. Sci. Technol*., 2011, **45**, 9582.

[17] S Bouchama, P. de Sainte-Claire, E. Arzoumanian, E. Oliveros, A. Boulkamh, C. Richard, *Environ. Sci Process Impact*, 2014, **16**, 839.

[18] A. ter Halle, D. Drancova, C. Richard, *Environ Sci Technol.*, 2006, **40**, 2989.

[19] A. ter Halle, A. Piquet, C. Richard, *Environ. Chem*., 2007, **4**, 256.

[20] J. M. Buth, M. Grandbois, P. J. Vikesland, K. McNeill, W. A. Arnold, *Environ. Toxicol. Chem.*, 2009, **28**, 2555.

[21] S. Kliegman, S. N. Eustis, W. A. Arnold, K. McNeill, *Environ. Sci. Technol*., 2013, **47**, 6756.

[22] D. Vialaton, J.F. Pilichowski, D. Baglio, A. Paya-Perez, B. Larsen, C. Richard, *J. Agric. Food Chem*., 2001, **49**, 5377.

[23] G. Nardi, M. Luisa Marin, P. A. de Souza, V. Lhiaubet-Vallet, M. A. Miranda, *RSC Adv.*, 2014, 4, 2687.

[24] T. Arai, K. Tokumaru, *Chem. Rev.*, 1993, **93**, 23.

[25] T. Mori, Y. Inoue, In *Synthetic Organic Photochemistry* (A. G. Griesbeck, J. Mattay, eds.), Marcel Dekker, New York, 2005, pp. 417-452.

[26] J. Saltiel, D. F. Sears, Jr., D-H. Ko, K.-M. Park, In *CRC Handbook of Organic Photochemistry and Photobiology* (W. M. Horspool, P.-S. Song, eds.) CRC Press, Boca Raton, 1995, pp. 3-15.

[27] P. J. Kropp, In *CRC Handbook of Organic Photochemistry and Photobiology* (W. M. Horspool, P.-S. Song, eds.) CRC Press, Boca Raton, 1995, pp. 16-28.

[28] G. O. Schenck, R. Steinmetz, *Tetrahedron Lett.,* 1960, **1**, 1.

[29] J. Saltiel, K. R. Neuberger, M. Wrighton, *J. Am. Chem. Soc.,* 1969, **91**, 3658.

[30] G. O. Schenck, R. Steinmetz, *Tetrahedron Lett.,* 1960, **1**, 1.

[31] J. Saltiel, K. R. Neuberger, M. Wrighton, *J. Am. Chem. Soc.,* 1969, **91**, 3658.

[32] A. Padwa, *Chem. Rev.,* 1977, **77**, 37.

[33] J. Chastain, A. ter Halle, P. de Sainte Claire, G. Voyard, M. Traikïa, C. Richard, *Photochem. Photobiol. Sci.*, 2013, **12**, 2076.

[34] J. M. Chovelon, A. Boudina, C. Emmelin, A. Baaliouamerand, O. Païssé, *Chemosphere*, 2007, **68**, 1280.

[35] P. Mazellier, C. Zamy, M. Sarakha, *Environ Chem Lett*, 2010, **8**, 19.

[36] P. Sandín-España, B. Sevilla-Morán, J. L. Alonso-Prados and I. Santín-Montanya, In *Activity of Cyclohexanedione Oxime Herbicides, in Herbicides – Properties, Synthesis and Control of Weeds Chemical Behaviour and Herbicidal*, ed. M. N. Abd El-Ghany, Agricultural and Biological Sciences series, 2012, pp. 75-102.

[37] L. N. Falb, D. C. Bridges, A. E. Smith, *J. Agric. Food Chem.*, 1990, **38**, 875.

[38] B. Sevilla-Morán, P. Sandín-España, M. J. Vicente-Arana, J. L. Alonso-Prados, J. M. García-Baudín, *J. Photochem. Photobiol. A*, 2008, **198**, 162.

[39] A. Padwa, F. Albrecht, *J. Am. Chem. Soc*., 1972, **94**, 1000.

[40] *Metabolic pathways of agrochemicals*, ed. T. R. Roberts, Royal Society of Chemistry, Cambridge, UK, 1998.

[41] S. Monadjemi, P. de Sainte-Claire, I. Abrunhosa-Thomas, C. Richard, *Photochem. Photobiol. Sci.*, 2013, **12**, 2067.

[42] F. D. Lewis, A. Beth, *Res. Chem. Intermed*., 1995, **21**, 749.

[43] D. A. Lightner, Y. T. Park, *J. Heterocycl. Chem.*, 1977, **14**, 415.

[44] D. Belluš, *Adv. Photochem.,* 1971, **8**, 109.

[45] M. A. Miranda, F. Galindo, In *Organic Photochemistry and Photobiology, 2nd Edition* (W. Horspool, F. Lenci, eds.), CRC Press, Boca Raton, 2004, pp. 42/1-42/11.

[46] J. C. Anderson, C. B. Reese, *Proceed. Chem. Soc.,* 1960, 217.

[47] L. S. Kaanumalle, A. Natarjan, V. Ramamurthy, In *Synthetic Organic Photochemistry* (A. G. Griesbeck, J. Mattay, eds.), Marcel Dekker, New York, 2005, pp. 553-618.

[48] D. Ravelli, M. Fagnoni, In *Organic Photochemistry and Photobiology, 3rd Edition, Vol. 1* (A. Griesbeck, M. Oelgemöller, F. Ghetti, eds.), CRC Press, Boca Raton, 2012, pp. 393-417.

[49] A.-L. Poquet, A. Feigenbaum, J.-P. Pete, *Tetrahedron Lett.,* 1986, **27**, 2975.

[50] T. S. Cantrell, W. S. Haller, J. C. Williams, *J. Org. Chem.,* 1969, **34**, 509.

[51] A. Amine-Khodja, A. Boulkamh, P. Boule, *Photochem. Photobiol. Sci*., 2004, **3**, 145.

[52] O. Brahmia, C. Richard, *J. Photochem. Photobiol. A*, 2003, **156**, 9.

[53] N.P. Gritsan, Y.P. Tsentalovich, A.V. Yurkovskaya and R.Z. Sadgeev, *J. Phys. Chem.*, 1996, **10**, 4448.

[54] F. Galindo, *J. Photochem. Photobiol. C,* 2005, **6**, 123.

[55] M. S. Kharasch, G. Stampa, W. Nudenbert, *Science,* 1952, **116**, 309.

[56] S. J. Harris, D. Murdock, M. P. Grubb, G. M. Greetham, I. P. Clark, M. Towrie, M. N. R. Ashfold, *Chem. Sci.,* 2014, **5**, 707.

[57] M. S. Syamala, V. Ramamurthy, *Tetrahedron,* 1988, **44**, 7223.

[58] J.P. Aguer, P. Boule, F. Bonnemoy, J.M. Chezal, J. M., *Pest. Sci.*, 1998, **54**, 253.

[59] J.P. Da Silva, E.V. Bastos, L.F.V. Ferreira, R.G. Weiss, *Photochem. Photobiol. Sci*., 2008, **7**, 69.

Captions for figures

Scheme 1: Basic photochemical processes involved in photochemical transformation

Scheme 2 : Photohydrolysis of 2,4-dichlorophenoxyacetic acid

Scheme 3 : Photolysis of chlorothalonil in apolar medium and in water/acetonitrile (80:20, v/v)

Scheme 4: Photoreduction of the triplet of chlorothalonil in the presence of an H-donor molecule (R-H)

Scheme 5: Photolysis of sulcotrione on paraffinic wax films

Scheme 6 : Dioxin formation upon irradiation of anionic triclosan

Scheme 7: Trapping of the biradical by d_8-2-propanol

Scheme 8: Formation of the biradical by intramolecular electron transfer

Scheme 9: Photocyclization of propiconazole

Scheme 10. E/Z photoisomerization of an alkene.

Scheme 11: Photoisomerization of azoxystrobin

Scheme 12: Photoisomerization of oxamyl

Scheme 13: Chemical structure of cycloxydim, a cyclohexanedione oxime herbicide and of its main photochemical and dark reactions

Scheme 14. Mechanism of the photo-Fries rearrangement.

Scheme 1

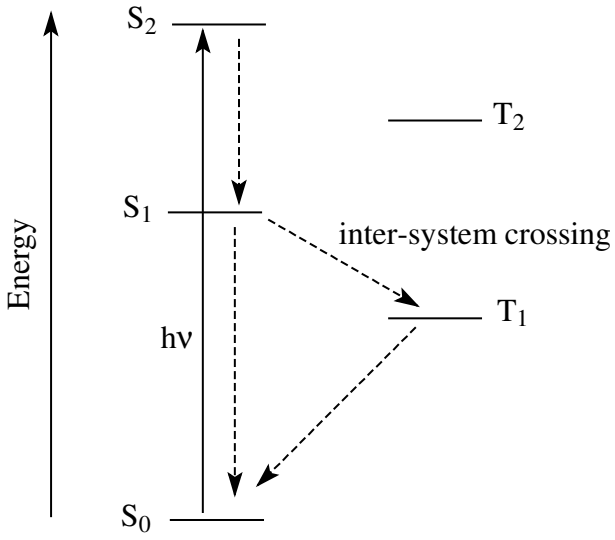

Scheme 2

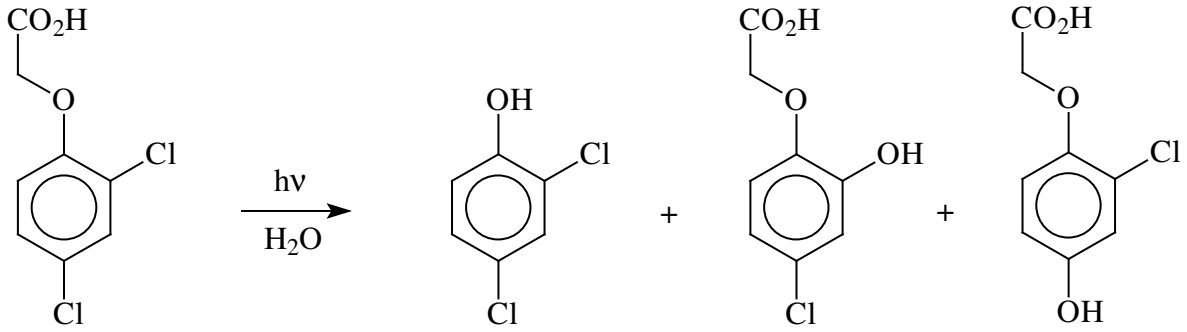

Scheme 3

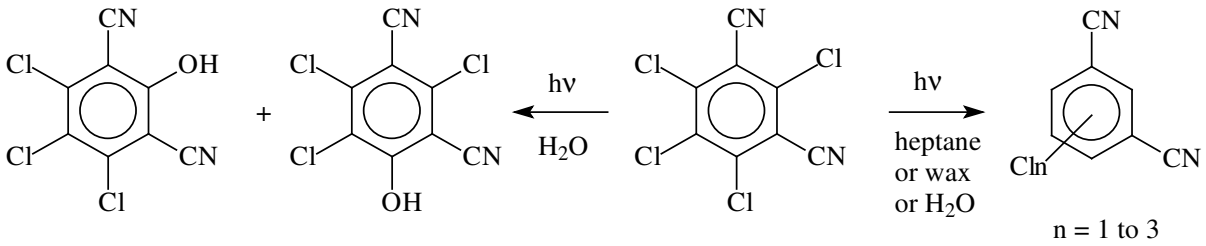
CN
Cl
OH
Cl
CN
Cl
+
CN
Cl
Cl
Cl
CN
OH
hν
H2O
CN
Cl
Cl
Cl
CN
Cl
hν
heptane
or wax
or H2O
CN
Cln
CN
n = 1 to 3

Scheme 4

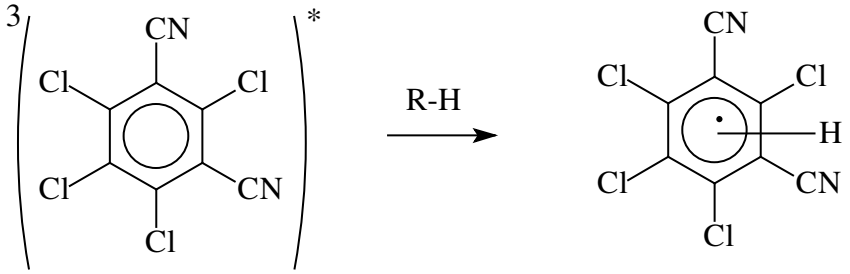

Scheme 5

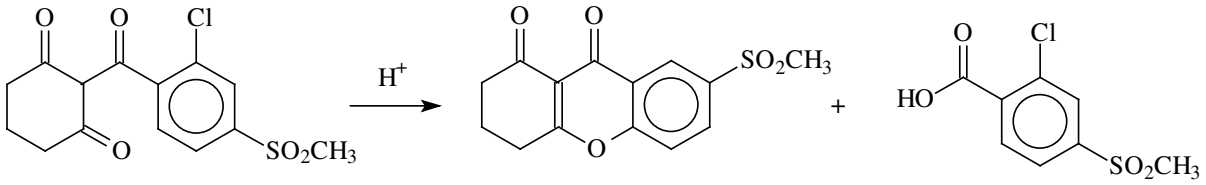

Scheme 6

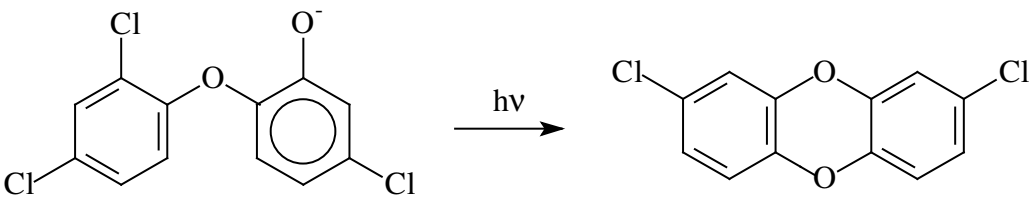

(chemical yield 4%)

Scheme 7

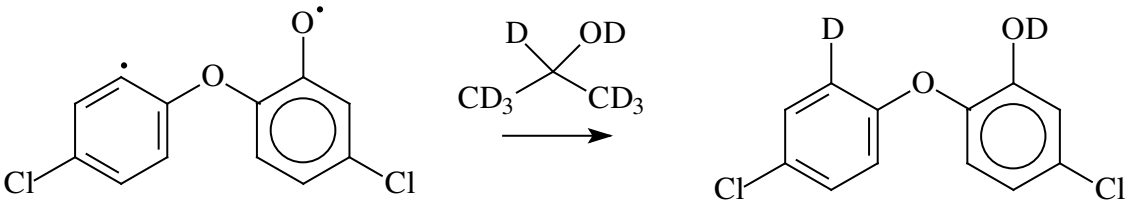

Scheme 8

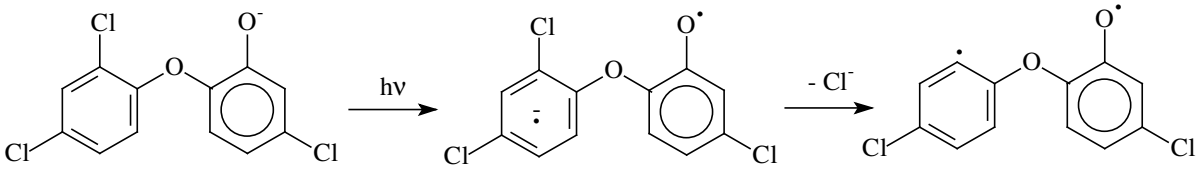

Scheme 9

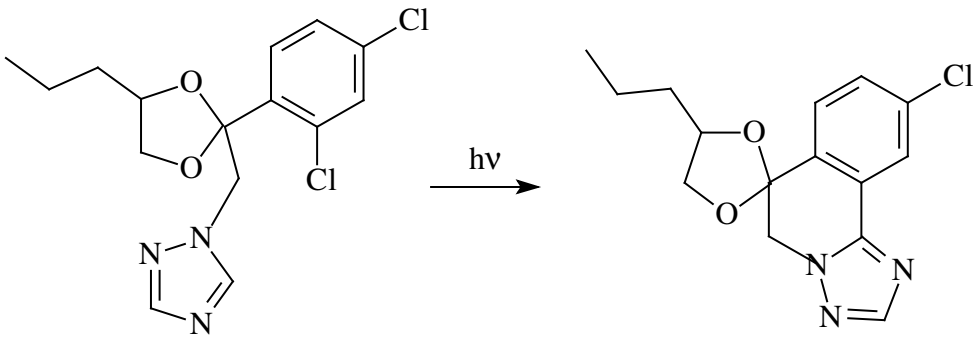

Scheme 10

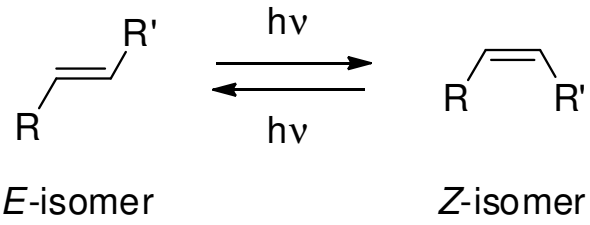

E-isomer *Z*-isomer

Scheme 11

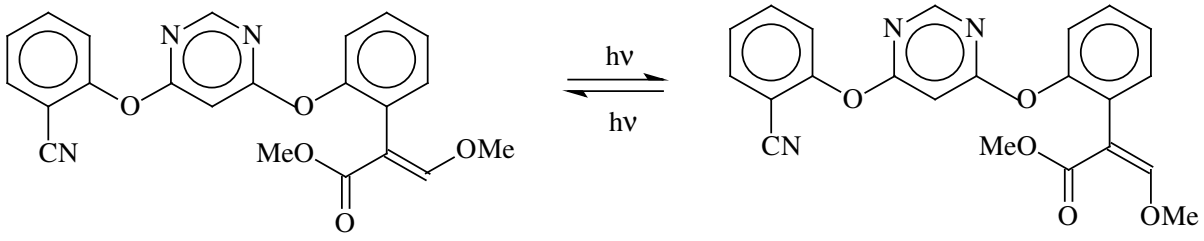

Azoxystrobin = Isomer E

Isomer Z

Scheme 12

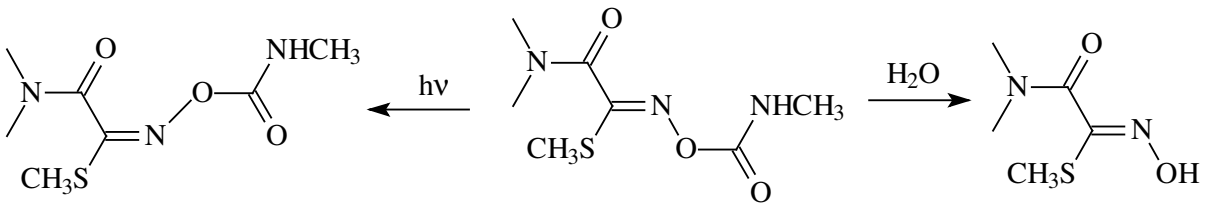

Scheme 13

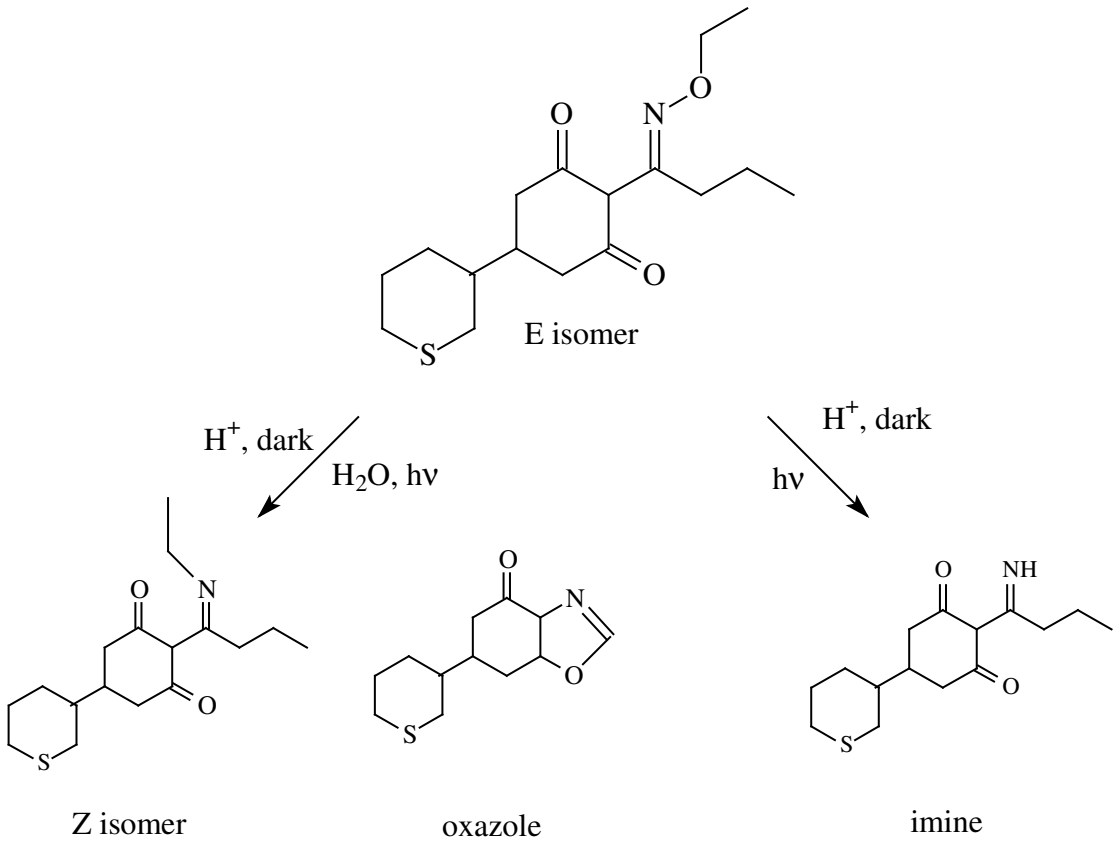
O
N
O
O
S
E isomer
H+, dark
H2O, hν
H+, dark
hν
O
N
O
S
Z isomer
O
N
O
S
oxazole
O
NH
O
S
imine

Scheme 14

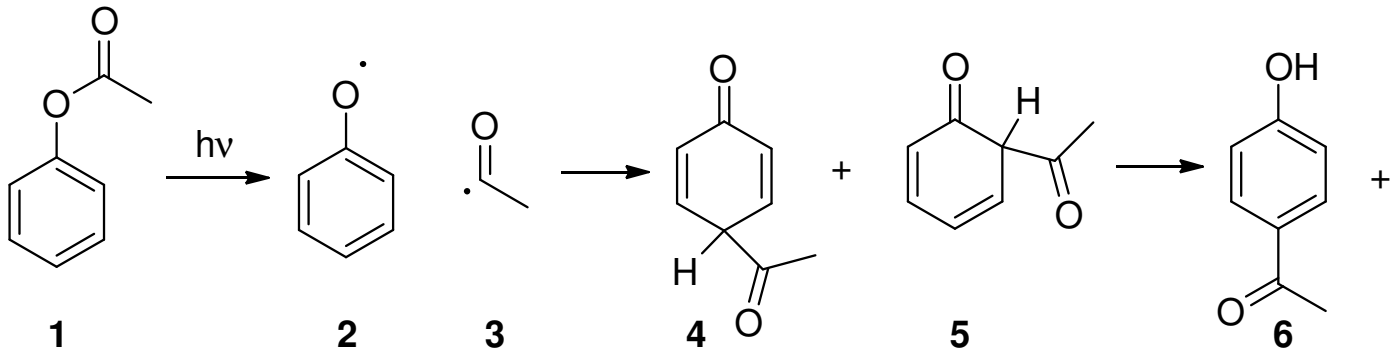

Chapter 5

Photochemical Reactivity of Organic Matter and its Size Fractions

Garrett McKay[1] and Fernando L. Rosario-Ortiz[1]*

[1]Department of Civil, Environmental and Architectural Engineering, 428 UCB, University of Colorado, Boulder, CO 80309, USA

Corresponding author: Fernando.rosario@colorado.edu; Phone: 303-492-7607

Abstract

The photochemical reactions that occur in natural water bodies play an important role in many biogeochemical processes, such as global carbon cycling and the fate of organic contaminants. Photochemically active compounds found in these systems include nitrate, nitrite, and dissolved organic matter (DOM). DOM is a major constituent in the water matrix and thus its photochemical reactions are central to understanding the photochemistry of natural waters. DOM is colored (typically yellow to brown) and absorbs light in the ultraviolet and visible range. Formation of excited states following DOM absorption leads to (sensitized) production of reactive intermediates, such as singlet oxygen, organic peroxyl radicals, hydrogen peroxide, hydroxyl radical, and excited triplet states. As DOM is a complex, heterogeneous material, a complete mechanistic understanding of these species' production has been difficult to obtain. The aim of this chapter is to develop a framework for understanding the mechanism of sensitized reactive intermediate production from DOM, with special attention to the role of DOM molecular size.

Table of Contents

1. Introduction

Dissolved organic matter (DOM), defined as the pool of carbonaceous compounds found ubiquitously in aqueous environments, represents the largest pool of reduced carbon in the biosphere.[1,2] DOM has been characterized as a complex mixture of organic compounds of varying molecular weight and composition, ranging from simple molecules composed of carbon, hydrogen and oxygen to more complex structures where heteroatoms such as nitrogen and sulfur are incorporated.[3]

Based on its source and subsequent physicochemical properties, DOM observed in surface waters can be classified into three main pools. These include terrestrial or allochthonous and aquatic or autochthonous DOM.[4-6] Both of these sources are considered to be end-members of geochemical importance and are frequently used to define boundaries with respect to the observed physicochemical properties of DOM in aquatic systems. A third component observed in surface waters under the influence of anthropigenic activities is the material derived from wastewater processes, referred to as effluent organic matter (EfOM). EfOM is composed of oxidized, recalcitrant DOM from drinking water sources as well as soluble microbial products (SMPs), a byproduct of biological treatment of wastewater.[7] The chemical composition of DOM includes lignin-type compounds, sugars, peptides, and polysaccharides; with phenolic, quinone, ketone, aldehyde, aromatic, carboxylic acid, amide, ester, and ether functional groups.

2. Molecular composition of DOM

The structural characterization of DOM has fascinated researchers since the published molecular formula of a humic substance ($C_{40}H_{30}O_{15}$) in 1840.[8] Historically, DOM has been quantified as dissolved or total organic carbon (DOC or TOC).[9,10] DOM has been represented as a combination of both humic and non-humic material,[1-3] with the humic material, commonly known as humic substances (HS) accounting for as much as 80% of the total DOM in fresh

waters.[3,11] HS are further classified into fulvic acid (FA) and humic acid (HA), based on their solubility at different pH values and chemical composition.[12] The non-humic component of DOM includes proteins, carbohydrates, and other organic compounds including low molecular weight acids.

The number of studies focusing on EfOM has lagged behind the progress made on DOM. However, analysis of the properties of EfOM suggest that it behaves differently from DOM. Briefly, the composition of EfOM could be sub-divided into three main groups: (1) background DOM originating from water supplies, (2) SMPs produced during biological wastewater treatment, and (3) natural and synthetic trace chemicals.[7] In terms of mass contribution, SMPs will dominate over the background DOM. The trace chemicals will contribute a minor part to the overall mass. SMPs are produced during biological processes in wastewater treatment plants and are divided into two categories: biomass-associated products (BAP) and utilization-associated products (UAP).[8,13] UAP are a result of microbial substrate intake, which is proportional to the amount of substrate available in the system, and BAP is a result of microbial endogenous decay, which correlates to biomass concentration in the biological reactor.[7,9,10,14] Operational parameters such as sludge retention time, organic loading rate, hydraulic retention time, and process temperature can alter the properties of SMPs, therefore impacting the overall chemistry of EfOM.[14-17]

In the past decade, DOM has been characterized using a wide array of analytical techniques, such as three-dimensional fluorescence excitation-emission spectroscopy,[18-20] high and ultra-high resolution mass spectrometry,[21-23] and NMR (carbon, nitrogen and phosphorous).[24-28] These techniques have allowed researchers to obtain chemical formulas and additional information of chemical functionalities. For example, Stenson et al. used Fourier

transform ion cyclotron resonance mass spectrometry (FTICR-MS) to determine the molecular formulas for 4626 individual components of Suwannee River Fulvic Acid (SRFA) and compared these data to degraded lignin.[21] This technique has also been applied to EfOM and shown that it has more diverse functional groups than DOM isolates from natural samples.[29] Furthermore, FTICR-MS has been used to characterize/compare EfOM derived from different activated sludge processes.[30]

The apparent molecular weight (AMW) of DOM has consistently been of interest to scientists and engineers examining the impact of DOM on natural and engineered processes.[31-33] Multiple techniques have been used to measure this property, including vapor pressure osmometry,[34,35] size exclusion chromatography (SEC),[36] small angle X-ray scattering,[35] ultracentrifugation,[37] and light scattering techniques.[38] Early on, researchers had a fairly good understanding of the molecular weight range (700-10,000 Da published in 1968)[39] of DOM and its metal-complexing abilities.[40,41] Based on all of the above techniques, the average molecular weight of DOM molecules is likely around 1 kDa.[42]

In addition, size fractionation of bulk DOM into its AMW fractions has been utilized as a tool to evaluate the physiochemical properties of DOM. Size fractionation has been performed using ultrafiltration membranes,[33,43,44] as well as by dialysis and SEC.[45] These techniques have provided greater insight into the physicochemical properties of DOM, which in turn has allowed for more advanced study of its photophysical and photochemical properties.

3. Photophysics of DOM

The first law of photochemistry states that the rate of direct photoreaction of a chemical is a function of the rate of light absorption. Therefore, in order to describe the photochemical properties of DOM and its molecular weight fractions, we start by describing the basic

photophysical processes that are in effect when DOM interacts with light. The potential photophysical processes upon DOM light absorption are shown in Fig. 1. The initially formed

[Fiure 1 near here]

singlet excited state, $^{1}DOM^{*}$, can undergo various processes, including internal conversion (IC), fluorescence (F), and intersystem crossing (ISC), which leads to a triplet excited state, $^{3}DOM^{*}$. Compared to individual organic molecules, DOM exhibits some complex optical properties that are difficult to describe. The difficulty is compounded by DOM's heterogeneity and inexact knowledge of its structure. In the following sections, a framework is developed for understanding the photophysics of DOM light absorption and luminescence so as to understand its photochemical pathways.

As light absorption is the initial step in the population of excited states that lead to reactive intermediates, it is useful to develop a framework for explaining this initial photophysical step. First, the types of chromophores in DOM and their electronic transitions as individual moieties will be discussed. We will subsequently review the relationships between absorption spectra and DOM physicochemical properties.

3.1 Light Absorption

Absorbance spectra of simple inorganic and organic compounds derive from energy differences between the lowest vibrational state of the electronic ground state and different vibrational states of higher electronic states. In aqueous solutions, vibrational structure is lost and mainly broad absorption bands are observed. For DOM, however, absorbance decreases exponentially (i.e. no prominent absorption bands) from ~ 200-600 nm.[46,47] Importantly, DOM spectra share these characteristics, regardless of source and physicochemical properties.

The most likely chromophores in DOM include various carbonyl-containing groups and aromatic rings. Electronic transitions in these groups involve excitation of electrons in non-

bonding or π bonding orbitals to a π* anti-bonding orbital (either $n \rightarrow \pi^*$ or $\pi \rightarrow \pi^*$). With respect to carbonyl compounds, the $n \rightarrow \pi^*$ transition is lower in energy than the $\pi \rightarrow \pi^*$ transition, but is also forbidden and therefore less intense. For example, Fig. 2 shows the maximum molar absorption coefficient ($\varepsilon_{\lambda,max}$) for the $n \rightarrow \pi^*$ and $\pi \rightarrow \pi^*$ transitions for acetone and 3-buten-2-one. If one considers the UV-visible spectrum of DOM to be due to individual

[Figure 2 near here]

chromophores, extremely conjugated carbonyl and olefin compounds would need to be present in order to achieve absorption into the near UV and visible wavelength range (e.g. the λ_{max} of β-Carotene which has 11 conjugated carbon-carbon double bonds is 452 nm).

Aromatic structures represent the other potential chromophore ($\pi \rightarrow \pi^*$ transition) in DOM. Sharpless and Blough have suggested that all DOM absorption and photochemistry results from these structures,[48] though this does not exclude carbonyl compounds conjugated to aromatic rings (e.g. aromatic ketones).[49-51] It has been suggested that lignin is a DOM-precursor in both marine DOM[52] as well as terrestrial DOM (SRFA).[21]. Lignin contains linked aromatic rings substituted with hydroxyl, alkoxy, and carboxyl groups that are electronically isolated by *o*-ether linkages. Empirical rules have been developed for benzoyl derivatives (present in lignin), correlating structure with λ_{max}. For example, consider Fig. 3 in which a benzoyl ring is substituted with a *p*-hydroxy and *m*-alkoxy group. Even with the presence of these electron-donating substituents, the calculated λ_{max} is only 262 nm. This value is in good

[Figure 3 near here]

agreement with the λ_{max} of 282 nm measured in lignin obtained from an un-treated wood powder.[53] Fused aromatic and heteroaromatic rings (e.g. anthracene and quinolone) have absorption bands that extend into the near UV (e.g. $\log_{10}(\varepsilon)$ of quinolone is ~ 3.1 at 310 nm).

Many parameters have been used to characterize DOM absorption spectra. For example, the spectral slope parameter (S), obtained from exponential fitting of the absorption spectrum, provides a quantitative measure of how rapidly absorption decreases as a function of wavelength. The E2:E3 and E4:E6 ratio (ratio of absorption at 254 nm to that at 365 nm and 465 nm to that at 665 nm, respectively) are other quantitative parameters used to describe that rate of absorbance decrease as a function of wavelength. Previous research has shown that both S and E2:E3 increases with decreasing molecular size fractions of DOM.[43,52,54,55] Addition of simple organic acids to DOM decreases its molecular size (shown by SEC), apparently by disrupting hydrophobic interactions, which in turn leads to a decrease in UV-visible absorbance.[56] In addition, reduction of DOM with borohydride as well as photobleaching results in a preferential loss of visible absorption.[57]

Our initial discussion of DOM chromophores highlighted that, except for very conjugated structures, absorption occurs mainly below 300 nm. If it is assumed that DOM absorption spectra are due to a superposition of individual chromophores, highly conjugated or heteroaromatic structures need be present in order to explain DOM's absorbance in the near UV and visible region of the spectrum. However, research suggests that these structures are not prevalent in DOM. It has been proposed that the complex optical properties of DOM result from intramolecular charge transfer (CT) complexes.[48,58,59] According to this model, intramolecular electron donors (D) and acceptors (A) within DOM can interact to form a donor-acceptor complex ($D + A \rightleftharpoons DA$). CT complexes ($D^+A^-$) can form directly upon excitation of ground state DA

$$DA + h\nu \rightarrow D^+A^- \qquad (1)$$

or following conversion of a singlet or triplet excited state.[60]

$$DA + h\nu \rightarrow {}^{1}(DA)^{*} \quad (2)$$

$${}^{1}(DA)^{*} \rightarrow D^{+}A^{-} \quad (3)$$

$${}^{1}(DA)^{*} \rightarrow {}^{3}(DA)^{*} \quad (4)$$

$${}^{3}(DA)^{*} \rightarrow D^{+}A^{-} \quad (5)$$

Additionally, CT states could be formed by electron transfer from short-range (but non-complexed) excited state donors and acceptors:[61]

$$D^{*} + A \rightarrow D^{\bullet+} + A^{\bullet-} \quad (6)$$

$$D + A^{*} \rightarrow D^{\bullet+} + A^{\bullet-} \quad (7)$$

For DOM, the CT state is represented by $DOM^{+\bullet/-\bullet}$, signifying a di-radical charge separation. Presence of short-range, CT interactions between electron-rich donors and electron-poor acceptors are capable of producing lower energy electronic transitions, thus, explaining the near UV and visible absorption properties of DOM. Assuming that lignin is the main DOM precursor, it is likely that hydroxy/methoxy substituted aromatics (e.g. phenols, methoxylated phenols) act as donors while carbonyl-containing structures (e.g. quinone, triplet aromatic ketones/aldehydes) act as acceptors. It is well known that triplet aromatic ketones ($E^{0}_{red} \approx 1.7$ V) oxidize electron-rich phenols,[49] and that DOM inhibits oxidation of electron-rich phenols.[62] Furthermore, kraft lignin (containing donor phenolic groups) and 3,5-di-*tert*-butyl-1,2-benzoquinone (an electron acceptor) interact to produce a CT absorption band.[63]

The CT model could also explain correlations between DOM physicochemical and optical properties. Observations of an inverse dependence of S on molecular weight are explained by the greater likelihood of CT interactions present for larger DOM molecules. Conversely, lower molecular weight DOM, having a less aggregated structure, should have less

CT interactions. An alternative explanation to the CT model is that higher molecular weight DOM molecules absorb more, possibly due to a greater degree of π electron conjugation.

3.2 Luminescence

Following excitation to a singlet excited state, ^{1}DOM* can undergo many photophysical processes (see Fig. 1). Vibrational relaxation of ^{1}DOM* from an excited vibrational state to the ground vibrational state of an excited electronic state occurs quickly (within picoseconds). The possible fates of ^{1}DOM* are reaction, fluorescence, internal conversion, or intersystem crossing.

The lifetime of ^{1}DOM* (τ_{1DOM*}) is related to the sum of its decay processes:

$$\tau_{1DOM*} = \frac{1}{k_F^0 + k_{IC}^0 + k_{ISC}^0} \quad (8)$$

Because of its short lifetime, it is intuitively unlikely that ^{1}DOM* has significant intermolecular reactions. However, research investigating the effect of halide quenching on DOM excited states and reactive intermediates has shown that photochemical production of hydroxyl radical ($HO^{\bullet}$) is correlated to fluorescence quantum yields (i.e. τ_{1DOM*}), but not triplet state quantum yields.[64] This does not exclude intramolecular electron transfer reactions, which as previously discussed could lead to CT states within DOM molecules.

Fluorescence quantum yields for DOM range from ~ 0.1-2% depending on the sample and excitation wavelength.[52,59,65] Interestingly, DOM fluorescence spectra do not seem to follow Kasha's rule, which states that fluorescence is expected to originate from the lowest vibrational excited state and thus a molecule will exhibit identical emission wavelength and quantum yield regardless of excitation wavelength. For simple organic molecules, Kasha's rule is explained by rapid (picosecond) internal conversion or vibrational relaxation of higher excited states to the lowest electronic excited state.

Model DOM compounds,[49-51] DOM isolates,[66] and EfOM[67] have been shown, in some cases, to increase the degradation rate of organic pollutants (relative to direct photolysis in pure water), apparently due to oxidation by ^{3}DOM*. It is therefore necessary to understand the rate of intersystem crossing as a function of AMW. Although the intersystem crossing quantum yields for DOM are difficult to measure these values are expected to be near 0.3-1, as evidenced by experimental measurements[68] and the expectation that carbonyls, a potentially important chromophore, have intersystem crossing values near unity.[69]

Phosphorescence of DOM (^{3}DOM* $\rightarrow$ ^{1}DOM) is weakly allowed by spin-orbit mixing and time-resolved measurements estimate ^{3}DOM* lifetimes of ~ 1-100 μs.[48] Some studies have reported direct observation of ^{3}DOM*.[70-72] Notably, there is some debate over whether the transient species observed in these studies is actually ^{3}DOM* (though no other suggestion for the transient has been advanced) as it was not quenched by alkyl phenols, a well-known ^{3}DOM* quencher. However, the apparent ^{3}DOM* signal is quenched by sorbic acid, a known triplet state quencher. [72]

4. Photochemical Formation of Reactive Intermediates

The photosensitized formation of reactive intermediates from DOM is a potential source of organic pollutant degradation in natural systems (e.g. estuaries, treatment ponds, rivers, lakes). Reactive intermediates include $HO^{\bullet}$, singlet oxygen ($^1O_2$), and ^{3}DOM*. In addition, photoionization of DOM can produce the aqueous electron, $e^-_{(aq)}$, however, dissolved oxygen ($[O_2]$ ~ 200 μM) effectively scavenges all $e^-_{(aq)}$ to form $O_2^{-\bullet}$ (k ~ 2 × 10^{10} $M^{-1}s^{-1}$).[73] Other photochemically produced species include H_2O_2 and peroxyl radicals (RO•).

The specific mechanism for the formation of reactive intermediates is described below using DOM as the starting material. After DOM absorbs light and electrons are promoted to an excited state, the system could return to the ground state following emission (fluorescence). A

fraction of the chromophores that were excited could also go through intersystem crossing and form ^{3}DOM*. The excited triplet state can be quenched by molecular oxygen, which results in the formation of $^1O_2$.[74]

$$^3O_2 + {}^3DOM^* \rightarrow {}^1O_2 + {}^1DOM \quad (9)$$

Due to the relatively low energy of $^1O_2$ (94 kJ mol^{-1}) this reaction occurs readily and it has been suggested that $^1O_2$ is essentially a probe for ^{3}DOM*.[48]

The formation of HO$^\bullet$ occurs through the photochemical reactions of DOM, however, the source of this radical is still under investigation.[75-78] At least two general pathways have been suggested: an H_2O_2-dependent and H_2O_2-independent pathway. In addition there is evidence that both free HO$^\bullet$ is produced as well as a so called lower-energy hydroxylating species. The H_2O_2-independent pathway is often portrayed as a ^{3}DOM* or a low-energy hydroxylating species abstracting hydrogen from water. Quinones are a potential model for these low-energy hydroxylating moieties in DOM. In fact, photochemical studies of 2-methyl-p-benzoquinone indicate that hydroxylation occurs through a water-quinone exciplex, and not free HO$^\bullet$.[76] Oxidation of water by an excited state DOM species has yet to be shown, however. Studies of HO$^\bullet$ production from DOM isolates using different probes and quenchers show that the H_2O_2-dependent pathway accounts for up to ~ 50% of HO$^\bullet$ production and that some probes (e.g. terephthalate and benzoate) are not specific for free HO$^\bullet$.[78]

Direct detection of reactive intermediates using time-resolved techniques is difficult, though some studies have utilized laser flash photolysis methods. Steady-state measurements using probe compounds is common. An excellent review of these methods has been written by Blough and Zepp[79] and the reader is referred there for complete details. In brief, $^1O_2$ is commonly measured by its reaction with dienes (dimethyl furan or furfuryl alcohol). Steady-state

concentrations of $^1O_2$ are calculated from the rate of diene loss and the known rate constant for the reaction between $^1O_2$ and the specific probe. Dienes (e.g. sorbic acid) are also used to probe ^{3}DOM* production rates[80] and energies.[81] As ^{3}DOM* is a strong oxidant, alkylated phenols such as 2,4,6-trimethylphenol are also commonly used to measure production rates of triplet states. Many probes have been used to monitor $HO^\bullet$ production rates, though it has been shown that hydroxylated products can result from hydroxylating species other than $HO^\bullet$.[78]

4.1 Observations for bulk DOM

Production of reactive intermediates from bulk DOM samples has been well studied for the past few decades. Specifically, many studies have quantified the production rate and quantum yield of reactive intermediates for natural samples of varying origin, while others have sought mechanistic understanding. Optical properties of DOM are closely tied to the formation of reactive intermediates.

For $^1O_2$, quantum yields on the order of 0.6-6% have been reported for various natural water samples,[58,82,83] from which steady-state concentrations can be calculated if the spectral irradiance is known. $HO^\bullet$ formation rates from DOM photolysis are on the order of 10^{-12} to 10^{-11} M s^{-1},[75,84,85] while quantum yields for this species are less commonly reported. However, values of 1.1 to 3.0 × 10^{-4} for three ocean waters and 7.5 × 10^{-5} for SRFA have been measured irradiating at 320 nm.[75] This same study measured nine $HO^\bullet$ quantum yields for SRFA over 290-360 nm, finding an average value of 5.4 × 10^{-5}. In particular, the $HO^\bullet$ quantum yield of SRFA peaked around 310 nm, and decreased at shorter and longer wavelengths. Steady state concentrations of ^{3}DOM are estimated at 10^{-15} to 10^{-13} M.[81] In addition, a pioneering study by Zepp et al. estimated ^{3}DOM* energy levels around 250 kJ mol^{-1} for natural samples and DOM isolates.[81] With respect to quantum yields and steady-state concentrations of reactive

intermediates, wastewater-derived EfOM has been shown to have higher values relative to DOM isolates, potentially due to non-humic material produced in water treatment (see section 2).[43,55,86]

In an effort to chemically alter the photosensitizing moieties of DOM, Mostafa and Rosario-Ortiz treated bulk EfOM with oxidizing NaOCl and O_3.[43] A decrease in absorbance and increase in E2:E3 accompanied DOM oxidation and resulted in an increase in singlet oxygen quantum yield. The decrease in absorbance is explained by oxidation of light-absorbing aromatic rings and olefins. The increase in singlet oxygen quantum yield indicates either the relative non-importance of the oxidized aromatic/olefin moieties as sensitizers in $^1O_2$ formation or a decrease in molecular weight following oxidation (see section 4.2). Conversely, Sharpless treated DOM isolates with reducing $NaBH_4$.[87] While a decrease in absorbance was noted, there was no apparent decrease in singlet oxygen quantum yield. These observations support the idea that, while chemical alteration of both electron donors (aromatics/olefins) and acceptors (carbonyls) may disrupt CT interactions and thus decrease absorbance, mainly carbonyl-containing compounds (acceptors) mediate the formation of $^1O_2$. Implicitly, this means that oxidation with NaOCl or O_3 does not alter the carbonyl-containing compounds in DOM.

Correlations between production of reactive intermediates and optical properties of bulk DOM samples have been reported for a variety of samples. Firstly, the correlation of singlet oxygen quantum yield to absorbance parameters (S, E2:E3, specific absorption coefficients) [43,58,83,87,88] probably reflects an increase in CT interactions in DOM with lower S and E2:E3. An increase in formation of CT complexes may decrease the efficiency of ^{3}DOM* formation (through production of CT states following absorption of a photon or reaction of $^1\text{DOM}^* \rightarrow \text{DOM}^{\bullet+/\bullet-}$ and $^3\text{DOM}^* \rightarrow \text{DOM}^{\bullet+/\bullet-}$).[48] Since ^{3}DOM* is the precursor to $^1O_2$, a decrease in singlet oxygen quantum yield would follow. A few studies report a positive correlation between

fluorescence quantum yield and hydroxyl radical quantum yield,[45,55,64] although it is unclear whether this relationship is due to molecular size parameters or some involvement of ^{1}DOM* in HO$^{\bullet}$ production (see section 4.2).[45,55]

With respect to DOM source, it has been shown that EfOM has larger quantum yields for reactive intermediates formation than DOM isolates.[86] As noted in section 2, EfOM is comprised of recalcitrant DOM from drinking water sources, SMPs, and trace organic contaminants. Organic contaminants in EfOM should have no contribution due to their very low concentration. It is possible that the difference in apparent quantum yields is due to the oxidation of DOM during chlorination in drinking water treatment. In fact, a positive correlation has been shown between oxidant dose and singlet oxygen quantum yield,[43] with the reason being attributed to either a decrease in molecular weight following oxidation or a chemical change in the sensitizing chromophores. The presence of SMPs in EfOM may also cause this increase, though apparent quantum yields of reactive intermediates from SMPs have not been measured.

4.2 Observations from different molecular weight fractions

Relatively few studies exist on the effect of molecular weight on reactive intermediates formation, however, there is a consistent trend of increasing apparent quantum yield for fluorescence and all reactive intermediates with decreasing size.[43-45,47,55,88] The results from these studies will be summarized in this section and a framework for understanding the physical and chemical basis is developed.

Wang et al. used ultrafiltration to separate a fulvic acid isolate and observed higher fluorescence intensities for lower AMW fractions, which were attributed to CT interactions within the DOM. This observation has been confirmed by further studies utilizing ultrafiltration for both EfOM[44,55] and a DOM isolate.[44] Fig. 4 shows the fluorescence quantum yields for

different AMW fractions of Suwannee River NOM (SRNOM) and an EfOM sample as a function of excitation wavelength. As shown, the fluorescence quantum yields are higher for

[Figure 4 near here]

EfOM than for SRNOM. The bottom part of the figure shows the peak emission wavelength as a function of excitation wavelength. A monotonic increase of the emission versus the excitation, as observed for SRNOM, has been used to rationalize CT interactions for DOM.[59] However, for EfOM, the monotonic increase in emission versus excitation is only observed for the lower AMW fraction. For the larger AMW fraction and bulk sample, there is a deviation at excitation wavelengths below 350 nm. Below this wavelength, it appears that fluorescence is following Kasha's rule, indicating differences in photophysical behavior and suggesting the presence of individual compounds that will also impact photochemical properties. The same deviation is observed between 400-420 nm excitation for smaller EfOM AMW fractions.

The increase in fluorescence quantum yield for lower AMW fractions could be due to either lower degrees of quenching of ^{1}DOM* or intrinsic fluorescence ability. For example, larger molecular weight DOM molecules may have a more aggregated three dimensional structure,[33,89] which would promote intramolecular quenching of ^{1}DOM*, resulting in a decrease in fluorescence quantum yield. Alternatively, lower AMW fractions could contain more potent fluorophores. However, considering that more conjugated structures generally have higher fluorescence quantum yields,[61] and that higher AMW fractions might be expected to have more conjugated structures relative to low AMW fractions, the first explanation (quenching of ^{1}DOM*) seems more likely.

With respect to reactive intermediates, an early study by Haag and Hoigné[88] used gel permeation chromatography to separate DOM samples into apparent molecular weight fractions

and quantified steady state $^1O_2$ concentrations ($[^1O_2]_{ss}$). Their results showed that 100-500 Da fractions had consistently higher, or at least equal, $[^1O_2]_{ss}$ as bulk samples. Richard et al. used SEC-Page to separate DOM isolate standards and soil DOM extracts in order to determine the effect of AMW on fluorescence and photosensitizing ability.[45] Fluorescence intensity was increased in low relative to high AMW fractions. Degradation of fenuron and 2,4,6-trimethylphenol (TMP), known to react with ^{3}DOM*,[49,50] was also increased in low AMW fractions, suggesting an increase in reactive intermediates formation. Rosario-Ortiz et al. have carried out studies on the effect of AMW on reactive intermediates quantum yields;[43,44,55] the general results are summarized in Fig. 5, which shows the apparent quantum yields for SRNOM

[Figure 5 near here]

and an EfOM sample. The bulk EfOM sample had higher quantum yields for the formation of $HO^{\bullet}$, $^1O_2$, and ^{3}DOM* compared to DOM.[44] After fractionation, lower AMW fractions of EfOM still had higher quantum yields than DOM. In addition the components associated with the lower AMW fraction of EfOM are much more reactive towards the formation of reactive intermediates. This fraction could be enriched in SMPs. The work done on AMW fractions could be rationalized by expecting that lower AMW components will have molecules with excited states separated by larger energy gaps, compared to larger (and more highly conjugated) components with faster internal conversion kinetics. It could also be that there are inherent differences in chromophore composition, and higher SMP reactivity overall.

It should be noted that the chemical probe used to measure $^1O_2$, furfuryl alcohol (FFA), is hydrophilic and is limited to reaction with bulk, aqueous phase $^1O_2$ and not $^1O_2$ in the DOM microenvironment.[90] Therefore, an increase in singlet oxygen quantum yields may reflect the greater amount of $^1O_2$ escaping the DOM microenvironment (and reaching the bulk phase)

before being quenched by DOM as would be expected with smaller molecular size DOM molecules. However, the fact that ^{3}DOM* quantum yields (measured by TMP) positively correlate with singlet oxygen quantum yields suggests another explanation, namely, that ^{3}DOM* itself (and not $^1O_2$ alone) may undergo intramolecular quenching. Higher AMW DOM has a more aggregated three-dimensional structure (see section 5) and thus increased intramolecular quenching is expected in these fractions.

Two studies have reported an increase in $HO^\bullet$ quantum yield with decreasing AMW.[44,55] In both instances, a concomitant increase in fluorescence quantum yield was observed in low AMW fractions. Sharpless and Blough have suggested that this is an indication of fewer CT interactions in low AMW fractions[48]. This seems plausible, as CT interactions would provide a relaxation pathway for excited state DOM molecules, which play a role in formation of $HO^\bullet$.

5. Scavenging of reactive intermediates by DOM

Central to the understanding of photochemical production of reactive intermediates from DOM photolysis is the recognition that DOM is reactive towards these very same reactive intermediates. In principle, both inter- and intramolecular reaction of reactive intermediates with DOM are possible. Wenk et al. studied quenching of model triplet excited states (quinones and aromatic ketones) by bulk DOM standards,[91] finding that only neutral or cationic sensitizers were quenched, likely due to complexation of these molecules by DOM. Based on rate constants measured for this system in aerated solution where triplet states are deactivated via reaction with oxygen, intermolecular quenching is insignificant below DOM concentrations of 22-72 $mg_C\ L^{-1}$, which is far below that of most natural systems. Intramolecular quenching of ^{3}DOM* has not yet been investigated and remains a possible pathway for ^{3}DOM* loss.

Other reactive intermediates have high reactivity with DOM, including $HO^\bullet$[16,33,92] and $^1O_2$.[93] Scavenging of these species by DOM can affect their steady-state concentrations and thus

their ability to degrade organic contaminants. Rate constants for the reaction of $HO^{\bullet}$ and $^1O_2$ with DOM are on the order of 10^{8-9} and 10^5 $M_C^{-1}s^{-1}$, respectively, where M_C is the molar concentration of carbon. Dong et al. showed that lower AMW fractions of EfOM were more reactive towards $HO^{\bullet}$ on a per carbon basis, explaining the result as geometric affect. In short, if high AMW fractions contain more aggregated three-dimensional structures, some carbon atoms are likely inaccessible to $HO^{\bullet}$. Conversely, less aggregated, low AMW fractions having a higher surface area-to-carbon atom ratio would exhibit higher reactivities on a molar basis based on this geometric effect.

5. Conclusions

Throughout this chapter, we have developed a framework for understanding the photophysical and photochemical processes in the complex material that is DOM. There are a few main conclusions that can be derived. One is that the optical properties (absorbance, fluorescence, phosphorescence) in DOM are influenced by interactions within DOM molecules. This may be influenced by the so-called charge transfer interactions as well as by molecular size. In addition, photochemical production of reactive intermediates (as well as fluorescence) clearly varies with molecular size. It is difficult at this point, however, to distinguish whether this is due to strictly molecular size (e.g. intramolecular quenching) or differences in chemical composition between the different fractions. More experiments are needed to clarify this matter. For example, reduction of molecular size fractions with borohydride to yield DOM with the same electron donating or accepting capacity would allow examination based solely on molecular size. Conversely, chemically modifying the same molecular fraction, or bulk DOM sample, via chemical or electrochemical oxidation or reduction would provide insight into the effects of chemical composition. In the context of natural systems, knowing the molecular size of the DOM in the system should provide a good surrogate to the expected steady-state concentrations of

reactive intermediates and thus provide estimations of indirect organic pollutant degradation rates.

6. Acknowledgements

The authors gratefully acknowledge financial support from the United States National Science Foundation (CBET #1235288). The authors also acknowledge Simón Mostafa for reviewing the manuscript.

Captions

Figure 1. Simplified Jablonski diagram representing the photophysical processes possible for DOM.
Figure 2. Maximum absorption coefficients (units of $M^{-1}cm^{-1}$) for acetone and 3-buten-2-one.

Figure 3. Calculation of maximum absorption wavelength for a typical DOM moiety based on empirical rules for benzoyl derivatives.
Figure 3. Calculation of maximum absorption wavelength for a typical DOM moiety based on empirical rules for benzoyl derivatives.
Figure 5. Quantum yields for the formation of reactive intermediates ($^1O_2$, ^{3}DOM*, $HO^{\bullet}$), for different size fractions normalized to the values of the unfractionated samples of SRNOM and Boulder Waste Water (BWW) sample. Quantum yields are reported as % to facilitate the display of the data. Figure adapted from Mostafa et al. 2014.[44]

Figures

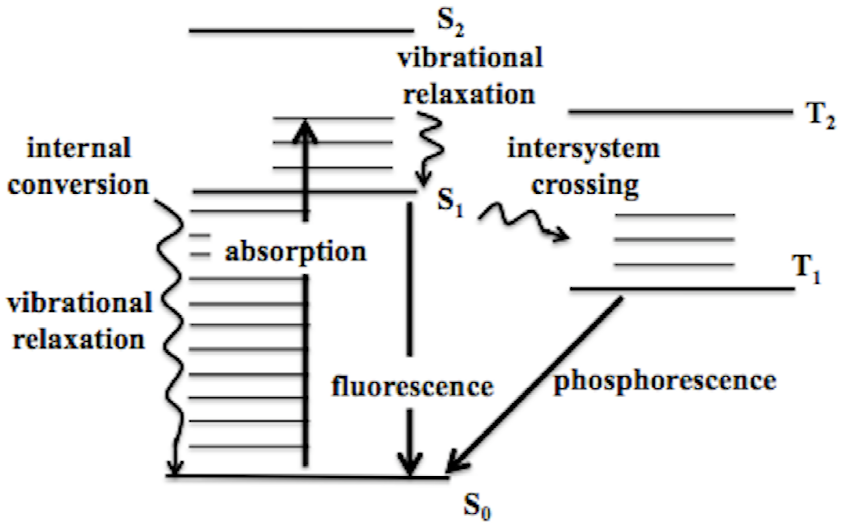

Figure 1. Simplified Jablonski diagram representing the photophysical processes possible for DOM.

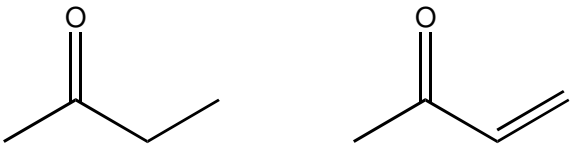

$\pi \longrightarrow \pi^*$	$\varepsilon_{189nm} = 900$	$\varepsilon_{213nm} = 7100$
$n \longrightarrow \pi^*$	$\varepsilon_{280nm} = 12$	$\varepsilon_{320nm} = 27$

Figure 2. Maximum absorption coefficients (units of $M^{-1}cm^{-1}$) for acetone and 3-buten-2-one.

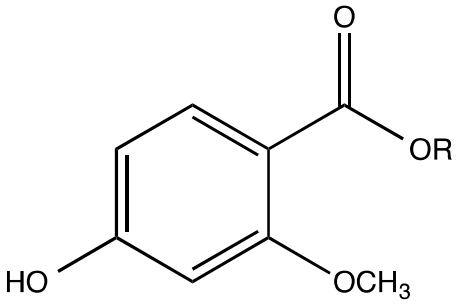

λ_{max} = 230 nm (parent chromophore) + 25 nm (*p*-OH) + 7 nm (*m*-OCH_3) = 262 nm

Figure 3. Calculation of maximum absorption wavelength for a typical DOM moiety based on empirical rules for benzoyl derivatives.

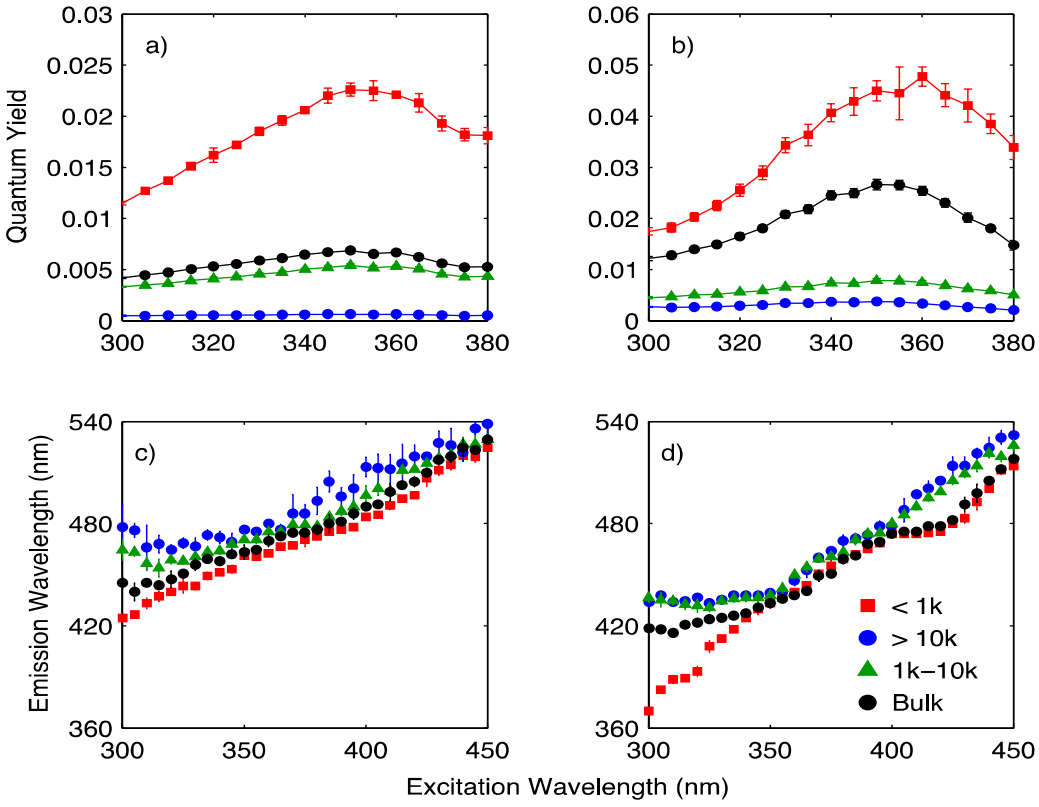

Figure 4. Fluorescence quantum yields as a function of excitation wavelength is presented for each size fraction in a) SRNOM and b) Boulder Waste Water (BWW). Peak emission wavelength as a function of excitation wavelength is depicted for each size fraction for c) SRNOM and d) BWW. Figure taken from Mostafa et al.[44]

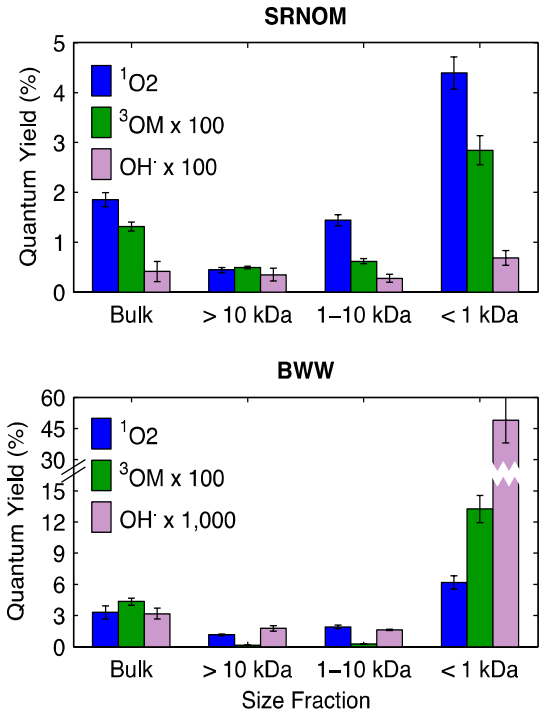

Figure 5. Quantum yields for the formation of reactive intermediates ($^1O_2$, ^{3}DOM*, $HO^{\bullet}$), for different size fractions normalized to the values of the unfractionated samples of SRNOM and Boulder Waste Water (BWW) sample. Quantum yields are reported as % to facilitate the display of the data. Figure adapted from Mostafa et al. 2014.[44]

7. References

1. J. I. Hedges and R. G. Keil, *Marine Chemistry*, 1995, **49**, 81–115.
2. J. I. Hedges, R. G. Keil, and R. Benner, *Organic geochemistry*, 1997, **27**, 195–212.
3. J. A. Leenheer and J.-P. Croué, *Environmental Science & Technology*, 2003, **37**, 18A–26A.
4. D. M. McKnight, E. W. Boyer, P. K. Westerhoff, P. T. Doran, T. Kulbe, and D. T. Andersen, *Limnology and Oceanography*, 2001, **46**, 38–48.
5. Y. Yamashita, R. Jaffé, N. Male, and E. Tanoue, *Limnology and Oceanography*, 2008, **53**, 1900.
6. M. Tzortziou, P. J. Neale, C. L. Osburn, J. P. Megonigal, N. Maie, and R. Jaffé, *Limnology and Oceanography*, 2008, **53**, 148.
7. H. K. Shon, S. Vigneswaran, and S. A. Snyder, *Critical reviews in environmental science and technology*, 2006, **36**, 327–374.
8. G. J. Mulder, *J. Prakt. Chem.*, 1840, **21**, 321–370.
9. A. KROGH and A. KEYS, 1934.
10. D. W. Menzel and R. F. Vaccaro, *Limnology and Oceanography*, 1964, **9**, 138–142.
11. C. Steinberg, *The Lakes Handbook: Limnology and Limnetic …*, 2008.
12. F. J. Stevenson, 1994.
13. E. Namkung and B. E. Rittmann, *Water Res.*, 1986.
14. D. J. Barker and D. C. Stuckey, *Water Res.*, 1999.
15. J. E. Grebel, J. J. Pignatello, and W. A. Mitch, *Environmental Science & Technology*, 2010, **44**, 6822–6828.
16. F. L. Rosario-Ortiz, S. P. Mezyk, D. F. R. Doud, and S. A. Snyder, *Environmental Science & Technology*, 2008, **42**, 5924–5930.
17. O. S. Keen, G. McKay, S. P. Mezyk, K. G. Linden, and F. L. Rosario-Ortiz, *Water Res.*, 2014, **50**, 408–419.
18. P. G. Coble, *Marine Chemistry*, 1996, **51**, 325–346.
19. C. A. Stedmon, S. Markager, and R. Bro, *Marine Chemistry*, 2003, **82**, 239–254.
20. R. Jaffé, K. M. Cawley, and Y. Yamashita, in *ACS Symposium Series*, ed. F. L. Rosario-Ortiz, American Chemical Society, Washington, DC, 2014, vol. 1160, pp. 27–73.
21. A. C. Stenson, A. G. Marshall, and W. T. Cooper, *Anal. Chem.*, 2003, **75**, 1275–1284.
22. R. L. Sleighter and P. G. Hatcher, *Marine Chemistry*, 2008, **110**, 140–152.
23. A. Stubbins, E. Hood, P. A. Raymond, G. R. Aiken, R. L. Sleighter, P. J. Hernes, D. Butman, P. G. Hatcher, R. G. Striegl, P. Schuster, H. A. N. Abdulla, A. W. Vermilyea, D. T. Scott, and R. G. M. Spencer, *Nature Geosci*, 2012, **5**, 198–201.
24. N. Hertkorn, R. Benner, M. Frommberger, P. Schmitt-Kopplin, M. Witt, K. Kaiser, A. Kettrup, and J. I. Hedges, *Geochimica et Cosmochimica Acta*, 2006, **70**, 2990–3010.
25. N. Maie, K. J. Parish, A. Watanabe, H. Knicker, R. Benner, T. Abe, K. Kaiser, and R. Jaffé, *Geochimica et Cosmochimica Acta*, 2006, **70**, 4491–4506.
26. H. Knicker, R. Nikolova, D. P. Dick, and R. S. D. Dalmolin, *Geoderma*, 2012, **181-182**, 11–21.
27. N. Hertkorn, M. Harir, B. P. Koch, B. Michalke, and P. Schmitt-Kopplin, *Biogeosciences*, 2013, **10**, 1583–1624.
28. E. C. Minor, M. M. Swenson, B. M. Mattson, and A. R. Oyler, *Environ. Sci.: Processes Impacts*, 2014, **16**, 2064.

29. M. Gonsior, M. Zwartjes, W. J. Cooper, W. Song, K. P. Ishida, L. Y. Tseng, M. K. Jeung, D. Rosso, N. Hertkorn, and P. Schmitt-Kopplin, *Water Res.*, 2011, **45**, 2943–2953.
30. L. Y. Tseng, M. Gonsior, P. Schmitt-Kopplin, W. J. Cooper, P. Pitt, and D. Rosso, *Environmental Science & Technology*, 2013, 130827102639005.
31. S. Tang, Z. Wang, Z. Wu, and Q. Zhou, *Journal of Hazardous Materials*, 2010, **178**, 377–384.
32. S. M. Louie, R. D. Tilton, and G. V. Lowry, *Environmental Science & Technology*, 2013, **47**, 4245–4254.
33. M. M. Dong, S. P. Mezyk, and F. L. Rosario-Ortiz, *Environmental Science & Technology*, 2010, **44**, 5714–5720.
34. C. S. CRONAN and G. R. AIKEN, *Geochimica et Cosmochimica Acta*, 1985, **49**, 1697–1705.
35. M. H. B. Hayes, P. MacCarthy, R. L. Malcolm, and R. S. Swift, *Humic substances II. In search of structure*, John Wiley & Sons Ltd, 1989.
36. Y.-P. Chin, G. Aiken, and E. O'Loughlin, *Environmental Science & Technology*, 1994, **26**, 1853–1858.
37. S. A. Visser, *Plant and Soil*, 1985, **87**, 209–221.
38. D. B. Wagoner, R. F. Christman, G. Cauchon, and R. Paulson, *Environmental Science & Technology*, 1997, **31**, 937–941.
39. M. Ghassemi and R. F. Christman, *Limnol. Oceanogr.*, 1968, **13**, 583.
40. J. Shapiro, *Journal (American Water Works Association)*, 1964, **56**, 1062–1082.
41. J. H. Reuter and E. M. Perdue, *Geochimica et Cosmochimica Acta*, 1977, **41**, 325–334.
42. E. M. Perdue and J. D. Ritchie, *Dissolved organic matter in freshwaters*, Elsevier Amsterdam, Netherlands, 2003, vol. 5.
43. S. Mostafa and F. L. Rosario-Ortiz, *Environmental Science & Technology*, 2013, 130712160648005.
44. S. Mostafa, J. A. Korak, K. Shimabuku, C. M. Glover, and F. L. Rosario-Ortiz, in *ACS Symposium Series*, American Chemical Society, Washington, DC, 2014, vol. 1160, pp. 159–179.
45. C. Richard, O. Trubetskaya, O. Trubetskoj, O. Reznikova, G. Afanas'eva, J. P. Aguer, and G. Guyot, *Environmental Science & Technology*, 2004, **38**, 2052–2057.
46. A. Bricaud, A. Morel, and L. Prieur, *Limnol. Oceanogr.*, 1981, **26**, 43–53.
47. Z.-D. Wang, B. C Pant, and C. H Langford, *Analytica Chimica Acta*, 1990, **232**, 43–49.
48. C. M. Sharpless and N. V. Blough, *Environ. Sci.: Processes Impacts*, 2014, **16**, 654.
49. S. Canonica, B. Hellrung, and J. Wirz, *J. Phys. Chem. A*, 2000, **104**, 1226–1232.
50. S. Canonica, B. Hellrung, P. Müller, and J. Wirz, *Environmental Science & Technology*, 2006, **40**, 6636–6641.
51. S. Canonica, *CHIMIA*, 2007, **61**, 641–644.
52. E. S. Boyle, N. Guerriero, A. Thiallet, R. D. Vecchio, and N. V. Blough, *Environmental Science & Technology*, 2009, **43**, 2262–2268.
53. H. Mikawa, K. Sato, C. Takasaki, and K. Ebisawa, *Bulletin of the Chemical Society of Japan*, 1956, **29**, 245–254.
54. J. R. Helms, A. Stubbins, J. D. Ritchie, E. C. Minor, D. J. Kieber, and K. Mopper, *Limnol. Oceanogr.*, 2008, **53**, 955–969.
55. E. Lee, C. M. Glover, and F. L. Rosario-Ortiz, *Environmental Science & Technology*, 2013, **47**, 12073–12080.

56. A. Piccolo, *Soil Science*, 2011, **166**, 1–23.
57. J. Ma, R. Del Vecchio, K. S. Golanoski, E. S. Boyle, and N. V. Blough, *Environmental Science & Technology*, 2010, **44**, 5395–5402.
58. R. M. Dalrymple, A. K. Carfagno, and C. M. Sharpless, *Environmental Science & Technology*, 2010, **44**, 5824–5829.
59. R. Del Vecchio and N. V. Blough, *Environmental Science & Technology*, 2004, **38**, 3885–3891.
60. J. B. Birks, *Photophysics of aromatic molecules*, John Wiley & Sons Ltd, 1970.
61. N. J. Turro, V. Ramamurthy, and J. C. Scaiano, *Modern Molecular Photochemistry of Organic Molecules*, University Science Books, Sausalito, California, 2012.
62. S. Canonica and H.-U. Laubscher, *Photochem. Photobiol. Sci.*, 2008, **7**, 547.
63. G. S. Furman and W. F. Lonsky, *Journal of Wood Chemistry and Technology*, 1988, **8**, 165–189.
64. C. M. Glover and F. L. Rosario-Ortiz, *Environmental Science & Technology*, 2013, **47**, 13949–13956.
65. J. J. Mobed, S. L. Hemmingsen, J. L. Autry, and L. B. McGown, *Environmental Science & Technology*, 1996, **30**, 3061–3065.
66. H. Xu, W. J. Cooper, J. Jung, and W. Song, *Water Res.*, 2011, **45**, 632–638.
67. M. M. Dong, R. Trenholm, and F. L. Rosario-Ortiz, *Journal of Hazardous Materials*, 2014.
68. A. Bruccoleri, C. Langford, and C. Arbour, *Env. Tech.*, 1990, **11**, 169–172.
69. A. A. Lamola and G. S. Hammond, *J. Chem. Phys.*, 1965, **43**, 2129.
70. A. M. Fischer, D. S. Kliger, J. S. Winterle, and T. Mill, *Chemosphere*, 1985, **14**, 1299–1306.
71. J. F. Power, D. K. Sharma, C. H. Langford, R. Bonneau, and J. Joussot-Dubien, *Photochemistry and Photobiology*, 1986, **44**, 11–13.
72. B. A. Cottrell, S. A. Timko, L. Devera, A. K. Robinson, M. Gonsior, A. E. Vizenor, A. J. Simpson, and W. J. Cooper, *Water Res.*, 2013, **47**, 5189–5199.
73. G. V. Buxton, C. L. Greenstock, W. P. Helman, A. B. Ross, and W. Tsang, *J. Phys. Chem. Ref. Data*, 1988, **17**, 513.
74. R. G. Zepp, N. L. WOLFE, G. L. BAUGHMAN, and R. C. HOLLIS, *Nature*, 1977, **267**, 421–423.
75. P. P. Vaughan and N. V. Blough, *Environmental Science & Technology*, 1998, **32**, 2947–2953.
76. A. Pochon, P. P. Vaughan, D. Gan, P. Vath, N. V. Blough, and D. E. Falvey, *J. Phys. Chem. A*, 2002, **106**, 2889–2894.
77. D. Gan, M. Jia, P. P. Vaughan, D. E. Falvey, and N. V. Blough, *J. Phys. Chem. A*, 2008, **112**, 2803–2812.
78. S. E. Page, W. A. Arnold, and K. McNeill, *Environmental Science & Technology*, 2011, **45**, 2818–2825.
79. N. V. Blough and R. G. Zepp, *Active Oxygen in Chemistry*, 1995, **2**, 280–333.
80. K. M. Parker, J. J. Pignatello, and W. A. Mitch, *Environmental Science & Technology*, 2013, **47**, 10987–10994.
81. R. G. Zepp, P. F. Schlotzhauer, and R. M. Sink, *Environmental Science & Technology*, 1985, **19**, 74–81.
82. W. R. Haag, J. R. Hoigne, E. Gassman, and A. M. Braun, *Chemosphere*, 1984, **13**, 641–

650.
83. B. M. Peterson, A. M. McNally, R. M. Cory, J. D. Thoemke, J. B. Cotner, and K. McNeill, *Environmental Science & Technology*, 2012, **46**, 7222–7229.
84. K. Mopper and X. Zhou, *Science*, 1990, **250**, 661–664.
85. D. Vione, G. Falletti, V. Maurino, C. Minero, E. Pelizzetti, M. Malandrino, R. Ajassa, R.-I. Olariu, and C. Arsene, *Environmental Science & Technology*, 2006, **40**, 3775–3781.
86. M. M. Dong and F. L. Rosario-Ortiz, *Environmental Science & Technology*, 2012, **46**, 3788–3794.
87. C. M. Sharpless, *Environmental Science & Technology*, 2012, **46**, 4466–4473.
88. W. R. HAAG and J. HOIGNE, *Environmental Science & Technology*, 1986, **20**, 341–348.
89. G. McKay, M. M. Dong, J. L. Kleinman, S. P. Mezyk, and F. L. Rosario-Ortiz, *Environmental Science & Technology*, 2011, **45**, 6932–6937.
90. D. E. Latch and K. McNeill, *Science*, 2006, **311**, 1743–1747.
91. J. Wenk, S. N. Eustis, K. McNeill, and S. Canonica, *Environmental Science & Technology*, 2013, **47**, 12802–12810.
92. P. Westerhoff, S. P. Mezyk, W. J. Cooper, and D. Minakata, *Environmental Science & Technology*, 2007, **41**, 4640–4646.
93. R. M. Cory, J. B. Cotner, and K. McNeill, *Environmental Science & Technology*, 2009, **43**, 718–723.

Chapter 6

Excitation Emission Matrices of Fluorescence - EEMF - For The Characterization of Organic Matter of Surface Waters

*CHRISTIAN COELHO [*1] AND GHISLAIN GUYOT [2,3]*

[1] UMR PAM Université de Bourgogne, AgroSupDijon, Institut Universitaire de la Vigne et du Vin, Jules Guyot, DIJON, France

[2] Université Clermont Auvergne, Université Blaise Pascal, Institut de Chimie de Clermont-Ferrand, BP 10448, F-63000 CLERMONT-FERRAND, France

[3] CNRS, UMR 6296, ICCF, F-63171 AUBIERE, France

*Corresponding author Email: christian.coelho@u-bourgogne.fr

ABSTRACT

Excitation Emission Matrices - EEMs - are three-dimensional representations of the total emissive light in terms of intensity and diversity of emission wavelengths one sample can gather when irradiated in a fixed range of excitation wavelength, generally between 200 nm and 700 nm. Excitation Emission Matrices of Fluorescence - EEMF - is an analytical tool of choice when investigating chromophoric complex systems made of several chemical compounds, as those of Dissolved Organic Matter - DOM - in surface waters.

The characterization of DOM via EEMF is non invasive and easily implementable in field sampling, making it more and more used. Additionally EEMF can inform on chemical composition of DOM, dissociate autochthonous from allochthonous organic matter production, visualize biological activities and investigate colloidal and particulate organic matter. Transept sampling approaches along watersheds enable to study DOM dynamics as well biotic (macrophyte inputs, phytoplankton blooms) as abiotic processes (photoprocesses, mineralization, water fluxes). When EEMF is coupled to data processing algorithms, like PARAFAC, hidden features from the temporal and spatial variability of DOM composition in surface waters can be revealed.

In order to go deeper in the study of molecular composition of fluorophores in DOM samples, EEMF could also be coupled with orthogonal analytical tools like ultra-high resolution mass spectrometry or nuclear magnetic resonance. Such strategy should in the future enable to target a set of chemical moieties or families responsible for DOM's cycling and reactivity, and strengthen the powerfulness of EEMF by increasing our knowledge on the fluorescent fingerprint gathered in a single EEM.

Table of Contents

1. INTRODUCTION

When studying surface water chemistry, fluorescence techniques are precious tools that have been widely used since they provide a wealth of biological and chemical information. Fluorescence spectroscopy was applied in the field of soil chemistry between the 1950's and 1970's thanks to emission/excitation and synchronous scan spectra [1-3] in order to discriminate between the various kinds of soil organic matter and to study their binding to metallic ions. In the 2000's, the first reports of Excitation-Emission Matrices (EEMs) appeared in the studies of the aquatic environment. Excitation-Emission Matrix Fluorescence (EEMF) allows evaluation of the quality of chromophoric dissolved organic matter (CDOM), differentiation of the colloidal from the dissolved organic matter, exploration of the dissolved organic matter (DOM) dynamics, traceability of an organic pollutant from the source, and optimization of the disinfection processes in water treatment plants.

CDOM originates from terrestrial, atmospheric and autochthonous sources, which are related to landscape (grassland, peatland, forest), hydrology (river flow, runoff, snowmelt) and anthropogenic activities (agriculture, industries) [4].

The fluorescence of DOM is widely reviewed in marine ecosystems as well as freshwaters and water treatment systems [5-11]. In this review, we will focus on the natural dissolved organic matter present in surface waters and on its characterization by EEMF, including the biotic and abiotic processes occurring in DOM that affect EEMs, the applications of chemometrics to a large set of EEM spectra and the future of EEMF in surface water chemistry to characterize the photoactive material.

2. EEMF AMONG FLUORESCENCE TECHNIQUES

Steady-state or time resolved measurements are used to determine spectroscopic characteristics of the fluorescence emission of a molecule (spectrum, fluorescence quantum yield and lifetime) [10, 12]. Steady-state measurements are the most easily implemented in scientific data. They are performed with a conventional spectrofluorimeter using a constant illumination and detection. The sample is excited with a continuous beam of light, generally produced from a xenon arc pulsed lamp and the intensity of the emission is detected by means of photomultiplier tubes or charge-

coupled devices. The excitation and emission wavelengths are chosen by the user according to the spectrum to be measured. In fact, emission, excitation and synchronous scan spectra can be collected, respectively by the measurement of the fluorescence intensity (i) at a fixed excitation wavelength and for a selected emission wavelength range, or (ii) at a fixed emission wavelength and a selected excitation wavelength, or (iii) by varying the excitation and emission wavelengths simultaneously, with an off-set wavelength of 20-30 nm.

These three types of measurements have been used in the study of the fluorescence of organic matter for specific applications such as the determination of the nature of DOM and the possible interactions with organic contaminants or trace metals [13-20].

Only a small fraction of the bulk DOM sample is investigated with these techniques. However, when studying DOM dynamics and biogeochemical cycles, all the fluorescence information should be exploited. Therefore, the total emission fluorescence spectra (that is EEM), flourished in the scientific community and particularly in the field of aquatic sciences, to obtain a more holistic view of ecosystems [21-25]. An EEM is a three-dimensional fluorescence picture, obtained for a range of emission wavelengths when excited at multiple wavelengths, as shown in the Figure 1. The x-axis and y-axis are respectively the range of excitation and emission scanned, while the z-axis represents the intensity of the emitted light symbolized by a chosen scale colour.

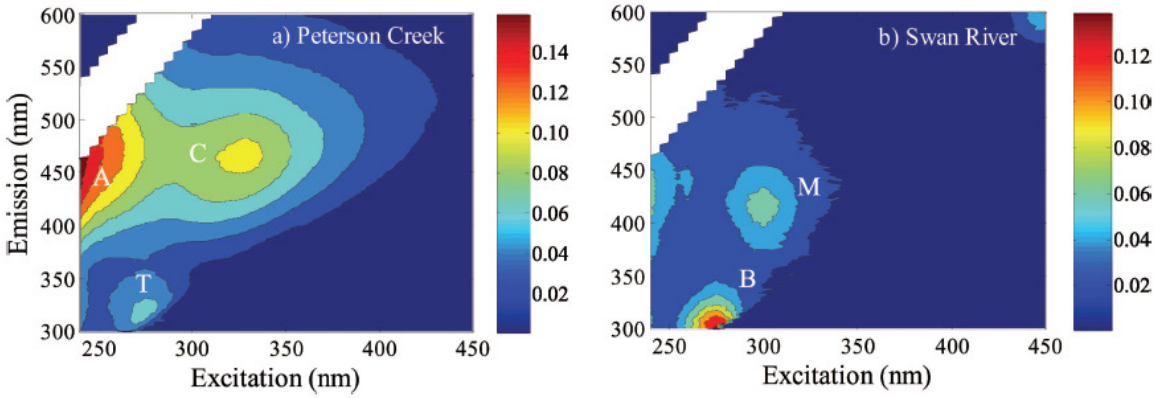

Figure 1 : Example of two EEMs from aqueous samples from (a) Peterson Creek, Juneau, Alaska and (b) Swan River, Perth, Australia, adapted from [7]. Letters A, B, C, M and T indicate the aquatic fluorophores as described in Table 1.

3. EEMF AS A TOOL TO STUDY CHROMOPHORIC DISSOLVED ORGANIC MATTER IN SURFACE WATERS

3.1. The chemical composition of fluorescent chromophoric dissolved organic matter

Surface waters (wetlands, springs, ponds, lakes, rivers, tributaries and estuaries) are rich in organic carbon constituents coming from dissolution, leaching or deposition of terrestrial and atmospheric organic matter[4, 26-28]. This organic matter is a complex macromolecular network made of ligno-cellulosic plant residues associated to organic compounds and other biomacromolecules such as proteins and lipids. The amount of DOM found in aquatic systems is quantified by the dissolved organic carbon (DOC), approximatively spanning from <1 $mg.L^{-1}$ to 20 $mg.L^{-1}$ or above [29-32]. Higher values of DOC are generally attributed to pollution events, as for untreated sewage waters. Variations of DOC levels show a good correlation with absorption parameters like the absorption coefficients and the spectral slope coefficients as defined in 2002 by Zepp et al. [31, 33].

Among the chromophoric dissolved organic matter, some chemical units have the ability to fluoresce. They include tyrosine and tryptophan moieties, phenolic structures as well as more condensed macromolecules, deriving from the fulvic and humic acids encountered in soils. They are denominated fulvic-like and humic-like structures. Such subunits, particularly the fulvic-like units [29], have been well correlated to DOC in freshwater samples.

With EEMs, all these aquatic fluorophores can be qualitatively and quantitatively visualized at a glance on EEMs. Their fluorescence parameters are listed in Table 1, as initially proposed [34, 35] by Coble (1996) and Parlanti (2000).

Table 1 : Aquatic Fluorophores found in EEMFs

Fluorophore according to [34]	Fluorophore according to [35]	λ_{ex} / nm	λ_{em} / nm	Fluorophore constituents
B	γ	275	310	Tyrosine-like
T	δ	275	340	Tryptophan-like
A	α’	260	380-460	Humic & Fulvic (terrestrial)
M	β	310-320	380-420	Humic (marine or autochthonous)
C	α	330-350	420-480	Humic & Fulvic (terrestrial)

EEMF has been developed in order to track the various kinds of dissolved organic matter in aquatic environments [36]. Optical measurements, and particularly fluorescence of humic-like structures were directly linked to their aromatic content [37].

3.2. Fluorescence indices for the interpretation of fluorescence data

In the same way as absorption parameters have been used to assess various kinds of DOM, fluorescence indices were developed specifically for aquatic environments. Even if these indices are helpful for data interpretation, they were used for specific aqueous compartments and much attention should be taken when expanding their use to other water environments.

Fluorescence indices represent generally the ratio of fluorescence intensities at specific analysed wavelengths. Mc Knight et al. (2001) have developed, for her research on rivers and lakes the fluorescence index (FI) that represents the ratio of emission intensities (450 nm / 500 nm) and characterizes the slope of the emission curve at an excitation of 370 nm [37]. The FI values determine the microbial or the terrestrial precursors of dissolved organic matter. The higher the FI value is (around 2.0) the higher the microbial activity that has produced aquatic organic matter. FI should be interpreted carefully when monitoring DOM cycling in estuaries [38], mangrove environments[39] and marine samples[40] due to other interfering physical-chemical processes (salinity, flocculation, water mixing, influence of marine/microbially-derived DOM).

In other cases, these indices are calculated in specific areas of the EEMs, like the humification index HIX and the freshness index BIX. The humification index HIX was introduced by Zsolnay et al. (1999). HIX is calculated as the ratio of the area 435-480 nm of the emission spectrum to the area 300-345 nm for an excitation wavelength set at 254 nm [41]. HIX represents the degree of humification of aqueous soil extracts.

Parlanti et al. (2000) calculated the freshness index BIX as the ratio of the intensities between the β peak and the α peak [35]. It represents the input of microbial organic matter compared to more decomposed organic matter. BIX is useful for determining rivers and tributaries inputs for estuaries and marine environments (Figure 1). An increase in the BIX value up to 0.9 for salinity values higher than 25, associated to the decrease of HIX, could be associated to a change of organic matter and a terrestrial organic matter removal source. Abiotic processes (water mixing area or photodegradation area) or

biological productivity, or combined abiotic and biotic processes could explain the evolution of these indices.

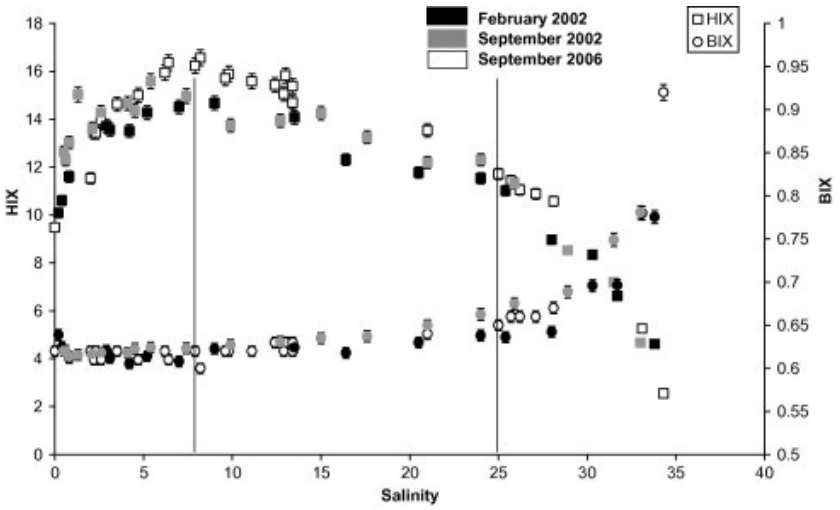

Figure 2 : Humification index (HIX) and the recent autochthonous contribution index (BIX) in an estuary environment (Gironde, France), adapted from [38]

An interesting volumetric integration under the five excitation emission regions of EEM has been suggested by Chen et al. (2003) for DOM fractions, marine water and freshwaters [42]. This regional integration enabled to dissociate the different forms of hydrophobic and hydrophilic DOM fractions.

A redox index was recently proposed by Miller et al. (2006). They compared the reduced quinone-like moieties to the total quinone-like input from specific fluorescent components obtained after a trilinear decomposition of EEMs [43, 44]. The redox index requires the statistical treatment of a large amount of EEMs, and it should be promising for understanding DOM redox states and the ability of DOM to produce e.g. disinfection by-products upon water treatment [45].

3.3. The fluorescence of colloidal organic matter

As proposed by Piccolo in 2001, humic substances can be viewed as supramolecular structures [46]. The first fractionation applied to natural organic matter (NOM) was the distinction between humic and fulvic acid, based on the difference of solubility in an acidic medium. Humic acid is insoluble at pH < 2 and fulvic acid is totally solubilised whatever the pH [47, 48]. Fractionation studies gained interest in the scientific community in order to inspect the colloidal organic matter in surface waters, using size exclusion

chromatography [21, 49-54], flow field fractionation [55-58], hydrophobic/hydrophilic resins [52, 59-62] and ultrafiltration [63-70].

There has been an increased interest to separate colloidal organic matter as a function of its hydrophobic/hydrophilic properties. Such separation can be performed after an acidification step, through XAD resins and acidic elution [59, 60]. Hydrophobic fractions present quantifiably larger overall fluorescence in riverine DOM, according to the EEMF volumetric integration proposed by Chen et al. (2003). ^{13}C NMR data suggest that these hydrophobic fractions have higher aromatic carbon content, too [42]. The Hydrophobic Organic Acid fraction (HPOA) has been used as a good proxy for differentiating CDOM terrestrial sources from autochthonous (algal, microbial) or photodegraded DOM [71].

Ultrafiltration is another fractionation tool used to concentrate DOM and remove water molecules and salts. Ultrafiltration requires membranes with specific molecular cut-offs. The cut-off range included between 0.5 and 5 kDa is generally used to differentiate the colloidal organic matter from the low molecular weight compounds. The combination of ultrafiltration with EEMF allows the detection and the isolation of fluorophores, which could not be achieved without the fractionation step. Ultrafiltration was performed on water from Amazonian rivers. Aquatic fluorophores A and C were present in all fractions and fluorophore C, generally attributed to higher molecular weight compounds, was preferentially retained with 5 kDa cut-off [63, 66]. The marine fluorophore M was present in the lowest size fraction (MW < 500 Da) [69]. In USA rivers from southeastern Georgia it has been observed that size distribution could affect the spectroscopic patterns (peak position and fluorescence intensity) [65].

Even if some spectroscopic shifts have been noticed with aquatic DOM fractions obtained via size exclusion chromatography (SEC) too, the similarity of the distribution of the fluorophores, especially peak A and C, is evident [21]. SEC presents the advantage to couple multiple spectroscopic detectors [49, 50]. It can inform on specific interactions, by interpreting the chromatographic behaviour. However, a major drawback is the hydrophobic interaction of DOM constituents with the stationary phase [49]. Interactions with metals have also been investigated [51]. A recent study consisting in measuring EEMs of surface fresh waters fractions obtained by SEC concluded that fluorescent moieties

are present in all the molecular weight continuum of DOM, which is in total agreement with the hypothesis of the supramolecular structure [54].

Field-Flow Fractionation (FFF) presents the advantage to avoid hydrophobic interactions with DOM. It was applied to follow two fluorescent colloidal fractions (around 2 kDa and 13 kDa) and it discerned DDOM inputs and photochemical processes from two southwestern Florida rivers [55]. Two colloid sizes have also been found in coastal waters, spanning at 1-5 kDa and 15-150 kDa. EEMF reveals that proteinaceous material dominates the smallest fraction and humic-like compounds mostly contribute to the larger one [56]. FFF brought new insights in the characterization and localization of fluorophores and chromophores in DOM from Canadian freshwaters [58].

Although fractionation techniques enable a better understanding of the aquatic fluorophores in DOM, unfractionated samples offer a more complete characterization of DOM molecular signatures. EEMs remain a valuable analytical tool for chemical fingerprinting of bulk DOM samples, evaluating biotic and abiotic processes involving fluorescent compounds.

4. DOM DYNAMICS ASSESSED BY EEMF

DOM in aqueous compartments can control ecological processes by influencing pH, it can be a substrate for biological activity [72-74], influence the availability of nutrients [75-78], control geochemical and photochemical reactions [63, 71, 79-86] and interact with trace metals [63, 78, 83, 87-94] and organic pollutants [95-101].

There's a need for developing analytical approaches that inform on both DOM composition and reactivity. Optical measurements have been developed for such purpose. EEMF is ideally suited for the investigation of DOM dynamics and chemical fingerprinting of DOM composition in all aquatic environments [7, 10, 42, 50, 102, 103].

Environmental biotic and abiotic processes can be tracked when looking at EEMs, as shown in the following sections.

4.1. Biotic processes

Biological activity is highlighted by an intense T-peak or a higher contribution of β peak compared to the α peak (elevated BIX value) [35, 38]. Aquatic macrophyte specific fluorophores correspond to the known protein-like peak and to autochthonous fluorescence below 400 nm, when the excitation wavelength is set under 300 nm [104]. Local phytoplankton blooms in some oceanic environments are also easily assessed via EEMF due to their predominant M peak [105]. The fluorescence index (FI) has been correlated to the relative contribution of microbial versus higher plant organic matter [37]. Chromophoric dissolved organic matter has been found to be directly or indirectly produced by marine phytoplankton [106, 107]. These fluorescent exudates, both fluorescent protein-like and marine humic-like material, should participate to surface water DOM biogeochemical dynamics. Phytoplankton can also bloom during the summer period in lakes, altering the DOM fluorophores composition, with a production of non−humic quinone-like and amino acid-like fluorophores [102]. Macrophytes have been shown to produce protein-like fluorescent DOM directly affecting the productivity of watersheds [104].

When looking at biogeochemical cycles, biotic processes cannot generally be distinguished from abiotic processes and particularly from photoprocesses. The microbially-derived non-humic and fulvic acid fractions of the DOM in a lake environment have been found to be associated to photodegraded quinone moieties [108].

4.2. Abiotic processes

One of the most interfering abiotic processes in surface waters is the direct and indirect photoprocesses generated from sunlight exposure [79, 83, 109]. Photoreactions are generally ascertained to induce seasonal variability in DOM [79, 110] or differences in water column composition and reactivity [18, 79]. Photobleaching directly impacts aquatic fluorophores chemistry, and the relevant EEMs are characterized by a reduction of the emission intensity and a blue shift (of the emission wavelength) [83, 111]. Photomineralisation changes the fluorophores matrices by bringing new chemical species such as dissolved inorganic carbon [112, 113] ammonia [114] or labile photoproducts [113]. FA-like fluorophores appeared to be more photodegraded compared with the protein-like fraction. Photosensitized reactions can totally change the reactivity of surface waters by generating transient species [85, 109, 113]. From this point of view, CDOM is a photochemical

source of transients in addition to being one of the substrates on which they act. Fluorescence of CDOM is usually reported to be a good proxy of CDOM photoactivity and it is correlated to singlet oxygen productivity in aquatic systems [115, 116].

Under redox conditions, the amount of DOM electron donating moieties can be tracked by EEMF [43, 117] The distribution between the oxidised and reduced quinones informs on the redox state of DOM samples and explains the variation in the fluorescence index.
DOM redox reactions directly impact the mobilisation, complexation or transport of metal species like arsenic [91] copper [118] mercury [88, 92, 119] or organic pollutants [96-98, 101], which interfere with the global cycling of DOM, and particularly DOM fluorophores.

Water fluxes and salinity gradient are two other abiotic processes that could dilute or otherwise affect aquatic fluorophores, and they are easily tracked in EEMs. It was even shown a reduction in the molecular mass for high salinity environments [120]. DOM is a useful tracer for water mixing in estuaries [38, 95, 121, 122]. Rhone river plumes and mixing in the Marseille bay have been shown to produce a specific biological activity [111]. New loads or fresh organic matter from tributaries can also be detected in river mixings [104, 123].

When studying environmental processes, scientists tend to accumulate a large amount of EEMs in the various sampling areas. In order to treat this large amount of information, chemometrics can help them to discriminate and validate models in large scale experimental fields.

5. EEM-PARAFAC

EEMs can be easily obtained all around the world, in water chemistry laboratories for a large set of samples. However, EEMs require a standardized protocol for each spectral acquisition, including caution for inner filter effects, optical corrections and normalizations [36, 124, 125]. An interlaboratory experiment conducted in 2010 by Murphy et al. [103] showed that EEM data were difficult to compare due to the lack of information on the way EEMs were acquired.

Once these analytical cares are validated, an EEM database can be created gathering as many matrices as sampled. Emission/excitation peak picking is generally the first operation carried out on EEM. This first step is essential for going further, but information contained in EEMs is often under-exploited compared to the potential of the technique. In 1997, Bro exposed a multi-way decomposition methodology, PARAFAC, which consists in a multi-dimensional generalization of the usual principal component analysis [126]. This way of treating data was pioneered by Stedmon et al. in 2003 in aquatic environmental compartments [36]. Since this time a number of scientific papers appeared, which used this methodology in several biological samples [127-129], food beverages [130-134] and environmental samples [4, 36, 102, 135-143].

Once PARAFAC is applied to an EEM database, each EEM is reduced into a set of trilinear terms and a residual matrix, as shown in Figure 3. This method uses an alternating least squares algorithm to minimize the sum of squared residuals in a trilinear model [36, 126, 144]

$$x_{ijk} = \sum_{f=1}^{N} a_{if} b_{jf} c_{kf} + \varepsilon_{ijk} \qquad i = 1,....,I;\ j = 1,....,J;\ k = 1,....,K$$

where x_{ijk} is the fluorescence intensity of the i[th] sample at j[th] emission wavelength and k[th] excitation wavelength. The scores, a_{if}, are directly proportional to the concentration of the f[th] fluorophore in the i[th] sample. The loadings, b_{jf} and c_{kf}, represent respectively emission and excitation spectra for the f[th] fluorophore. The variable, N, represents the number of fluorophores. The residual ε_{ijk} corresponds to the unexplained variation of the PARAFAC model.

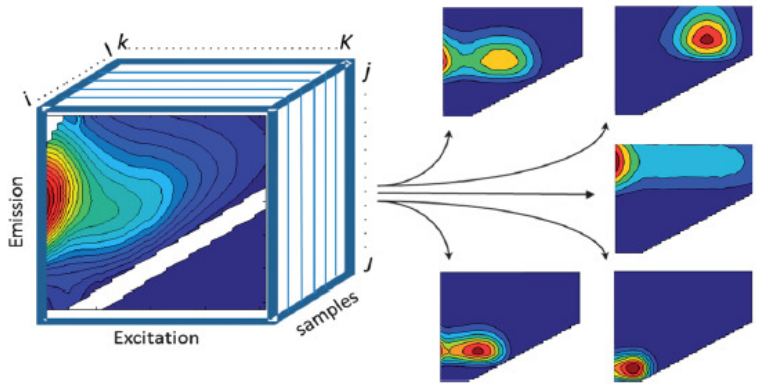

Figure 3 : Multi-way decomposition of EEMs database into five PARAFAC components, adapted from [144].

As a function of the relative abundance of aquatic fluorophores in water samples, a minimum of five PARAFAC components are found to explain the global information

contained in EEMs databases [36, 135, 136, 143, 145]. The number of components can increase up to thirteen under specific red/ox conditions and potential presence of anthropogenic organic pollutants [43, 45, 102, 104, 108].

EEM-PARAFAC enables to gather temporal and spatial variability of DOM composition in surface waters [140, 145-148] which, in the context of global warming, appears to be a crucial step, for collecting historical information on climatic events. These scientific studies highlight DOM sources and sinks, in connection with the local and the global aquatic ecosystems [145]. Hydrological connectivity between water masses can be assessed as well [104] and the transport of DOM components can be followed in a riverine, lacustrine, estuarine and oceanic continuum [38, 149].
The impact of anthropogenic activities can be traced [141, 143, 150-154] with specific PARAFAC components. Biogeochemical changes impact the aquatic fluorophores composition, which could be attributed to specific contributions of anthropogenic relative to autochthonous DOM or to a seasonal effect. The latter issues make the interpretation difficult but they reinforce the powerfulness of PARAFAC treatment to a large set of EEMs, acquired in the spatio-temporal context of DOM dynamics.

Climatic events (flooding and drought periods, sunlight irradiance, storm/hurricane events) affect the aquatic fluorescent CDOM quality and quantity in water reservoirs [138, 155, 156]. For instance, the contribution of humic-like substances to CDOM in Lake Tianhmuhu in China appears to be higher in wet seasons, characterized by an elevated frequency of rainfall and runoff, compared to the proteinaceous components [138].

6. CAN EEMF BRING NEW INSIGHTS INTO DOM CHEMICAL DIVERSITY?

EEM measurements boomed in the past decades as they allow since global information on aquatic fluorophores to be gathered thanks to an untargeted approach. They are presently inseparable from the investigation of biogeochemical cycles in all water compartments. Statistical deconvolution of the original signal enables interpretation and explanation of biotic and abiotic processes occurring in aqueous continuums. The parallel factor analysis, PARAFAC, is the nowadays-privileged signal processing method.

Other statistical treatments have been recently applied to dissolved organic matter, including self-organising maps (SOM) and correlation analysis [157, 158] or independent component analysis [159, 160]. The combination of PARAFAC and SOM clarifies pH-induced changes in DOM [158]. The use of SOM and artificial neural networks for the decomposition of EEMs appears to be helpful in the monitoring of organic matter removal in wastewater treatment processes [161, 162]. Independent component analysis presents the advantage of classifying the constitutive components of EEM matrices of removing interfering fluorescent components, facilitating a future characterization of aquatic fluorophores [159].

For a better knowledge of fluorescent dissolved aquatic matter, EEMs are acquired concomitantly with ultra-high resolution mass spectrometry, thereby getting a global overview of aquatic DOM complexity [163-167].

A Spearman rank correlation between PARAFAC components intensities and FTICR-MS peak intensities has been proposed to discriminate the variations of fluorescent DOM pool constituents [164, 165, 167]. Humic-like fluorophores (peak A) appeared to be made of compounds rich in oxygen, with a relatively high double bond equivalent. The molecular formula $C_{17}H_{14}O_{11}$ presents an elevated Pearson correlation level [165]. Such observation means that this hypothetical isomer presents common seasonal and spatial covariations in water reservoirs under environmental conditions.

Another big step that is being made and that will increase in the next years is the use of EEMF in aquatic ecosystems to track the fluorescing components as well as the non-fluorescing families that should evolve with similar variations, presenting common sinks, productions or transports in ecosystems [167]. It was shown that non coloured and photo-labile aliphatics (carboxylic-rich alicyclic molecules) co-vary in the same manner as actual known fluorophores present in the Congo River, when the river water was photo-irradiated [163]. Such observation surely requires more research but it is evident that future studies should integrate these kinds of orthogonal analytical tools in order to go further in the knowledge concerning the links between aquatic fluorophores and their environment. When orthogonal tools (fluorescence, nuclear magnetic resonance, mass spectrometry, X-ray photoelectron spectroscopy, direct scan voltammetry) are used, it is possible to highlight some DOM organic moieties facilitating electron transfer reactions. This is of fundamental importance in DOM cycling and reactivity problems [168].

The dynamics of DOM fluorophores are not totally understood, especially under extreme conditions [109, 141, 166]. EEMF has brought new insights in chemical processes involving N and S compounds produced by specific microbial activity in an arctic lake [166] or new photoactive compounds presenting a high degree of transients species production on Antarctic waters [109]. The links between all the ecosystems parameters (microbiology, topology and hydrology) should be taken into account to go further in the DOM cycling understanding [141].

Another challenge that should emerge in the future is the detection of untargeted compounds that could reach surface waters, due to their intrinsic fluorescence properties or by their associations to humic compounds. Correlation between elemental formulas and fluorescent PARAFAC components will help in this sense. Recently, the fluorescent humic-like component appeared to be correlated to disinfection by-products content (trihalomethanes and haloacetic acids) due to chlorine reactivity towards DOM [45, 169]. Other emerging pollutants such as benzene or naphthalene-like compounds due to oil spills events [170-172] or oxidant agents (whitening agents, detergents, chlorinated compounds) due to sewage treatments [6, 83, 173] are directly fluorescing components that can reach water systems and change the fluorescence signature of DOM. In a recent study some oil-derived components were still detected, via EEM-PARAFAC, in deep ocean waters, two years after the oil spill in the Gulf of Mexico [172] **.**

EEMF should help in the future to assess the precise impact of these organic molecules on aquatic DOM diversity. An important advantage of EEMF is that it permits a non-invasive, fast and cheap screening of complex systems that should be coupled to other analytical tools dealing with structural aspects.

References

1. M. Levesque, *Soil Sci.*, 1972, 113, 346-353.
2. N. Senesi, T. M. Miano, M. R. Provenzano and G. Brunetti, *Soil Sci.*, 1991, 152, 259-271.
3. K. Kalle, *Deutsche Hydr. Zeits.*, 1949, 2, 117.
4. C. J. Williams, Y. Yamashita, H. F. Wilson, R. Jaffe and M. A. Xenopoulos, *Limnol. Oceanogr.*, 2010, 55, 1159-1171.
5. P. G. Coble, *Chemical Reviews*, 2007, 107, 402-418.
6. N. Hudson, A. Baker and D. Reynolds, *River Research and Applications*, 2007, 23, 631-649.

7. J. B. Fellman, E. Hood and R. G. M. Spencer, *Limnol. Oceanogr.*, 2010, 55, 2452-2462.
8. A. Andrade-Eiroa, M. Canle and V. Cerda, *Appl. Spectrosc. Rev.*, 2013, 48, 1-49.
9. A. Andrade-Eiroa, M. Canle and V. Cerda, *Appl. Spectrosc. Rev.*, 2013, 48, 77-141.
10. P. G. Coble, Lead, J., Baker, A., Reynolds, D.M. and Spencer R.G.M., *Aquatic Organic Matter Fluorescence*, Cambridge University Press, 2014.
11. E. C. Minor, M. M. Swenson, B. M. Mattson and A. R. Oyler, *Environ. Sci.: Processes Impacts*, 2014, DOI: 10.1039/c4em00062e, Ahead of Print.
12. J. R. Lakowicz, *Principles of fluorescence spectroscopy, 3rd Edition, Joseph R. Lakowicz, editor*, Springer Science, 2010.
13. P. G. Coble, S. A. Green, N. V. Blough and R. B. Gagosian, *Nature (London)*, 1990, 348, 432-435.
14. S. A. Green and N. V. Blough, *Limnol. Oceanogr.*, 1994, 39, 1903-1916.
15. B. A. Poulin, J. N. Ryan and G. R. Aiken, *Environ. Sci. Technol.*, 2014, 48, 10098-10106.
16. S. E. Cabaniss and M. S. Shuman, *Mar. Chem.*, 1987, 21, 37-50.
17. M. J. Pullin and S. E. Cabaniss, *Limnol. Oceanogr.*, 1997, 42, 1766-1773.
18. K. Mopper and C. A. Schultz, *Mar. Chem.*, 1993, 41, 229-238.
19. M. Newson, A. Baker and S. Mounsey, *Hydrological Processes*, 2001, 15, 989-1002.
20. A. Baker and J. Lamont-Black, *Ground Water*, 2001, 39, 745-750.
21. J. J. Alberts, M. Takács and P. K. Egeberg, *Organic Geochemistry*, 2002, 33, 817-828.
22. J. J. Alberts and M. Takács, *Organic Geochemistry*, 2004, 35, 243-256.
23. A. Baker, *Environ. Sci. Technol.*, 2002, 36, 1377-1382.
24. E. M. Carstea, A. Baker, G. Pavelescu and I. Boomer, *Hydrological Processes*, 2009, 23, 1937-1946.
25. M. Bieroza, A. Baker and J. Bridgeman, *Sci. Total Environ.*, 2009, 407, 1765-1774.
26. R. M. B. O. Duarte, C. A. Pio and A. C. Duarte, *Anal. Chim. Acta*, 2005, 530, 7-14.
27. H. F. Wilson and M. A. Xenopoulos, *Nat. Geosci.*, 2009, 2, 37-41.
28. N. Mladenov, M. W. Williams, S. K. Schmidt and K. Cawley, *Biogeosciences*, 2012, 9, 3337-3355.
29. S. A. Cumberland and A. Baker, *Hydrological Processes*, 2007, 21, 2093-2099.
30. A. Baker, S. Cumberland and N. Hudson, *Area*, 2008, 40, 117-127.
31. R. G. M. Spencer, P. J. Hernes, R. Ruf, A. Baker, R. Y. Dyda, A. Stubbins and J. Six, *Journal of Geophysical Research: Biogeosciences*, 2010, 115, G03013.
32. R. G. M. Spencer, K. D. Butler and G. R. Aiken, *Journal of Geophysical Research: Biogeosciences*, 2012, 117, G03001.
33. C. Hu, F. E. Muller-Karger and R. G. Zepp, *Limnol. Oceanogr.*, 2002, 47, 1261-1267.
34. P. G. Coble, *Mar. Chem.*, 1996, 51, 325-346.
35. E. Parlanti, K. Worz, L. Geoffroy and M. Lamotte, *Org. Geochem.*, 2000, 31, 1765-1781.
36. C. A. Stedmon, S. Markager and R. Bro, *Mar. Chem.*, 2003, 82, 239-254.
37. D. M. McKnight, E. W. Boyer, P. K. Westerhoff, P. T. Doran, T. Kulbe and D. T. Andersen, *Limnol. Oceanogr.*, 2001, 46, 38-48.
38. A. Huguet, L. Vacher, S. Relexans, S. Saubusse, J. M. Froidefond and E. Parlanti, *Org. Geochem.*, 2009, 40, 706-719.
39. R. Jaffe, J. N. Boyer, X. Lu, N. Maie, C. Yang, N. M. Scully and S. Mock, *Mar. Chem.*, 2004, 84, 195-210.

40. M. Gonsior, B. M. Peake, W. J. Cooper, R. Jaffe, H. Young, A. E. Kahn and P. Kowalczuk, *Aquat. Sci.*, 2008, 70, 397-409.
41. A. Zsolnay, E. Baigar, M. Jimenez, B. Steinweg and F. Saccomandi, *Chemosphere*, 1998, 38, 45-50.
42. W. Chen, P. Westerhoff, J. A. Leenheer and K. Booksh, *Environ. Sci. Technol.*, 2003, 37, 5701-5710.
43. R. M. Cory and D. M. McKnight, *Environ. Sci. Technol.*, 2005, 39, 8142-8149.
44. M. P. Miller, D. M. McKnight, R. M. Cory, M. W. Williams and R. L. Runkel, *Environ. Sci. Technol.*, 2006, 40, 5943-5949.
45. K. M. H. Beggs, R. S. Summers and D. M. McKnight, *J. Geophys. Res., [Biogeosci.]*, 2009, 114, G04001/04001-G04001/04010.
46. A. Piccolo, *Soil Sci.*, 2001, 166, 810-832.
47. Aiken GR, McKnight D, Weshaw RL and M. P., *An introduction to humic substances in soil, sediment and water.*

Humic Substances in Soil, Sediment and Water, John Wiley & Sons: NewYork, 1985.

48. P. MacCarthy, *Spec. Publ. - R. Soc. Chem.*, 2001, 273, 19-30.
49. C. H. Specht and F. H. Frimmel, *Environ. Sci. Technol.*, 2000, 34, 2361-2366.
50. N. Her, G. Amy, D. McKnight, J. Sohn and Y. Yoon, *Water Res.*, 2003, 37, 4295-4303.
51. J.-H. Park, *Chemosphere*, 2009, 77, 485-494.
52. H. V.-M. Nguyen, J. Hur and H.-S. Shin, *Water, Air, Soil Pollut.*, 2010, 212, 395-406.
53. M. Halim, R. Spaccini, E. Parlanti, A. Amezghal and A. Piccolo, *J. Geochem. Explor.*, 2013, 129, 23-27.
54. C. Romera-Castillo, M. Chen, Y. Yamashita and R. Jaffé, *Water Research*, 2014, 55, 40-51.
55. E. Zanardi-Lamardo, C. D. Clark, C. A. Moore and R. G. Zika, *Environ. Sci. Technol.*, 2002, 36, 2806-2814.
56. J. Boehme and M. Wells, *Mar. Chem.*, 2006, 101, 95-103.
57. B. Stolpe, L. Guo, A. M. Shiller and M. Hassellöv, *Marine Chemistry*, 2010, 118, 119-128.
58. C. Gueguen and C. W. Cuss, *J. Chromatogr. A*, 2011, 1218, 4188-4198.
59. G. R. Aiken, E. M. Thurman, R. L. Malcolm and H. F. Walton, *Anal. Chem.*, 1979, 51, 1799-1803.
60. J. A. Leenheer and J.-P. Croue, *Environ. Sci. Technol.*, 2003, 37, 18A-26A.
61. H. Humbert, H. Gallard, H. Suty and J.-P. Croue, *Water Res.*, 2005, 39, 1699-1708.
62. C. Wang, X. Zhang, J. Wang and C. Chen, *J. Environ. Sci. (Beijing, China)*, 2013, 25, 85-95.
63. S. Mounier, N. Patel, L. Quilici, J. Y. Benaim and C. Benamou, *Water Research*, 1999, 33, 1523-1533.
64. T. M. Miano and J. J. Alberts, *Spec. Publ. - R. Soc. Chem.*, 1999, 247, 157-167.
65. J. J. Alberts, M. Takacs, M. McElvaine and K. Judge, *Apparent size distribution and spectral properties of natural organic matter isolated from six rivers in southeastern Georgia, USA. In: Ghabbour, E., Davies, G. (Eds.), Humic Substances, Structures, Models and Functions. The Royal Society of Chemistry, Cambridge, UK, pp. 179–190.*, 2001.
66. N. Patel-Sorrentino, S. Mounier and J. Y. Benaim, *Water Research*, 2002, 36, 2571-2581.
67. S. Schwede-Thomas, Y.-P. Chin, K. Dria, P. Hatcher, E. Kaiser and B. Sulzberger, *Aquatic Sciences*, 2005, 67, 61-71.
68. C. Belzile and L. Guo, *Mar. Chem.*, 2006, 98, 183-196.

69. A. Huguet, L. Vacher, S. Saubusse, H. Etcheber, G. Abril, S. Relexans, F. Ibalot and E. Parlanti, *Org. Geochem.*, 2010, 41, 595-610.
70. T. J. Boyd, B. P. Barham, G. J. Hall, B. S. Schumann, R. W. Paerl and C. L. Osburn, *Journal of Geophysical Research: Biogeosciences*, 2010, 115, G00F14.
71. R. M. Cory, D. M. McKnight, Y.-P. Chin, P. Miller and C. L. Jaros, *J. Geophys. Res., [Biogeosci.]*, 2007, 112, G04S51/01-G04S51/14.
72. R. G. Wetzel, P. G. Hatcher and T. S. Bianchi, *Limnol. Oceanogr.*, 1995, 40, 1369-1380.
73. L. J. Tranvik, *Ecol. Stud.*, 1998, 133, 259-283.
74. J. V. Goldstone, M. J. Pullin, S. Bertilsson and B. M. Voelker, *Environ. Sci. Technol.*, 2002, 36, 364-372.
75. M. McCarthy, T. Pratum, J. Hedges and R. Benner, *Nature (London)*, 1997, 390, 150-154.
76. J. L. Klug, *Can. J. Fish. Aquat. Sci.*, 2005, 62, 472-481.
77. S. E. Tank, M. Manizza, R. M. Holmes, J. W. McClelland and B. J. Peterson, *Estuaries Coasts*, 2012, 35, 401-415.
78. S. Nishimura, K. Kuma, S. Ishikawa, A. Omata and S.-i. Saitoh, *J. Geophys. Res.: Oceans*, 2012, 117, C02025/02021-C02025/02013.
79. D. P. Morris and B. R. Hargreaves, *Limnol. Oceanogr.*, 1997, 42, 239-249.
80. R. D. Vinebrooke and P. R. Leavitt, *Limnol. Oceanogr.*, 1998, 43, 1065-1081.
81. R. G. M. Spencer, B. A. Pellerin, B. A. Bergamaschi, B. D. Downing, T. E. C. Kraus, D. R. Smart, R. A. Dahlgren and P. J. Hernes, *Hydrological Processes*, 2007, 21, 3181-3189.
82. R. G. M. Spencer, A. Stubbins, P. J. Hernes, A. Baker, K. Mopper, A. K. Aufdenkampe, R. Y. Dyda, V. L. Mwamba, A. M. Mangangu, J. N. Wabakanghanzi and J. Six, *Journal of Geophysical Research: Biogeosciences*, 2009, 114, G03010.
83. K. M. G. Mostofa, F. Wu, C.-Q. Liu, D. Vione, T. Yoshioka, H. Sakugawa and E. Tanoue, *Geochem. J.*, 2011, 45, 235-254.
84. J. R. Helms, A. Stubbins, E. M. Perdue, N. W. Green, H. Chen and K. Mopper, *Mar. Chem.*, 2013, 155, 81-91.
85. A. Bianco, M. Minella, E. De Laurentiis, V. Maurino, C. Minero and D. Vione, *Chemosphere*, 2014, 111, 529-536.
86. J. R. Helms, D. A. Glinski, R. N. Mead, M. W. Southwell, G. B. Avery, R. J. Kieber and S. A. Skrabal, *Org. Geochem.*, 2014, 73, 83-89.
87. X. Lu and R. Jaffe, *Water Research*, 2001, 35, 1793-1803.
88. P. Fu, F. Wu, C. Liu, F. Wang, W. Li, L. Yue and Q. Guo, *Appl. Geochem.*, 2007, 22, 1668-1679.
89. F. F. Sodre and M. T. Grassi, *J. Braz. Chem. Soc.*, 2007, 18, 1136-1144.
90. Y. Yamashita and R. Jaffe, *Environ. Sci. Technol.*, 2008, 42, 7374-7379.
91. N. Mladenov, Y. Zheng, M. P. Miller, D. R. Nemergut, T. Legg, B. Simone, C. Hageman, M. M. Rahman, K. M. Ahmed and D. M. McKnight, *Environ Sci Technol*, 2010, 44, 123-128.
92. W. Zheng, L. Liang and B. Gu, *Environ. Sci. Technol.*, 2012, 46, 292-299.
93. S. Orsetti, J. L. Marco-Brown, E. M. Andrade and F. V. Molina, *Environ. Sci. Technol.*, 2013, 47, 8325-8333.
94. Y. Wang, D. Zhang, Z.-y. Shen, C.-h. Feng and X. Zhang, *Environ. Sci. Pollut. Res.*, 2014, DOI: 10.1007/s11356-014-3380-z, Ahead of Print.
95. J. E. Dorsch and T. F. Bidleman, *Estuarine, Coastal Shelf Sci.*, 1982, 15, 701-707.
96. J. L. Beltran, R. Ferrer and J. Guiteras, *Anal. Chim. Acta*, 1998, 373, 311-319.

97. R. D. JiJi, G. A. Cooper and K. S. Booksh, *Anal. Chim. Acta*, 1999, 397, 61-72.
98. M. L. Nahorniak and K. S. Booksh, *Analyst (Cambridge, U. K.)*, 2006, 131, 1308-1315.
99. T. Kusakabe, K. Ikeda, Y. Shimizu, S. Higashi, Y. Kawabata, T. Kitamura and Y. Suzuki, *Water Sci. Technol.*, 2008, 58, 1609-1614.
100. W. G. Mendoza, D. D. Riemer and R. G. Zika, *Environ. Sci.: Processes Impacts*, 2013, 15, 1017-1030.
101. N. Ferretto, M. Tedetti, C. Guigue, S. Mounier, R. Redon and M. Goutx, *Chemosphere*, 2014, 107, 344-353.
102. M. P. Miller and D. M. McKnight, *J. Geophys. Res., [Biogeosci.]*, 2010, 115, G00F12/01-G00F12/14.
103. K. R. Murphy, K. D. Butler, R. G. M. Spencer, C. A. Stedmon, J. R. Boehme and G. R. Aiken, *Environ. Sci. Technol.*, 2010, 44, 9405-9412.
104. J.-F. Lapierre and J.-J. Frenette, *Aquat. Sci.*, 2009, 71, 15-24.
105. P. G. Coble, C. E. Del Castillo and B. Avril, *Deep-Sea Res., Part II*, 1998, 45, 2195-2223.
106. E. J. Rochelle-Newall and T. R. Fisher, *Mar. Chem.*, 2002, 77, 7-21.
107. C. Romera-Castillo, H. Sarmento, X. A. Alvarez-Salgado, J. M. Gasol and C. Marrase, *Limnol. Oceanogr.*, 2010, 55, 446-454.
108. M. P. Miller, D. M. McKnight and S. C. Chapra, *Aquat. Sci.*, 2009, 71, 170-178.
109. L. E. De, S. Buoso, V. Maurino, C. Minero and D. Vione, *Environ Sci Technol*, 2013, 47, 14089-14098.
110. A. Vodacek, N. V. Blough, M. D. Degrandpre, E. T. Peltzer and R. K. Nelson, *Limnol. Oceanogr.*, 1997, 42, 674-686.
111. J. Para, P. G. Coble, B. Charriere, M. Tedetti, C. Fontana and R. Sempere, *Biogeosciences*, 2010, 7, 4083-4103.
112. W. Graneli, M. Lindell and L. Tranvik, *Limnol. Oceanogr.*, 1996, 41, 698-706.
113. W. L. Miller, M. A. Moran, W. M. Sheldon, R. G. Zepp and S. Opsahl, *Limnol. Oceanogr.*, 2002, 47, 343-352.
114. J. M. Morell and J. E. Corredor, *J. Geophys. Res., [Oceans]*, 2001, 106, 16807-16813.
115. C. Coelho, G. Guyot, A. ter Halle, L. Cavani, C. Ciavatta and C. Richard, *Environ. Chem. Lett.*, 2011, 9, 447-451.
116. B. M. Peterson, A. M. McNally, R. M. Cory, J. D. Thoemke, J. B. Cotner and K. McNeill, *Environ. Sci. Technol.*, 2012, 46, 7222-7229.
117. L. Klapper, D. M. McKnight, J. R. Fulton, E. L. Blunt-Harris, K. P. Nevin, D. R. Lovley and P. G. Hatcher, *Environmental Science & Technology*, 2002, 36, 3170-3175.
118. S. Mounier, R. Braucher and J. Y. Benaim, *Water Res.*, 1999, 33, 2363-2373.
119. W. B. Chen, D. S. Smith and C. Gueguen, *Chemosphere*, 2013, 92, 351-359.
120. E. R. Stabenau and R. G. Zika, *Mar. Chem.*, 2004, 89, 55-67.
121. G. P. Klinkhammer, C. Wilson, C. S. Chin and M. D. Rudnicki, 1996.
122. G. P. Klinkhammer, C. S. Chin, C. Wilson, M. D. Rudnicki and C. R. German, *Mar. Chem.*, 1997, 56, 1-14.
123. C. E. Del Castillo, F. Gilbes, P. G. Coble and F. E. Muller-Karger, *Limnol. Oceanogr.*, 2000, 45, 1425-1432.
124. T. Ohno, *Environ. Sci. Technol.*, 2002, 36, 742-746.
125. R. G. Zepp, W. M. Sheldon and M. A. Moran, *Mar. Chem.*, 2004, 89, 15-36.
126. R. Bro, *Chemom. Intell. Lab. Syst.*, 1997, 38, 149-171.
127. B. Lin, M. S. Bergholt, D. P. Lau and Z.-W. Huang, *Analyst (Cambridge, U. K.)*, 2011, 136, 3896-3903.

128. D.-M. Fang, H.-L. Wu, Y.-J. Ding, L.-Q. Hu, A. L. Xia and R.-Q. Yu, *Talanta*, 2006, 70, 58-62.
129. A. C. d. O. Neves, R. F. d. A. Junior, A. L. C. d. S. L. Oliveira, A. Antunes de Araujo and K. M. Gomes de Lima, *Analyst (Cambridge, U. K.)*, 2014, 139, 2423-2431.
130. D. Airado-Rodriguez, T. Galeano-Diaz, I. Duran-Meras and J. P. Wold, *J. Agric. Food Chem.*, 2009, 57, 1711-1720.
131. R. M. Callejon, J. M. Amigo, E. Pairo, S. Garmon, J. A. Ocana and M. L. Morales, *Talanta*, 2012, 88, 456-462.
132. D. Markechova, P. Majek and J. Sadecka, *Food Chem.*, 2014, 159, 193-199.
133. M. Silvestri, A. Elia, D. Bertelli, E. Salvatore, C. Durante, M. Li Vigni, A. Marchetti and M. Cocchi, *Chemom. Intell. Lab. Syst.*, 2014, 137, 181-189.
134. C. Coelho, A. Aron, C. Roullier-Gall, M. Gonsior, P. Schmitt-Kopplin and R. D. Gougeon, to be submitted.
135. T. Ohno and R. Bro, *Soil Sci. Soc. Am. J.*, 2006, 70, 2028-2037.
136. P. Kowalczuk, M. J. Durako, H. Young, A. E. Kahn, W. J. Cooper and M. Gonsior, *Mar. Chem.*, 2009, 113, 182-196.
137. P. Kowalczuk, W. J. Cooper, M. J. Durako, A. E. Kahn, M. Gonsior and H. Young, *Mar. Chem.*, 2010, 118, 22-36.
138. Y. Zhang, Y. Yin, L. Feng, G. Zhu, Z. Shi, X. Liu and Y. Zhang, *Water Res.*, 2011, 45, 5110-5122.
139. C. L. Osburn, L. T. Handsel, M. P. Mikan, H. W. Paerl and M. T. Montgomery, *Environ Sci Technol*, 2012, 46, 8628-8636.
140. M. Chen, N. Maie, K. Parish and R. Jaffe, *Biogeochemistry*, 2013, 115, 167-183.
141. S. A. Walker, R. M. W. Amon and C. A. Stedmon, *J. Geophys. Res.: Biogeosci.*, 2013, 118, 1689-1702.
142. H. Chen, B.-h. Zheng and L. Zhang, *Environ. Sci.: Processes Impacts*, 2013, 15, 485-493.
143. J. D. Hosen, O. T. McDonough, C. M. Febria and M. A. Palmer, *Environmental Science & Technology*, 2014, 48, 7817-7824.
144. K. R. Murphy, C. A. Stedmon, D. Graeber and R. Bro, *Anal. Methods*, 2013, 5, 6557-6566.
145. Y. Yamashita, N. Maie, H. Briceno and R. Jaffe, *J. Geophys. Res., [Biogeosci.]*, 2010, 115, G00F10/01-G00F10/15.
146. M. Borisover, Y. Laor, A. Parparov, N. Bukhanovsky and M. Lado, *Water Research*, 2009, 43, 3104-3116.
147. Y. Yamashita, A. Panton, C. Mahaffey and R. Jaffé, *Ocean Dynamics*, 2011, 61, 569-579.
148. K. Mueller, C. Fortin and P. C. Campbell, *Aquat Geochem*, 2012, 18, 21-44.
149. K. R. Murphy, C. A. Stedmon, T. D. Waite and G. M. Ruiz, *Mar. Chem.*, 2008, 108, 40-58.
150. S. A. Walker, R. M. W. Amon, C. Stedmon, S. Duan and P. Louchouarn, *Journal of Geophysical Research: Biogeosciences*, 2009, 114, G00F06.
151. J. B. Fellman, K. C. Petrone and P. F. Grierson, *Limnol. Oceanogr.*, 2011, 56, 243-256.
152. K. M. Cawley, K. D. Butler, G. R. Aiken, L. G. Larsen, T. G. Huntington and D. M. McKnight, *Mar. Pollut. Bull.*, 2012, 64, 1678-1687.
153. F. Meng, G. Huang, Z. Li and S. Li, *Industrial & Engineering Chemistry Research*, 2012, 51, 6212-6218.

154. K. G. Dahm, C. M. Van Straaten, J. Munakata-Marr and J. E. Drewes, *Environ. Sci. Technol.*, 2013, 47, 649-656.
155. S. Inamdar, S. Singh, S. Dutta, D. Levia, M. Mitchell, D. Scott, H. Bais and P. McHale, *J. Geophys. Res.: Biogeosci.*, 2011, 116, G03043/03041-G03043/03023.
156. L. Yang, W. Guo, N. Chen, H. Hong, J. Huang, J. Xu and S. Huang, *Appl. Geochem.*, 2013, 28, 164-171.
157. E. Ejarque-Gonzalez and A. Butturini, *PLoS ONE*, 2014, 9, e99618.
158. C. W. Cuss, Y. X. Shi, S. M. McConnell and C. Gueguen, *J. Geophys. Res.: Biogeosci.*, 2014, 119, 1850-1860.
159. G. J. Hall and J. E. Kenny, *Anal. Chim. Acta*, 2007, 581, 118-124.
160. F. Ammari, R. Bendoula, D. Jouan-Rimbaud Bouveresse, D. N. Rutledge and J.-M. Roger, *Talanta*, 2014, 125, 146-152.
161. M. Bieroza, A. Baker and J. Bridgeman, *Environmetrics*, 2011, 22, 256-270.
162. H. Yu, Y. Song, R. Liu, H. Pan, L. Xiang and F. Qian, *Chemosphere*, 2014, 113, 79-86.
163. A. Stubbins, R. G. M. Spencer, H. Chen, P. G. Hatcher, K. Mopper, P. J. Hernes, V. L. Mwamba, A. M. Mangangu, J. N. Wabakanghanzi and J. Six, *Limnol. Oceanogr.*, 2010, 55, 1467-1477.
164. G. A. Singer, C. Fasching, L. Wilhelm, J. Niggemann, P. Steier, T. Dittmar and T. J. Battin, *Nature Geosci*, 2012, 5, 710-714.
165. P. Herzsprung, W. von Tuempling, N. Hertkorn, M. Harir, O. Buettner, J. Bravidor, K. Friese and P. Schmitt-Kopplin, *Environ. Sci. Technol.*, 2012, 46, 5511-5518.
166. J. D'Andrilli, C. M. Foreman, A. G. Marshall and D. M. McKnight, *Org. Geochem.*, 2013, 65, 19-28.
167. A. Stubbins, J. F. Lapierre, M. Berggren, Y. T. Prairie, T. Dittmar and P. A. del Giorgio, *Environ. Sci. Technol.*, 2014, 48, 10598-10606.
168. R. L. Fimmen, R. M. Cory, Y.-P. Chin, T. D. Trouts and D. M. McKnight, *Geochim. Cosmochim. Acta*, 2007, 71, 3003-3015.
169. K. M. H. Beggs and R. S. Summers, *Environmental Science & Technology*, 2011, 45, 5717-5724.
170. Z. Zhou, L. Guo, A. M. Shiller, S. E. Lohrenz, V. L. Asper and C. L. Osburn, *Mar. Chem.*, 2013, 148, 10-21.
171. W. G. Mendoza, D. D. Riemer and R. G. Zika, *Environ Sci Process Impacts*, 2013, 15, 1017-1030.
172. T. S. Bianchi, C. Osburn, M. R. Shields, S. Yvon-Lewis, J. Young, L. Guo and Z. Zhou, *Environmental Science & Technology*, 2014, 48, 9288-9297.
173. R. K. Henderson, A. Baker, K. R. Murphy, A. Hambly, R. M. Stuetz and S. J. Khan, *Water Res*, 2009, 43, 863-881.

Chapter 7

Phototransformation induced by HO• radicals

By

Khan M. G. Mostofa[1,2*], Cong-Qiang Liu[2*], Hiroshi Sakugawa[3], Pingqing Fu[4], Marco Minella[5], Davide Vione[5], Daisuke Minakata[6], Feng-Chang Wu[7], Lin Zhai[8], M. Golam Mortuza[9], Fahad A. Al-Misned[9], Jingwen Chen[10], Jie Yuan[11], and Li Si-liang[2]

[1]Institute of Surface Earth System Sciences, Tianjin University, Tianjin 300072, P. R. China.

[2]State Key Laboratory of Environmental Geochemistry, Institute of Geochemistry, Chinese Academy of Sciences, Guiyang 550002, P. R. China.

[3]Graduate School of Biosphere Science, Department of Environmental Dynamics and Management, Hiroshima University, 1-7-1, Kagamiyama, Higashi-Hiroshima 739-8521, Japan.

[4]State Key Laboratory of Atmospheric Boundary Layer Physics and Atmospheric Chemistry, Institute of Atmospheric Physics, Chinese Academy of Sciences, Beijing 100029, China.

[5]Università degli Studi di Torino, Dipartimento di Chimica, Via P. Giuria 5, 10125 Torino, Italy and Centro Interdipartimentale NatRisk, Via Leonardo da Vinci 44, 10095 Grugliasco (TO), Italy.

[6]Department of Civil and Environmental Engineering, Michigan Technological University 1400 Townsend Drive, Houghton, MI. 49931, U.S.A.

[7]State Key Laboratory of Environmental Criteria and Risk Assessment, Chinese Research Academy of Environmental Sciences, Chaoyang, 100012, China.

[8]School of Environmental Science and Engineering, Tianjin University, Tianjin 300072, P. R. China.

[9]Department of Zoology, College of Science, King Saud University, Riyadh 11451, Saudi Arabia

[10]Key Laboratory of Industrial Ecology and Environmental Engineering (MOE), Department of Environmental Science and Technology, Dalian University of Technology, Linggong Road 2, Dalian 116024, P. R. China

[11]Institute of Geology and Geophysics, Chinese Academy of Sciences, Beitucheng Western Road, Chaoyang District, 100029, Beijing, P. R. China

[*]Corresponding address: E-mail: Mostofa KMG (mostofa@tju.edu.cn) or Liu CQ (liucongqiang@vip.skleg.cn)

Abstract

The hydroxyl radical ($HO^{\bullet}$) is a strong oxidizing agent that can transform dissolved organic matter (DOM) into many intermediate photoproducts and byproducts which include low molecular weight (LMW) DOM, hydrogen peroxide (H_2O_2), CO_2, dissolved inorganic carbon (DIC: dissolved CO_2, H_2CO_3, HCO_3^-, and CO_3^{2-}), NO_3^-, NH_4^+, and so on in surface waters. Furthermore, $HO^{\bullet}$ has a prominent role in the transformation of recalcitrant pollutants into more biodegradable compounds. This chapter discusses the key sources of $HO^{\bullet}$ in natural waters and elucidates the phototransformation pathways of high molecular weight (HMW) and LMW DOM induced by $HO^{\bullet}$. As an example, the photooxidation of methylmercury chloride (MeHgCl) by hydroxyl radicals is discussed along with its reaction mechanism. Among the possible indicators of DOM transformation, the decrease in the fluorescence intensity of autochthonous fulvic acid is discussed based on field observations. The presented results suggest that $HO^{\bullet}$ may be involved in the photooxidation of both HMW and LMW DOM in surface waters.

Table of Contents

5.1 Introduction

Phototransformation of dissolved organic substances including organic pollutants is a natural phenomenon in rivers, ponds, lakes, estuaries and oceans, induced by natural sunlight. Sunlight primarily initiates phototransformation processes, also through the generation of reactive transients. They include the hydroxyl radical ($HO^{\bullet}$) that is produced by irradiation of photosensitizers such as nitrate, nitrite and dissolved organic matter (DOM) in surface waters. Experimental studies on surface waters have shown that $HO^{\bullet}$ can be produced, among others, by the photo-Fenton reaction[1-5] , through H_2O_2 photogenerated by DOM[6, 7], as well as from NO_3^- and/or NO_2^- photolysis.[4, 5, 7-10] The radical $HO^{\bullet}$ is a reactive and efficient electrophile that can react non-selectively with a wide range of dissolved compounds at reaction rates often limited by mass transfer diffusion phenomena. It is also a strong oxidant ($E° = 2.32$ V vs NHE at 298 K and pH 7)[11] that it is used to achieve complete mineralization of emerging organic contaminants in advanced oxidation processes (AOPs), such as O_3/H_2O_2, UV/H_2O_2, UV/TiO_2, etc.[12, 13] when HO• is generated in engineered water treatment systems. In natural waters the reaction between hydroxyl radicals and biorecalcitrant pollutants is often an important degradation pathway which can give an increment of the biodegradability and consequently promote the transformation of emerging contaminants till, in some case, a complete mineralization.[14, 15]

The mechanism behind the phototransformation of organic compounds by $HO^{\bullet}$ is a complex process that depends on molecular size, occurrence of functional groups and their chemical behavior.[16-19] For HMW DOM, it has been shown that successive

photooxidation of specific functional groups by $HO^{\bullet}$ occurs sequentially.[20-23] Simultaneously, $HO^{\bullet}$ can react with low molecular weight compounds while HMW DOM (e.g. humic acids) may act as photosensitizer.[17, 18, 24] While $HO^{\bullet}$ can be involved in the phototransformation of DOM in surface waters,[25-28] the complexity of the process as far as natural DOM is concerned makes it difficult to assess the importance of $HO^{\bullet}$ in field observations. Indications can be obtained from the decrease in DOM fluorescence[27, 28] and from the diurnal variations of H_2O_2[6] produced from DOM upon sunlight exposure during the daytime.

This chapter will give a general overview on the mechanism of production and on the reactivity of $HO^{\bullet}$ in surface waters and on the associated phototransformation mechanisms of both HMW and LMW DOM. It will also discuss the phototransformation of a common organic pollutant, methylmercury chloride, and the decrease in fluorescence of fulvic acid as a useful indicator for photooxidation in surface-water photochemistry.

5.2 Sources of $HO^{\bullet}$ upon irradiation of surface waters

The radical $HO^{\bullet}$ can be produced in aqueous solution upon irradiation of nitrate, nitrite and several organic compounds. Production rates vary widely depending on the $HO^{\bullet}$ source (see Table 5.1).[3, 10, 29-35]

[Table 5.1 near here]

Photoproduction rates of $HO^{\bullet}$ from small molecules (*e.g*. phenylalanine, diaminostilbene type-DAS1 or peracetic acid; see Table 5.1) are usually lower compared to relatively large compounds such as standard Suwanne River Humic and Fulvic Acids (SRHA and SRFA), extracted fulvic acids or DOM. After a certain limit, however, an elevated molecular weight becomes detrimental to photoreactivity, which will be the topic of another chapter of this book. Because of the abundance of humic substances (fulvic and humic acids) in natural DOM, they play a significant role in the in-situ photooxidation of smaller molecules and organic pollutants.[18, 24, 36, 37]

The contribution of NO_3^- and NO_2^- to $HO^{\bullet}$ in natural waters depends on their concentration, that is controlled by several processes that are not necessarily of photochemical nature. For instance, NO_3^- is one of the key nutrients which fuels on primary productivity[38, 39], although primary producers (*e.g*. phytoplankton) and nitrification processes ($NH_4^+ \rightarrow NO_2^- \rightarrow NO_3^-$ or $NH_4^+ + 2\ O_2 \rightarrow NO_3^- + 2\ H^+ + H_2O$) can regenerate NO_3^- in waters under both photoinduced and microbial conditions.[39, 40] Moreover, denitrification ($NO_3^- \rightarrow NO_2^- \rightarrow NO \rightarrow N_2O \rightarrow N_2$), caused by denitrifying bacteria[41] or anaerobic ammonium oxidation, ANAMMOX ($NH_4^+ + NO_2^- \rightarrow N_2H_4 \rightarrow N_2$), carried out by Anammox bacteria[42] are all processes that can limit the concentration of nitrate and nitrite in natural waters.

For this reason, although nitrate and nitrite can be key $HO^{\bullet}$ sources in some environments, DOM would often play a more important role. Part of the $HO^{\bullet}$ photoproduction by DOM is promoted by the generation of H_2O_2 that is then involved in several processes including the Fenton and photo-Fenton ones.[22, 24, 30, 43-47] It has

been estimated that the photo-Fenton process would contribute to 2-70% of $HO^{\bullet}$ photoproduction in freshwater.[3-5, 10, 24, 29] Up to 50 % of the hydroxyl radical generation by irradiated DOM is thought to take place through reaction pathways involving H_2O_2, while the exact nature of the H_2O_2-independent pathway(s) is still elusive.[24, 48]

5.2.1 $HO^{\bullet}$ from photo-Fenton reaction

The photo-Fenton reaction requires iron species, H_2O_2 and radiation. Trace metal ions, particularly Fe^{3+}/Fe^{2+}, occur in a variety of natural waters, from freshwater to seawater. H_2O_2 is produced in sunlit surface waters and has strong diurnal variations, with concentrations that gradually increase before sunrise to noon and then gradually decrease after sunset, see as example the case reported in (Fig. 5.1).[6]

[Figure 5.1 near here]

In the reported case the higher H_2O_2 concentration at noon time is mostly caused by light intensity, which is more important than other factors such as water flow rates.[6] Diurnal variations of H_2O_2 in the surface waters are commonly measured in natural surface waters.[6,49-54] The photo-Fenton reaction has been observed in the surface water of the open ocean and it can be for instance detected as an anticorrelation between the vertical profiles of Fe(II) and H_2O_2, suggesting a reaction between the two species.[55] Interestingly, photochemical reactions involving the direct photolysis

of H_2O_2 have been shown to be also important in the production of $HO^{\bullet}$ upon UVC irradiation of DOM, which is of interest for water treatment.[56]

H_2O_2 is primarily generated by DOM, mostly humic substances (fulvic and humic acids), upon irradiation of surface water.[6] The production rate of H_2O_2 by Standard Suwannee River Humic Acids (SRHA) is approximately 2.6-fold higher compared to SRFA when they are illuminated in ultrapure (Milli-Q) waters (Fig. 5.2).[6]

[Figure 5.2 near here]

This issue might be offset by the three-fold reactivity toward HO• of SRHA compared to SRFA.[57] Note that aqueous solutions (1 mg L^{-1}) of standard organic substances are used for production of HO• radicals. Note also that all data depicted in the Figure 5.2 are calibrated for natural sunlight on 6 July 2004 at Hiroshima University Campus at noon under clear sky conditions, which was 4.05-fold higher than the artificial Xenon lamp used as solar simulator.

The mechanism of H_2O_2 production from DOM probably involves several reactions.[4, 6, 54, 56, 58-60] Photoexcited DOM can release aqueous electrons (e^-) (Eq 5.1) or oxidize dissolved compounds (R) yielding DOM radical anions ($DOM^{-\bullet}$). In both cases, the reaction with the molecular oxygen would produce the superoxide radical anion ($O_2^{\bullet-}$) (Eq 5.2, 5.3). The dismutation of superoxide and its conjugated acid, hydroperoxide ($HO_2^{\bullet}$, pKa = 4.8)[61] would then yield H_2O_2. Once H_2O_2 is formed, it is

involved in the Fenton and photo-Fenton reaction to produce $HO^{\bullet}$ in the presence of Fe(III)/Fe(II) species and sunlight (Eqs 5.6-5.7).[1, 4, 55]

The whole reaction scheme is shown below:

$$DOM + h\upsilon \rightarrow {}^{3}DOM^{*} \rightarrow e^{-} + DOM^{+\bullet} \quad (5.1)$$

$$e^{-} + O_2 \rightarrow O_2^{\bullet-} \quad (5.2)$$

$${}^{3}DOM^{*} + R \rightarrow DOM^{\bullet-} + R^{+\bullet} \quad (5.3)$$

$$DOM^{\bullet-} + O_2 \rightarrow DOM + O_2^{\bullet-} \quad (5.3)$$

$$O_2^{\bullet-} + H^{+} \rightarrow HO_2^{\bullet} \quad (5.4)$$

$$HO_2^{\bullet} + O_2^{\bullet-} + H^{+} \rightarrow H_2O_2 + O_2 \quad (5.5)$$

$$FeOH^{2+} + h\upsilon \rightarrow Fe^{2+} + HO^{\bullet} \quad (5.6)$$

$$Fe^{2+} + H_2O_2 \rightarrow Fe^{3+} + HO^{\bullet} + HO^{-} \quad (5.7)$$

Synergistic photogeneration of reactive oxygen species (*e.g.* $O_2^{\bullet-}$) by dissolved organic matter (*e.g.* fulvic and humic acids) and C_{60} in the aqueous phase can be interpreted on the basis of the above mentioned reaction scheme.[62]

5.2.2 In situ Generation of $HO^{\bullet}$ from DOM via H_2O_2

Another important source of $HO^{\bullet}$ is the in situ generation of $HO^{\bullet}$ from DOM.[30, 60, 62] The process may at least partially occur upon photoinduced generation of HO• from H_2O_2, which is primarily produced from DOM components such as Fluorescent Dissolved Organic Matter (FDOM) or Colored Dissolved Organic Matter

(CDOM) by the above mentioned reactions (Eqs 5.1-5.5). The key reaction processes can be depicted as follows:

$$FDOM + O_2 + H_2O + H^+ + h\upsilon \rightarrow H_2O_2 + FDOM^{\bullet +} + HO^{\bullet} \quad (5.8)$$

$$H_2O_2 \rightarrow 2\ HO^{\bullet} \quad (5.9)$$

It has been estimated that FDOM could contribute to 10-40% of $HO^{\bullet}$ production in freshwater streams.[29] Note that the direct oxidation of H_2O/OH^- by the photoproduced triplet states of the DOM is a very intriguing topic, but a complete clarification of the role of this process in the photogeneration of $HO^{\bullet}$ is far to be obtained, even because it is difficult, with real samples, to discriminate between the Fenton/photo-Fenton pathways and possible direct oxidative processes.

5.3 Phototransformation induced by $HO^{\bullet}$

Phototransformation of DOM by $HO^{\bullet}$ is a general phenomenon in surface water photochemistry because the DOM the main sink of $HO^{\bullet}$, although its actual importance is still under debate.[4, 16, 18, 24, 26, 28, 35, 63] Photooxidation of DOM can be a complex phenomenon due to the wide variations in DOM composition (both natural and anthropogenic DOM) in natural waters. Natural DOM includes HMW components such as allochthonous humic substances (fulvic and humic acids) of terrestrial origin , autochthonous fulvic acids of phytoplankton origin or extracellular polymeric substances, as well as the LMW components such as amino acids, carbohydrates, phenols, and so on.[64-66] On the other hand, anthropogenic DOM includes emerging organic contaminants such as endocrine disruptors,

pharmaceuticals and personal care products (PPCPs), pesticides, herbicides, detergents or fluorescent whitening agents (FWAs), including mostly diaminostilbene type (DAS1) and distyryl biphenyl (DSBP), protein-like components, sterols, and so on.[13, 63, 67, 68] An important difference between both natural and anthropogenic DOM is the low production of H_2O_2 by the latter solar exposure,[6,7, 47] An important difference between natural and anthropogenic DOM is the low production of H_2O_2 by the latter upon solar exposure, which is probably linked to a lower capacity to absorb sunlight.[24, 47]

DOM as photosensitizer can produce reactive species upon sunlight absorption, which can induce the transformation of the photosensitizing molecule and/or of other dissolved organic compounds. From another point of view, a DOM component can be transformed by reactive species photoproduced by itself (or simply upon other sunlight-induced photoreactions) or by other photosensitizers (e.g. DOM, nitrate, nitrite). The two processes are named direct and indirect photooxidation, respectively, and the extent to which they occur depends on DOM photoreactivity (direct photooxidation is for instance favored with the most photoreactive DOM components/moieties).[6,2-4, 8, 9, 24, 69-79]

5.3.1 Phototransformation of HMW DOM by $HO^{\bullet}$

Self-photooxidation is common with humic substances such as fulvic and humic acids.[22, 24, 80] These substances absorb sunlight and subsequently produce H_2O_2, and then $HO^{\bullet}$, through several chain reactions (Eqs 5.1-5.7) as discussed before. They

can also react with photogenerated transients, including $HO^{\bullet}$. Light-induced phototrasformation is consistent with the decreasing electron-donating capacities of humic substances under irradiation, due to selective destruction of their photosensitizing chromophores.[81]

The ability of organic compounds to react with $HO^{\bullet}$ can be assessed by using the group contribution method (GCM) to predict the aqueous phase HO• rate constants for many functional groups including (1) H-atom abstraction, (2) HO• addition to alkenes, (3) HO• addition to aromatic compounds, and (4) HO• interaction with sulfur (S)-, nitrogen (N)-, or phosphorus (P)-atom-containing compounds.[16] Although the GCM cannot be used for humic substances (HSs), it has been shown that HSs are more reactive toward HO• than "average" organic molecules.[57] Therefore, highly susceptible specific functional groups in humic substances could easily be degraded upon reaction with $HO^{\bullet}$ as well as with other transients. Important uncertainties concerning the degradation pathway(s) still remain, including for instance the possible formation of $[DOM–HO]^{*}$ adducts upon radical addition of $HO^{\bullet}$ to the phenolic moieties of DOM.

5.3.2 Photooxidation of LMW DOM or organic pollutants: Methylmercury chloride as an example

Phototransformation of LMW DOM can take place by reaction with $HO^{\bullet}$, generated by photosensitizers.[17, 18, 24, 82] Smaller molecules are generally less photoactive than humic substances because of the small molecular structure and few

functional groups. Moreover, different LMW DOM components show different phototransformation pathways upon sunlight exposure. Under irradiation of one specific substance (e.g. phenol), some new component can be produced (e.g. hydroquinone), which in some cases may be more photosensitive and could consequently produce more H_2O_2 upon irradiation.[6,7] Therefore, photooxidation of LMW DOM components in surface waters is a complex phenomenon that could be strongly affected by the chemical nature (molecular structure and weight) of the organic substance.

As an example, here it will be discussed the photooxidation of methyl mercury chloride (CH_3HgCl), a neurotoxin, which is one of the most toxic form of mercury that occurs in natural waters.[17, 18, 36, 83, 84] CH_3HgCl is readily biomagnified up aquatic food chains to levels harmful to both humans and wildlife, and it is of concern because of the increasing worldwide pollution by mercury.[17, 83, 85] Photooxidation of CH_3Hg^+ is one of its main removal pathways from natural waters, and it has been shown to occur in the presence of DOM but not in ultra-pure water.[18, 84] Mechanisms for the photodegradation of CH_3Hg^+ have been proposed by several studies, but several uncertainties still remain.[18, 36, 84] Our proposed mechanism is connected with two key facts based on the electronic configuration of complexes formed between Hg^+ and the functional groups of DOM.[19]

First, formation of π-electron bonding systems occurs between CH_3Hg^+ [Hg^{1+} = $1s^2 2s^2 2p^6 3s^2 3p^6 4s^2 3d^{10} 4p^6 5s^2 4d^{10} 5p^6 6s^1 4f^{14} 5d^{10}$] and DOM ($CH_3Hg$—DOM), through electron donation from the functional groups of high-molecular-weight DOM

to an empty *s*-orbital of CH_3Hg^+ (ligand-to-metal charge transfer).[86, 87] The overall conditional complexation constants (K'_{DOM}) between Hg(II) and dissolved organic matter (extracted humic acids, fulvic acids and hydrophobic acids) show very strong interactions ($K'_{DOM} = 10^{23.2\pm1.0}$ L kg^{-1}) at Hg/DOM ratios below approximately 1 μg Hg/mg DOM, which are indicative of strong mercury–thiol bonds.[88] In contrast, much weaker interactions ($K'_{DOM} = 10^{10.7\pm1.0}$ L kg^{-1}) are observed at Hg/DOM ratios above approximately 10 μg Hg/mg DOM, coherently with Hg binding to oxygen functional groups.[88] These π-electrons are loosely bound and they are highly susceptible to radiative excitation.[86, 87, 88] A ligand-to-metal charge transfer could be triggered by photolysis of the complex $H_3C–Hg^+←DOM$ (where the "←" indicates electron donation), which could take place as follows (Eq 5.10):

$$H_3C–Hg^+←DOM + h\nu \rightarrow H_3C–Hg^{\bullet} + DOM^{+\bullet} \qquad (5.10)$$

The quenching of the fluorescence signals of biofilm extracellular polymeric substances was reported in the presence of Hg^{+2} ions, which is an experimental evidence of the energy transfer between the DOM ligand and the Hg^{2+} centre in $R–Hg^+–DOM$ complexes.[65]

Oxidized DOM ($DOM^{+\bullet}$) could undergo several processes. Interestingly, similar phenomena involving the charge-transfer photolysis of Fe(III)-DOM complexes would ultimately cause DOM mineralization *via* decarboxylation.[36] The species $H_3C–Hg^{\bullet}$ might for instance react with $HO^{\bullet}$ and/or $^1O_2$.[36, 84] Oxidizing transients are expected to preferentially react with the methyl moiety of $H_3C–Hg^{\bullet}$, because the

coordination π-electron bonding system would provide an increased electron density on the methyl group and would lower the excitation energy of the carbon-mercury bond.[89] Such processes would lead to the demethylation of $H_3C–Hg^{\bullet}$, with formation of elemental Hg and oxidation of the methyl group (Eq 5.11).

$$H_3C–Hg^{\bullet} + {}^1O_2/HO^{\bullet} \rightarrow Hg + \text{oxidized } CH_3 \qquad (5.11)$$

The occurrence of inorganic compounds can also be important: for instance, increasing salinity can decrease the photodegradation of CH_3Hg^+ by several processes[17], including: *(i)* the scavenging of $HO^{\bullet}$ by bromide (the main $HO^{\bullet}$ scavenger in seawater)[90, 91], and *(ii)* the different speciation of the CH_3Hg^+ cation in seawater compared to freshwater. In seawater, the formation of stable complexes/ion pairs with anions such as Cl^- and Br^- may hinder the formation of the photolabile species $H_3C–Hg^+–DOM$.

5.4 Estimation of the phototransformation of DOM by $HO^{\bullet}$

An increase of H_2O_2 from its initial level before sunrise is related to an $HO^{\bullet}$ production through direct photochemistry or Fenton processes, and to the subsequent decomposition of $DOM^{+\bullet}$ formed upon reaction between DOM and $HO^{\bullet}$. Because DOM is a major $HO^{\bullet}$ sink, each mole of produced H_2O_2 can potentially yield a mole of $DOM^{+\bullet}$,[6] which is typically susceptible to decompose during the day time in surface water. In the Kurose River, Hiroshima Prefecture, Japan, the diurnal H_2O_2 production in stream water has been measured and it was, on average, equal to 5 nM

in between 5:30-8:00 Japan Standard Time (JST), 14 nM in between 8:00-10:00 JST, 28 nM in between 10:00-11:00 JST, 34 nM in between 11:00-12:00 JST, 31 nM in between 12:00-13:00 JST, 25 nM in between 13:00-14:00 JST, 18 nM in between 14:00-17:00 JST and 0 nM in between 17:00-19:00 JST (Fig. 5.1). By deduction of H_2O_2 concentration before sunrise (5:30 am period), the total H_2O_2 production during the day light period is 222 nM for 13.5 hours.

In downstream river water, H_2O_2 production was on average 12 nM in between 5:30-8:00 JST, 27 nM in between 8:00-10:00 JST, 55 nM in between 10:00-11:00 JST, 59 nM in between 11:00-12:00 JST, 65 nM in between 12:00-13:00 JST, 65 nM in between 13:00-14:00 JST, 58 nM in between 14:00-15:00 JST, 58 nM in between 15:00-17:00 JST and 16 nM in between 17:00-19:00 JST. Total H_2O_2 production during the day light period was thus 534 nM for 13.5 hours. Note that H_2O_2 production was estimated for each hour during its measurement for more than one hour. The phototransformation per day of DOM by $HO^{\bullet}$ could be approximated by using a simple equation:

Cumulated $[H_2O_2(nM)]$ = Cumulated $[HO^{\bullet}]$ = Cumulated $[DOM^{+\bullet}]$

For stream water, $\Sigma[DOM^{+\bullet}] = \Sigma[H_2O_2(nM)] = 222$ nM for 13.5 hours.

For downstream river water, $\Sigma[DOM^{+\bullet}] = \Sigma[H_2O_2(nM)] = 534$ nM for 13.5 hours.

$[DOM^{+\bullet}]$ represents the decomposition of DOM by $HO^{\bullet}$ produced from H_2O_2, either by photo-Fenton reaction or other photoinduced processes (e.g. the direct decomposition: $H_2O_2 + h\nu \rightarrow 2\ HO^{\bullet}$). In the case under study, the decomposition of DOM by $HO^{\bullet}$ in stream water would be 2.4-fold lower (222 nM for 13.5 hours) than

for downstream river waters (534 nM for 13.5 hours). This difference could result from several facts: first, the in-flowing rate of upstream river water was apparently higher compared to the downstream rivers, which would decrease the ability of sunlight to thoroughly illuminate the stream water. Second, DOM contents are relatively higher in downstream rivers (326-384 μM C) than in upstream rivers (118-239 μM C).[63] Third, the upper locations for in-flowing upstream water are mostly shaded by forest plants[63] that can decrease the solar irradiance on the water surface and subsequently lower the H_2O_2 concentrations in the sampling site.

Diurnal variation of H_2O_2 is commonly measured in rivers[6,54], lakes[49], estuaries[50], and oceans.[51-53] The amplitude of the H_2O_2 diurnal cycle (highest concentration at noon time minus concentration during the period before sunrise) was measured in different ecosystems and resulted equal to 35-65 nM in rivers, 790 nM in lake, 36-183 nM in estuary and 20-476 nM in coastal and open ocean.[47,65] Because it is readily measured, H_2O_2 concentration could be a useful indicator to estimate DOM photooxidation by $HO^{\bullet}$, produced by photosensitizers in surface waters.

5.4.1 Decrease in fluorescence of fulvic acid as a useful indicator for photooxidation in surface water photochemistry: A field observation

Detection of photooxidation of DOM upon solar exposure in surface waters is a critical phenomenon in field observation. In fact, although dissolved organic carbon (DOC) concentrations (used as measurement of DOM) generally decrease upon irradiation in the laboratory,[92-96] this is not always the case for field studies of in-

flowing waters (streams and rivers) or stagnant surface waters (lakes, estuaries and oceans). In streams and rivers, the water flow continuously carries fresh DOM and the photoinduced degradation effect caused by sunlight is relatively small compared to that of stagnant waters. On the other hand, DOM in stagnant waters is substantially enhanced during the summer seasons in the surface water compared to deeper waters.[27, 28, 97, 98]. Therefore, in addition to photoinduced degradation, one has a significant input of autochthonous DOM by phytoplankton under both photoinduced and microbial conditions.[28, 66, 99] On the other hand, photooxidation of DOM upon solar exposure in surface waters can be monitored by the decrease in the fluorescence intensity of high molecular weight DOM, particularly humic substances (fulvic and humic acids) of terrestrial origin and autochthonous fulvic acid-like (C-like) substances of phytoplankton origin. The relevant studies can be carried out by comparing the fluorescence peak intensities in the Excitation Emission Matrix (EEM) spectra recorded for surface and deeper waters.

Autochthonous DOM is for instance produced in the surface waters of Lake Hongfeng and Lake Baihua during the summer season. By using fluorescence spectroscopy, three components can be identified: fulvic acid-like (M-like), autochthonous fulvic acid-like (C-like) and tryptophan-like (peaks T and T_{UV}) components identified using fluorescence spectroscopy.[27] PARAFAC modeling on the EEM spectra of eutrophic Lake Hongfeng and Lake Baihua demonstrates that the fulvic acid (C-like) component is the key one among those identified during the summer stratification period (Fig. 5.3).

[Figure 5.3 hear here]

Based on the difference between surface and deeper water, it has been possible to estimate the photooxidative decrease in fluorescence intensity of the fulvic acid (C-like) component (Table 5.2; Fig. 5.4). Indeed, during the winter vertical mixing period the fluorescence intensity of DOM and all other parameters undergo very limited variations, followed by a decrease when the stratification period is started in early summer (Fig. 5.4).

[Figure 5.4 near here]

In the surface waters of Lake Hongfeng, the fluorescence intensity of the fulvic acid (C-like) component is decreased by approximately 2-29% for peak C and 0-29% for peak A during the summer period from May to September (Table 5.2).

[Table 5.2 near here]

Interestingly, the fluorescence intensity in the surface layer is lower than in deeper water during summer, but it becomes higher in November (Figure 5.4). This observation can be accounted for by the low degree of DOM photodegradation in the surface water layer in the early winter, for which reason the generation of new DOM including autochthonous fulvic acid from primary production could easily offset the relatively low photooxidative loss of autochthonous fulvic acid.[27, 66] Coherently, the

primary production (chlorophyll *a*) is significantly higher in surface water (15.0-20.5 μg/L, mean = 19.1 μg/L at 0-3 m depths in February) than in the deeper layer (2.7-19.1 μg/L, mean = 8.6 μg/L at 10-25 m depths) during the winter period.[27] On the other hand, in the surface waters of Lake Baihua, the photooxidative decrease in fluorescence intensity of the fulvic acid (C-like) component is significantly higher in July (58-65%) and September (26-29%) compared to the deeper water layers (Table 5.2). The decrease in fluorescence is relatively low in November (15-21%), February (12-23%) and May (10-16%), but it is observed throughout the summer and winter period. Such differences are probably caused by the mixing of wastewater released from industries in the waters of Lake Baihua[27], which may reduce the winter vertical mixing and decrease the primary production.[27] The reduction of vertical mixing enhances the solar exposure of surface-water DOM, thereby enhancing photodegradation, while a lower primary production would generate smaller amounts of autochthonous fulvic acid. The outcome is a decrease of fulvic acid fluorescence, which is more marked in the surface waters of Lake Baihua (highest: 58-65% in July) than in Lake Hongfeng (highest: 29% in July).[27]

The fluorescence of the fulvic acid (C-like) component could thus be a useful indicator for photooxidation processes in surface waters including rivers[63] and lakes.[27, 28] Many photooxidation experiments have been carried out using water from rivers, lakes and marine ecosystems,[93, 94, 96, 100-102] but, due to the complexity of the factors involved, the decrease of DOM in field observation is rarely observed.[27, 28, 63] Indeed, the autochthonous DOM from primary production (*e.g.* phytoplankton or

algae) under both light and dark conditions [39, 66, 99] enhances the DOM contents in the surface water layer during the summer stratification period.[27, 28, 97, 98, 103] However, when measuring fluorescence intensity instead of the DOC, the photooxidation-induced decrease is so high that it cannot be compensated for by the production of fresh DOM. In this way, it is possible to highlight the photodegradation of fulvic acids in surface waters.

On the basis of the arguments discussed in previous paragraphs, it can be easily imagined that $HO^{\bullet}$ would play a role in the photooxidation of DOM. However, the exact importance of the $HO^{\bullet}$ radical in the observed photodegradation processes still needs to be clarified and quantified.

5.5 Factors affecting surface water photochemistry

Photooxidation processes mostly occur in the photic or mixing zone of surface waters. On the other hand, the extent of the photic or mixing zone of lakes or oceans depends on water depth, on the presence of total suspended solids (TSS) and total DOM and, for lakes, also on size and location (for instance, the action of wind may enhance the mixing zone).[104-107] Such phenomena substantially affect the Secchi disk readings in a variety of lake waters. For instance, a ~75% decrease of TSS effluent loadings from waste-water treatment plants can cause a ~25% increase of Secchi depths.[105] Because of its high ability to absorb sunlight, DOM can also limit the photic zone in waters as it can inhibit the penetration of solar radiation into the deeper layers.[104, 107] Correspondingly, waters with high contents of DOM can limit the

photoinduced decomposition of DOM itself. For example, in the same experimental conditions over a 13-day irradiation period, it has been demonstrated that the percentage of DOM photodegradation was significantly higher (36% *vs*. 16%) in stream water with low contents of DOM (100 μM C) compared to downstream river water with higher contents of DOM (200 μM C).[96] Similarly, exposure to light of waters with similar contents of DOM (2046 and 1972 μM C) yielded similar fractions of decomposition under the same experimental conditions (31 and 36%, respectively).[94] Similar results are also found in earlier studies.[100, 101] Although the photodegradation of DOM also depends on its nature.[22], the low extent of photooxidation in waters with high contents of DOM may be connected to the absorption of radiation by organic compounds. DOM contents could, therefore, limit photodecomposition processes altering the depth of the photic zone. The key factors that affect surface water photochemistry can be summarized as follows: (1) sunlight irradiance; (2) water temperature; (3) concentration of inorganic species in water (in particular iron species, NO_2^-, NO_3^-, pH, alkalinity, salinity and ionic strength); (4) nature and concentration of DOM; (5) dissolved oxygen and consequently the redox potential of the water; (6) depth of the water and (7) its dynamic in the mixing zone (hypolimnion).[22] Note that some of the above reported factors are strongly influenced by local and global changes such as the increment of UV-radiation during ozone hole events, the global warming and the modification of the average atmospheric composition (e.g. increase of the CO_2 concentration).

5.6 Consequences and implications of phototransformations induced by $HO^{\bullet}$

Phototransformation processes, which include the reactions induced by $HO^{\bullet}$, play an important role in surface waters, particularly in lakes, estuaries and oceans. These processes can interact with other biogeochemical and global cycles and the possible implications can be summarized as follows:

(1) Under the global warming conditions that enhance the phototransformation of DOM by increasing the stratification of the surface water layer, numerous intermediate products including nutrients (NO_3^-, NO_2^-, NH_4^+, and PO_4^{3-}), CO_2, DIC (dissolved CO_2, H_2CO_3, HCO_3^-, and CO_3^{2-}), LMW DOM and so on can be produced.[22, 39, 103, 108-111] Such photoproducts can further fuel the primary productivity[39] and enhance the biota growth in natural waters.[112]

(2) The synergistic effects of seawater acidification and high temperature[113, 114] are expected to enhance the production of reactive oxygen species (ROS), including $HO^{\bullet}$, in surface waters (e.g. through photo-Fenton processes).

(3) ROS production can have an impact on living organisms.[30, 115, 116] The radical $HO^{\bullet}$ can damage the photosystem II activities and finally cause cell death. [30, 117]

(4) Transformation of organic pollutants including cyanobacterial toxins, induced by photochemical processes including reactions with $HO^{\bullet}$ [118-120], can produce labile LMW DOM and other mineralization products such as CO_2, CO, DIC, etc. Such photooxidation processes could play an important role in reducing the harmful effects of organic pollutants to organisms including humans.

The described processes and interactions account for the importance of elucidating the role of $HO^{\bullet}$ in the transformation and mineralization of natural DOM and organic pollutants.

Acknowledgements

This work was supported by the Institute of Surface Earth System Sciences, Tianjin University, China. The authors would like to extend their sincere appreciation to King Saud University, Deanship of Scientific Research, College of Science, Research Center for its support, and to University of Torino - EU Accelerating Grants, project TO_Call2_2012_0047.

References

1. R.G. Zepp, B.C. Faust and J. Hoigne, *Environ. Sci. Technol.*, 1992, **26**, 313.
2. B.A. Southworth and B.M. Voelker, *Environ. Sci. Technol.*, 2003, **37**, 1130.
3. E.M. White, P.P. Vaughan and R.G. Zepp, *Aquat. Sci.*, 2003, **65**, 402.
4. D. Vione, G. Falletti, V. Maurino, C. Minero, E. Pelizzetti, M. Malandrino, R. Ajassa, R.I. Olariu and C. Arsene, *Environ. Sci. Technol.*, 2006, **40**, 3775.
5. N. Nakatani, M. Ueda, H. Shindo, K. Takeda and H. Sakugawa, *Anal. Sci.*, 2007, **23**, 1137.
6. K.M.G. Mostofa and H. Sakugawa, *Environ. Chem.*, 2009, **6**, 524.
7. C.D. Clark, W. de Bruyn and J.G. Jones, *Mar. Pollut. Bull.*, 2014, **79**, 54.
8. M.W. Lam, K. Tantuco and S.A. Mabury, *Environ. Sci. Technol.*, 2003, **37**, 899.
9. R.G. Zepp, J. Hoigne and H. Bader, *Environ. Sci. Technol.*, 1987, **21**, 443.
10. K. Takeda, H. Takedoi, S. Yamaji, K. Ohta and H. Sakugawa, *Anal. Sci.*, 2004, **20**, 153.
11. P.M. Wood, *Biochem. J.*, 1988, **253**, 287.
12. E.J. Rosenfeldt and K.G. Linden, *Environ. Sci. Technol.*, 2004, **38**, 5476.
13. P. Westerhoff, Y. Yoon, S. Snyder and E. Wert, *Environ. Sci. Technol.*, 2005, **39**, 6649.
14. B. Sur, E. De Laurentiis, M. Minella, V. Maurino, C. Minero and D. Vione, *Sci. Total Environ.*, 2012, **426**, 296
15. J. Kochany and J.R. Bolton, *J. Phys. Chem.*, 1991, **95**, 5116
16. D. Minakata, K. Li, P. Westerhoff and J. Crittenden, *Environ. Sci. Technol.*, 2009, **43**, 6220.
17. F.J. Black, B.A. Poulin and A.R. Flegal, *Geochim Cosmochim Acta*, 2012, **84**, 492.
18. C. Tai, Y. Li, Y. Yin, L.J. Scinto, G. Jiang and Y. Cai, *Environ. Sci. Technol.*, 2014, **48**, 7333.
19. K.M.G. Mostofa, C.Q. Liu, M. Minella, D.Vione, *Sci. Total Environ.,* 2015, **(submitted)**.
20. H. Xie, O.C. Zafiriou, W.J. Cai, R.G. Zepp and Y. Wang, *Environ. Sci. Technol.*, 2004, **38**, 4113.
21. K. Li and J. Crittenden, *Environ. Sci. Technol.*, 2009, **43**, 2831.
22. K.G.M. Mostofa, C.Q. Liu, D. Minakata, F. Wu, D. Vione, M.A. Mottaleb, T. Yoshioka and H. Sakugawa, *Photobiogeochemistry of Organic Matter*, ed. K.M.G. Mostofa, T. Yoshioka, A. Mottaleb and D. Vione, Springer, Berlin Heidelberg, 1st edition, 2013, Chapter 4, pp. 273-364.
23. J.A. Amador, M. Alexander and R.G. Zika, *Appl. Environ. Microbiol.*, 1989, **55**, 2843.
24. S.E. Page, W.A. Arnold and K. McNeill, *Environ. Sci. Technol.*, 2011, **45**, 2818.
25. X. Ma and S.A. Green, *J. Great Lakes Reser.*, 2004, **30**, 97.

26. K.M.G. Mostofa, T. Yoshioka, E. Konohira and E. Tanoue, *Water Air Soil Pollut.*, 2007, **184**, 157.
27. P.Q. Fu, K.M.G. Mostofa, F.C. Wu, C.Q. Liu, W. Li, H. Q. Liao, L. Y. Wang, J. Wang and Y. Mei, *Geochem. J.*, 2010, **44**, 99.
28. K.M.G. Mostofa, T. Yoshioka, E. Konohira, E. Tanoue, K. Hayakawa and M. Takahashi, *Limnology*, 2005, **6**, 101.
29. M. Chiwa, N. Higashi, K. Otsuki, H. Kodama, T. Miyajima, K. Takeda and H. Sakugawa, *Chemosphere*, 2015, **119**, 1386.
30. K.M.G. Mostofa, C.Q. Liu, H. Sakugawa, D. Vione, D. Minakata, M. Saquib and M. A. Mottaleb, *Photobiogeochemistry of Organic Matter: Principles and Practices in Water Environments*, ed. K.M.G. Mostofa, T. Yoshioka, A. Mottaleb and D. Vione, Springer, Berlin Heidelberg, 1st edition, 2013, Chapter 3, pp. 209-272.
31. A. Grannas, C. Martin, Y.-P. Chin and M. Platz, *Biogeochemistry*, 2006, **78**, 51.
32. C. Anastasio and J.T. Newberg, *J. Geophys. Res.*, 2007, **112**, 10306.
33. K. Mopper and X. Zhou, *Science*, 1990, **250**, 661.
34. T. Arakaki and B.C. Faust, *J. Geophys. Res.*, 1998, **103**, 3487.
35. D. Vione, M. Minella, V. Maurino and C. Minero, *Chem.– A Eur. J.*, 2014, **20**, 10590.
36. C.R. Hammerschmidt and W.F. Fitzgerald, *Environ. Sci. Technol.*, 2010, **44**, 6138.
37. E.M. Janssen, P.R. Erickson and K. McNeill, *Environ. Sci. Technol.*, 2014, **48**, 4916.
38. R.W. Howarth, *Harmful Algae*, 2008, **8**, 14.
39. K.M.G. Mostofa, C.Q. Liu, D. Vione, K. Gao and H. Ogawa, *Environ. Pollut.*, 2013, **182**, 461.
40. S.C. Doney, N. Mahowald, I. Lima, R.A. Feely, F.T. Mackenzie, J.F. Lamarque and P.J. Rasch, *Proc. Nat. Acad. Sci.*, 2007, **104**, 14580.
41. Y. Pan, B.-J. Ni and Z. Yuan, *Environ. Sci. Technol.*, 2013, **47**, 11083.
42. B.B. Ward, *Science*, 2013, **341**, 352.
43. J. Jeong and J. Yoon, *Water Res.*, 2005, **39**, 2893.
44. D.L. Sedlak and J. Hoigné, *Atmos. Environ.*, 1993, **27**, 2173.
45. L. Sun and J.R. Bolton, *J. Phys. Chem.*, 1996, **100**, 4127.
46. D. Vione, V. Maurino, C. Minero and E. Pelizzetti, *Chemosphere*, 2001, **45**, 903.
47. K.M.G. Mostofa, C.Q. Liu, H. Sakugawa, D. Vione, D. Minakata and F. Wu, *Photobiogeochemistry of Organic Matter: Principles and Practices in Water Environments*, ed. K.M.G. Mostofa, T. Yoshioka, A. Mottaleb and D. Vione, Springer, Berlin Heidelberg, 1st edition, 2013, Chapter 2, pp. 139-207.
48. B. Sur, M. Rolle, C. Minero, V. Maurino, D. Vione, M. Brigante and G. Mailhot, *Photochem. Photobiol. Sci.*, 2011, **10**, 1817
49. W. Cooper, D. Lean, *Environ. Sci. Technol.*, 1989, **23**, 1425.
50. R.J. Kieber and G.R. Helz, *Estuar., Coast. Shelf Sci.*, 1995, **40**, 495.

51. H. Sakugawa, T. Yamashita and K. Fujiwara, *Global Fluxes of Carbon and Its Related Substances in the Coastal Sea-ocean-atmosphere System: Proceedings of the 1994 Sapporo IGBP Symposium, 14-17 November 1994, Hokkaido University, Sapporo Hokkaido, Japan*, M & J International, 1995.
52. J. Yuan and A.M. Shiller, *Deep Sea Res. Part II*, 2001, **48**, 2947.
53. G.B. Avery Jr, W.J. Cooper, R.J. Kieber and J.D. Willey, *Mar. Chem.*, 2005, **97**, 236.
54. L.E. Richard, B.M. Peake, S.A. Rusak, W.J. Cooper and D.J. Burritt, *Environ. Chem.*, 2007, **4**, 49.
55. P.L. Croot, P. Laan, J. Nishioka, V. Strass, B. Cisewski, M. Boye, K.R. Timmermans, R.G. Bellerby, L. Goldson, P. Nightingale and H.J.W. de Baar, *Mar. Chem.*, 2005, **95**, 65.
56. Y. Lester, C.M. Sharpless, H. Mamane and K.G. Linden, *Environ. Sci. Technol.*, 2013, **47**, 11726.
57. E. Appiani, S.E. Page and K. McNeill, *Environ. Sci. Technol.*, 2014, **48**, 11794.
58. R.G. Petasne and R.G. Zika, *Nature*, 1987, **325**, 516.
59. C.A. Moore, C.T. Farmer and R.G. Zika, *J. Geophys. Res.*, 1993, **98**, 2289.
60. A. Marchisio, M. Minella, V. Maurino, C. Minero and D. Vione, *Water Res.*, 2015, **73**, 145.
61. M.J. Zhan, *J. Environ. Sci*, 2009, **21**, 303
62. Y. Li, J. Niu, E. Shang and J.C. Crittenden, *Environ. Sci. Technol.*, 2015, **49**, 965.
63. K.M.G. Mostofa, Y. Honda and H. Sakugawa, *Geochem. J.*, 2005, **39**, 257.
64. Y.L. Zhang, M.A. van Dijk, M.L. Liu, G.W. Zhu and B.Q. Qin, *Water Res.*, 2009, **43**, 4685.
65. D. Zhang, X. Pan, K.M.G. Mostofa, X. Chen, G. Mu, F. Wu, J. Liu, W. Song, J. Yang and Y. Liu, *J. Hazard. Mater.*, 2010, **175**, 359.
66. K.M.G. Mostofa, C.Q. Liu, T. Yoshioka, D. Vione, Y. Zhang and H. Sakugawa, *Photobiogeochemistry of Organic Matter: Principles and Practices in Water Environments*, ed. K.M.G. Mostofa, T. Yoshioka, A. Mottaleb and D. Vione, Springer, Berlin Heidelberg, 1st edition, 2013, Chapter 6, pp. 429-559.
67. S.D. Richardson, *Anal. Chem.*, 2007, **79**, 4295.
68. M.A. Mottaleb, S. Usenko, J.G. O'Donnell, A.J. Ramirez, B.W. Brooks and C.K. Chambliss, *J. Chromatogr. A*, 2009, **1216**, 815.
69. H. Gao and R.G. Zepp, *Environ. Sci. Technol.*, 1998, **32**, 2940.
70. W.R. Haag and Hoigné J., *Chemosphere*, 1985, **14**, 1659-1671.
71. J.M. Allen, S.Lucas and S.K. Allen, *Environ. Toxicol. Chem.*, 1996, **15**, 107.
72. S.F. Canonica, M., *Environ. Sci. Technol.*, 2001, **35**, 690.
73. Y.P. Chin, P.L. Miller, L. Zeng, K. Cawley and L.K. Weavers, *Environ. Sci. Technol.*, 2004, **38**, 5888.
74. S.A. Timko, C. Romera-Castillo, R. Jaffe and W.J. Cooper, *Environ. Sci.: Processes Impacts*, 2014, **16**, 866.

75. H. Katsumata, S. Kaneco, T. Suzuki, K. Ohta and Y. Yobiko, *Chem. Engineer. J.*, 2005, **108**, 269.
76. W.C. Paterlini and R.F.P. Nogueira, *Chemosphere*, 2005, **58**, 1107.
77. P. Miró, A. Arques, A. M. Amat, M. L. Marin and M. A. Miranda, *Appl. Catal. B: Environ.*, 2013, **140–141**, 412.
78. P.L. Brezonik and J. Fulkerson-Brekken, *Environ. Sci. Technol.*, 1998, **32**, 3004.
79. S. Nélieu, M.V. Shankar, L. Kerhoas and J. Einhorn, *J. Photochem. Photobiol. A: Chem.*, 2008, **193**, 1.
80. Y. Chen, S. Khan and M. Schnitzer, *Soil Sci. Soc. Am. J.*, 1978, **42**, 292.
81. C.M. Sharpless, M. Aeschbacher, S.E. Page, J. Wenk, M. Sander and K. McNeill, *Environ. Sci. Technol.*, 2014, **48**, 2688.
82. S.J. Canonica, U. Stemmler, K. Hoigne, *Environ. Sci. Technol.*, 1995, **29**, 1822.
83. A.M. Scheuhammer, M.W. Meyer, M.B. Sandheinrich and M.W. Murray, *Ambio*, 2007, **2007**, 12.
84. T. Zhang and H. Hsu-Kim, *Nature Geosci.*, 2010, **3**, 473.
85. D.G. Streets, M.K. Devane, Z. Lu, T.C. Bond, E.M. Sunderland and D.J. Jacob, *Environ. Sci. Technol.*, 2011, **45**, 10485.
86. K.M.G. Mostofa, F. Wu, C.Q. Liu, D. Vione, T. Yoshioka, H. Sakugawa and E. Tanoue, *Geochem. J.*, 2011, **45**, 235.
87. K.M.G. Mostofa, C.Q. Liu, T. Yoshioka, D. Vione, Y. Zhang and H. Sakugawa, *Photobiogeochemistry of Organic Matter: Principles and Practices in Water Environments*, ed. K.M.G. Mostofa, T. Yoshioka, A. Mottaleb and D. Vione, Springer, Berlin Heidelberg, 1st edition, 2013, Chapter 9, pp. 769-849.
88. M. Haitzer, G.R. Aiken and J.N. Ryan, *Environ. Sci. Technol.*, 2002, **36**, 3564.
89. B. Ni, J.R. Kramer, R.A. Bell and N.H. Werstiuk, *J. Phys. Chem. A*, 2006, **110**, 9451.
90. J. Goldstone, M. Pullin, S. Bertilsson and B. Voelker, *Environ. Sci. Technol.*, 2002, **36**, 364.
91. R. Das, B. Dutta, V. Maurino, D. Vione and C. Minero, *Environ. Chem. Lett.*, 2009, **7**, 337.
92. A.V. Vähätalo and R.G. Wetzel, *Mar. Chem.*, 2004, **89**, 313
93. A. Skoog, M. Wedborg and E. Fogelqvist, *Mar. Chem.*, 1996, **55**, 333.
94. M.A. Moran, W.M. Sheldon and R.G. Zepp, *Limnol. Oceanogr.*, 2000, **45**, 1254.
95. A.V. Vähätalo and R.G. Zepp, *Environ. Sci. Techn.*, 2005, **39**, 6985.
96. K.M.G. Mostofa, T. Yoshioka, E. Konohira and E. Tanoue, *Geochem. J.*, 2007, **41**, 323.
97. T. Yoshioka, S. Ueda, T. Khodzher, N. Bashenkhaeva, I. Korovyakova, L. Sorokovikova and L. Gorbunova, *Limnology*, 2002, **3**, 0159.
98. H. Ogawa and E. Tanoue, *J. Oceanogr.*, 2003, **59**, 129.
99. M.L. Brooks, J.S. Meyer and D.M. McKnight, *Hydrobiologia*, 2007, **579**, 95.

100. J.R. Helms, A. Stubbins, J.D. Ritchie, E.C. Minor, D.J. Kieber and K. Mopper, *Limnol. Oceanogr.*, 2008, **53**, 955.
101. C.L. Osburn, D.W. O'Sullivan and T.J. Boyd, *Limnol. Oceanogr.*, 2009, **54**, 145.
102. M. Xiao, F. Wu, L. Wang, X. Li and R. Huang, *J. Environ. Sci.*, 2013, **25**, 237.
103. D.P. Morris, H. Zagarese, C.E. Williamson, E.G. Balseiro, B.R. Hargreaves, B. Modenutti, R. Moeller and C. Queimalinos, *Limnol. Oceanogr.*, 1995, 1381.
104. D.G. Borkman and T.J. Smayda, *ICES J. Mar. Sci.*, 1998, **55**, 668.
105. A.V. Vahatalo, M. Salkinoja-Salonen, P. Taalas and K. Salonen, *Limnol. Oceanogr.*, 2000, **45**, 664.
106. K.M.G. Mostofa, C.Q. Liu, D. Vione, M.A. Mottaleb, H. Ogawa, S.M.Tareq and T. Yoshioka, *Photobiogeochemistry of Organic Matter: Principles and Practices in Water Environments*, ed. K.M.G. Mostofa, T. Yoshioka, A. Mottaleb and D. Vione, Springer, Berlin Heidelberg, 1st edition, 2013, Chapter 5, pp. 365-428.
107. W. Graneli, M. Lindell and L. Tranvik, *Limnol. Oceanogr.*, 1996, **41**, 698.
108. W.L. Miller and R.G. Zepp, *Geophys. Res. Lett.*, 1995, **22**, 417.
109. E. Ortega-Retuerta, U. Passow, C.M. Duarte and I. Reche, *Biogeosciences*, 2009, **6**, 3071.
110. M. Xiao and F. Wu, *J. Environ. Sci.*, 2014, **26**, 935.
111. J. Kopáćek, J. Hejzlar, P. Porcal, S. and Klementová, *Limnol. Oceanogr.*, 2003, **48**, 106.
112. D.G. Boyce, M.R. Lewis and B. Worm, *Nature*, 2010, **466**, 591.
113. K. Gao, J. Xu, G. Gao, Y. Li, D. A. Hutchins, B. Huang, L. Wang, Y. Zheng, P. Jin and X. Cai, *Nature Climate Change*, 2012, **2**, 519.
114. J.A. Dykens, J.M. Shick, C. Benoit, G.R. Buettner and G.W. Winston, *J. Exp. Biol.*, 1992, **168**, 219.
115. P.R. Maddigapu, M. Minella, D. Vione, V. Maurino and C. Minero, *Environ. Sci. Technol.*, 2010, **45**, 209.
116. O. Blokhina, E. Virolainen and K.V. Fagerstedt, *Ann. Bot.*, 2003, **91**, 179.
117. K. Govindan, M. Raja, M. Noel and E.J. James, *J. Hazard. Mater.*, 2014, **272**, 42.
118. O.S. Keen, G. McKay, S.P. Mezyk, K.G. Linden and F.L. Rosario-Ortiz, *Water Res.*, 2014, **50**, 408.
119. X. He, G. Zhang, A.A. de la Cruz, K.E. O'Shea and D.D. Dionysiou, *Environ. Sci. Technol.*, 2014, **48**, 4495.

Figure captions

Fig. 5.1

Diurnal variations of H_2O_2 concentration in the upstream waters collected on August 23, 2003 and the downstream waters collected on September 26, 2003 in the Kurose River, Hiroshima Prefecture, Japan. The upstream course of the river is mostly surrounded by dense forests, while the downstream river was substantially polluted by household effluents from undeveloped sewage treatment systems in Higashi-Hiroshima during the sampling period (see Mostofa et al. 2005a for details).

Fig. 5.2

Photoinduced generation of H_2O_2 and $HO^{\bullet}$ from standard Suwannee River Fulvic Acid (a) and standard Suwannee River Humic Acid (b) in photoexperiments conducted using a solar simulator. Aqueous solutions (1 mg L^{-1}) of the standard two substances are used for production of H_2O_2 and $HO^{\bullet}$. All data depicted in these Figures are calibrated for natural sunlight on 6 July 2004 at Hiroshima University Campus at noon under clear sky conditions.

Fig. 5.3

The autochthonous fulvic acid-like (C-like) substance is identified using parallel factor (PARAFAC) modeling on the EEM spectra of the lake waters at different vertical depths, collected from Lake Hongfeng (HF) and Lake Baihua (BH), China.

Fig. 5.4

Photoinduced decrease in the fluorescence intensity of fluorescence peaks (peak C and peak A) of autochthonous fulvic acid-like (C-like) substance of phytoplankton (or algal) origin in the surface waters of Lake Hongfeng (HF) and Lake Baihua (BH), China, compared to the deeper water layers. Water samples were collected from two sites of each lake (southern site = HF-S and northern site = HF-N for Lake Hongfeng, BH-1 and BH-2 for Lake Baihua).

Fig. 1

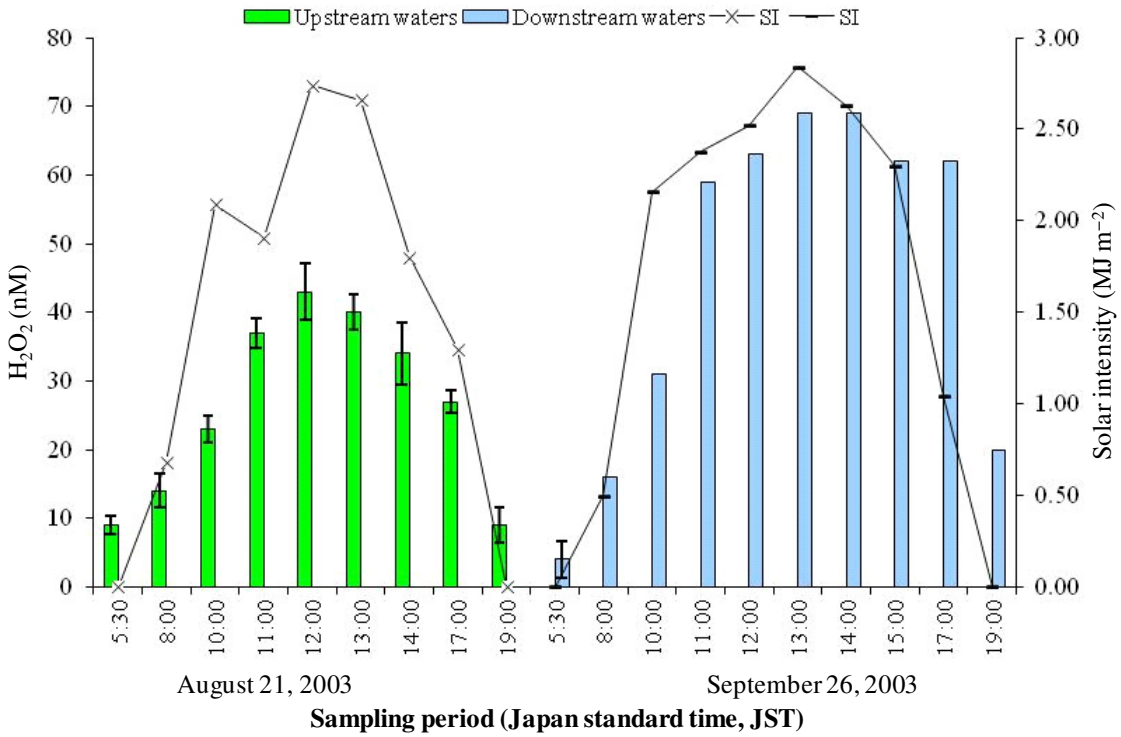
Upstream waters
Downstream waters
SI
SI
H_2O_2 (nM)
Solar intensity (MJ m^{-2})
0
10
20
30
40
50
60
70
80
0.00
0.50
1.00
1.50
2.00
2.50
3.00
5:30
8:00
10:00
11:00
12:00
13:00
14:00
17:00
19:00
5:30
8:00
10:00
11:00
12:00
13:00
14:00
15:00
17:00
19:00
August 21, 2003
September 26, 2003
Sampling period (Japan standard time, JST)

Fig. 2

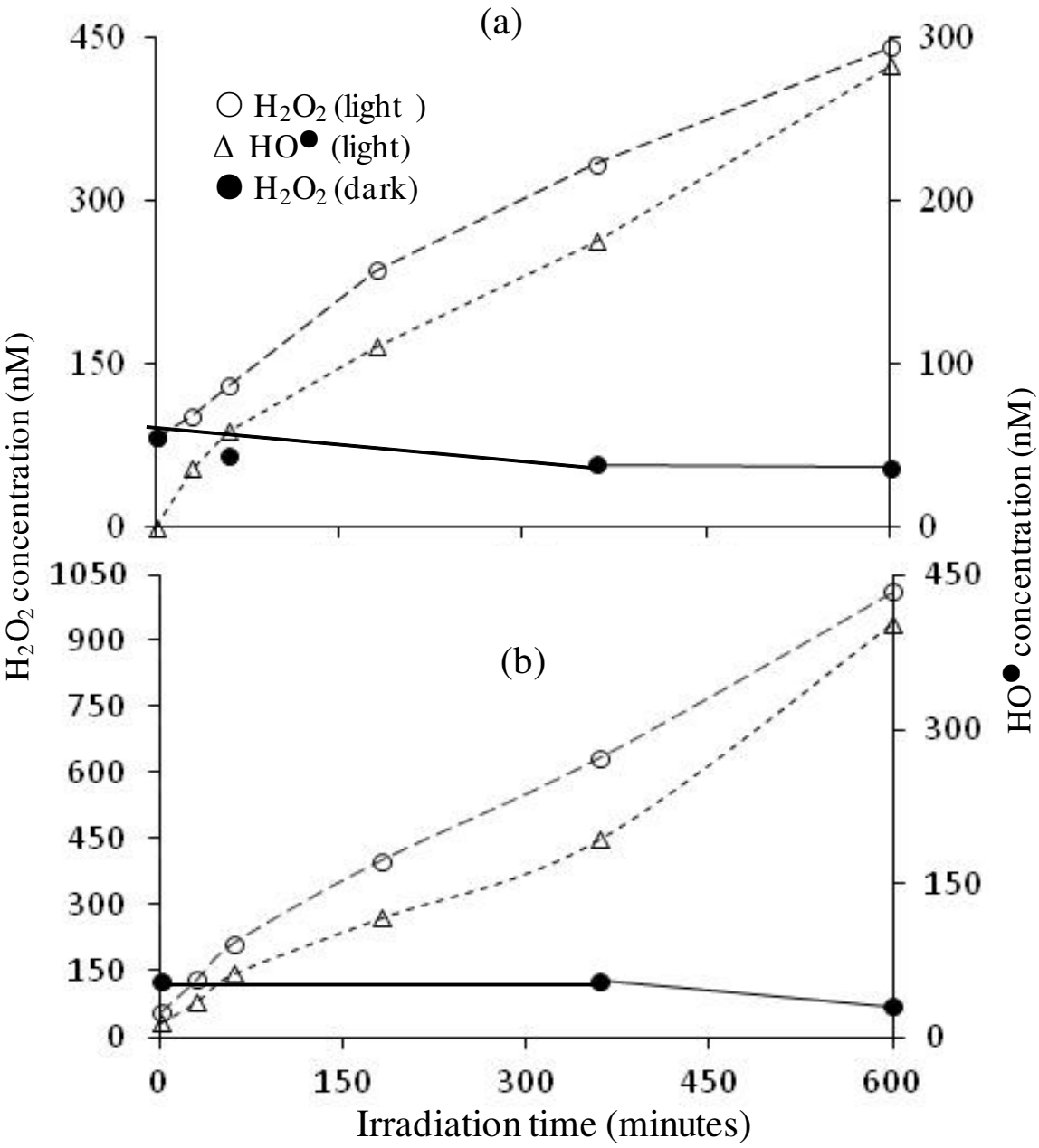
(a)
○ H_2O_2 (light)
Δ HO● (light)
● H_2O_2 (dark)
450
300
150
0
300
200
100
0
(b)
1050
900
750
600
450
300
150
0
450
300
150
0
0
150
300
450
600
Irradiation time (minutes)
H_2O_2 concentration (nM)
HO● concentration (nM)

Fig. 3

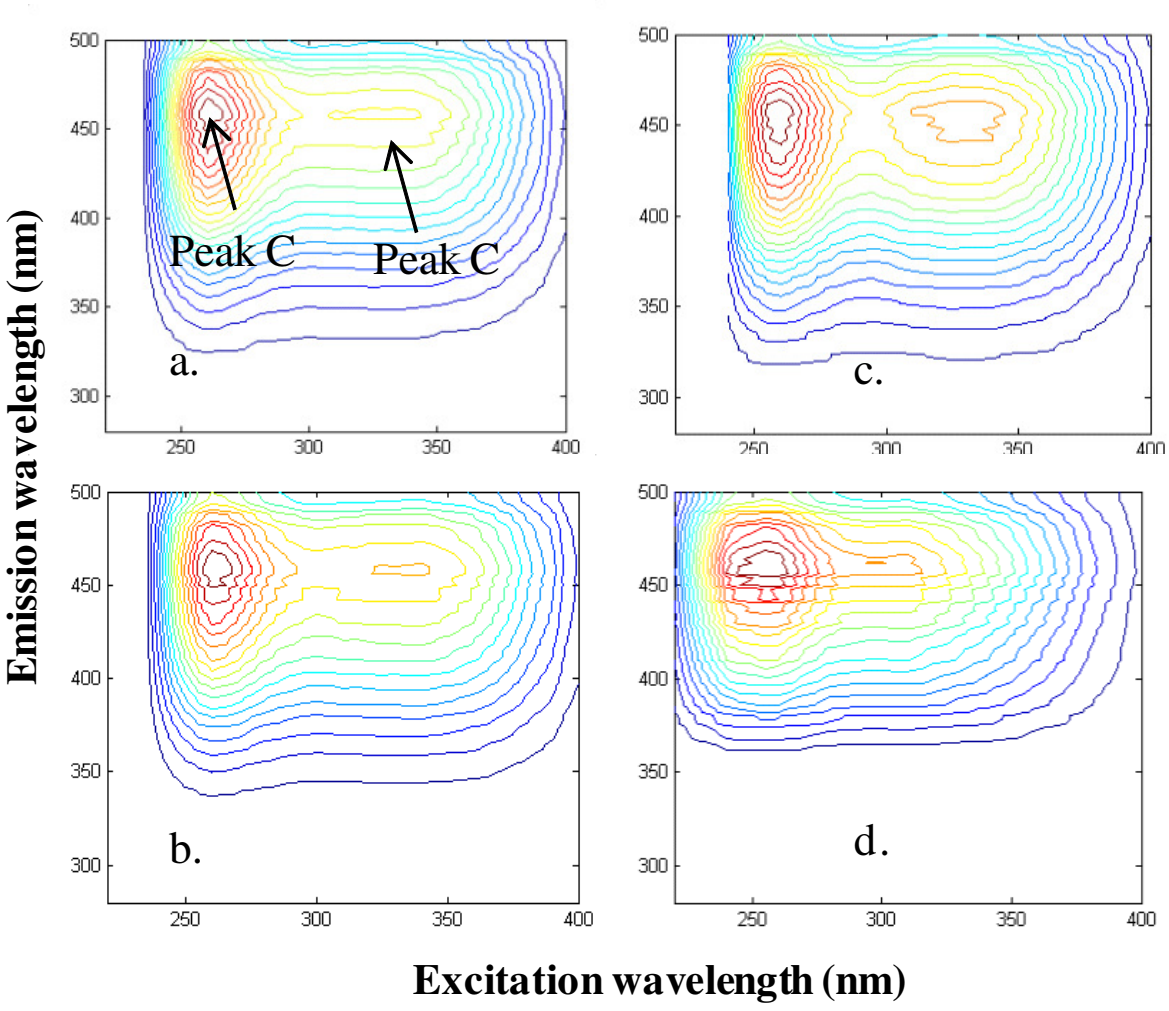
Emission wavelength (nm)
Excitation wavelength (nm)
Peak C
Peak C
a.
b.
c.
d.
500
450
400
350
300
250
300
350
400

Fig. 4

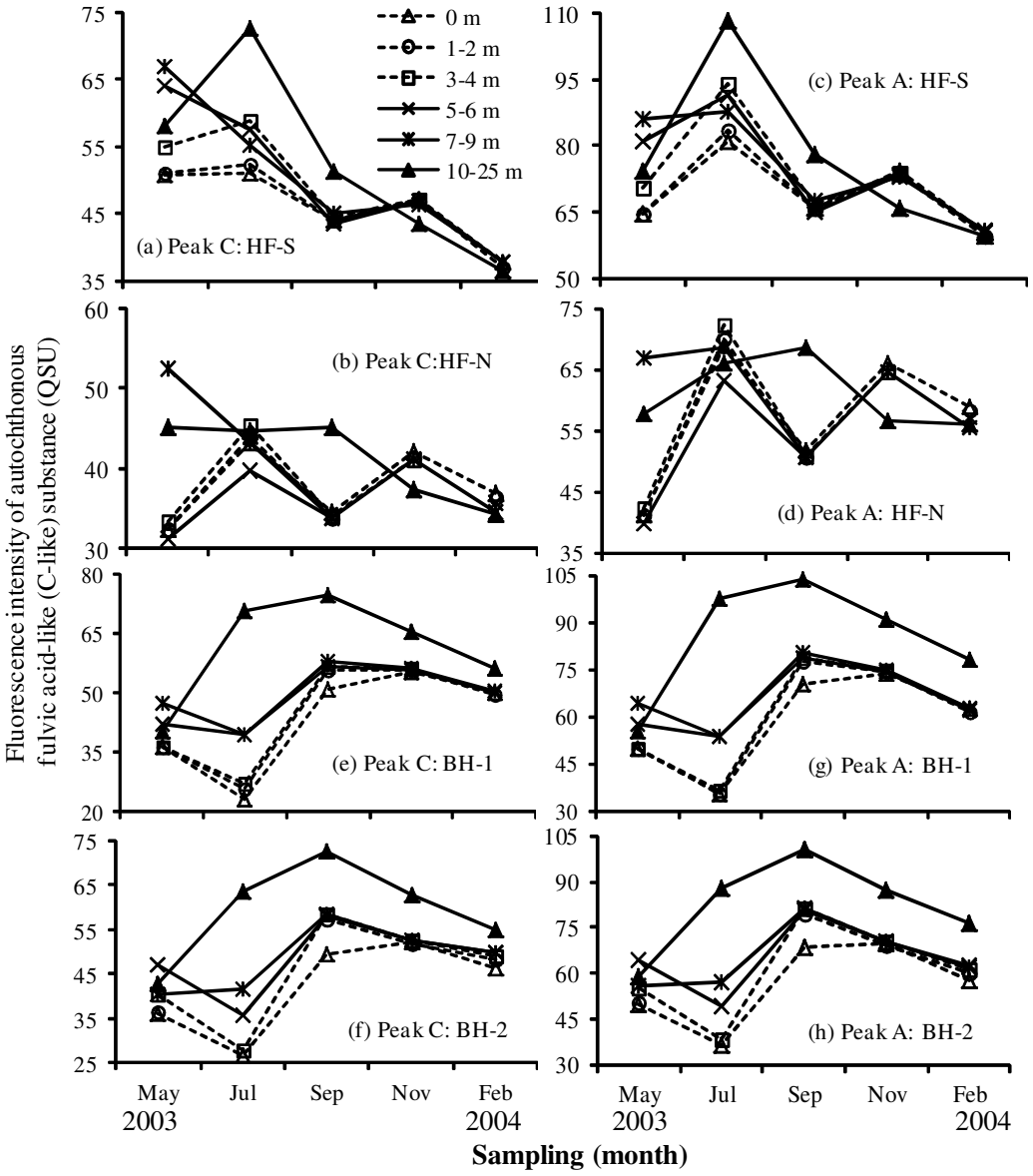
0 m
1-2 m
3-4 m
5-6 m
7-9 m
10-25 m
(a) Peak C: HF-S
(b) Peak C:HF-N
(c) Peak A: HF-S
(d) Peak A: HF-N
(e) Peak C: BH-1
(f) Peak C: BH-2
(g) Peak A: BH-1
(h) Peak A: BH-2
Fluorescence intensity of autochthonous fulvic acid-like (C-like) substance (QSU)
May
Jul
Sep
Nov
Feb
2003
2004
Sampling (month)

Chapter 8

The role of singlet oxygen in surface water photochemistry

Douglas E. Latch

Department of Chemistry, Seattle University, 901 12th Avenue, Seattle, WA 98122

latchd@seattleu.edu

Table of Contents

Abstract

Singlet oxygen, ($^1O_2$, $^1\Delta_g$), is a selective oxidant produced in sunlit surface waters. It is an electrophile produced from the quenching of excited state triplet natural organic matter (^{3}NOM) by dissolved oxygen and it reacts with electron-rich alkenes, sulfides, and phenols. The concentration of $^1O_2$ is high near the NOM molecules that sensitize its production and significantly decreases moving away from the NOM source. This chapter discusses the formation, quenching, reactivity, and detection of $^1O_2$ and includes examples of surface water contaminants that react with $^1O_2$.

8.1 Introduction

Singlet oxygen, ($^1O_2$, $^1\Delta_g$), an excited state of molecular oxygen, is one of several photochemically produced reactive intermediates (PPRIs) found in sunlit natural waters.[1-11] The presence of singlet oxygen in sunlit natural waters has been known since Zepp, et al. detected $^1O_2$ in 1977.[1] The first electronic excited state of molecular oxygen, $^1O_2$ is formed in a sensitization process in which energy is transferred from triplet states of photosensitizer species to molecular oxygen.[2,3,11-13] Compared to most other PPRIs produced from indirect photochemical processes, $^1O_2$ is a selective oxidant.[2,9,10] Its formation in the environment has been determined to be dependent upon the presence of both sunlight and chromophores in the water that can act as sensitizers.[1-5,8-10] In laboratory studies and the few field measurements that have been undertaken, $^1O_2$ displays fairly specific reactivity.[2-3,11,13] Singlet oxygen may be a key intermediate species in the transformation and fate of both pollutants and naturally occurring refractory organic compounds that abound in natural systems.

Singlet oxygen is the first electronic excited state of ground state molecular oxygen, O_2, which has two unpaired electrons in its valence shell (making it a triplet). Upon energy transfer from a sensitizer excited to its triplet state (^{3}sens), O_2 is converted to $^1O_2$. As shown in Figure 8.1, $^1O_2$ ($^1\Delta_g$) is 22.5 kcal/mole higher in energy than in the spin-unpaired ground state.[11,12,14] A more energetic form of singlet oxygen, $^1\Sigma_g$, can also be formed, but it quickly decays to $^1O_2$ ($^1\Delta_g$) in solution and will not be discussed

further in this chapter; the term $^1O_2$ is commonly used to refer to the $^1\Delta_g$ species and that convention will be used here from this point forward.[11,12,14] Since the energy gap between ground state oxygen and $^1O_2$ is relatively small, many sensitizers are capable of efficiently producing $^1O_2$.[15] Phosphorescence measurements have been utilized to monitor the radiative decay of $^1O_2$ back to the ground state.[16-19] This spin-forbidden luminescence is seen in the near infrared region of the spectrum at 1270 nm. The lifetime of $^1O_2$ is relatively long in the gas phase ($\tau = 2.58 \times 10^3$ s), but $^1O_2$ is efficiently deactivated by many solvents.[20] In aqueous solutions, solvent deactivation is the primary relaxation mode for $^1O_2$; the lifetime of $^1O_2$ in water is 4 μs.[20,21] In chemical reactions $^1O_2$ is an electrophile, reacting with electron rich alkenes and aromatic compounds, phenols, and sulfides.[2,3,11]

The importance of $^1O_2$ in the transforming organic compounds in natural waters has been the subject of debate. Because its reactivity is limited to a few general reaction types and is rapidly deactivated by water, some have thought that $^1O_2$ is a relatively insignificant oxidant in natural systems.[2,13] Some researchers rationalize that other PPRIs react more rapidly and with more types of organic molecules than does $^1O_2$, thereby making the reactions of $^1O_2$ inconsequential in the degradation of most aquatic pollutants. While $^1O_2$ may not be as active as hydroxyl radical and other PPRIs in the degradation of many organic molecules, it may be important to the fates of compounds containing certain electron rich functional groups or hydrophobic species that associate with natural organic matter (NOM; an important photosensitizer of $^1O_2$ in natural waters).

8.2 Quenching and Reactivity of Singlet Oxygen in Aqueous Solutions

8.2.1 Physical Deactivation of $^1O_2$ and the Steady-state Approximation

In solution, solvent deactivation is the primary relaxation mode for $^1O_2$. Water physically quenches $^1O_2$ with a solvent deactivation rate constant (k_{solv}) of 2.5×10^5 s^{-1}.[20,21] Organic compounds in solution are also capable of physically quenching $^1O_2$ without reacting with it. Amines such as diazobicyclo[2,2,2]octane (DABCO) exhibit this quenching behavior, as do sodium azide and β-

carotene.[20,22] Addition of these species in solutions containing $^1O_2$ leads to predictable decreases in $^1O_2$ concentrations based on the amount of quencher added and its $^1O_2$ quenching rate constant (k_q). This predictable quenching effect can be used as a diagnostic test for the involvement of $^1O_2$ in photochemical reactions. The steady-state concentration of $^1O_2$ ($[^1O_2]_{SS}$) in sunlit natural waters can be approximated based on the species that produce it and those that quench it. Equation 1 gives the rate law for $^1O_2$ formation and decay for the simple case where solvent quenching is the only significant deactivation route. In this equation, k_f is the rate constant for $^1O_2$ formation in a given solution (in units of M/s). This $^1O_2$ photosensitization rate constant depends on the concentration of excited triplet state sensitizer and the rate constant (k) at which it creates $^1O_2$ ($k_f = k[^3sens]$). Because things like light intensity and the amount of dissolved oxygen in solution impact $[^3sens]$ and k, k_f will also be dependent on these factors.

$$\frac{d[^1O_2]}{dt} = k_f - k_{solv}[^1O_2] \qquad (1)$$

In this scenario, $[^1O_2]_{SS}$ can be expressed as a balance of production and loss processes, as in equation 2.

$$[^1O_2]_{SS} = \frac{k_f}{k_{solv}} \qquad (2)$$

Upon addition of additional physical quenchers of $^1O_2$ (Q) or substrates that chemically react with $^1O_2$ (S), the $^1O_2$ rate law and $[^1O_2]_{SS}$ equations include additional terms, as shown in equations 3 and 4. In these equations k_{rxn} is the bimolecular rate constant for chemical reaction of the substrate with $^1O_2$ and k_q is for physical deactivation of $^1O_2$. In most natural water systems, physical deactivation by the water solvent dominates the denominator and the other terms can be neglected (and equation 2 can be used). Equation 4 can be useful in laboratory studies where added $^1O_2$ quenchers and reactants can be added to help determine the extent of involvement of $^1O_2$ in a given photoreaction.

$$\frac{d[^1O_2]}{dt} = k_f - k_{solv}[^1O_2] - k_q[Q][^1O_2] - k_{rxn}[S][^1O_2] \qquad (3)$$

$$[^1O_2]_{SS} = \frac{k_f}{k_{solv} + k_q[Q] + k_{rxn}[S]} \qquad (4)$$

8.2.2 General Chemical Reactions Involving $^1O_2$

In addition to radiative decay and physical quenching, $^1O_2$ also undergoes a series of specific chemical reactions.[2,3,11,20] Examples of these chemical-quenching methods are shown in Figure 8.2. One of the most studied reactions involving $^1O_2$ is the [4+2] cycloaddition reaction that it undertakes with conjugated dienes.[2,3,11] Several studies have shown that $^1O_2$ reacts with acyclic, cyclic, and heterocyclic dienes, and Wilkinson, et al. (1995) have compiled bimolecular rate constants for many such reactions.[20] This reaction class is analogous to Diels-Alder reactions that occur between dienes and alkenes that are commonly taught in introductory organic chemistry courses. The initial product of the [4+2] cycloaddition reaction is an endoperoxide. Oftentimes, however, the endoperoxide is too unstable to be isolated, and it undergoes further reactions that are indicative of the endoperoxide intermediate.[11] The most important [4+2] cycloadditions that are used in environmental analyses of $^1O_2$ are those with furan-based molecules that have been employed as $^1O_2$ sensors.[1,23-26]

Singlet oxygen also participates in [2+2] cycloadditions.[2,11] This reaction occurs between one electron-rich carbon-carbon double bond and $^1O_2$ to form 1,2-dioxetane products. Most dioxetanes are unstable due to the strain in forming the 4-membered ring and break down to form other products shortly after being formed.[11] Certain sterically protected dioxetanes, however, are quite stable. A third reaction mode that exists between $^1O_2$ and unsaturated organic molecules is the ene reaction.[11] This reaction yields hydroperoxide products.

In addition to reacting with alkenes, $^1O_2$ has also been shown to be reactive towards sulfides.[2,11,20,27,] Ackerman demonstrated that electron-rich sulfides are more reactive to singlet-oxygenation than electron-poor species; this is consistent with $^1O_2$ electrophilic character.[27] Compilations of rate constants exist for the reaction of different sulfides with $^1O_2$.

Perhaps the most studied $^1O_2$ reaction in the environment is the singlet-oxygenation of phenolic molecules.[28-35] Since the phenolic moiety is an important part of many organic substances found in natural, drinking, and wastewaters, Tratnyek and Hoigné studied the interaction between $^1O_2$ and various

phenolic compounds in aqueous environments.[31] With knowledge that the more electron rich phenolate ion reacts more quickly with $^1O_2$ than does the parent phenol, they studied various substituted phenols in aqueous solutions over a range of pH values. Their work has made it possible to predict the rate of oxidation of differently substituted phenols as a function of the basicity of the water.[31,3]

8.3 Singlet Oxygen Detection Techniques

Quantifying the presence of PPRIs such as $^1O_2$ under field conditions can be difficult due to their low concentrations, limited sensitivity of the measurement methods, and non-specific reactivity of sensor molecules.[9,10, 36,37] Various measurement techniques have been employed to quantify the presence of $^1O_2$ in laboratory and field settings. Most molecular probes for $^1O_2$ have been designed based on its selective reactivity with electron rich alkenes. In laboratory settings, one can also directly monitor the phosphorescence emitted as $^1O_2$ decays back to ground-state O_2.[15-19] The following sections highlight the direct and indirect techniques often used to assess the concentration of $^1O_2$ in solution.

8.3.1 Singlet Oxygen Probe Molecules

Most environmental reports of $^1O_2$ detection involve molecular probes, in which the degradation of a compound with known reactivity with $^1O_2$ or the formation of the products of a singlet-oxygenation reactions are followed during the course of a photolysis experiment.[1,23,26,36,37] This technique necessitates removing a water sample from the system of interest, adding the trapping agent to the water sample, and irradiating the mixture. The loss of the probe molecule or the formation of $^1O_2$-specific reaction products is then tracked (usually by high performance liquid chromatography) over time. The probe molecule should be carefully chosen to react selectively with $^1O_2$ in a well-controlled, predictable manner. The rate at which the probe molecule (P) degrades (or products form) is then used as an indirect method to calculate $[^1O_2]_{SS}$, as depicted in equations 5 - 7. Equation 5 is the rate law for probe loss due to $^1O_2$ and equation 6 is a linearized form that can be plotted to give the observed degradation rate constant (k_{obs}).

This can be used with the probe's known rate constant for reaction with $^1O_2$ to determine $[^1O_2]_{SS}$ as shown in equation 7.

$$-\frac{d[P]}{dt} = k_{rxn}[P][^1O_2]_{SS} \quad (5)$$

$$\ln\left(\frac{[P]_t}{[P]_0}\right) = -k_{rxn}[^1O_2]_{SS}t = -k_{obs}t \quad (6)$$

$$[^1O_2]_{SS} = \frac{k_{obs}}{k_{rxn}} \quad (7)$$

Zepp, et al. provided an early example of using molecular probes to detect $^1O_2$ in irradiated natural waters.[1] In their seminal work, they capitalized on the fact that $^1O_2$ reacts quickly with 2,5-dimethylfuran (DMF). An additional consideration in choosing DMF as a $^1O_2$ probe was the fact that its photooxygenation products are well characterized.[1,9,37] This means that the loss of DMF or the formation of its known $^1O_2$ reaction products could be tracked to determine how much $^1O_2$ was present in irradiated natural waters. Figure 8.3 shows the structure of DMF and its reaction products.

In the years following the work of Zepp, et al., it was reported that H_2O_2 was a possible interfering oxidant in the determination of $[^1O_2]$ by DMF.[8-10] As a result, Haag and coworkers developed a new probe for selectively detecting $^1O_2$ in natural waters.[23] The researchers outlined the characteristics of a good $^1O_2$ probe molecule:

A good $^1O_2$ probe should exhibit:

- no direct photolysis or self-sensitization
- no radical-initiated autooxidation or polymerization
- no interference by its own photooxygenation products
- no quenching of sensitizer triplets
- no physical quenching of $^1O_2$ (or a small, known fraction)
- high rate constant for reaction with $^1O_2$
- rate constant independent of pH (or with known dependence)
- high water solubility

Taking these factors into account, furfuryl alcohol (FFA) was employed as a $^1O_2$-trapping agent.[23-25] Like with DMF, FFA's singlet-oxygenation products are well known, as seen in Figure 8.3.[3,9,37]

An experimental advantage that FFA has over DMF is the fact that it is less volatile and more water-soluble than DMF. These two considerations allow for less demanding sampling techniques. The sensitivity of FFA, however, does not match that of DMF, as the rate constant for reaction with $^1O_2$ is about five times lower for FFA.

Aguer and Richard studied the reactivity of another furan-based molecule, furoin, as a probe for PPRIs.[26] Not only did they find that furoin reacts with both $^1O_2$ and hydroxyl radical (•OH), it was also determined that different products resulted depending on which PPRI was present. Since the relative contribution of •OH reaction with furoin could be differentiated from that of $^1O_2$, this research highlighted the promise of using furoin as a probe for the simultaneous measurement of both $^1O_2$ and •OH.

In an attempt to improve indirect chemical trapping methods for $^1O_2$, Nardello, et al. employed non-furanyl compounds as probe molecules.[38-39] A primary motivation for developing these probes was the uncertainty in which furanyl probe photooxidation products could be attributed to reaction with $^1O_2$. The probe molecules that they developed reacted quantitatively with $^1O_2$ to form a stable endoperoxide as the major/only product. An advantage of isolating the endoperoxide product is that other oxidants that could conceivably react with the probe would not produce an endoperoxide, thereby giving evidence to the direct involvement of $^1O_2$. A recent review of methods for detecting PPRIs in aqueous systems identified only FFA and 1,3-cyclohexadiene-1,4-diethanoate (CHDDE), one of the probes developed by Nardello, et al., as the only two probe molecules that fit Nardello's definition of a good $^1O_2$ probe (as articulated in references 37 and 39).[38] Figure 8.3 also shows the reactivity of CHDDE with $^1O_2$. Major advantages of FFA are the copious prior studies using it as a $^1O_2$ probe to use as reference and its wide commercial availability. Although FFA has been widely adopted as a $^1O_2$ probe molecule, it does have some shortcomings. Other PPRIs such as •OH and excited state triplet organic matter (^{3}OM) can react with FFA and degrade it. The extent to which the different pathways are involved in FFA degradation can be deduced by tracking the formation of $^1O_2$ specific FFA degradation products, calculating the expected contribution of •OH to FFA loss based on independent measurements of $[•OH]_{SS}$ and the known rate constant for reaction of •OH with FFA, and through the use of $^1O_2$ quenchers to identify any additional

loss of FFA not attributable to $^1O_2$ or •OH. Al Housari, et al. provide a thorough description of this process of delineating the specific pathways responsible for FFA photodegradation.[40]

Luminescence-based $^1O_2$ probes have also been developed, but none have been widely adopted in the detection of $^1O_2$ in surface waters.[37] One pair of chemiluminescent probes that have been used to detect $^1O_2$ in environmental samples will be described later (in section 8.5).[41-43]

8.3.2 Direct Detection of Singlet Oxygen Phosphorescence

Phosphorescent measurements of the relaxation of $^1O_2$ back to ground state O_2 were first utilized in the 1960s to determine the pure radiative lifetime of $^1O_2$.[15] While initial studies examined the luminescent properties of $^1O_2$ in the gas phase, good solution phase results proved to be more elusive. Krasnovsky was the first researcher to monitor the phosphorescent signal emitted by $^1O_2$ in solution.[16] With sensitizers dissolved in air-saturated solutions of carbon tetrachloride, a phosphorescent signal centered at 1270 nm was observed when the solutions were irradiated in a steady-state fashion. In addition to observing the radiative decay of $^1O_2$, Krasnovsky also noted that the signal was proportional to the amount of sensitizer present in solution. Following this study, Krasnovsky developed a phosphoroscope instrument to monitor the 1270 nm luminescence signal.[17] Among other things, this instrument was used to study the efficacy of different sensitizers as $^1O_2$ generators and the effect of solvent on the lifetime and quantum yield of $^1O_2$. The next major improvement in directly observing $^1O_2$ luminescence was the application of short duration laser pulses as the source of excitation.[18,19] Laser flash photolysis (LFP) systems that arose from these technological improvements are now used in environmental laboratories to study the reactivity of pollutants and other chemicals found in surface waters with $^1O_2$ and to measure quantum yields of $^1O_2$ production.[7,44-46]

8.4 Production of Singlet Oxygen

8.4.1 Photochemical Production from Dissolved Natural Organic Matter in Natural Waters

Zepp and co-workers showed that aquatic natural organic matter can act as sensitizers for the production of $^1O_2$ in natural waters.[1,4,5] Their findings were reinforced by many other researchers studying the photochemical properties of NOM, a few of which will be presented here. Frimmel et al. have measured quantum yields of $^1O_2$ production (Φ_Δ) for several NOM samples.[7] The Φ_Δ is defined as how many $^1O_2$ molecules are produced per photon absorbed by the sensitizer. Using laser flash photolysis methods, they measured $^1O_2$ quantum yields of between 1.5 – 3.0 % for a variety of NOM source materials, with a soil NOM sample giving a particularly high yield relative to aqueous NOM. Sandvik, et al. examined $^1O_2$ production from NOM along salinity transects in an estuary.[17] They report Φ_Δ values ranging from 1.7 – 6.1 %. They also found that NOM of lower molecular weights gave larger Φ_Δ, and that NOM isolated from different locations along a salinity gradient gave similar Φ_Δ.

Paul, et al. used a laser flash photolysis method and monitored the phosphorescence of $^1O_2$ to determine Φ_Δ for NOM samples isolated from several aquatic, soil, swamp, and peat sources.[45] They report Φ_Δ values ranging between 0.16 – 0.91 % for aquatic NOM, 0.26 – 2.69 % for soil NOM, 0.81 – 0.83 % for peat NOM, and 0.61 % for the one swamp source tested. In addition to reporting higher Φ_Δ for soil NOM, they also found that a synthetic OM was a very poor producer of $^1O_2$.

Several studies have been undertaken to correlate Φ_Δ with other measurable characteristics of NOM. Dalrymple, et al. studied the production of $^1O_2$ from various aquatic NOM samples and found that Φ_Δ correlates well with the E2/E3 ratio (ratio of the absorbance at 254 nm to absorbance at 365 nm) of the NOM.[48] Measured Φ_Δ values ranged from 0.59 – 4.5 %. They also showed that while Φ_Δ decreases as pH increases for a given NOM sample, solution pH alone is a poor predictor of Φ_Δ. Peterson, et al. also observed a positive correlation between Φ_Δ and E2/E3 ratio.[49] They measured Φ_Δ and $^1O_2$ formation rates from Lake Superior water collected near shore to more interior regions of the lake. These water samples varied considerably in NOM content and the extent to which they were influenced by riverine sources

draining into the lake. They found that $^1O_2$ formation rates were much higher near the shore where NOM concentrations were significantly higher, but that Φ_Δ was greater in the open lake (where the NOM had high E2/E3 signatures).

Marchisio, et al. found that Φ_Δ increases as excitation wavelength decreases for NOM collected from several lakes, but the effect is much less dramatic than that observed for hydroxyl radical and ^{3}NOM.[50] They report Φ_Δ values ranging from 0.4 – 1.7 %, with the lowest value measured with the longest irradiation wavelength (420 nm) and the highest value measured upon excitation with the shortest wavelength (313 nm). The authors used the wavelength dependence of Φ_Δ in modeling the expected decrease in $[^1O_2]_{SS}$ with depth of the water column.

Sharpless examined $^1O_2$ photoproduction from NOM samples that had been reduced with $NaBH_4$.[51] His experiments showed that the Φ_Δ is negligibly impacted upon NOM reduction, with Φ_Δ ranging from 1.4 to 3.2 %. Various NOM sources gave different Φ_Δ that scaled with E2/E3 ratios and overall $^1O_2$ production rates decreased upon NOM reduction due to associated decreases in NOM absorbance. He proposes that borohydride reducible species such as aromatic ketones are involved in the $^1O_2$ sensitization process. Like Marchisio, et al., Sharpless also found that Φ_Δ increased as excitation wavelengths decreased. In another study, Sharpless, et al. examined the effects of photooxidation on NOM's ability to produce $^1O_2$.[52] They report Φ_Δ values between ~1.4 and 2.0 % for two aquatic NOM and one soil NOM prior to irradiation and that the values increase to ~ 1.7 and 2.7 % following photooxidation of the NOM. Photooxidation of the NOM thus leads to more efficient production of $^1O_2$. It should be noted that photoweathering of the soil sample tested led to more dramatic increases in Φ_Δ, even though its E2/E3 ratio increased much less dramatically upon light exposure than those of the aquatic NOM tested. The Φ_Δ values reported in this study scale with the E2/E3 ratio when following the evolution of these parameters upon photooxidation of a given NOM sample; the trends differ considerably when comparing across NOM sample types. Measured Φ_Δ values showed a weak negative correlation with the electron donating and electron accepting capacities of the NOM, indicating that NOM containing a high

percentage of redox active functional groups are slightly less efficient sensitizers of $^1O_2$ than NOM with fewer redox active sites.

8.4.2 Photochemical Production from Effluent Organic Matter in Natural Waters

In addition to NOM, other organic matter found in natural waters can sensitize the production of $^1O_2$. Several recent papers report on the ability of effluent organic matter (EfOM) from wastewater treatment plants or samples collected from EfOM-impacted surface waters to produce $^1O_2$. Mostafa and Rosario-Ortiz report that EfOM is an efficient producer of $^1O_2$, giving higher Φ_Δ values (2.8 – 4.7 %) than commonly used NOM sources (1.6 – 2.1 %).[53] Increases in Φ_Δ upon oxidation of the EfOM were observed (reaching as high as 9.3 %), which is consistent with the photooxidation results for NOM reported by Sharpless, et al. A study by Zhang, et al. gave similar results.[54] They found that an EfOM also had a higher Φ_Δ than several NOM samples (2.66 % versus 1.34 – 1.85 %). They also measured Φ_Δ of different EfOM fractions and found that the hydrophilic fraction gave the highest value (8.16 %; transphilic and hydrophobic fractions gave Φ_Δ values of 2.45 and 3.24 %, respectively). They deduce that the hydrophilic fraction dominates $^1O_2$ production in EfOM. Bodhipaksha, et al. studied the photochemical properties of EfOM-impacted waters.[55] They examined whole water samples and isolates and found that Φ_Δ correlated with the production efficiency of ^{3}OM, which is to be expected based on $^1O_2$ being a downstream product of ^{3}OM. Like others, they found that Φ_Δ scaled with E2/E3 ratio and that Φ_Δ decreased as the electron donating capacity of the OM increased. They report greater photochemical reactivity of the whole water samples than that of the isolates, cautioning against the sole use of isolates in photochemical studies. In experiments where EfOM and DOM solutions were mixed in various proportions, no increases in $^1O_2$ production due to EfOM (the more efficient producer of $^1O_2$) were observed, which was ascribed to EfOM quenching ^{3}NOM.

8.4.3 Photochemical Production from Particulate Natural Organic Matter in Natural Waters

The photosensitizing properties of particulate organic matter (POM) are not well understood. A recent paper used synthetic POM (silica particles coated with commercial OM) to explore the ability of the POM to produce $^1O_2$.[56] Through the use of probe molecules capable of sorbing to the POM, they found that POM is a poorer sensitizer of $^1O_2$ relative to dissolved NOM, but that the sorbed probes degraded more rapidly than in DOM solutions in the absence of POM due to the relatively high [$^1O_2$] at the POM surface. This is consistent with a pair of studies describing the heterogeneous distribution of $^1O_2$ in irradiated DOM solutions (see section 8.5). For moderately hydrophobic pollutants that are reactive toward $^1O_2$ (log K_{OC} ~ 3 – 5), these particles could be important in their fates. A model is given to show how observed $^1O_2$ concentrations are expected to change for substrates of varying hydrophobicity upon filtration of POM from photolysis solutions.

8.4.4 Steady-state Concentrations of $^1O_2$ in Surface Waters

The relatively low quantum yields of $^1O_2$ production by surface water constituents and rapid deactivation by water leads to low steady-state $^1O_2$ concentrations in natural waters. Studies have reported $[^1O_2]_{SS}$ ranges between 10^{-15} and 10^{-12} M at the surface.[8-10,37] Concentrations of $^1O_2$ are expected to decrease with depth and will depend on the how colored the water is.[2,3,49,50] Marchisio, et al. model the predicted depth profile for [$^1O_2$] for two different NOM concentrations based on light filtering through the water column and Φ_Δ measured at different excitation wavelengths.[50]

8.4.5 Other $^1O_2$ Sources for use in the Laboratory

In laboratory studies, one can choose synthetic photosensitizers that produce $^1O_2$ with high quantum efficiencies. Methylene Blue, Rose Bengal, and perinaphthenone are a few examples of such sensitizing dyes, with quantum efficiencies of 0.50, 0.75, and 0.95, respectively.[20,58] Such high quantum yields are not observed with the materials present in natural waters, and these synthetic sensitizers can be used to assess the reactivity and reaction mechanisms of $^1O_2$ with various substrates. This is a common

method used to measure bimolecular rate constants for reaction with $^1O_2$. Singlet oxygen can also be generated in non-photochemical reactions.[11] These reactions can be useful for measuring a substrate's reactivity with $^1O_2$ in the absence of other light induced processes (i.e. direct photolysis or reaction with other PPRIs). Foote and Clennan describe several of these relatively clean methods for producing $^1O_2$.[11]

8.5 Microheterogeneous Distribution of Singlet Oxygen in Natural Waters

8.5.1 Microheterogeneous $^1O_2$ Distributions

One important finding from non-environmental photochemical studies is that $^1O_2$ exhibits heterogeneous concentration profiles in multiphasic media; the presence of microphases that co-localize and concentrate the sensitizer and substrate leads to enhanced $^1O_2$ reaction rate.[58,59] A set of recent studies have shown that aqueous solutions of NOM act in a similar fashion, with regions of high $^1O_2$ localized in and near the photosensitizing NOM molecules and much lower concentrations in the bulk aqueous phase.[42-43] The production and distribution of $^1O_2$ and the partitioning of probe molecules between the NOM microsphere and the bulk aqueous phase is shown in Figure 8.4. This microheterogeneity of $^1O_2$ distributions is potentially important because hydrophobic pollutants can partition into NOM and potentially witness much higher $^1O_2$ concentrations than molecules freely dissolved in the aqueous phase. Such hydrophobes could thus degrade more quickly than would be expected based on $[^1O_2]_{SS}$ values measured by hydrophilic probes. For this reason, Hassett described NOM as possibly being a potent microreactor for breaking down hydrophobic pollutants.[60]

To demonstrate microheterogeneous $^1O_2$ distributions in aqueous NOM solutions, chemiluminescent hydrophobic probe molecules capable of partitioning into the NOM microphase and reacting selectively with $^1O_2$ were analyzed alongside FFA.[41] Figure 8.5 shows these probes and their detection scheme. Specifically, spiroadamantyildene-substituted vinyl ethers (**1a** and **1b** in Figure 8.5) reacted with $^1O_2$ to form stable dioxetane products (**2a** and **2b**). Following trapping, the dioxetanes are induced to decompose with luminescence upon addition of tetra-n-butylammonium fluoride (TBAF); this type of trap-and-trigger luminescence technique gives good sensitivity. When aqueous NOM solutions

were irradiated in the presence of the various probes, the hydrophobic probe molecules that associate with the NOM microphase reported much greater $^1O_2$ concentrations than FFA did, thus supporting the microheterogeneous distribution of $^1O_2$ in sunlit surface waters.[42,43]

A probe molecule or pollutant will witness an apparent $^1O_2$ concentration ($[^1O_2]_{app}$) that is a function of its partitioning between the NOM and bulk aqueous phases and the volume averaged $^1O_2$ concentrations in the NOM and aqueous phases, as shown in equation 8. The $[^1O_2]_{app}$ that a given probe molecule sees can be easily calculated based on the probe's loss rate (or product formation rate), the probe concentration, and the probe's k_{rxn} with $^1O_2$, as shown in equations 9 and 10. These equations would also apply to hydrophobic pollutants.

$$[^1O_2]_{app} = f_{NOM}[^1O_2]_{NOM} + f_{aq}[^1O_2]_{aq} \quad (8)$$

$$-\frac{d[P]}{dt} = k_{rxn}[P][^1O_2]_{app} \quad (9)$$

$$[^1O_2]_{app} = \frac{\left(\frac{-d[P]}{dt}\right)}{k_{rxn}[P]} \quad (10)$$

A model was developed to account for and provide a visual representation of the microheterogeneous distribution of $^1O_2$ produced from the irradiation of NOM. In this model, NOM is considered to be a distinctive phase comprised of many spherically shaped monodisperse NOM particles inside which the sensitizing chromophores are evenly distributed. According to this description, $^1O_2$ is produced only in the NOM microenvironment. Upon irradiation a concentration gradient develops between the NOM microphase and the surrounding aqueous environment. This gradient drives a net flux of $^1O_2$ out of the NOM and into the aqueous phase. Singlet oxygen has a limited diffusion distance due to its rapid deactivation by water. The $[^1O_2]$ is thus reduced over time as the $^1O_2$ diffuses away from the NOM region. Equation 11 shows how the concentration decreases over time ($[^1O_2]_t$) relative to its initial concentration in the NOM region ($[^1O_2]_0$).

$$[^1O_2]_t = [^1O_2]_0 e^{-k_D t} \text{ and } t = \frac{l^2}{D} \qquad (11)$$

One can convert this time-based change in $[^1O_2]$ to distance from the NOM phase with knowledge of the length (l) a transient species can diffuse over time. Here D is the diffusivity of O_2 in water and k_D is the aqueous phase $^1O_2$ deactivation rate constant ($k_D = k_{solv} + k_q[Q]_{aq}$, where $[Q]_{aq}$ is the aqueous phase concentration of a quencher of $^1O_2$). Figure 8.6 shows a cartoon depiction of the dramatic effect of aqueous phase quenching of $^1O_2$ as it diffuses from the NOM region to the aqueous phase. Very recently, $^1O_2$ microheterogeneity was reported in the particulate organic matter (POM) sensitized production of $^1O_2$, as described above (section 8.4.3).

8.5.2 Effects of Quenchers and the Kinetic Solvent Isotope Effect on Microheterogeneous $^1O_2$ Distributions

Common tests used to confirm the involvement of $^1O_2$ in aqueous phase reactions did not appreciably alter the responses of the hydrophobic probe molecules and cannot be used as diagnostics for $^1O_2$ reactions in the NOM microenvironment. Experiments in aqueous solutions with NOM and added $^1O_2$ quencher sodium azide were performed to determine its effects on $[^1O_2]_{NOM}$ and $[^1O_2]_{aq}$. Addition of azide caused a predictable decrease in FFA photodegradation rate, due to a precipitous drop in the average $[^1O_2]_{aq}$ in the presence of the additional quencher. In contrast to the FFA results, the data obtained for the hydrophobic probes display a much smaller quenching effect; these probe molecules sample the $^1O_2$ in the hydrophobic NOM microenvironment that is inaccessible by the hydrophilic azide ion quencher.

The hydrophobic $^1O_2$ quencher β-carotene was also added to solutions of the most hydrophobic probe and NOM to determine its effect on $^1O_2$ contained in the environment of the NOM microphase. Based on a known β-carotene quenching rate constant and the nominal quencher concentrations in the experiments, the magnitude of the quenching at these concentrations was much higher than predicted by the conventional homogeneous $^1O_2$ distribution model. The enhanced reactivity displayed by β-carotene is a consequence of the actual sample volume that it occupies; due to its low aqueous solubility and

extremely high hydrophobicity, β-carotene is expected to be present predominately in the NOM microphase, which occupies a much smaller volume than the bulk solution. This leads to higher effective β-carotene concentrations within the NOM region and efficient quenching of $[^1O_2]_{NOM}$.

The kinetic solvent isotope effect measured by the hydrophobic probes was also much different than that observed with hydrophilic probes. Only minimal solvent effects were seen with the hydrophobic probes when the solvent was changed from H_2O to D_2O, whereas this change in solvent composition normally would lead to about thirteen-fold increases in loss rates of aqueous phase probe molecules due to the longer $^1O_2$ lifetime in D_2O.[20,21,42] This result was consistent with numeric modeling results that predicted little change in $[^1O_2]_{NOM}$ upon changing the solvent from H_2O to D_2O.[42]

8.6 Examples of Aquatic Species Potentially Transformed by Singlet Oxygen in Surface Waters

Despite the fact that many pollutants contain functional groups that are known to react with $^1O_2$, few studies report its involvement in the degradation of pollutants. Oftentimes pollutants that are prone to reaction with $^1O_2$ also are susceptible to direct photolysis or reactions with other PPRIs. This section describes some of the surface water species that are reactive toward $^1O_2$ to varying degrees.

8.6.1 Cimetidine and Ranitidine

Cimetidine and ranitidine are two high use antacids that have been detected in surface waters.[61,62] Both were found to be photoreactive, with ranitidine degrading mostly through direct photolysis with a small contribution (~10 %) due to $^1O_2$ in Mississippi River water.[44] The photodegradation of cimetidine, however, is dominated by reaction with $^1O_2$. The photochemical behavior of cimetidine is thus highlighted here because it is the rare aquatic pollutant whose photochemical fate is attributed solely to reaction with $^1O_2$. The role of $^1O_2$ in the degradation of cimetidine was deduced from quenching studies that clearly implicated $^1O_2$ and ruled out radical species. The reactivities of cimetidine and model compounds of cimetidine were assessed using steady state and laser flash photolysis experiments with

efficient, synthetic sensitizers of $^1O_2$. Figure 8.7 summarizes some of this work. The model studies show that the cyanoguanidine unit of cimetidine is unreactive toward $^1O_2$, ruling out reaction at that site. Both the substituted imidazole ring and the sulfide site showed reactivity with $^1O_2$, with the sulfide site reacting about an order of magnitude slower than the imidazole and cimetidine parent species. This means that the majority of the $^1O_2$-induced degradation of cimetidine is likely to occur at the imidazole ring. Only one product (in low yield) was identified, cimetidine sulfoxide; sulfoxides are common products of $^1O_2$ reactions with sulfides. The low yield of this product is consistent with the sulfide site contributing only slightly to the degradation of cimetidine. Additional studies at different pH values showed that the reaction of $^1O_2$ with cimetidine was highly sensitive to pH due to the basicity of the imidazole nitrogen. Since protonation of the imidazole ring creates a positive charge, reactivity with the electrophilic $^1O_2$ is significantly altered, with much lower rate constants at low pH ($k_{rxn} = 2.2 \times 10^8$ $M^{-1}s^{-1}$ at pH 8 and $k_{rxn} = 3.3 \times 10^6$ $M^{-1}s^{-1}$ at pH 4). The half-lives of cimetidine are expected to vary considerably from site to site based on differences in $[^1O_2]_{SS}$ and pH across various surface waters. Peterson, et al. calculated expected cimetidine half-lives across an NOM gradient in Lake Superior.[49] They predicted near surface half-lives ranging from less than 4 h near shore where riverine NOM at relatively high concentrations dominates to 120 h in the open lake where NOM concentrations are much lower. When accounting for loss of cimetidine throughout the entire water column, half-lives were predicted to be considerably larger due to light attenuation; calculated half-lives ranged from 44 to 155 days depending on season and location within the lake.

8.6.2 Pesticides

Pesticides are well-studied pollutants in terrestrial and aquatic systems. The photochemical behaviors of a great variety of pesticides from various chemical classes have been reported. Few of these reports implicate $^1O_2$ in the surface water photodegradation of pesticides under environmentally relevant conditions. Two reviews regarding the photochemical fates of pesticides, however, report that some pesticides such as thiobencarb, carboxine, uracil herbicides and pyrimidine fungicides are degraded when

irradiated in the presence of synthetic sensitizers of $^1O_2$.[63,64] These pesticides may also be subject to $^1O_2$ reactions in sunlit surface waters. The pesticides that have been reported to degrade by $^1O_2$ under field relevant conditions are described here, and the structures of these species can be seen in Figure 8.8 Mesotrione is a triketone herbicide that has been introduced to the market relatively recently. It undergoes a self sensitized reaction with $^1O_2$ under direct photolysis conditions, but its photodegradation rate in NOM solutions was accelerated relative its direct photolysis rate.[65] The study's authors attributed the rate enhancement to reaction with $^1O_2$. Zeng and Arnold studied the photochemical fates of sixteen pesticides in prairie pothole lake water.[66] The NOM from these pothole lakes led to the increased removal rate of the pesticides. The extent of indirect photolysis was assessed relative to direct photolysis by comparing loss rates in buffered pure water to those in the pothole water. Quenching studies were conducted to assess the relative importance of individual PPRI on the indirect photodegradation of the pesticides. Their results show that $^1O_2$ contributed to the degradation of several pesticides to varying degrees. About 10 % of the loss of mesotrione was attributed to $^1O_2$ in this system, with the majority being due to ^{3}NOM. The role of $^1O_2$ was more substantial in the loss of bentazon (~40 % of its total degradation was due to $^1O_2$), clopyralid (~45 %), chlorpyrifos (~30 %), and propiconazole (~70 %). Fenthion undergoes a self-sensitized reaction with $^1O_2$ whereby it forms a stable sulfoxide product.[64] The formation of a sulfoxide product in environmentally relevant indirect photolysis experiments provides evidence for some involvement of $^1O_2$ in the oxidation of disulfoton.

8.6.3 Hormones and Hormone Mimics

Estrogenic steroid hormones have been widely studied in surface waters due to their potent biological activity. Grebel, et al. show that the photochemical fate of 17β-estradiol (E2) is expected to be strongly influenced by salinity (see Figure 8.8 for the structure of E2 and the other chemicals listed included in this section).[67] They report that the contribution of $^1O_2$ to the photodegradation of E2 is negligible in freshwater and that the E2 photodegradation rate was reduced by 90 % in saline waters. They also found that the relative contributions of different PPRIs changed in moving from freshwater to

seawater, with $^1O_2$ responsible for 42 % of the indirect loss rate in the saline system. In a study of the photochemical behavior of synthetic growth promoters, Qu, et al. found that direct photolysis was the primary loss pathway for the trenbolone acetate and melengestrol acetate families, while zeranol, β-zearalanol and zearalanone degraded by indirect photolysis.[68] Quenching studies conducted at various pH values indicated that $^1O_2$ may be a contributor to the indirect photolysis of these synthetic hormones only in basic solutions. The pH behavior is consistent with the electrophilic $^1O_2$ reacting much more rapidly with deprotonated hydroxyaromatic compounds than with the undissociated neutral species. Phytoestrogens are plant-derived chemicals that may act as endocrine disruptors. Kelly and Arnold determined that the phytoestrogen daidzein photodegrades mainly through direct photolysis with some additional loss due to reaction with $^1O_2$.[69] The phytoestrogens biochanin A, genistein, and equol were found to be susceptible to indirect photolysis, with $^1O_2$ and ^{3}NOM being responsible for the degradation.[70] The extent of $^1O_2$ involvement was shown to increase at higher pH values when the hydroxyaromatic rings would be more deprotonated and electron rich.

8.6.4 Biomolecules such as Amino Acids and Proteins

Biomolecules found in surface waters may be susceptible to photooxidation. Boreen, et al., studied the indirect photochemistry of eighteen free amino acids.[71] Four (histidine, His; methionine, Met; tyrosine, Tyr; and tryptophan, Trp) showed some reactivity with $^1O_2$. Each of these amino acids contains a functional group that is known to react with $^1O_2$: His has an imidazole ring, Met has a sulfide site, Tyr has a phenolic group, and Trp has an indole ring system (see Figure 8.8 for the structures). Depending on the source of the seven natural waters tested, $^1O_2$ contributed from 70 to 100 % of the photochemical loss of His, 35 to 62 % for Met, 3 to 33 % for Tyr, and 3 to 11 % for Trp. The involvement of $^1O_2$ varied considerably with the water source. A recent paper by Chu, et al. found that protonated His and histamine (a His metabolite) photodegradation rates are enhanced relative to their neutral species.[72] This result would not be expected based on the reactivity of the protonated imidazole rings with $^1O_2$, as the protonated form exhibits lower inherent reactivity toward electrophilic $^1O_2$. The enhancement was

attributed to reaction with $^1O_2$ by protonated His and histamine molecules that were sorbed to the NOM sensitizer. In this scenario, His and histamine witnessed higher $[^1O_2]_{app}$ than their unprotonated analogs would witness in the bulk aqueous phase. This behavior was further detailed by adding competitive sorbates that displaced the protonated His and histamine species. When cosorbates were added, the degradation rate enhancements due to the high relative $[^1O_2]_{app}$ at the NOM surface was drastically reduced.

Lundeen and McNeill studied the reactivity of an intact protein (glyceraldehyde-3-phosphate dehydrogenase; GAPDH) with $^1O_2$.[73] They tracked the oxidation of His residues within the GAPDH structure under singlet-oxygenation conditions. They found that the position of the His within the GAPDH structure was critically important in their rates of oxidation, with surface exposed His residues oxidized much more rapidly than His residues buried deep within the protein matrix. Singlet oxygen accessible surface areas ($^1O_2$-ASAs) were calculated from GAPDH's crystal structure and the oxidation rates of His residues showed a strong correlation to the His $^1O_2$-ASAs. Results of this study may be useful in predicting photooxidation rates for proteins and oligopeptides in surface waters.

8.6.5 Viruses

The ability of $^1O_2$ to inactivate viruses has recently been explored in an effort to better understand the fates of waterborne pathogens and potentially reduce their impacts on the environment and society. Kohn and Nelson explored the direct and indirect photoinactivation of MS2, a bacteriophage commonly used as a surrogate for human enteric viruses, in the presence of various sensitizers.[74] Indirect photochemistry mediated by $^1O_2$ was found to be critically important in the inactivation of MS2. Quenching studies and experiments performed in D_2O (to capitalize on $^1O_2$'s well known kinetic solvent isotope effect) were used to identify $^1O_2$ as the inactivating species. Commercial and natural organic matter led to faster inactivation rates than OM from a waste stabilization pond (WSP). A later study using additional NOM samples and WSP water gave similar results.[75] The MS2 was found to associate with the NOM and inactivation was rapid in these solutions due to the high $[^1O_2]_{app}$ at the NOM interface. The

inactivation of MS2 was attributed to $^1O_2$ produced exogenously (i.e. by the NOM) rather than to any direct or endogenous (i.e. self sensitized) production of PPRIs. MS2 did not associate with WSP water and a large degradation rate enhancement due to the high $[^1O_2]_{app}$ at the NOM surface was not observed for this sample. The importance of exogenous sensitizers was further detailed by Silverman, et al.[76] They found that unfiltered surface water samples from five locations significantly increased the rates of inactivation of one virus and two bacteriophages. One virus, poliovirus type 3, however, appeared to degrade primarily via endogenous reaction pathways rather than due to $^1O_2$ generated by NOM from the surface water samples.

Rule-Wigginton, et al. determined that a site-specific oxidation of an amino acid residue on the outer surface of the major capsid protein of MS2 was found to occur upon irradiation of MS2 in the presence of Rose Bengal (a synthetic $^1O_2$ sensitizer).[77] This type of $^1O_2$ reaction mechanism may be important in the photooxidation of waterborne viruses.

Mattle, et al. have developed a predictive photochemical model to assess the relative roles of direct photolysis and various PPRIs in the inactivation of MS2, adenovirus, and phiX174.[78] To do so, they determined reaction rate constants for different PPRIs and the viruses. They also measured direct photolysis quantum yields. These parameters and steady-state concentrations of the PPRIs were then used to predict inactivation rates and parse out which pathways are responsible for virus inactivation. Their results implicated mostly direct photolysis in the inactivation of these viruses, with some disinfection due to $^1O_2$ for MS2 and adenovirus.

8.6.6 Other Species

The photochemical fate of the high use flame retardant tetrabromobisphenol A (TBBPA) was examined in a set of studies.[79,80] TBBPA was shown to rapidly quench $^1O_2$, particularly when the phenolic TBBPA molecule was deprotonated (see Figure 8.8 for TBBPA's structure). A TBBPA photoproduct from reaction with $^1O_2$ was identified by electron paramagnetic resonance (EPR) spectroscopy when TBBPA was irradiated in the presence of synthetic sensitizers.[79] Similar results were obtained when a

commercial humic acid was used as sensitizer.[80] The $^1O_2$ quencher sodium azide inhibited the growth of the TBBPA $^1O_2$ product and limited uptake of oxygen by TBBPA. These results suggest that TBBPA may be rapidly oxidized in natural waters due to reaction with $^1O_2$.

The bacteriostatic antibiotic trimethoprim undergoes indirect photolysis via reaction with $^1O_2$ and •OH.[81,82] The involvement of $^1O_2$ was determined by tracking reaction products, including those that evolve from the breakdown of a [2+2] cycloaddition of $^1O_2$ to a trimethoprim double bond. About 20 % of the trimethoprim photodegradation was attributed to $^1O_2$. The aquaculture antibiotic ormetoprim photodegrades due to direct and indirect processes.[83] Most of the indirect photodegradation is due to •OH, but $^1O_2$ was also believed to be involved. Many sulfonamide antibiotics have been studied.[46,84-87] Their photodegradation is expected to be mostly due to direct photolysis and reaction with ^{3}NOM, but $^1O_2$ may also contribute to some minor extent.[46,86,87]

In addition to sensitizing the production of PPRI, NOM can also quench and react with PPRIs. This dual role of NOM is a potentially important aspect of the global carbon cycle. Phototransformations initiated by PPRIs may conceivably reintroduce refractory NOM molecules into the bioavailable fraction of DOM in natural waters. Machado, et al. provide evidence that phenolic functionalities on lignin molecules undergo reactions with $^1O_2$.[88] McNally, et al. used model compounds to demonstrate that $^1O_2$ is likely to be important in the degradation of lignin molecules only at deprotonated phenolic sites.[89] These electron-rich phenolate sites were found to react with $^1O_2$ with k_{rxn} on the order of 10^7 $M^{-1}s^{-1}$. Total $^1O_2$ quenching rate constants were considerably lower for the undissociated phenolic sites, and reaction with excited state sensitizer was favored under these conditions. Cory, et al., measured the uptake of $^1O_2$ by NOM in Rose Bengal sensitized experiments by measuring the loss of dissolved oxygen upon irradiation and employing several standard diagnostic tests for the involvement of $^1O_2$.[90] Between 64 – 70 % of the uptake of oxygen by NOM was due to $^1O_2$ under the study conditions. They determined that NOM was capable of both physically and chemically quenching $^1O_2$ with rate constants that were similar to phenols and aromatic amines on a per carbon basis.

Singlet oxygen is also reputed to be involved in the cycling of metals in surface waters. Zhang and Hsu-Kim have implicated $^1O_2$ as the primary species involved in the photodemethylation of the toxic species methylmercury in surface waters.[91] Two recent studies by Garg and co-workers show that $^1O_2$ is involved in the redox cycling of iron in surface waters.[92,93] Specifically, $^1O_2$ oxidizes semiquinone-like Fe(II)-oxidizing species that are stable in the dark. These oxidants are thus capable of oxidizing Fe(II) to Fe(III) in the dark when $^1O_2$ is not present, but are quickly oxidized by $^1O_2$ produced upon irradiation. As such, the studies' authors identify other processes that are responsible for the oxidation of Fe(II) to Fe(III) in sunlit surface waters.

8.7 Acknowledgements

I gratefully acknowledge Seattle University's Center for Environmental Justice and Sustainability for support and Prof. Kris McNeill for helpful discussions.

8.8 References

1. Zepp R. G., Wolfe N. L., Baughman G. L., and Hollis R. C. (1977). Singlet oxygen in natural waters. *Nature*, **267**, 421-423.
2. Larson R. A. and Weber E. J. (1994). Reaction Mechanisms in Environmental Organic Chemistry. CRC Press, Inc. Boca Raton, FL.
3. Schwarzenbach R. P., Gschwend P. M., Imboden, D. M. (2002). Environmental Organic Chemistry, 2nd ed. Wiley-Interscience: New York.
4. Zepp R. G., Baughman G. L., and Schlotzhauer P. F. (1981). Comparison of the photochemical behavior of various humic substances in water: I. Sunlight induced reactions of aquatic pollutants photosensitized by humic substances. *Chemosphere*, **10**, 109-17.
5. Zepp R. G., Baughman G. L., and Schlotzhauer P. F. (1981). Comparison of photochemical behavior of various humic substances in water: II. Photosensitized oxygenations. *Chemosphere*, **10**, 119-26.
6. Zepp R. G., Schlotzhauer P. F., and Sink R. M. (1985). Photosensitized transformations involving electronic energy transfer in natural waters: role of humic substances. *Environmental Science and Technology*, **19**, 48-55.
7. Frimmel F. H., Bauer H., Putzien J., Murasecco P., and Braun A. M. (1987). Laser flash photolysis of dissolved aquatic humic material and the sensitized production of singlet oxygen. *Environmental Science and Technology*, **21**, 541-545.
8. Hoigné J., Faust B. C., Haag W. R., Scully F. E., and Zepp R. G. (1989). Aquatic humic substances as sources and sinks of photochemically produced transient reactants. In: Aquatic Humic Substances, Suffet I. H. and MacCarthy P., (Eds.), American Chemical Society: Washington, D.C., 363-81.
9. Cooper W. J., Zika R. G., Petasne R. G., Fischer A. M. (1989). Sunlight-induced photochemistry of humic substances in natural waters: major reactive species. In: Aquatic Humic Substances, Suffet I. H. and MacCarthy P., (Eds.), American Chemical Society: Washington, D.C., 333-362.
10. Blough N. V. and Zepp, R. G. (1995). Reactive oxygen species in natural waters. In: Active Oxygen in Chemistry, Foote C., Valentine J., Greenberg A., Liebman S. (Eds), Chapman and Hall: New York, 280-333.
11. Foote C. S. and Clennan E. L. (1995). Properties and reactions of singlet oxygen. In: Active Oxygen in Chemistry, Foote C., Valentine J., Greenberg A., Liebman S. (Eds), Chapman and Hall: New York, 105-140.
12. Greer A. (2006). Christopher Foote's discovery of the role of singlet oxygen [$^1O_2$ ($^1\Delta_g$)] in photosensitized oxidation reactions. *Accounts of Chemical Research*, **39**, 797-804.
13. Larson R. A. and Marley K. A. (1999). Singlet oxygen in the environment. *Handbook of Environmental Chemistry*, **2**,123-137.
14. Paterson M. J., Christiansen O., Jensen F., and Ogilby P. R. (2006) Overview of theoretical and computational methods applied to the oxygen-organic molecule photosystem. *Photochemistry and Photobiology*, **82**, 1136-1160.
15. Turro, N. J. (1991). Modern Molecular Photochemistry; University Science Books: Sausalito, California.
16. Krasnovsky A. A. (1976). Photosensitized luminescence of singlet oxygen in solution. *Biofizika*, **21**, 748-749.
17. Krasnovsky A. A. (1977). Photoluminescence of singlet oxygen in solutions of chlorophylls and pheophytins. *Biofizika*, 1977, **22**, 927-928.
18. Byteva I. M. and Salokhiddinov K. I. (1980). Lifetime of singlet oxygen in different solvents. *Biofizika*, **25**, 358.
19. Nonell S. and Braslavsky S. E. (2000). Time-resolved singlet oxygen detection. *Methods in Enzymology*, **319**, 37-49.
20. Wilkinson F., Helman W. P., Ross A. B. (1995). Rate constants for the decay and reactions of the lowest electronically excited singlet state of molecular oxygen in solution. An expanded and revised compilation. *Journal of Physical Chemistry Reference Data*, **24**, 663-1021.

21. Merkel P. B., Nilsson R., and Kearns D. R. (1972). Deuterium effects on singlet oxygen lifetimes in solutions. New test of singlet oxygen reactions. *Journal of the American Chemical Society*, **94**, 1030-1031.

22. Haag W. R. and Mill T. (1987). Rate constants for interaction of singlet oxygen ($^1\Delta g$) with azide ion in water. *Photochemistry and Photobiology*, **45**, 317-321. *Environmental Science and Technology*, **42**, 166-172.

23. Haag W. R., Hoigné J., Gassman E., and Braun A. M. (1984). Singlet oxygen in surface waters - part I: furfuryl alcohol as a trapping agent. *Chemosphere*, **13**, 631-640.

24. Haag W. R., Hoigne J., Gassman E., and Braun A. M. (1984). Singlet oxygen in surface waters - part II: quantum yields of its production by some natural humic materials as a function of wavelength. *Chemosphere*, **13**, 641-650.

25. Haag W. R. and Hoigné J. (1986). Singlet oxygen in surface waters. 3. Photochemical formation and steady-state concentrations in various types of waters. *Environmental Science and Technology*, **20**, 341-8.

26. Aguer J. P. and Richard C. (1993). Use of furoin as probe molecule for the involvement of singlet oxygen in aqueous phase photoinduced transformations. *Toxicological and Environmental Chemistry*, **39**, 217-227.

27. Ackerman R. A., Pitts Jr. J. N., Rosenthal I. (1971). Singlet oxygen in the environmental sciences. Reactions of singlet oxygen, O2(1Δg) with olefins, sulfides, and compounds of biological significance. *American Chemical Society, Division of Petroleum Chemistry,* **16**, A25-A34.

28. Scully F. E. and Hoigné J. (1987). Rate constants for reactions for singlet oxygen with phenols and other compounds in water. *Chemosphere*, **16**, 681-694.

29. Palumbo M. C. and Garcia N. A. (1988). On the mechanism of quenching of singlet oxygen by chlorinated phenolic pesticides. *Toxicological and Environmental Chemistry*, **17**, 103-116.

30. Palumbo M. C., Garcia N. A., Gutierrez M. I., Luiz M. (1990). Singlet molecular oxygen-mediated photooxidation of monochloro and mononitrophenols. A kinetic study. *Toxicological and Environmental Chemistry*, **29**, 85-94.

31. Tranyek P. G. and Hoigne, J. (1991). Oxidation of substituted phenols in the environment: a QSAR analysis of rate constants for reaction with singlet oxygen. *Environmental Science and Technology*, **25**, 1596-1604

32. Tratnyek, P. G. and Hoigné, J. (1994). Photo-oxidation of 2,4,6-trimethylphenol in aqueous laboratory solutions and natural waters: kinetics of reaction with singlet oxygen. *Journal of Photochemistry and Photobiology A.*, **84**, 153-160.

33. Garcia N. A. (1994). New trends in photobiology: Singlet-molecular-oxygen-mediated photodegradation of aquatic phenolic pollutants. A kinetic and mechanistic overview. *Journal of Photochemistry and Photobiology*, *22*, 185-196.

34. Richard C. and Grabner G. (1999). Mechanism of phototransformation of phenol and derivatives in aqueous solution. *Handbook of Environmental Chemistry*, **2**, 217-240.

35. Canonica S. and Tratnyek, P. G. (2003). Quantitative structure-activity relationships for oxidation reactions of organic chemicals in water. *Environmental Toxicology and Chemistry*, **22**, 1743-1754.

36. Zafiriou O. C., Blough N. V., Micinski E., Dister B., Kieber D., and Moffett, J. (1990). Molecular probe systems for reactive transients in natural waters. *Marine Chemistry*, **30**, 45-70.

37. Burns J. M., Cooper W. J., Ferry J. L., King D. W., DiMento B. P., McNeill K., Miller C. J., Miller W. L., Peake B. M., Rusak S. A., Rose A. L., and Waite T. D. (2012). Methods for reactive oxygen species (ROS) detection in aqueous environments. *Aquatic Sciences*, **74**, 683-734.

38. Nardello V., Azaroual N., Cervoise I., Vermeersch G., and Aubry, J. M. (1996). Synthesis and photooxidation of sodium 1,3-cyclohexadiene-1,4-diethanoate: a new colorless and water-soluble trap of singlet oxygen. *Tetrahedron*, **52**, 2031-2046.

39. Nardello V., Brault D., Chavalle P., and Aubry J. M. (1997). Measurement of photogenerated singlet oxygen ($^1O_2(^1\Delta_g)$) in aqueous solutions by specific chemical trapping with sodium 1,3-cyclohexadiene-1,4-diethanoate. *Journal of Photochemistry and Photobiology, B*, **39**, 146-155.

40. Al Housari F., Vione D., Chiron S., Barbati S. (2010). Reactive photoinduced species in estuarine waters. Characterization of hydroxyl radical, singlet oxygen and dissolved organic matter triplet state in natural oxidation processes. *Photochemical and Photobiological Sciences*, **9**, 78-86.

41. MacManus-Spencer L. A., Latch D. E., Kroncke K. M., and McNeill K. (2005). Stable dioxetane precursors as selective trap-and-trigger chemiluminescent probes for singlet oxygen. *Analytical Chemistry*, **77**, 1200-1205.
42. Latch D. E. and McNeill, K. (2006). Microheterogeneity of singlet oxygen distributions in irradiated humic acid solutions. *Science*, **311**, 1743-1747.
43. Grandbois M., Latch D. E., and McNeill, K. (2008). Microheterogeneous concentrations of singlet oxygen in natural organic matter isolate solutions. *Environmental Science and Technology*, **42**, 9184-9190.
44. Latch D. E., Stender B. L., Packer J. L., Arnold W. A., and McNeill, K. (2003). Photochemical Fate of Pharmaceuticals in the Environment: Cimetidine and Ranitidine. *Environmental Science and Technology*, **37**, 3342-3350.
45. Paul A., Hackbarth S., Vogt R. D., Roeder B., Burnison B. K., and Steinberg C. W. (2004). Photogeneration of singlet oxygen by humic substances: comparison of humic substances of aquatic and terrestrial origin. *Photochemical and Photobiological Sciences*, **3**, 273-280.
46. Boreen A. L., Arnold W. A., and McNeill K. (2005). Triplet-sensitized photodegradation of sulfa drugs containing six-membered heterocyclic groups: Identification of an SO_2 extrusion photoproduct. *Environmental Science and Technology*, **39**, 3630-3638.
47. Sandvik S. L. H., Bilski, P., Pakulski J. D., Chignell, C. F., and Coffin, R. B. (2000). Photogeneration of singlet oxygen and free radicals in dissolved organic matter isolated from the Mississippi and Atchafalaya River plumes*Marine Chemistry*, **69**, 139-152.
48. Dalrymple R. M., Carfagno A. K., and Sharpless C. M. (2010). Correlations between dissolved organic matter optical properties and quantum yields of singlet oxygen production and hydrogen peroxide. *Environmental Science and Technology*, **44**, 5824-5829.
49. Peterson B. M., McNally A. M., Cory R. M., Thoemke J. D., Cotner J. B., and McNeill K. (2012). Spatial and temporal distribution of singlet oxygen in Lake Superior. *Environmental Science and Technology*, **46**, 7222-7229.
50. Marchisio, A., Minella M., Maurino V., Minero C., and Vione D. (2015). Photogeneration of reactive transient species upon irradiation of natural water samples: Formation quantum yields in different spectral intervals, and implications for the photochemistry of surface waters. *Water Research*, **73**, 145-156.
51. Sharpless C. M. (2012). Lifetimes of triplet dissolved natural organic matter (DOM) and the effect of $NaBH_4$ reduction on singlet oxygen quantum yields: Implications for DOM photophysics. *Environmental Science and Technology*, **46**, 4466-4473.
52. Sharpless C. M., Aeschbacher M., Page S. E., Wenk J., Sander M., and McNeill, K. (2014). Photooxidation-induced changes in optical, electrochemical and photochemical properties of humic substances. *Environmental Science and Technology*, **48**(5), 2688-2696.
53. Mostafa S. and Rosario-Ortiz F. L. (2013). Singlet oxygen formation from wastewater organic matter. *Environmental Science and Technology*, **47**, 8179-8186.
54. Zhang D., Yan S., and Song W. (2014). Photochemically induced formation of reactive oxygen species (ROS) from effluent organic matter. *Environmental Science and Technology*, 48, 12645-12653.
55. Bodhipaksha L. C., Sharpless C. M., Chin Y. P., Sander M., Langston W. K., and MacKay A. A. (2015). Triplet photochemistry of effluent and natural organic matter in whole water and isolates from effluent-receiving rivers. *Environmental Science and Technology*, **49**, 3453-3463.
56. Appiani E. and McNeill K. (2015). Photochemical production of singlet oxygen from particulate organic matter. *Environmental Science and Technology*, **49**, 3514-3522.
57. Schmidt R., Tanielian C., Dunsbach R., Wolff C.J. (1994). Phenalenone, a universal reference compound for the determination of quantum yields of singlet oxygen ($O_2{}^1\Delta_g$) sensitization. Photochemistry and Photobiology A, **79**, 11-17.
58. Neckers D. C. and Paczkowski J. (1986). Microheterogeneous photooxidation. *Journal of the American Chemical Society*, **108**, 291-292.
59. Hecht S. and Frechet J. M. J. (2001). Light-Driven Catalysis within Dendrimers: Designing Amphiphilic Singlet Oxygen Sensitizers. *Journal of the American Chemical Society*, **123**, 6959-6960.
60. Hassett J. P. (2006). Dissolved organic matter as a microreactor. *Science*, **311**, 1723 – 1724.

61. Kolpin D. W., Furlong E. T., Meyer M. T., Thurman E. M., Zaugg S. D., Barber L. B., and Buxton H. T. (2002). Pharmaceuticals, Hormones, and Other Organic Wastewater Contaminants in U.S. Streams, 1999-2000: A National Reconnaissance. *Environmental Science and Technology*, **36**, 1202-1211.
62. Zuccato E., Calamari D., Natangelo M., and Fanelli R. (2000). Presence of therapeutic drugs in the environment. *Lancet*, **355**, 1789-1790.
63. Burrows H. D., Canle L M., Santabella J. A., and Steenken S. (2002). Reaction pathways and mechanisms of photodegradation of pesticides. *Journal of Photochemistry and Photobiology B*, **67**, 71-108.
64. Remucal, C. K. (2014). The role of indirect photochemical degradation in the environmental fate of pesticides: A review. *Environmental Science: Processes and Impacts*, **16**, 628-653.
65. Ter Halle A. and Richard C. (2006). Simulated solar light irradiation of mestrione in natural waters. *Environmental Science and Technology*, **40**, 3842-3847.
66. Zeng T., Arnold W. A. (2013). Pesticide Photolysis in Prairie Potholes: Probing Photosensitized Processes. *Environmental Science and Technology*, **47**, 6735-6745.
67. Grebel J. E., Pignatello J. J., and Mitch W. A. (2012). Impact of halide ions on natural organic matter-sensitized photolysis of 17β-estradiol in saline waters. *Environmental Science and Technology*, **46**, 7128-7134.
68. Qu S., Kolodziej E. P., and Cwiertny D. M. (2012). Phototransformation Rates and Mechanisms for Synthetic Hormone Growth Promoters Used in Animal Agriculture. *Environmental Science and Technology*, **46**(24), 13202–13211.
69. Kelly M. M. and Arnold W. A. (2012). Direct and indirect photolysis of the phytoestrogens genistein and daidzein. *Environmental Science and Technology*, **46**(10), 5396-5403.
70. Felcyn J. R., Davis J. C. C., Tran L. H., Berude J. C., and Latch, D. E. (2012). Aquatic photochemistry of isoflavone phytoestrogens: Degradation kinetics and pathways. *Environmental Science and Technology*, **46**, 6698-6704.
71. Boreen A. L., Edhlund B. L., Cotner J. B., and McNeill K. (2008). Indirect photodegradation of dissolved free amino acids: The contribution of singlet oxygen and the differential reactivity of DOM from various sources. *Environmental Science and Technology*, **42**, 5492-5498.
72. Chu C., Lundeen R. A., Remucal C. K., Sander M., and McNeill K. (2105). Enhanced indirect photochemical transformation of histidine and histamine through association with chromophoric dissolved organic matter. *Environmental Science and Technology*, **49**, 5511-5519.
73. Lundeen R. A. and McNeill K. (2013). Reactivity differences of combined and free amino acids: Quantifying the relationship between three-dimensional protein structure and singlet oxygen reaction rates. *Environmental Science and Technology*, **47**, 14215-14223.
74. Kohn T. and Nelson K. L. (2007). Sunlight-mediated inactivation of MS2 coliphage via exogenous singlet oxygen produced by sensitizers in natural waters. *Environmental Science and Technology*, **41**, 192-197.
75. Kohn T., Grandbois M., McNeill K., and Nelson, K. L. (2007) Association with Natural Organic Matter Enhances the Sunlight-Mediated Inactivation of MS2 Coliphage by Singlet Oxygen. *Environmental Science and Technology*, **41**, 4626-4632.
76. Silverman A. I., Peterson B. M., Boehm A. B., McNeill K., and Nelson K. L. (2013). Sunlight inactivation of human viruses and bacteriophages in coastal waters containing natural photosensitizers. *Environmental Science and Technology*, **47**, 1870-1878.
77. Rule-Wigginton K., Menin L., Montoya J. P., and Kohn T. (2010). Oxidation of virus proteins during UV_{254} and singlet oxygen mediated inactivation. *Environmental Science and Technology*, **44**, 5437-5443.
78. Mattle M. J., Vione D., and Kohn T. (2014). Conceptual Model and Experimental Framework to Determine the Contributions of Direct and Indirect Photoreactions to the Solar Disinfection of MS2, phiX174, and Adenovirus *Environmental Science and Technology*, **49**, 334-342.
79. Han S. K., Bilski P., Karriker B., Sik R. H., and Chignell C. F. (2008). Oxidation of flame retardant tetrabromobispenol A by singlet oxygen.
80. Han S. K., Sik R. H., Motten A. G., Chignell C. F., and Bilski P. J. (2009). Photosensitized oxidation of tetrabromobisphenol A by humic acid in aqueous solution. *Photochemistry and Photobiology*, **85**, 1299-1305.

81. Luo X., Zheng Z., Greaves J., Cooper W. J., and Song W. (2012). Trimethoprim: Kinetic and mechanistic considerations in photochemical environmental fate and AOP treatment. *Water Research*, **46**, 1327-1336.

82. Pace A. and Barreca S. (2013). Environmental organic photochemistry: Advances and perspectives. *Current Organic Chemistry*, **17**, 3032-3041.

83. Guerard J. J. and Chin Y. P. (2012). Photodegradation of ormetoprim in aquaculture and stream-derived dissolved organic matter. *Journal of Agricultural and Food Chemistry*, **60**, 9801-9806.

84. Boreen A. L., Arnold W. A., and McNeill K. (2004). Photochemical fate of sulfa drugs in the aquatic environment: Sulfa drugs containing five-membered heterocycic groups. *Environmental Science and Technology*, **38**, 3933-3940.

85. Guerard J. J., Chin Y.-P., Mash H., and Hadad C. M. (2009). Photochemical fate of sulfadimethoxine in aquaculture waters. *Environmental Science and Technology*, **43**, 8587-8592.

86. Challis J. K., Carlson J. C., Friesen K. J., Hanson M. L., and Wong C. S. (2013). Aquatic photochemistry of the sulfonamide antibiotic sulfapyridine. *Journal of Photochemistry and Photobiology A.*, **262**, 14-21.

87. Challis J. K., Hanson M. L., Friesen K. J., and Wong C. S. (2014). A critical assessment of the photodegradation of pharmaceuticals in aquatic environments: defining our current understanding and identifying knowledge gaps. *Environmental Science Processes & Impacts*, **16**, 672-696.

88. Machado A. Ed. H., Ruggiero R., Neumann M. G. (1994). The photodegradation of lignins in the presence of hydrogen peroxide. *Journal of Photochemistry and Photobiology A*, **81**, 107-15.

89. McNally A. M., Moody E. C., and McNeill K. (2005). Kinetics and mechanism of the sensitized photodegradation of lignin model compounds. *Photochemical and Photobiological Sciences*, **4**, 268-274.

90. Cory R. M., Cotner J. B., and McNeill K. (2009). Quantifying interactions between singlet oxygen and aquatic fulvic acids. *Environmental Science and Technology*, **43**, 718-723.

91. Zhang T. and Hsu-Kim H. (2010). Photolytic degradation of methylmercury enhanced by binding to natural organic ligands. *Nature Geoscience*, **3**(7), 473-476.

92. Garg S., Ito H., Rose A. L., and Waite T. D. (2013). Mechanism and kinetics of dark iron redox transformations in previously photolyzed acidic natural organic matter solutions. *Environmental Science and Technology*, **47**, 1861-1869.

93. Garg S., Jiang C., Miller C. J., Rose A. L., and Waite T. D. (2013). Iron redox transformations in continuously photolyzed solutions containing natural organic matter: Kinetic and mechanistic insights. *Environmental Science and Technology*, **47**, 9190-9197.

8.9 Figures

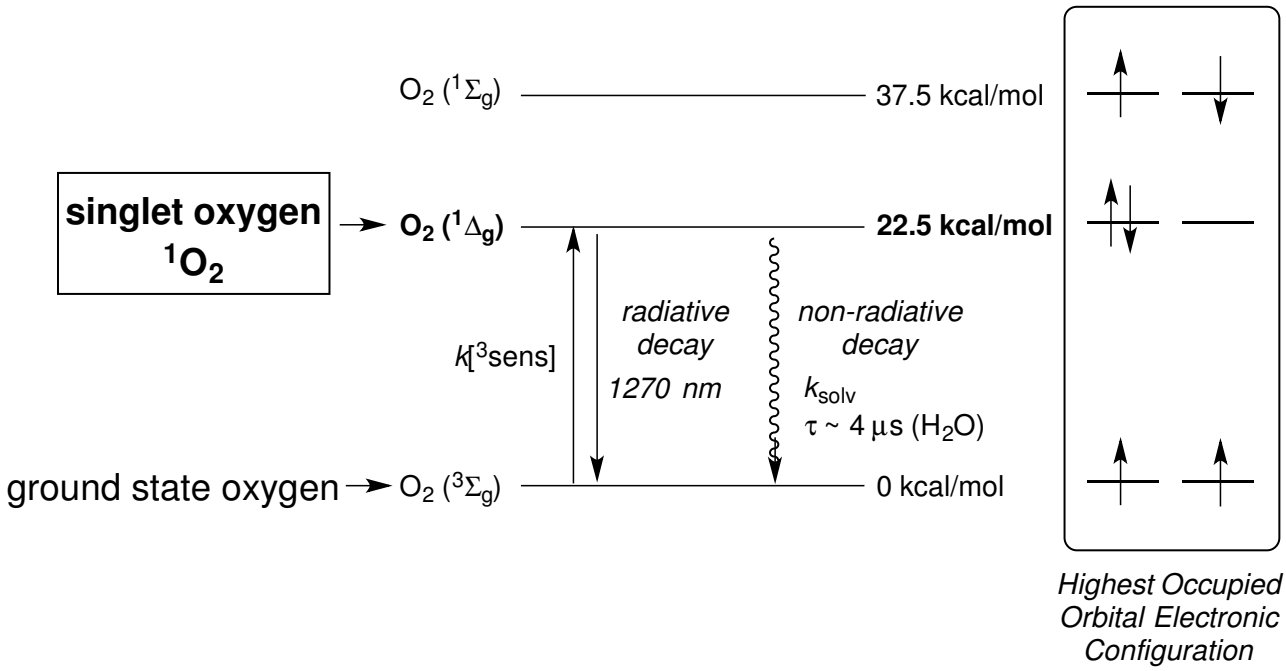

Figure 8.1 Physical properties of $^1O_2$ and ground state oxygen (adapted from references 11, 12, and 14).

[4+2] cycloaddition

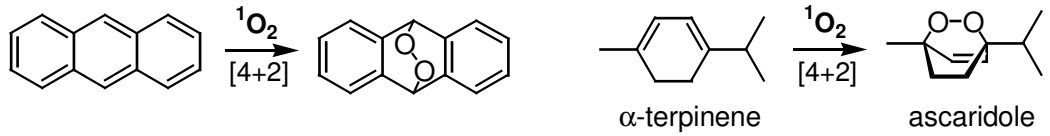

[2+2] cycloaddition

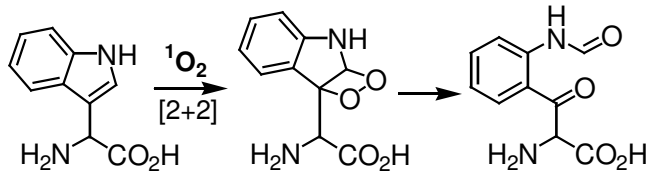

ene reaction

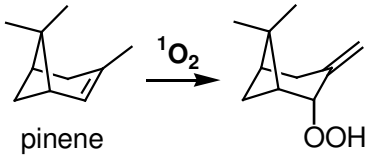

phenol oxidation

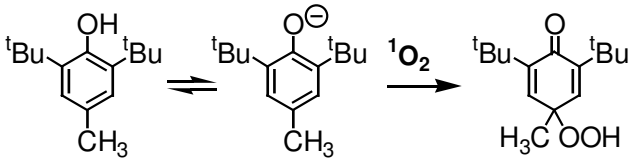

sulfide oxidation

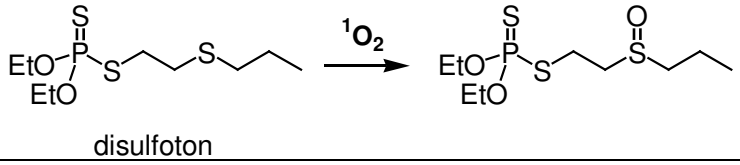

Figure 8.2 Characteristic reactions involving $^1O_2$ (adapted from references 2 and 11).

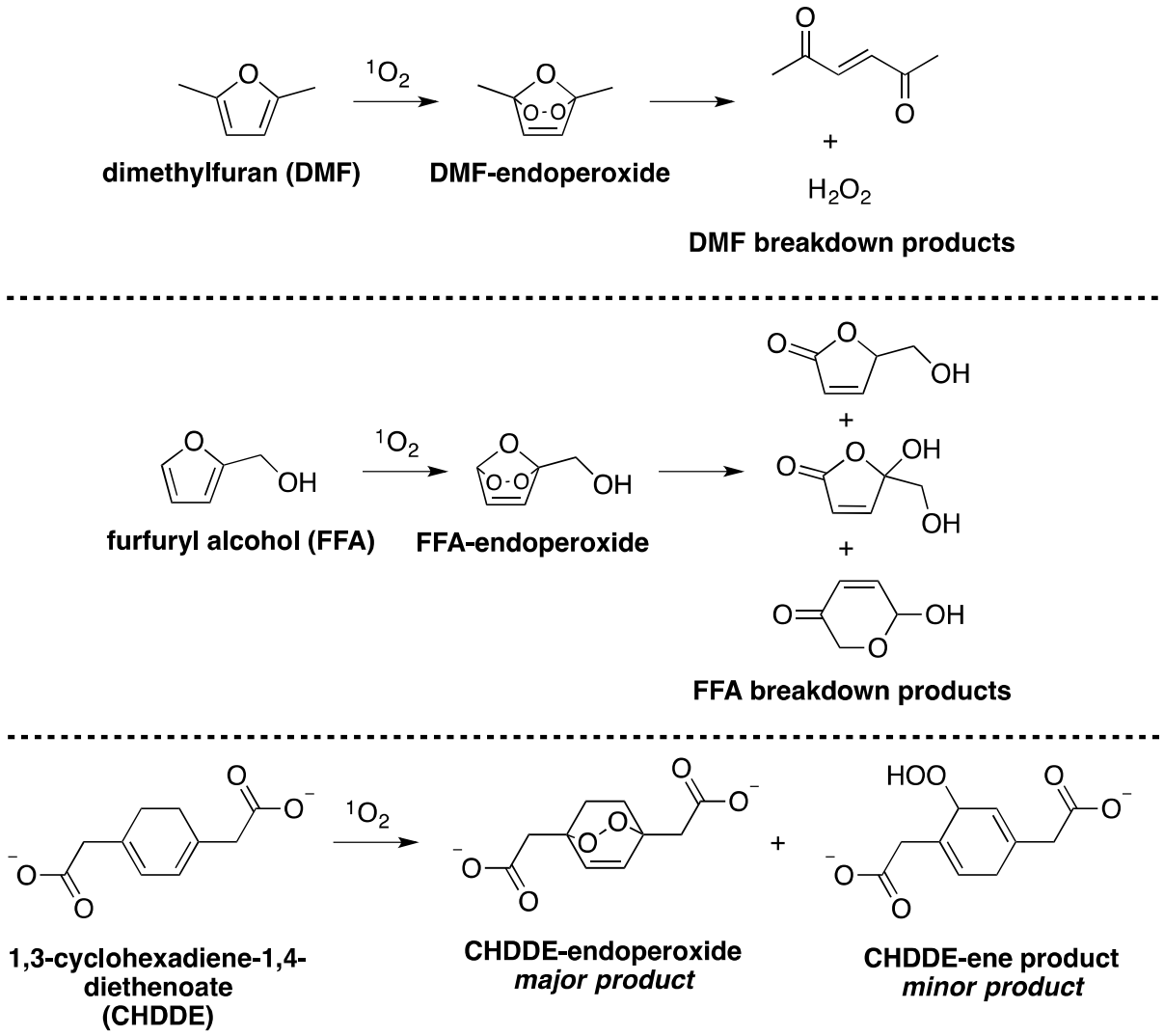

Figure 8.3 Molecular probe molecules used to detect $^1O_2$ (adapted from references 1, 10, 23, 37-39)

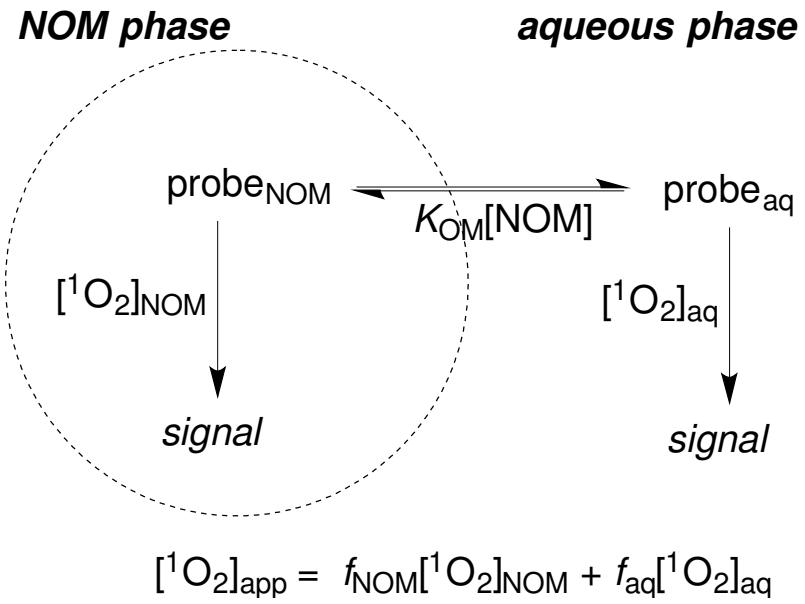

$$[^1O_2]_{app} = f_{NOM}[^1O_2]_{NOM} + f_{aq}[^1O_2]_{aq}$$

Figure 8.4 Schematic depiction of $^1O_2$ production and measurement in aqueous NOM solutions (adapted from references 42 and 43).

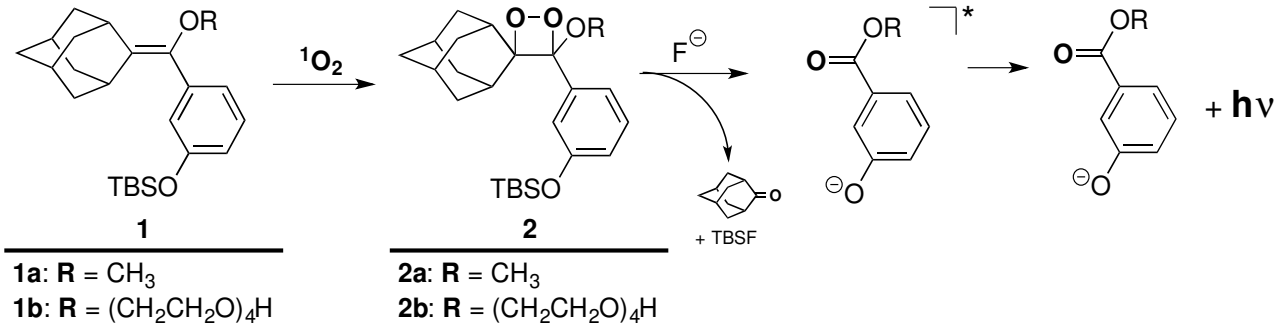

1a: **R** = CH_3
1b: **R** = $(CH_2CH_2O)_4H$

2a: **R** = CH_3
2b: **R** = $(CH_2CH_2O)_4H$

Figure 8.5 Trap-and-trigger $^1O_2$ detection scheme of hydrophobic probes **1a** and **1b**. The probes react with $^1O_2$ to form stable dioxetanes **2a** and **2b**. Upon triggering with TBAF, the dioxetanes decompose through an electron-exchange mechanism in which the oxybenzoate ester anion is formed in an electronic excited state. The anion luminesces as it relaxes to its ground state. The amount of light released depends on the amount of $^1O_2$ trapped and can thus be used to determine $^1O_2$ concentrations. (Adapted from reference 41.)

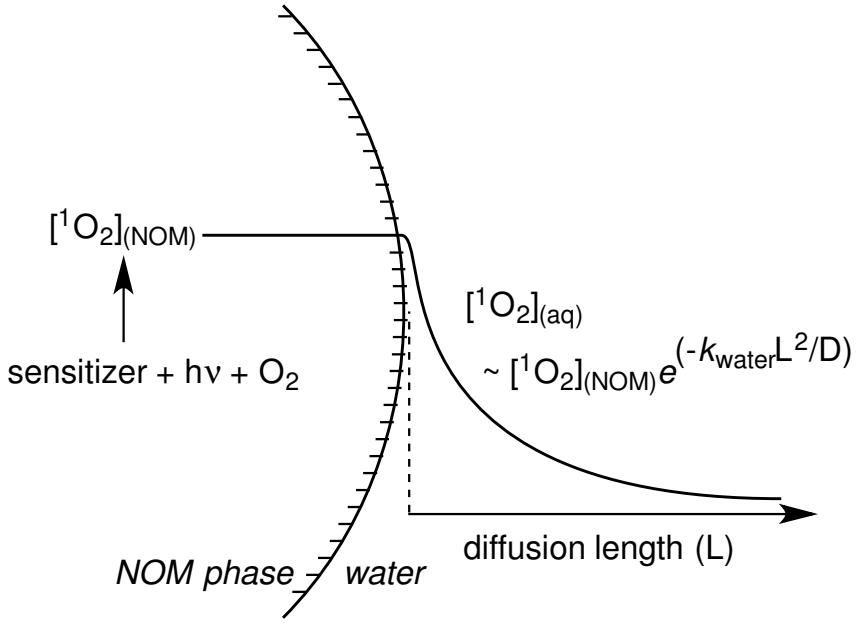

Figure 8.6 Depiction of $^1O_2$ production within an NOM microsphere and its deactivation as it diffuses through the aqueous phase.

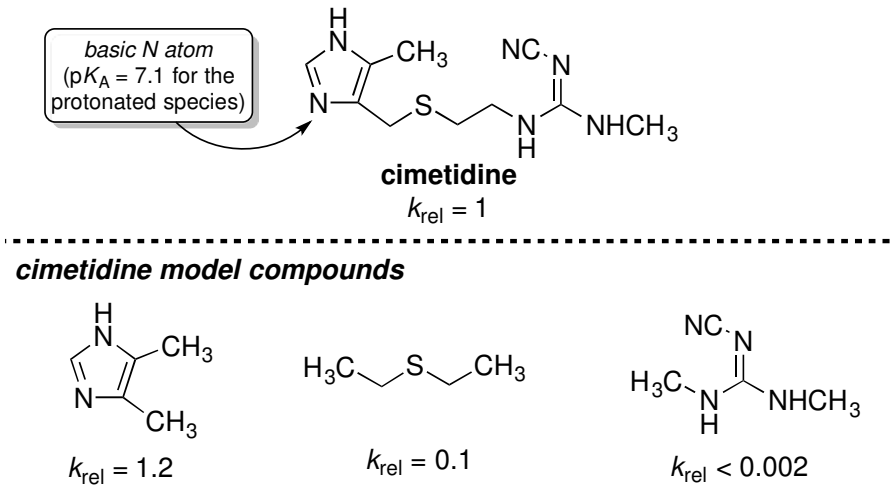

Figure 8.7 Structures of cimetidine and cimetidine model compounds used to assess the reactivity of different functional groups with $^1O_2$, as determined by laser flash photolysis (Latch, et al., 2003). Here k_{rel} are $^1O_2$ quenching rate constants for each species relative to that measured for the neutral cimetidine parent compound. These results implicate the imidazole ring as the most likely reaction site, although the identification of cimetidine sulfoxide as a reaction product provides evidence that some reaction also occurs at the sulfide site. As the indicated N-atom of cimetidine's imidazole ring is protonated in acidic media, reaction rates slow considerably due to the reduced electron density of the heterocycle. (Adapted from reference 44.)

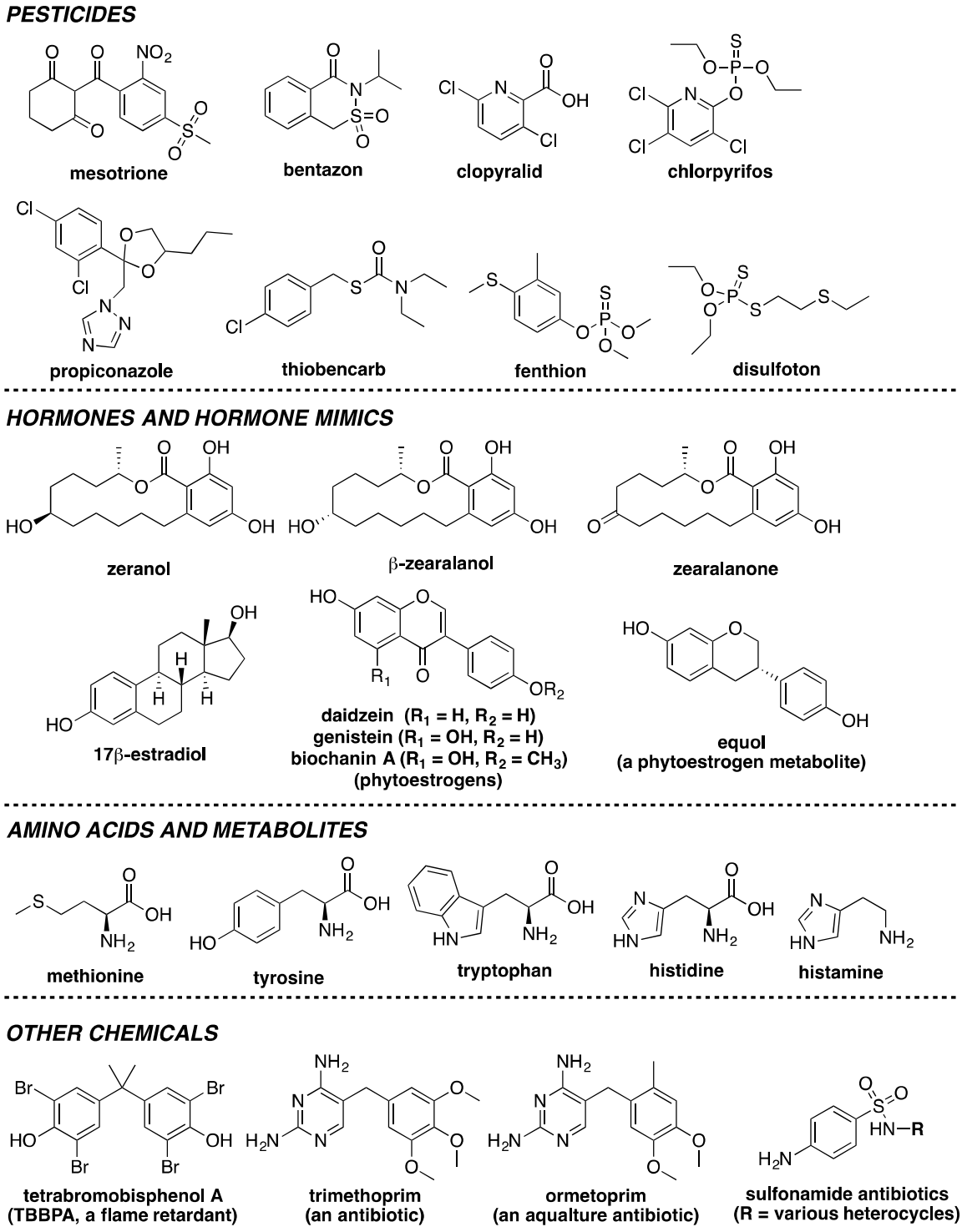

Figure 8.8 Structures of several environmentally relevant chemicals that may undergo reaction with $^1O_2$ to some extent in sunlit surface waters.

Chapter 9

PHOTOTRANSFORMATION OF ORGANIC COMPOUNDS INDUCED BY IRON SPECIES

Marcello Brigante [a,b] and Gilles Mailhot *[a,b]

[a] Clermont Université, Université Blaise Pascal, Institut de Chimie de Clermont-Ferrand (ICCF), BP 10448, F-63000 Clermont-Ferrand, France

[b] CNRS, UMR 6296, Institut de Chimie de Clermont-Ferrand, F-63171 Aubière, France

Corresponding Author Email: gilles.mailhot@univ-bpclermont.fr

Abstract

The present chapter describes firstly the iron chemistry in aqueous solution in all its complexity. The photochemical properties are then presented in detail for the main forms of iron complexes found in aquatic compartments or used in advanced oxidation processes. In the third part of the chapter, the photochemical impact of different iron complexes on the degradation of water-dissolved organic compounds is explained in detail and the significance of different physico-chemical parameters is evaluated. Some examples of the use of iron species in advanced oxidation processes are presented to show their positive effects on water treatment.

Table of Contents

9.1 Iron

Iron is the most abundant transition metal in the earth's crust (average concentration is about 5.6%). It is also the metal most used by modern human society. In the environment, it is present primarily in rocks as well as in soils but also, in lower amounts, in water systems (dissolved or suspended) and in atmospheric solid or liquid phases. Moreover, it is one of the most significant elements for almost all living organisms including humans. Iron is also an essential element because it plays a central role in many biological and chemical processes.

In the solid phase, iron is generally found as oxides or oxyhydroxides, and among them the most frequent are hematite, magnetite, limonite, goethite and lepidocrocite. These forms of iron are scarcely soluble in water, but their solubility can be increased in the presence of siderofores and they can also undergo a process of photodissolution upon absorption of visible and UV light[1]. In the aquatic environment, iron is present at different concentrations that are lowest in sea water (between 0.2 and 4 nmol L^{-1}) and highest in the atmosphere (fogs and clouds), from few µmol L^{-1} up to 400 µmol L^{-1} [2-4]. In the continental aquatic compartment, the average concentration of dissolved iron is equal to few µM but the highest concentrations can reach about 150 µM.

This short introduction shows the key role that iron species can have on environmental processes and more generally the importance of this element for life on earth.

In this chapter, iron chemistry in water is firstly described in detail, then the main photochemical processes involving different iron species are presented with

qualitative and quantitative results. Finally, in the last section, the impact of iron complexes in the aquatic environment and their use for advanced oxidation processes (AOPs) are discussed.

9.1.1 Iron in water: speciation and physicochemical properties

9.1.1.1 Iron in natural waters

Iron in natural waters is present as ferric (Fe(III)) or ferrous (Fe(II)) oxidation state which depends on pH, on the oxidative and reductive processes and also on the presence of organic or inorganic complexing agents. The ability of the ferric/ferrous couple to be reduced or oxidized is an important feature for the chemical and biological processes in aquatic environment. Fe(II) is naturally present in anaerobic environment, while Fe(III) is the most stable form in aerobic water. Fe(III) is present as soluble complex species such as: $[Fe(H_2O)_6]^{3+}$, $[Fe(H_2O)_5(OH)]^{2+}$, $[Fe(H_2O)_4(OH)_2]^{+}$, $[Fe(H_2O)_3(OH)_3]$, $[Fe(H_2O)_2(OH)_4]^{-1}$, and possibly $[Fe_2(H_2O)_8(OH)_2]^{4+}$, depending on the physico-chemical conditions (e.g. pH and Fe concentrations). However, these iron aquacomplexes account for a minor part of the total iron present in natural waters.[5] Eberle and Palmer have measured the concentrations of iron and identified different soluble species in the Rhine river (Europe): of the 407 µg L^{-1} total Fe(III), only 1.6 µg L^{-1} Fe(III) was really dissolved (after filtering the solution with a 0.4 µm filter). In the filtrate, 39% of the Fe(III) was in the form of $[Fe(H_2O)_4(OH)_2]^{+}$, 28% as $[Fe(H_2O)_3(OH)_3]$ and 13% as $[Fe(H_2O)_2(OH)_4]^{-1}$. The rest was not identified, but it was probably in the form of

soluble Fe(III) colloids. The large difference between really dissolved Fe(III) species and the total concentration of iron can be attributed to oxides and complexes with organic matter or polycarboxylic acids.

As mentioned above, iron plays an important role in the biological and chemical cycles of different elements present in water. For example, a low iron concentration can limit the growth of phytoplankton in the oceans.[6] Iron is also an important element in the atmosphere or in natural waters, as described by Behra and Sigg[7] or Sulzberger et al.[1].

9.1.1.2 Hydrolysis of Fe(III) salts

The hydrolysis of Fe(III) salts in aqueous solution is a complicated process, leading to different iron species depending on several parameters like pH, initial concentration of Fe(III) salts, temperature, ionic strength of the solution, type of the counter anion, presence of complexing agents, etc. To explain this phenomenon it is necessary to divide the process of hydrolysis of ferric salts into four stages:[8]

- Formation of low molecular weight species (monomers and dimers).
- Formation of red cationic polymer.
- Ageing and oxidation of the red polymer.
- Formation of ferric oxides and hydroxides by precipitation of low molecular weight precursors.

<u>The low molecular weight complexes are as follows:</u>

- Monomer $[Fe(H_2O)_6]^{3+}$, corresponding to Fe^{3+} cation surrounded by six water

molecules placed in an octaedric structure.

- Monomer $[Fe(H_2O)_5(OH)]^{2+}$ or $Fe(OH)^{2+}$, where one water molecule is substituted by an hydroxyl group.

- Monomer $[Fe(H_2O)_4(OH)_2]^{+}$ or $Fe(OH)_2^{+}$, where two water molecules are substituted by two hydroxyl groups.

- Dimer $[Fe_2(H_2O)_8(OH)_2]^{4+}$ or $Fe_2(OH)_2^{4+}$, a dimer complex with two metal centers. Its structure has been discussed for a long time. Nowadays, the structure is supposed to be a *dihydroxy*-form, corresponding to the molecular formula $[(H_2O)_4Fe(OH)_2Fe(H_2O)_4]^{4+}$, where the atoms of iron are connected by two hydroxyl bridges. In contrast, the *oxo* form $[(H_2O)_5FeOFe(H_2O)_5]^{4+}$ where the atoms of iron are connected by a single oxygen bridge is less probable.

The hydrosoluble Fe(III) polymers are:

- A trimer form, for which two formulas are proposed, $[Fe_3(OH)_3(H_2O)_{12}]^{6+}$ (or $Fe_3(OH)_3^{6+}$), and $[Fe_3(OH)_4(H_2O)_{14}]^{5+}$ (or $Fe_3(OH)_4^{5+}$).

- Fe(III) oligomers, polymers or soluble aggregates; they are also present in water but their structures are never been identified.

The list of Fe(III) species, which are found in natural waters, is completed by ferric oxides or oxyhydroxides in the form of colloidal or suspended particles, for example *goethite* α-FeO(OH), *lepidocrocite* γ-FeO(OH), *hematite* α-Fe_2O_3, *maghemite* γ-Fe_2O_3 or *ferrihydrite* $Fe(OH)_3$. These species are scarcely soluble in water[9] and can undergo a process of photodissolution[1] (or can be solubilized by chemolitothrophic bacteria), with formation of soluble Fe(II) or Fe(III) species.

To simplify the chemical formulas of the iron complexes, the water molecules will not written in the following part of this chapter. Therefore, for instance, Fe^{3+} corresponds hereafter to $[Fe(H_2O)_6]^{3+}$.

Influence of pH:

The pH plays a crucial role on the dissociation equilibrium of the Fe(III) species and on their distribution in the aquatic environment. In the area of neutral and basic pH, iron is present in the oxidized form and tends to agglomerate or precipitate. The dissociation equilibria and related constants were determined by Faust and Hoigné for an ionic strength of 0.03 M: [10]

$$Fe^{3+} + H_2O \rightarrow Fe(OH)^{2+} + H^+ \qquad K_1 = 2.7\times10^{-3}\ \text{M} \qquad (9.1)$$

$$Fe^{3+} + 2H_2O \rightarrow Fe(OH)_2^{+} + 2H^+ \qquad K_2 = 1.3\times10^{-8}\ \text{M}^2 \qquad (9.2)$$

$$2Fe^{3+} + 2H_2O \rightarrow Fe_2(OH)_2^{4+} + 2H^+ \qquad K_3 = 6.0\times10^{-4}\ \text{M} \qquad (9.3)$$

The distribution of Fe(III) monomeric complexes at pH < 5 is presented in the following figure (Figure 9.1):

[Figure 9.1 near here]

Influence of iron concentration:

The iron species present in solution depend also on the initial Fe(III) concentration. Flynn[8] has established a diagram of predominance of low molecular mass ferric species as a function of both concentration and pH. The results show that hydroxylated monomeric forms are present at higher pH. The higher is the pH, the more the monomeric species is hydroxylated, while iron dimer complexes exist in solution only at relatively elevated Fe(III) concentrations (> 5×10^{-2} M).

9.1.1.3 Spectral properties of iron aquacomplexes

Figure 9.2 presents the different absorption spectra of low molecular mass iron complexes. Strong differences can be noticed between the different complexes.

[Figure 9.2 near here]

- The absorption spectrum of the Fe^{3+} complex is characterized by a maximum at 240 nm, with molecular absorption coefficient between 3850 and 4500 M^{-1} cm^{-1}.[11-13]
- The absorption spectrum of the $FeOH^{2+}$ complex presents a maximum at 297 nm, with a molecular absorption coefficient around 2000 M^{-1} cm^{-1}.[10]
- The absorption spectrum of the $Fe(OH)_2^{+}$ complex has also a maximum at 297 nm, but the molar absorption coefficient is not well defined; it is variably reported as 1100[14] or 1800 M^{-1} cm^{-1}.[12] This ferric complex is quite unstable and tends to precipitate.
- The dimer $Fe_2(OH)_2^{4+}$ has a maximum at 335 nm with a molecular absorption coefficient between 3500[13] and 8300 M^{-1} cm^{-1}.[12]
- The soluble aggregates of Fe(III) give a continuously increasing absorption from 500 to 200 nm, without notable maxima.

9.1.1.4 Other complexes of iron

In the presence of high concentrations of sulfates and in acidic environment, the following inorganic complexes can be formed: $[FeSO_4]^{+}$, $[Fe(SO_4)_2]^{-}$, $[FeHSO_4]^{2+}$. With high concentration of chlorides one can observe the formation of $[FeCl]^{2+}$ and

$[FeCl_2]^+$. The presence of phosphates leads to iron hydrogen- and dihydrogenphosphates and, depending on the concentration of oxygen, soluble ferrous or insoluble ferric forms are created. Dissolved iron often makes complexes with organic polycarboxylic acids such as citrate, oxalate, malonate etc. This phenomenon will be described in section 9.2.2.

9.2 Photochemistry of iron complexes

9.2.1 Aquacomplexes

The first observation of the photochemical activity of iron salts was given by Evans and Uri in 1949[15]. They demonstrated the photopolymerization of acrylonitrile and methylmethacrylate in a solution of $FeCl_3$.

In 1953, Bates and Uri[16] have shown the activity of ferric ions in the presence of a UV light source. Oxidation of organic compounds present in the system was observed under UV irradiation. As an agent responsible for this reaction, the hydroxyl radical formed via photodissociation of $Fe(OH)^{2+}$ was supposed:

$$Fe(OH)^{2+} \xrightarrow{h\nu} Fe^{2+} + HO^{\bullet} \qquad (9.4)$$

The photochemical behaviour of various Fe(III) aquacomplexes has been the main objective of many studies, especially in later decades. Two major types of processes, where iron plays a role of photoinducer of pollutants degradation, can be highlighted:

• The first mechanism is based on the Fe(III) complexed solely by *hydroxyl/water groups*, where the pollutant can react with hydroxyl radicals generated by photodissociation of the complex(es). [17]

• The second mechanism concerns the complexation of Fe(III) by *organic complexing agents*, which could be the pollutant (like nitrilotriacetic acid NTA), the solvent etc. Absorption of light induces an intramolecular photoredox process, reducing Fe(III) to Fe(II) and oxidizing the complexing agent. [18]

The formation of hydroxyl radicals from Fe(III) aquacomplexes under irradiation is explained by an energy diagram of transition metal complexes (Figure 9.3).

[Figure 9.3 near here]

Among the transitions indicated in the diagram, the ”B” transitions are the most frequent and relevant to photochemical processes. Irradiation of metal complexes at a suitable wavelength lets the intramolecular redox processes take place. Under irradiation, the energy of the photons is absorbed and the complex gets excited. In the excited state, the metal and ligand are likely to undergo redox reactions. Deactivation of the excited state leads to either transfer of charge from ligand to metal (LMCT), liberating reduced metal and oxidized ligand ($HO^{\bullet}$ for Fe(III) aquacomplexes), or to the regeneration of the initial complex by non-redox radiation.

The $HO^{\bullet}$ formation efficiency depends strongly on the Fe(III) speciation and on the irradiation wavelength. This efficiency is often represented as a quantum yield, which is defined as the ratio of transformed or formed molecules to the number of absorbed photons during the same period of time. The quantum yields of hydroxyl radical formation are presented in Table 9.1:[11,19,20]

[Table 9.1 near here].

Table 9.1 shows that the monomeric complexes $Fe(OH)^{2+}$ and $Fe(OH)_2^{+}$ are the most

photoactive species for the hydroxyl radical formation. The other Fe(III) species form also some hydroxyl radical under irradiation, but with a much smaller quantum yield. Moreover, it is important to notice that at pH > 5 the concentration of $Fe(OH)_2^+$ is higher (Figure 9.1), but one also observes the precipitation of iron hydroxides and thus the main source of hydroxyl radicals (soluble Fe(III) species) is rapidly dried out.

Table 9.1 also shows that the efficiency of hydroxyl radical formation is wavelength-dependent, and that the relevant quantum yields decrease with increasing wavelength. For shorter wavelengths the energy of the photons is higher, which is in agreement with the fact that the release of hydroxyl radicals from the solvent cage needs an amount of additional energy to that needed for the electron transfer.

During the irradiation of solutions of Fe(III) aquacomplexes, the redox process leads to the formation of iron in the ferrous oxidation state. In Table 9.2,[10,11,21] the quantum yields of Fe(II) formation are gathered for different wavelengths of irradiation and different chemical compositions of the solutions. The percentage of the monomer complexes is another parameter that should be taken into consideration. It is defined as the ratio of the concentration of monomer complexes to the total concentration of Fe(III).

[Table 9.2 near here].

This table confirms also that the efficiency of the process of Fe(II) formation is strongly dependent on both Fe(III) speciation and the irradiation wavelength.

The degradation of pollutants in the aqueous phase, photoinduced by Fe(III) aquacomplexes, have been widely studied in the 1990s and 2000s. Various pollutants

have been tested, especially herbicides of the triazine[22] and phenylurea groups,[23,24] tenzides,[25] derivates of benzene[17] and phenolic derivates.[26] These compounds generally do not undergo direct photodegradation under sunlight ($\lambda > 290$ nm). For these different molecules, the primary degradation step is the same: formation of hydroxyl radicals which react with pollutants at different sites, according to their chemical structure. More details are given in section 9.3.

The reported data concerning the primary process (quantum yield) of the photochemical reaction clearly show that Fe(III) speciation and wavelength of irradiation are two important parameters controlling the efficiency of the photochemical process and, therefore, the production of hydroxyl radicals.

The principal role of Fe(II) in the general processes involving iron species in aquatic media lies in the Fenton reaction. In fact, the reaction of Fe(II) with hydrogen peroxide, in oxygenated solution, could provide an additional source of hydroxyl radicals.

$$Fe(II) + H_2O_2 \rightarrow Fe(III) + {}^{-}OH + HO^{\bullet} \quad k = 53\ M^{-1}\ s^{-1}.\ ^{27} \quad (9.5)$$

Hayon and Weiss[28] also reported the reaction of Fe(II) in an aquatic oxygenated solution upon irradiation at 254 nm, leading via electron transfer to the formation of the superoxide radical anion.

$$Fe(II) + O_2 \xrightarrow{h\nu} Fe(III) + O_2^{\bullet -} \quad (9.6)$$

Despite low absorbance below 300 nm, it was described that this process could occur under irradiation at wavelength higher than 300 nm,[29] but the efficiency in such conditions is very low.

It is also known that the superoxide radical anion can recombine with its protonated form, the hydroperoxide radical (pKa = 4.8), to give molecular oxygen and hydrogen peroxide:

$HO_2^{\bullet} + O_2^{\bullet -} + H_2O \rightarrow H_2O_2 + O_2 + {}^{-}OH$ k = 9.7×10^7 M^{-1} s^{-1} (9.7)[30]

Hydrogen peroxide can also be formed by recombination of hydroperoxide radicals, but with a lower rate constant:

$HO_2^{\bullet} + HO_2^{\bullet} \rightarrow H_2O_2 + O_2$ k = 8.3×10^5 M^{-1} s^{-1} (9.8)[31]

The second important role of ferrous ions is their oxidation to ferric ions by reaction with the hydroxyl radicals, superoxide anion and hydroperoxide. In all the cases, Fe(III) is generated but with different rate constants.

$Fe(II) + HO^{\bullet} \rightarrow Fe(III) + {}^{-}OH$ k = 3×10^8 M^{-1} s^{-1} [33] or k = 4.6×10^8 M^{-1} s^{-1} (9.9)[30]

$Fe(II) + HO_2^{\bullet} + H^+ \rightarrow Fe(III) + H_2O_2$ k = 1.2×10^6 M^{-1} s^{-1} (9.10)[33]

$Fe(II) + O_2^{\bullet -} \xrightarrow{+H^+, H_2O_2} Fe(III) + H_2O_2$ k = 1.0 x 10^7 $M^{-1}s^{-1}$ (9.11)[34]

These reactions lead again to the formation of Fe(III) and, therefore, a continuous photochemical source of radicals is present in such systems. However, the first reaction with the hydroxyl radicals consumes a strong oxidant ($HO^{\bullet}$ itself), which is detrimental for the process of organic compound oxidation. On the contrary, the two other reactions with hydroperoxide radical or superoxide radical anion are very positive for the regeneration of Fe(III) and so for the photochemical production of hydroxyl radicals. This regeneration of hydroxyl radical species could explain the complete mineralization of pollutants that is often observed in the photochemical processes involving iron species.

9.2.2 Organic complexes

Polycarboxylates such as citrate, malonate and oxalate are common constituents of precipitation, fog, surface waters and soil solutions.[35] They can form strong complexes with Fe^{3+} and enhance the dissolution of iron in natural waters through photochemical processes.

Aminopolycarboxylic acids (APCAs) like EDTA (Ethylenediaminetetraacetic acid) or EDDS (Ethylenediamine-N,N'-disuccinic acid) may behave similarly to polycarboxylic acids.[36] In fact, APCAs have a strong ability to solubilize and inactivate metal ions (and particularly iron) by complex formation.

The stability constants K of metal-organic ligand complexes are defined and determined as follows, whenever possible:

$$ML_{n-1} + L \leftrightarrow ML_n$$

$$K_n = [ML_n] / [ML_{n-1}] [L]$$

The following table shows literature values of stability constants of iron (ferric and ferrous) complexes with different organic ligands (polycarboxylic or aminopolycarboxylic acids) (Table 9.3).

[Table 9.3 near here]

From the table it is clear that the stability constants of the complexes can vary widely and that the organic compounds have not the same ability to complex ferric or ferrous iron in aqueous solution. In addition, we note that the stability constants with ferric iron are systematically higher than those with ferrous iron.

Moreover, the formed Fe-ligand complexes can absorb radiation at much longer wavelengths (generally until 500 nm, which allows them to absorb sunlight) than the non-complexed polycarboxylic or aminopolycarboxylic acids, which do not absorb sunlight. The following figure shows an example of the structure of the FeNTA complex (NTA = nitrilotriacetic acid) and its UV-visible spectrum (Figure 9.4).

[Figure 9.4 near here]

The polycarboxylate or aminopolycarboxylate complexes undergo rapid photochemical reactions under sunlight irradiation, leading to the formation of oxidizing species.[37,38] Therefore, the presence of polycarboxylates or aminopolycarboxylates affects the speciation of iron in surface waters and the biogeochemical cycles of iron and other elements. It was reported that light irradiation of Fe(III)-polycarboxylate or Fe(III)-aminopolycarboxylate complexes could produce both Fe(II) and ligand-free radicals by the ligand-to-metal charge transfer (LMCT) reactions (9.12). The photogenerated radical could react with Fe(III) species or O_2 to form Fe(II) species or the superoxide radical anion $O_2^{\bullet-}$ (9.13), respectively. The relative rates of the reactions of the radical with O_2 or Fe(III) are very important for determining the steady state concentration of Fe(II) and $O_2^{\bullet-}$. As mentioned before, $O_2^{\bullet-}$ and its acid conjugated form $HO_2^{\bullet}$ (pKa = 4.8 for the $HO_2^{\bullet}$/ $O_2^{\bullet-}$ couple) can participate in further reactions, including the generation of H_2O_2 (reactions (9.14) to (9.17)).[32] The yield of H_2O_2 depends critically on the competition between H_2O_2-producing reactions (reactions (9.14) to (9.17)) and the O_2-producing reactions ((9.18) and (9.19)).

$$Fe(III)-L \xrightarrow{h\nu} \left[Fe(III)-L\right]^{*} \rightarrow Fe(II)+L^{\bullet} \qquad (9.12)$$

$$L^{\bullet} + O_2 \rightarrow O_2^{\bullet -} + L_{ox} \qquad (9.13)$$

$$Fe(II) + O_2^{\bullet -} \xrightarrow{H^+} Fe(III) + H_2O_2 \qquad k = 1.0 \times 10^7\ M^{-1}\ s^{-1} \qquad (9.14)$$

$$Fe(II) + HO_2^{\bullet} \xrightarrow{H^+} Fe(III) + H_2O_2 \qquad k = 1.2 \times 10^6\ M^{-1}\ s^{-1} \qquad (9.15)$$

$$HO_2^{\bullet} + O_2^{\bullet -} \xrightarrow{H^+} H_2O_2 + O_2 + {}^{-}OH \qquad k = 9.7 \times 10^7\ M^{-1}\ s^{-1} \qquad (9.16)$$

$$HO_2^{\bullet} + HO_2^{\bullet} \xrightarrow{H^+} H_2O_2 + O_2 \qquad k = 8.3 \times 10^5\ M^{-1}\ s^{-1} \qquad (9.17)$$

$$Fe(III) + HO_2^{\bullet} \rightarrow Fe(II) + O_2 + H^+ \qquad k < 1 \times 10^3\ M^{-1}s^{-1} \qquad (9.18)$$

$$Fe(III) + O_2^{\bullet -} \rightarrow Fe(II) + O_2 \qquad k = 5 \times 10^7\ M^{-1}\ s^{-1} \qquad (9.19)$$

From these reactions it seems very likely that the concentrations of $HO_2^{\bullet}/O_2^{\bullet -}$ and Fe(III)/Fe(II) and, as a consequence, the formation of H_2O_2 in water are intertwined. In fact, it is well known that $HO^{\bullet}$ can be formed upon oxidation of Fe(II) by H_2O_2 in the so-called Fenton reaction (9.20).[39] The rate constant proposed by Gallard and collaborators[40] is close to those proposed in 1951 by Barb and coworkers.[27]

$$Fe(II) + H_2O_2 \rightarrow Fe(III) + HO^{\bullet} + {}^{-}OH \qquad k = 63\ M^{-1}\ s^{-1} \qquad (9.20)$$

Reactions (9.12) to (9.20) are similar to those described for iron aquacomplexes, but the formation of the superoxide radical anion and, therefore, of hydrogen peroxide is more efficient with organic complexes that with aquacomplexes.

The pH is an important parameter that governs the efficiency of the photochemical process. Interestingly, contrary to aquacomplexes or polycarboxylate complexes, a very efficient photochemical process is observed until pH 9.0 with aminopolycarboxylate complexes of Fe(III).[40] The increase of the pH range for the photochemical process is particularly interesting in terms of the natural environment,

and it reinforces the fact that iron complexes may have an impact on the environment. In the following section, different examples of photochemical reactions involving different kinds of iron complexes are presented.

9.3 Phototransformation of organic compounds in the presence of iron

Degradation by light, reaction with the hydroxyl radical $HO^{\bullet}$ and hydrolysis are important processes of pollutant abiotic degradation in the environment and can provide an alternative way to biodegradation. The major abiotic reactions (except for the hydrolysis) are connected with irradiation by sunlight. If the pollutant absorbs solar light, it can undergo photolysis that may lead to its transformation. If the pollutant does not absorb sunlight, its transformation can be induced by different absorbing species present in or added to the aquatic medium (e.g. nitrate, humic substances, Fe(III) complexes, H_2O_2). A common feature of these species is the formation under irradiation of highly oxidative transients, mainly the hydroxyl radicals $HO^{\bullet}$, which degrade many organic compounds in water with rate constants close to the diffusion control [41]. The formation of oxidizing transients has been used in different chemical processes, designated as advanced oxidation processes (AOP's), to eliminate organic compounds from aqueous solutions. Among the different AOP's, the TiO_2 photocatalysis, the photo-Fenton reaction using Fe(III) species, H_2O_2 and UV-Visible radiation and the photooxidation process of Fe(III) complexes or Fe(III) aquacomplexes are commonly used to transform (mineralize) pollutants.

9.3.1 Impact in the aquatic compartments

9.3.1.1 Fe(III) complexing agents

The first studies on the impact of the photochemistry of iron complexes in aqueous solution were performed on the fate of strong chelating agents used in the domestic and industrial domains, to remove metal cations including iron species. Aminopolycarboxylic acids such as nitrilotriacetic acid (NTA) were used to complex divalent and trivalent cations, for example in the formulation of detergents. Since Fe(III) is one the most widely present cations in natural waters, nitrilotriacetic acid will exist in waste water principally as Fe(III) nitrilotriacetate Fe(NTA). As it is shown in Figure 9.4, the absorption spectrum shows a tail up to the visible domain. As a result, Fe(NTA) undergoes transformation under solar irradiation and it is of great importance to know its photochemical behavior to understand the fate of NTA in the environment.

According to a study of Andrianirinaharivelo and collaborators,[18] the photodegradation of Fe(NTA) in aqueous solution does not occur by a single process. The conjunction of the excitation wavelength and pH makes the overall phenomenon quite complicated, but pH seems to be the most important parameter. The monohydroxyanion, the species present in neutral solution (Figure 9.4), can undergo at 365 nm a simple photosolvation leading to hydrous Fe(III) oxide and NTA. Upon excitation at 254 nm the Fe-O bond can be activated, giving rise to $HO^{\bullet}$ radicals and Fe(II). In acidic medium the molecular form of the complex Fe(NTA) reacts by charge transfer, either between Fe(III) and the carboxylate group at 365 nm or between Fe(III)

and the H_2O ligand at 254 nm. In addition, the oxidation rate of Fe(II) species is quite different in neutral and acidic solution.

The nature of the photoproducts is also dependent on pH and wavelength: Fe(III), Fe(II), NTA, IDA (iminodiacetic acid), CO_2 and HCHO can all be produced. Accordingly, in terms of the fate of Fe(NTA) at pH 5.5 to 7.0 and $\lambda < 290$ nm, all the above described photoreactions and photoproducts are involved.

Another study performed by Andrianirinaharivelo and Bolte[42] on the transformation of iminodiacetic acid, photo-induced by complexation with Fe(III), shows that the degradation of the aminopolycarboxylic acid can continue until complete transformation into CO_2 (Figure 9.5).

[Figure 9.5 near here]

9.3.1.2 Fe(III) aquacomplexes

The photosensitizing role of aqueous Fe(III) species was a subject of interest for environmental photochemistry in surface[43-47] and cloud[10,48-51] waters as well as for pollutant degradation.[24,25,29,52,53] In the absence of chelating agents, the most photoactive species is $Fe(OH)^{2+}$ that is the main aquacomplex present in moderately acidic solution (see paragraph 9.2).[10]

In our group, for the studies performed on the transformation of pollutants photoinduced by Fe(III) aquacomplexes, we investigated the transformation of the pollutant from the first transient species formed to the complete mineralization, via the identification of several photoproducts to establish a mechanism of degradation as

in the paper of Mailhot and co-workers.[17] In this particular paper, presenting the degradation of 4-chloroaniline, the authors identified three different mechanisms of transformation as a function of the experimental conditions:

- ring substitution
- rind opening
- oligomerization processes.

In the paper of Galichet and co-workers,[54] the toxicity of the solution was monitored at the same time as the degradation process of isoproturon. The evolution of the toxicity during the early stages of the degradation showed a strong increase from the starting toxicity of isoproturon (Figure 9.6). However, the degradation process was very efficient and after 6h the toxicity came back to the initial level, after which the mineralization process caused a further toxicity decrease. These results suggest that the degradation of pollutants has to be monitored throughout the process. In fact, some photoproducts can be more toxic than the starting compound and this may cause a serious problem for the aquatic environment.

[Figure 9.6 near here]

The studies performed with Fe(III) aquacomplexes lead, in most cases, to the complete mineralization of the pollutant. This very important result is based on a homogenous photocatalytic process based on the couple Fe(III)/Fe(II), which produces a continuous formation of radical species (mainly the hydroxyl radical, Figure 9.7). The oxidation of Fe(II) into Fe(III), which is the limiting step of the process, is favoured by i) the presence of oxygen and a complexing agent of Fe(III), ii)

the attack of the radical species formed on Fe(II) and iii) the oxygen photoassisted oxidation of Fe(II), giving rise to Fe(III) and the superoxide radical anion.[29]

[Figure 9.7 near here]

These different research works give evidence for the efficiency of pollutant removal from water by a process of homogenous photocatalysis.

9.3.1.3 Fe(III) organic complexes

The photochemistry of Fe(III)-organic complexes is also used for the degradation of organic pollutants. The reactivity of two main organic complexes, namely Fe(III)-nitrilotriacetic acid (FeNTA) and Fe(III)-ethylenediamine-N,N'-disuccinic acid (FeEDDS) is here reported.

FeNTA was studied in the presence of 4-chlorophenol (4-CP) adopted as target pollutant.[62] The quantum yields of the photodecomposition of the complex FeNTA and of Fe(II) formation by an intra-molecular photoredox process (the first stage of the reaction) were evaluated and presented in the following table (Table 9.4):

[Table 9.4 near here]

The quantum yields are high and the photoredox process is efficient over a large range of pH values. This is a very different finding compared to the results obtained with the Fe(III) aquacomplexes, which are efficient only until pH 4.0. However, while pH plays a significant role on the quantum yields of the first step (FeNTA disappearance), its effect is far less pronounced as far as 4-CP degradation is concerned.

The effect of FeNTA concentration on the kinetics of 4-CP disappearance gave clear

evidence that the species generated upon irradiation of FeNTA are able to induce the degradation of 4-CP (Figure 9.8). Indeed, no degradation of 4-CP was observed without FeNTA, and the rate of 4-CP degradation increased with increasing FeNTA concentration.

[Figure 9.8 near here]

The short-lived transients produced during the process were clearly identified and the two mechanisms leading to 4-CP degradation were elucidated.

At long wavelength irradiation (i.e., low energy), the $RCO_2^{\bullet}$ radical is formed upon intramolecular electron transfer between the carboxylate group and Fe(III), which is reduced to Fe(II). In the presence of oxygen, an hydrogen atom is abstracted from the R function of the $RCO_2^{\bullet}$ radical to produce $HO_2^{\bullet}$ and, upon dismutation, H_2O_2. 4-CP degradation results from the attack by $HO^{\bullet}$ generated by a Fenton reaction (Figure 9.9). At shorter wavelength irradiation (i.e. higher energy) the main detected radical species is $CO_3^{\bullet-}$, together with $HO^{\bullet}$. In this case, there is an electron transfer from the OH^- or H_2O ligand to Fe(III) (Figure 9.9).

[Figure 9.9 near here]

Carbonate radical ($CO_3^{\bullet-}$) requires the presence of oxygen to be formed; on the contrary, $R\text{-}CO_2^{\bullet}$ is formed even in the absence of oxygen. However, whatever the mechanism of FeNTA degradation, 4-CP requires the presence of oxygen to be degraded. Due to the elevated photolysis quantum yield of FeNTA, the resulting photoinduced pollutant degradation appears to be an efficient way of self-decontamination in the natural environment.

The second study presented here describes the impact of the photochemistry of the complex FeEDDS on the degradation of 4-tert-butylphenol (4-t-BP) in aqueous solution.[40] The detailed chemical structure of the complex between Fe(III) and EDDS and the predominance of the different forms with respect to pH were also obtained by ab initio calculations. In fact, pH is the main parameter influencing the photodegradation efficiency and the study was thus performed in a large range of pH. In the following figure (Figure 9.10) the effect of pH is clearly demonstrated.

[Figure 9.10 near here]

The observed increase of the degradation rate of 4-t-BP ($R_{4\text{-t-BP}}$) until pH 8.0 is due to the iron cycle and the relative concentration of the Fe(III) and Fe(II) species. These concentrations are strongly impacted by the presence of $HO_2^{\bullet}/O_2^{\bullet-}$, photogenerated by the complex FeEDDS. Above pH 8.0, the degradation rate of 4-t-BP decreases because of the presence of another less photoactive form of the complex. Indeed, the most photoactive form of the FeEDDS complex is the non hydroxylated one.

The reported results show that pH is a key parameter for iron complexes, thus it is very important to know their speciation for their use and optimization in water treatment processes.

9.3.2 Iron use in advanced oxidation processes

Advanced oxidation processes that employ titanium dioxide, hydrogen peroxide and iron species have been extensively studied over the last two decades.[56,57] In the following part of this paragraph, three different studies using iron species in advanced

oxidation processes are presented.

9.3.2.1 Fe(III) aquacomplexes

The principle of heterogeneous photocatalysis with titanium dioxide is a well known process: by irradiation of TiO_2 with light of energy higher than the band gap ($\lambda < 400$ nm), a pair of charge carriers (electron/hole) is formed. Photogenerated charge carriers can react with molecules adsorbed on the surface of TiO_2 particles. The most important reaction is oxidation of adsorbed water molecules, dissociated or nor, by holes to generate the hydroxyl radicals.

In the paper of Mestankova et al. (2005),[58] the authors investigated the influence of ferrous and/or ferric ions on TiO_2 efficiency. The kinetics of oxidative photodegradation of Monuron (3-(4-chlorophenyl)-1,1-dimethylurea), an herbicide of the phenylurea family, in different photocatalytic systems (iron, TiO_2 and combined system iron + TiO_2) were investigated and compared. It was studied the influence of iron addition on the TiO_2 photocatalyst and of TiO_2 on the photocatalytic cycle, observing a very positive effect of iron addition. The latter was more pronounced when TiO_2 concentration was lower. In a suspension of TiO_2 (24 mg L^{-1}) with addition of Fe(III) (3×10^{-4} mol L^{-1}), the measured rate constant of Monuron degradation was similar to that obtained in a suspension of TiO_2 with a concentration 20 times higher (500 mg L^{-1}). The mechanistic approach allowed the authors to identify the main reactions governing the combined system and to propose a photochemical cycle (Figure 9.11).[58]

[Figure 9.11 near here]

Two interactions between iron and TiO_2 appear to be essential for the efficiency of such process: i) the reaction of Fe(II) with oxidizing species generated upon irradiation of TiO_2 (H_2O_2, $HO_2^{\bullet}/O_2^{\bullet-}$) induces an additional formation of $HO^{\bullet}$ from the well-known Fenton process and regenerates the highly photoactive Fe(III) species; ii) the reaction of Fe(III) with photogenerated electrons can decrease the reactivity of monomeric Fe(III) species (highly photoactive) but increase degradation in the presence of soluble aggregates of Fe(III) (poorly photoactive).[58]

The mechanistic understanding of the combined system iron-TiO_2[58] helps optimizing the water treatment process. Indeed, optimization is reached when each photocatalyst plays a specific role. Fe(III) aquacomplexes are the main sources of hydroxyl radicals and TiO_2 is mainly used as a source of oxidative species for the oxidation of Fe(II) into Fe(III), thereby favoring the photocatalytic cycle Fe(III)/Fe(II).

9.3.2.2 Fe(III) organic complexes

The Fenton or photo-Fenton processes are efficient methods for the removal of many kinds of contaminants including pesticides, dyes, insecticides, pharmaceuticals, etc.[59-62] However, there are some defects in the traditional Fenton or photo-Fenton processes. Firstly, low efficiency is usually observed when the process is taking place at neutral or alkaline pH. Secondly, high concentrations of iron salts and peroxide are necessary to achieve an efficient rate of removal of the substrate. In fact, as it is mentioned in the beginning of this chapter, most of the iron in natural waters exists in the form of insoluble ferric oxides and (hydr)oxides. Due to the insolubility of Fe(III)

at neutral pH, the Fenton or photo-Fenton processes are unstable under such conditions where they afford low generation of hydroxyl radicals in the presence of H_2O_2. In order to overcome this limitation, polycarboxylates such as citrate, malonate and oxalate or aminopolycarboxylates such as EDTA and NTA are used as organic ligands, to complex iron and maintain it in solution. Very recently and for the first time, our group used a strong complexing agent, ethylenediamine-N,N'-disuccinic acid (EDDS), in the homogeneous Fenton-like and photo-Fenton-like processes.[63,64]

- Fenton-like process.

The effect of H_2O_2 concentration, Fe(III)-EDDS concentration, pH value and oxygen concentration on the homogeneous Fenton degradation of Bisphenol A (BPA), used as a model pollutant, was investigated. The most significant effect was observed in the experiments carried out at different pH values. Surprisingly, the performance of the EDDS-driven Fenton reaction toward BPA oxidation was found to be much higher at near neutral or basic pH than at acidic pH (Figure 9.12).

[Figure 9.12 near here]

Inhibition and probe studies, with 2-propanol used as an hydroxyl radical scavenger and chloroform used as a superoxide radical anion ($O_2^{\bullet -}$) scavenger, were conducted to ascertain the role of these radicals on BPA degradation. The two sets of experiments with both scavengers led to important conclusions on the mechanism involved in the Fenton-like process, using Fe(III)-EDDS complexes. The radical $HO^{\bullet}$ is mainly responsible for the BPA degradation. However, its formation from the Fenton process strongly depends (80 %) on the presence of the superoxide radical anion. Indeed, only

20% of $HO^{\bullet}$ formation results from the following classical reactions, where superoxide radical anions are not needed.

$$Fe(III) - EDDS + H_2O_2 \rightarrow Fe(II) - EDDS + HO_2^{\bullet} + H^+ \qquad (9.20)$$

$$Fe(II) - EDDS + H_2O_2 \rightarrow Fe(III) - EDDS + HO^{\bullet} + OH^- \qquad (9.21)$$

The other 80% of $HO^{\bullet}$ formation comes as well from the Fenton process but through the reduction of Fe(III)-EDDS into Fe(II)-EDDS by $O_2^{-\bullet}$, in a similar way as what happens for Fe(III) aquacomplexes:

$$Fe(III) + O_2^{\bullet -} \rightarrow Fe(II) + O_2 \qquad (9.22)$$

The following figure summarizes this interesting result (Figure 9.13).

[Figure 9.13 near here]

The unexpected effect of pH on the Fenton reaction efficiency could be due to the formation of $HO_2^{\bullet}$ or $O_2^{\bullet -}$ radicals, but also to the presence of different forms of the complex Fe(III)-EDDS as a function of pH.[41] Indeed, the reduction of Fe(III)-EDDS to Fe(II)-EDDS is a crucial step that governs the formation of hydroxyl radicals, mainly responsible for BPA degradation. In addition to its ability to maintain iron in soluble form, EDDS acts as a superoxide radical-promoting agent, enhancing the generation of Fe(II) (the rate limiting step) and therefore the production of $HO^{\bullet}$ radicals. These results are very encouraging for the application of the EDDS-driven Fenton process in conditions of neutral pH, closer to natural conditions encountered in the environment.

- Photo-Fenton-like process

The same kinds of experiments were carried out in the photo-Fenton-like process,

assessing the effect of the Fe(III)-EDDS complex under irradiation. The main focus was on $HO^{\bullet}$ formation and BPA degradation. Figure 9.14 shows that Fe(III)-EDDS had important effects on both $HO^{\bullet}$ radical formation and BPA degradation in the photo-Fenton system at neutral pH.

[Figure 9.14 near here]

As it was demonstrated for the Fenton-like process, this is mainly due to the presence of EDDS, which can stabilize Fe(III) in aqueous solution between pH 3 and 9 and thus prevent its precipitation. In experiments carried out by varying concentrations, the increase of H_2O_2 and Fe(III)-EDDS were found to enhance the degradation rate of BPA. However, when the concentrations of Fe(III)-EDDS and/or H_2O_2 were too high, a competition for the reactivity of $HO^{\bullet}$ was observed between BPA and Fe(II)-EDDS or H_2O_2, thereby lowering BPA degradation. The experiments performed at different pH values demonstrated that BPA can be efficiently degraded at acidic, neutral and alkaline pH, which means that the addition of EDDS can widen the applicable pH range of the photo-Fenton system. It was also shown that oxygen is an important parameter for the oxidation of BPA.

It was concluded that the addition of EDDS enhanced the production of $HO^{\bullet}$ and the degradation of BPA, which is very interesting for water treatment processes. The high efficiency of the photo-Fenton process using Fe(III)-EDDS as iron source allows for keeping complex and H_2O_2 concentrations low and for operating over a wider pH range, which is very encouraging for the application of the photo-Fenton process at neutral pH.

As for the Fenton-like process, the use of Fe(III)-EDDS makes this system an encouraging method for the treatment of organic pollutants in the natural aquatic environment.

9.4 Conclusion

In this chapter the complexity of iron chemistry in aqueous solution is discussed, but at the same time the significant impact of iron species on the chemical composition of different aquatic media is highlighted all along the chapter. To assess the role of iron compounds in aqueous solution it is really necessary to understand the speciation of iron. The main parameters influencing the iron speciation are the presence of organic complexing agents and the pH, which both govern the presence, the concentration and the formation of the different forms of iron complexes in aqueous solution. The use of iron in water treatment, through its introduction in different advanced oxidation processes and its positive effect in terms of pollutant removal, seems to be a very promising technique to preserve water quality.

Acknowledgements

The authors gratefully acknowledge the Blaise Pascal University in Clermont-Ferrand, France and the CNRS. This work was supported by the “Federation des Recherches en Environnement” through the CPER “Environnement” founded by the “Région Auvergne”, the French Government and FEDER from the European community.

References

1. G. R. Helz, R. G. Zepp, D. G. Crosby, *Aquatic and Surface Photochemistry*, Lewis Publishers, 1994, 53- 73.
2. J. H. Martin, R. M. Gordon, S. E. Fitzwater, *Nature*, 1990, **345**, 156.
3. K. S. Johnson,R. M. Gordon, K. H. Coale, *Mar. Chem.*, 1997, **57**, 137.
4. M. H. Conklin, M. R. Hoffmann, *Environ. Sci. Technol.*, 1988, **22**, 899.
5. S. H. Eberle, W. Palmer, *Z. Wasser. Abwass. For.*, 1986, **19**, 233.
6. J. H. Martin, S. E. Fitzwater, *Nature*, 1988, **331**, 341.
7. P. Behra, L. Sigg, *Nature*, 1990, **344**, 419.
8. C. M. Flynn, *Chem. Rev.*, 1984, **84**, 31.
9. D. Langmuir, D. O. Whittemore, *Adv. Chem. Ser.*, 1971, **106**, 209.
10. B.C. Faust, J. Hoigné, *Atmos. Environ.*, 1990, **24**, 79.
11 C. H. Langford, J. H. Carey, *Can. J. Chem.*, 1975, **53**, 2430.
12 R. J. Knight, R. N. Sylva, *J. Inorg. Nucl. Chem.*, 1975, **37**, 779.
13 R. M. Milburn, *J. Am. Chem. Soc.*, 1956, **79**, 537.
14 M. T. Escot, Thèse de doctorat en Pharmacie, Université d'Auvergne, Clermont-Ferrand (France) 1973.
15 M. G. Evans, N. Uri, *Nature*, 1949, **164**, 404.
16 H. G. C. Bates, M. G. Evans, N. Uri, *J. Am. Chem. Soc.*, 1953, **75**, 2754.
17 G. Mailhot, L. Hykrdová, J. Jirkovský, K. Lemr, G. Grabner, M. Bolte, *Appl. Catal., B*, 2004, **50**, 25.

18 S. L. Andrianirinaharivelo, P. Jirkovský, M. Bolte, *Trans. Met. Chem.*, 1993, **18**, 37.

19 H. J. Benkelberg, P. J. Warneck, *J. Phys. Chem.*, 1995, **99**, 5214.

20 H. J. Benkelberg, A. Schäfer, P. Warneck, *Air Pollution research Report 33: Atmospheric Oxidation Processes*, ed. Becker K.-H., CEC, Brussel, 1991, 130.

21 P. Mazellier, G. Mailhot, M. Bolte, *New J. Chem.*, 1997, **21**, 389.

22 H. Krýsová, J. Jirkovský, J. Krýsa, G. Mailhot, M. Bolte, *Appl. Catal., B*, 2003, **40**, 1.

23 L. Poulain, G. Mailhot, P. Wong-Wah-Chung, M. Bolte, *J. Photochem. Photobiol., A*, 2003, **159**, 81.

24 P. Mazellier, J. Jirkovský, M. Bolte, *Pestic. Sci*., 1997, **49**, 259.

25 N. Brand, G. Mailhot, M. Bolte, *Environ. Sci. Technol.*, 1998, **32**, 2715.

26 H. Kawaguchi, A. Inagaki, *Chemosphere*, 1994, **28**, 57.

27 W. G. Barb, J. H. Baxendale, P. George, K. R. Hargrave, *Trans. Faraday Soc.* 1951, **47**, 462.

28 E. Hayon, J. Weiss, *J. Chem. Soc.*, 1960, **0**, 3866.

29 C. Catastini, M. Sarakha, G. Mailhot, M. Bolte, *Sci. Total Environ.*, 2002, **298**, 219.

30 H. Christensen, K. Sehested, *J. Phys. Chem.*, 1988, **92**, 3007.

31 B. H. J. Bielski, D. E. Cabelli, R. L. Arudi, A. B. Ross, *J. Phys. Chem. Ref. Data*, 1985, **14**, 1041.

32 Z. Stuglik, Z. P. Zagorski, *Radiat. Phys. Chem.* 1981, **17**, 229.

33 G. G. Jayson, B. J. Parson, A. J. Swallow, *J. Chem. Soc. Faraday Trans. 1* , 1973, **69**, 236.

34 J. D. Rush, B. H. J. J. Bielski, *J. Phys. Chem*. 1985, **89**, 5062.

35 K. Kawamura, S. Steinberg,I. R. Kaplan, *Int. J. Environ. Anal. Chem*. 1985, **19**, 175.

36 J. Li, G. Mailhot, F. Wu, N. Deng, *Photochem. Photobiol. Sci.*, 2012, **11**, 1880.

37 B. C. Faust, R. G. Zepp, *Environ. Sci. Technol*. 1993, **27**, 2517.

38 D. Panias, M. Taxiarchou, I. Paspaliaris, A. Kontopoulos, *Hydrometallurgy* 1996, **42**, 257.

39 H. Gallard, J. De Laat, B. Legube, *New J. Chem.*, 1988, **22**, 263.

40 Y. Wu, M. Brigante, W. Dong, P. de Sainte-Claire, G. Mailhot, *J. Phys Chem, A*, 2014, **118**, 396.

41 G. V. Buxton, C. L. Greenstock, W. P. Helman, A. P. Ross, *J. Phys. Chem. Ref. Data*, 1985, **17**, 513.

42 L. Andrianirinaharivelo, M. Bolte, *Chemosphere*, 1992, **24**, 953.

43 K. S. Johnson, K. H. Coale, V. A. Elrod, N. W. Tindale, *Mar. Chem*., 1994, **46**, 319.

44 W. L. Miller, D. W. King, J. Lin, D. R. Kester, *Mar. Chem.*, 1995, **50**, 63.

45 B. M. Voelker, F. M. M. Morel, B. Sulzberger, *Environ. Sci. Technol.*, 1997, **31**, 1004.

46 D. C. Hrncir, D. McKnight, *Environ. Sci. Technol*., 1998, **32**, 2137.

47 L. Emmenegger, R. Schoenenberger, L. Sigg, B. Sulzberger, *Limnol. Oceanogr*.,

2001, **46**, 49.

48 G. S. Zhuang, Z. Yi, R. A. Duce, P. R. Brown, *Glob. Biogeochem. Cycl.*, 1992, **6**, 161.

49 S. O. Pehkonen, R. L. Siefert, M. R. Hoffmann, *Environ. Sci. Technol*., 1995, **29**, 215.

50 T. Arakaki, B. C. Faust, *J. Geophys. Res. D*, 1998, **103**, 3487.

51 Y. G. Zuo, *Chemosphere*, 2003, **51**, 175.

52 N. Brand, G. Mailhot, M. Bolte, *Chemosphere*, 2000, **40**, 395.

53 G. Mailhot, N. Brand, M. Astruc, M. Bolte, *Appl. Organomet. Chem.*, 2002, **16**, 27.

54 F. Galichet, G. Mailhot, F. Bonnemoy, J. Bohatier, M. Bolte, *Pest. Mang. Sci.*, 2002, **58**, 707.

55 A. Otman, G. Mailhot, M. Litter, M. Bolte, *Photochem. Photobil. Sci.*, 2006, **5**, 395.

56 M. R. Hoffmann, S. T. Martin, W. Choi, D. W. Bahnemann, *Chem. Rev.*, 1995, **95**, 69.

57 J. J. Pignatello, E. Oliveros, A. MacKay, *Crit. Rev. Environ. Sci. Technol.*, 2006, **36**, 1.

58 H. Mestankova, J. Krysa, J. Jirkovsky, G. Mailhot, M. Bolte, *Appl. Catal. B*, 2005, **58**, 185.

59 P. L. Huston, J. J. Pignatello, *Water Res.*, 1999, **33**, 1238.

60 T. Maezono, M. Tokumura, M. Sekine, Y. Kawase, *Chemosphere*, 2011, **82**, 1422.

61 E. Evgenidou, I. Konstantinou, K. Fytianos, I. Poulios, *Water Res.*, 2007, **41**, 2015.

62 F. Ménndez-Arriaga, S. Esplugas, J. Giménez, *Water Res.*, 2010, **44**, 589.

63 W. Huang, M. Brigante, F. Wu, K. Hanna, C. Mousty, G. Mailhot *Environ. Sci. Technol.,* 2013*,* **47**, 1952.

64 W. Huang, M. Brigante, F. Wu, K. Hanna, G. Mailhot, *J. Photoch. Photobiol. A,* 2012, **239**, 17.

Table Caption

Table 9.1: Quantum yields of hydroxyl radical formation for different Fe(III) species.

Table 9.2: Quantum yields of Fe(II) formation for different solutions of Fe(III).

Table 9.3: Fe(III) or Fe(II) complexes stability constants with different organic compounds.

Table 9.4: Quantum yields of FeNTA and 4-CP disappearance and Fe(II) formation at pH 4.0 and 6.0 and wavelengths 365 and 313 nm. The values in parenthesis correspond to the quantum yields in the absence of 4-CP.

Table 9.1:

Fe(III) aquacomplex	λ_{irr} [nm]	$\Phi_{\bullet OH}$	Reference
Fe^{3+}	254	0.065	11
	< 300	~ 0.05	20
$Fe(OH)^{2+}$	280	0.31	20
	300	0.19	20
	313	0.14	20
	373	0.065	20
$Fe(OH)_2^{+}$	280	0.30	21
	360	0.071	
$Fe_2(OH)_2^{4+}$	350	0.007	11

Table 9.2:

	λ_{irr} [nm]	$\Phi_{Fe(II)}$	Reference
$Fe_2(OH)_2^{4+}$	350	0.010	19
$Fe(OH)^{2+}$	313	0.140	10
Presence of $HO^{\bullet}$ scavenger	360	0.017	
$[Fe^{III}]_0 = 1\times10^{-4}$ mol.L^{-1}	313	0.080	22
92 % $Fe(OH)^{2+}$	360	0.055	
$[Fe^{III}]_0 = 1\times10^{-4}$ mol.L^{-1}	313	0.020	22
10 % $Fe(OH)^{2+}$	365	0.008	

Table 9.3:

Complex	**Log K**
Fe(III)	
EDTA	25.7
EDDS	22.0
HEDTA	19.1
Salicylic acid	16.3

NTA	15.9
Citric acid	11.8
Glycine	10.0
Oxalic acid	9.4
Tartaric acid	7.5
Succinic acid	7.5
Lactic acid	6.4
Glycolic acid	4.7
Propionic acid	3.4
Formic acid	3.1
Fe(II)	
o-phenantroline	21.3
Ferrocine	16.2
EDTA	14.3
NTA	8.8
Salicylic acid	6.5
IDA	5.8
Oxalic acid	> 4.7
Glutamic acid	4.6
Glycine	4.3
Citric acid	3.2

Table 9.4:

	$\Phi_{FeNTA\ disappearance}$		$\Phi_{Fe(II)\ formation}$		$\Phi_{4\text{-}CP\ disappearance}$	
λ(nm)	pH = 4.0	pH = 6.0	pH = 4.0	pH = 6.0	pH = 4.0	pH = 6.0
365	0.27 (0.25)	0.04 (0.03)	0.28 (0.21)	0.04 (0.02)	0.011	0.012
313	0.50 (0.35)	0.17 (0.11)	0.46 (0.34)	0.16 (0.09)	0.018	0.030

Figure caption

Figure 9.1: Diagram of distribution of monomer complexes of Fe(III) as a function of pH. Temperature = 298 K and ionic strength = 0.03 M.

Figure 9.2: UV-visible absorption spectra of Fe(III) complexes, molar absorption coefficient as a function of wavelength.

Figure 9.3: Energetic diagram of a transition metal complex. A: Metallic transition d-d due to the degeneration of the ligand field. B and C: ligand to metal charge transfer. D: intra-ligand transition.

Figure 9.4: FeNTA Chemical structure of the two forms (molecular form and monohydroxyanion form with a pKa = 5.5), FeNTA UV-visible spectrum at pH 3.6 and solar spectra during winter and summer.

Figure 9.5: Photodegradation of the FeNTA complex ; from NTA to CO_2.

Figure 9.6: Comparison of (□) the toxicity EC_{50} evolution and the formation of the main primary photoproducts (■,○, ▲).

Figure 9.7: Iron photchemical cycle in aqueous solution.

Figure 9.8: Kinetics of 4-CP (0.2 mM) photodegradation at different FeNTA concentrations. pH = 4.0, λ irradiation = 365 nm.

Figure 9.9: FeNTA photochemical process at longer wavelength.

Figure 9.10: Effect of pH value on the degradation rate of 4-t-BP (5×10^{-5} M) in the presence of Fe(III)-EDDS (1×10^{-4} M) under polychromatic irradiation.

Figure 9.11: Photochemical cycle of combined system iron-TiO_2.

Figure 9.12: Initial degradation rate of BPA 20 µM in the presence of Fe(III)-EDDS 0.5 mM, H_2O_2 5 mM, at different pHs. The error bars represent the ±3σ based on the

fit of the experimental data. The solid line (sigmoid equation) represents only a visual guide.

Figure 9.13: Simplified mechanism of Fenton acceleration attributed to the positive effect of the superoxide radical anion ($O_2^{\bullet -}$) during regeneration of Fe(II) from Fe(III) at pH = 6.2 ± 0.1.

Figure 9.14: BPA degradation in different photo-oxidation systems at pH 6.2. Initial concentrations were 20 μM BPA, 0.1 mM Fe(III)-EDDS, 0.1 mM Fe(III), and 0.1 mM H_2O_2. The lines show an exponential decay fit and are presented only to guide the eyes.

Figure 9.1:

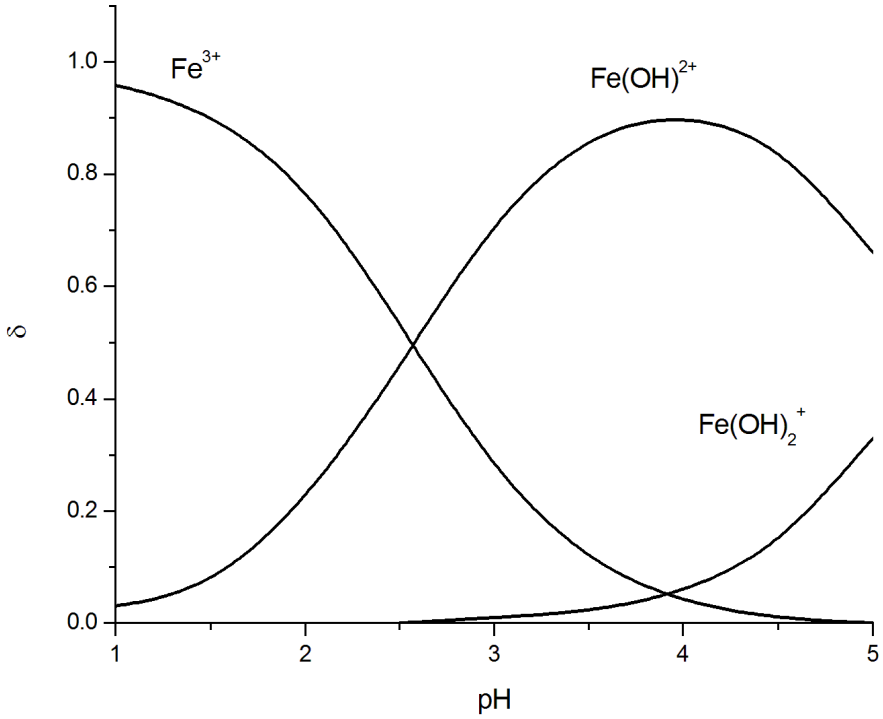

Figure 9.2:

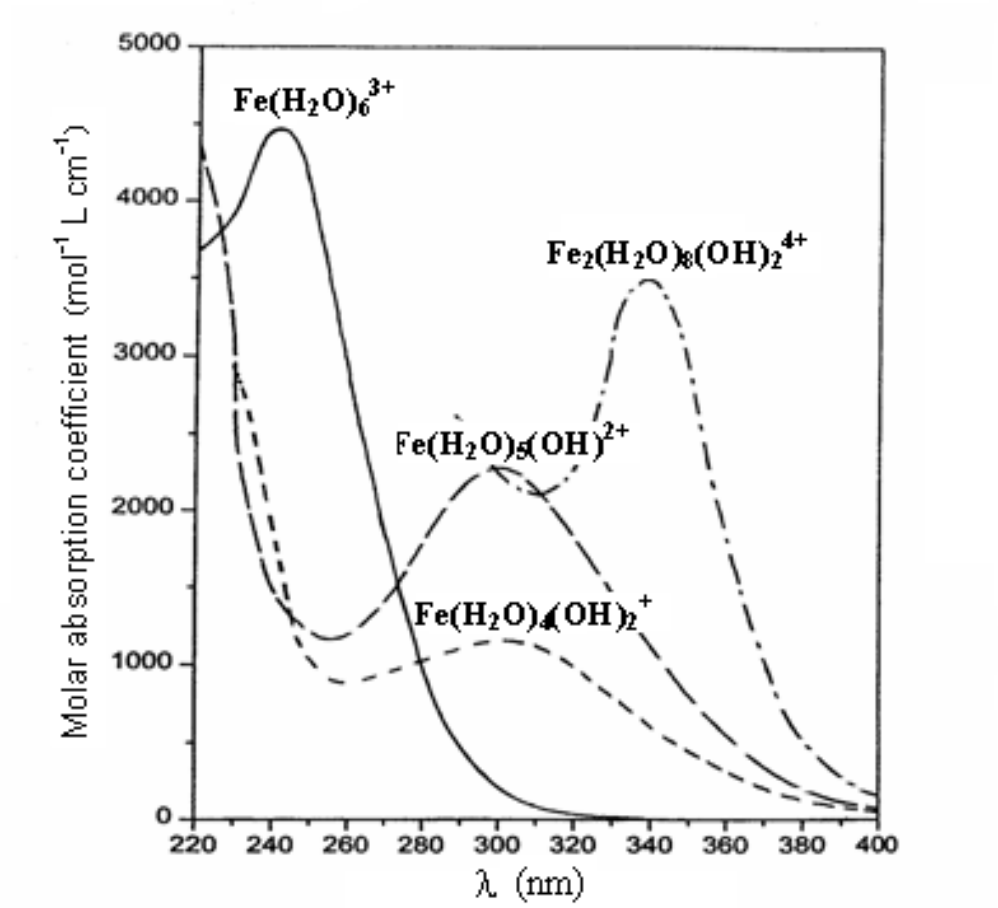
Molar absorption coefficient (mol^{-1} L cm^{-1})
λ (nm)
$Fe(H_2O)_6^{3+}$
$Fe_2(H_2O)_8(OH)_2^{4+}$
$Fe(H_2O)_5(OH)^{2+}$
$Fe(H_2O)_4(OH)_2^{+}$
0
1000
2000
3000
4000
5000
220
240
260
280
300
320
340
360
380
400

Figure 9.3:

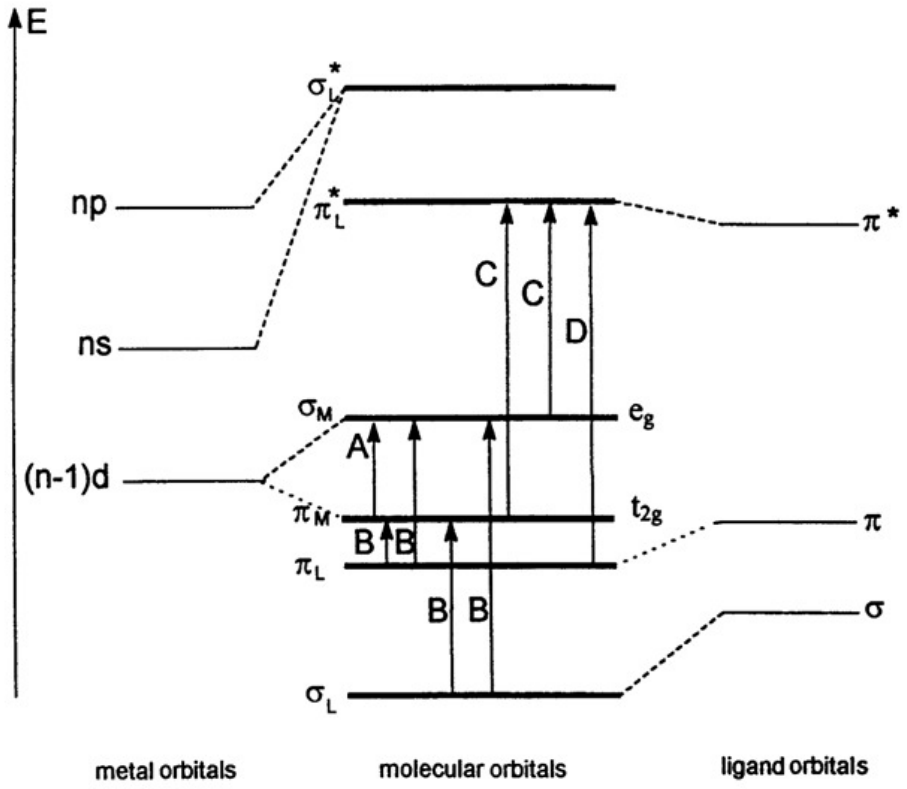
E
σ_L^*
np
π_L^*
π^*
C
C
D
ns
σ_M
e_g
A
(n-1)d
π_M
t_{2g}
π
B
B
π_L
B
B
σ
σ_L
metal orbitals
molecular orbitals
ligand orbitals

Figure 9.4:

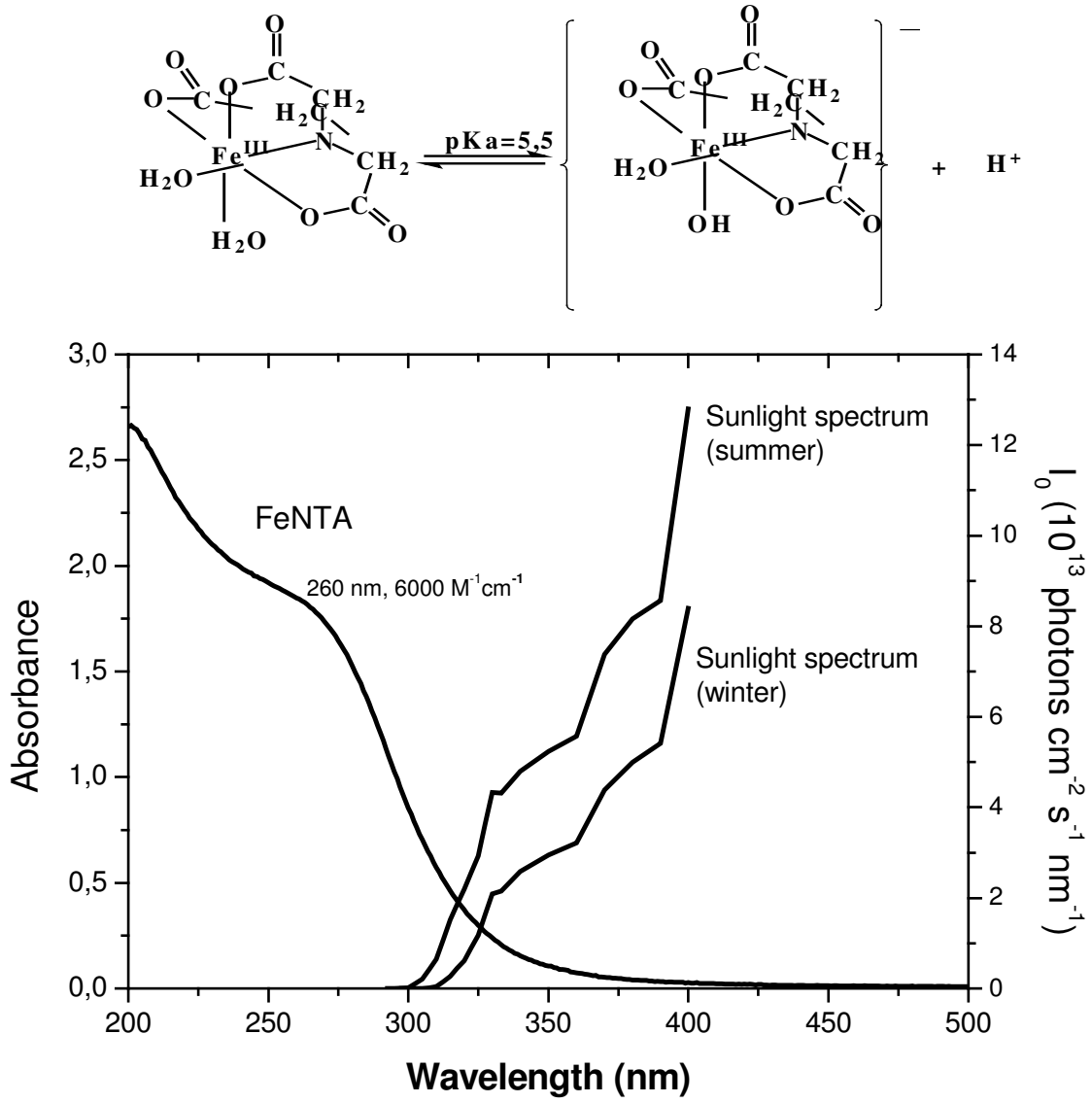
pKa=5,5
+ H+
FeNTA
260 nm, 6000 M-1cm-1
Sunlight spectrum (summer)
Sunlight spectrum (winter)
Absorbance
I0 (10^13 photons cm-2 s-1 nm-1)
Wavelength (nm)
3,0
2,5
2,0
1,5
1,0
0,5
0,0
14
12
10
8
6
4
2
0
200
250
300
350
400
450
500

Figure 9.5:

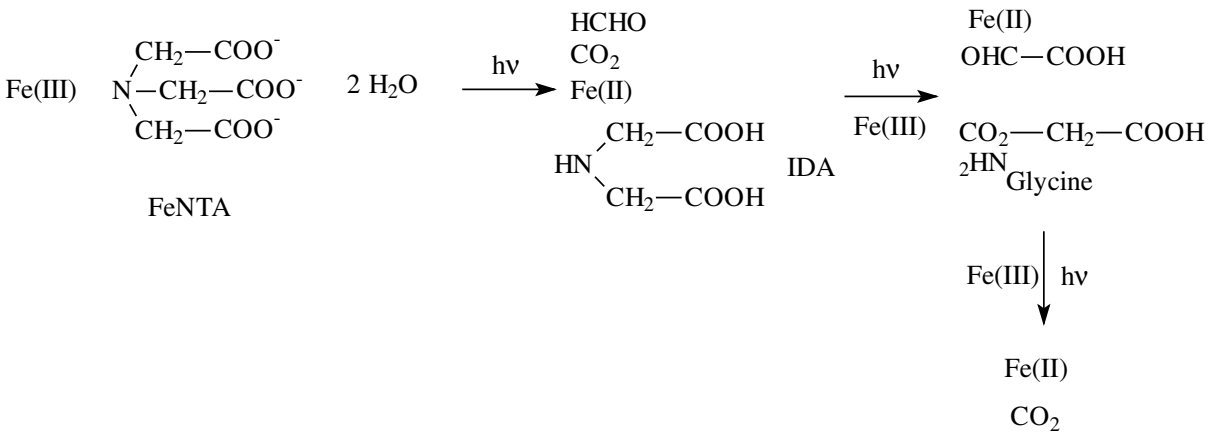
Fe(III)
CH2—COO-
N—CH2—COO-
CH2—COO-
FeNTA
2 H2O
hν
HCHO
CO2
Fe(II)
CH2—COOH
HN
CH2—COOH
IDA
hν
Fe(III)
Fe(II)
OHC—COOH
CO2—CH2—COOH
2HN
Glycine
Fe(III)
hν
Fe(II)
CO2

Figure 9.6:

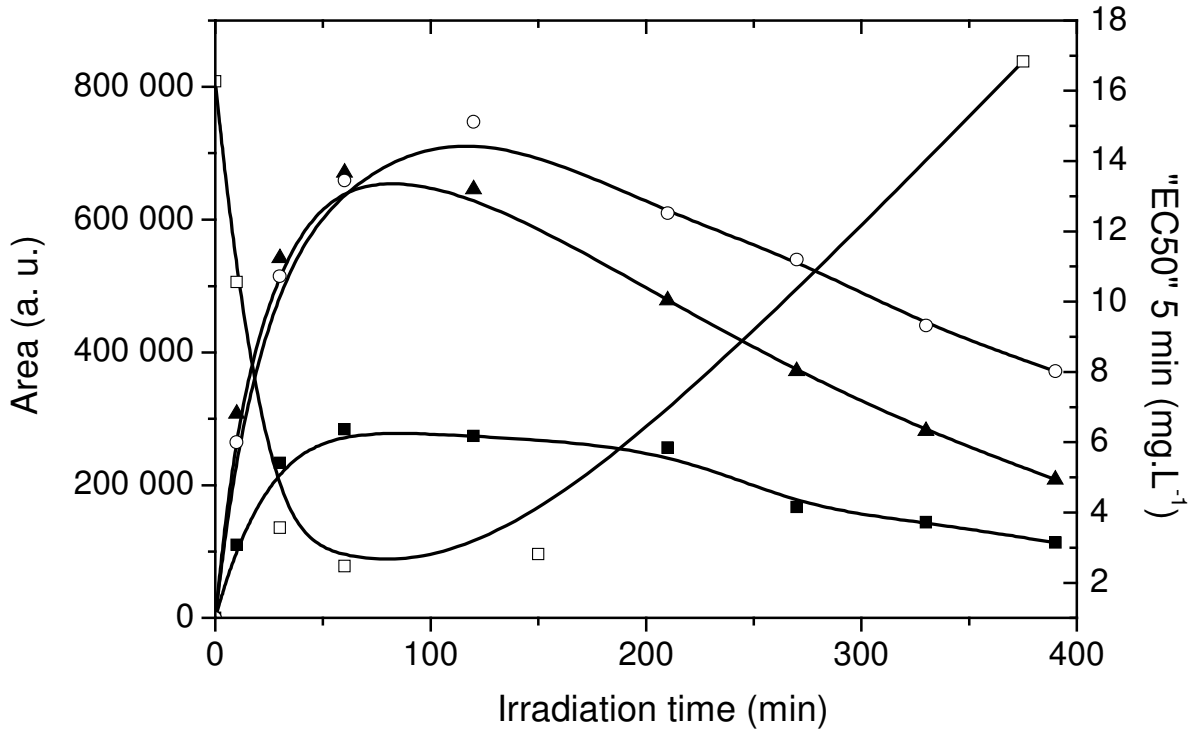
Area (a. u.)
800 000
600 000
400 000
200 000
0
0
100
200
300
400
Irradiation time (min)
18
16
14
12
10
8
6
4
2
"EC50" 5 min (mg.L-1)

Figure 9.7:

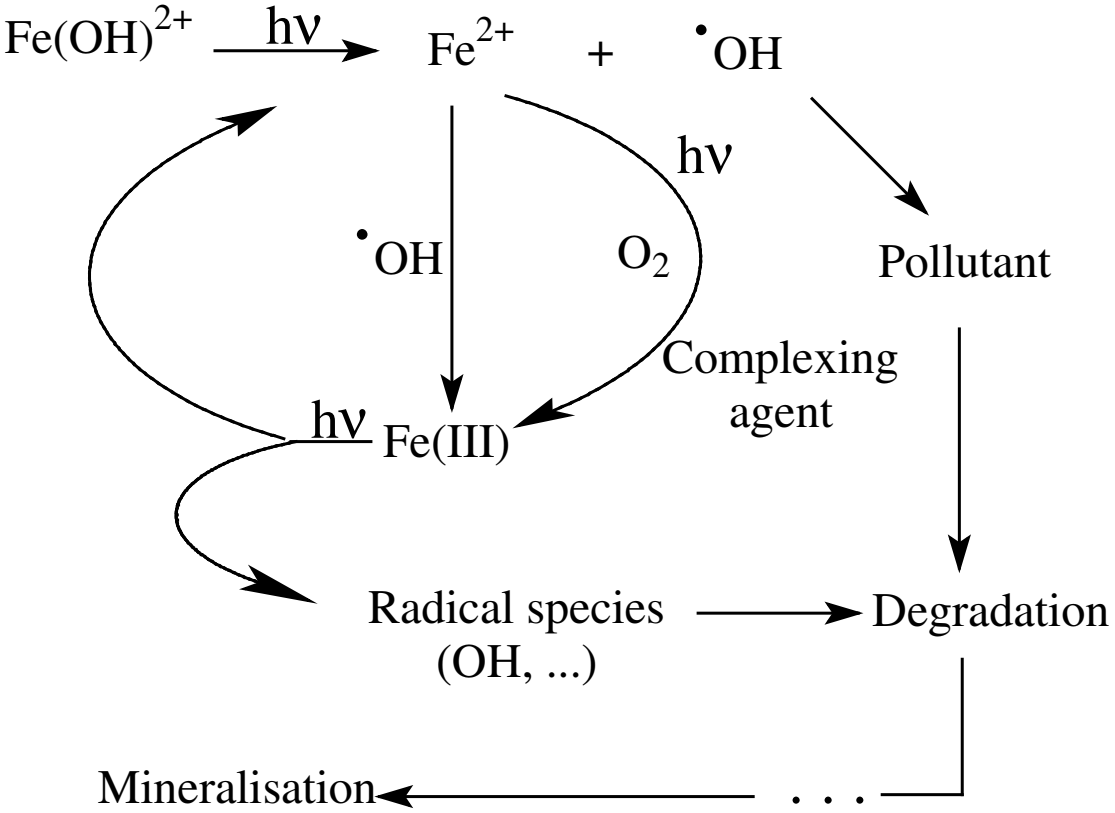
Fe(OH)2+
hν
Fe2+
+
•OH
hν
•OH
O2
Pollutant
Complexing
agent
hν
Fe(III)
Radical species
(OH, ...)
Degradation
Mineralisation
. . .

Figure 9.8:

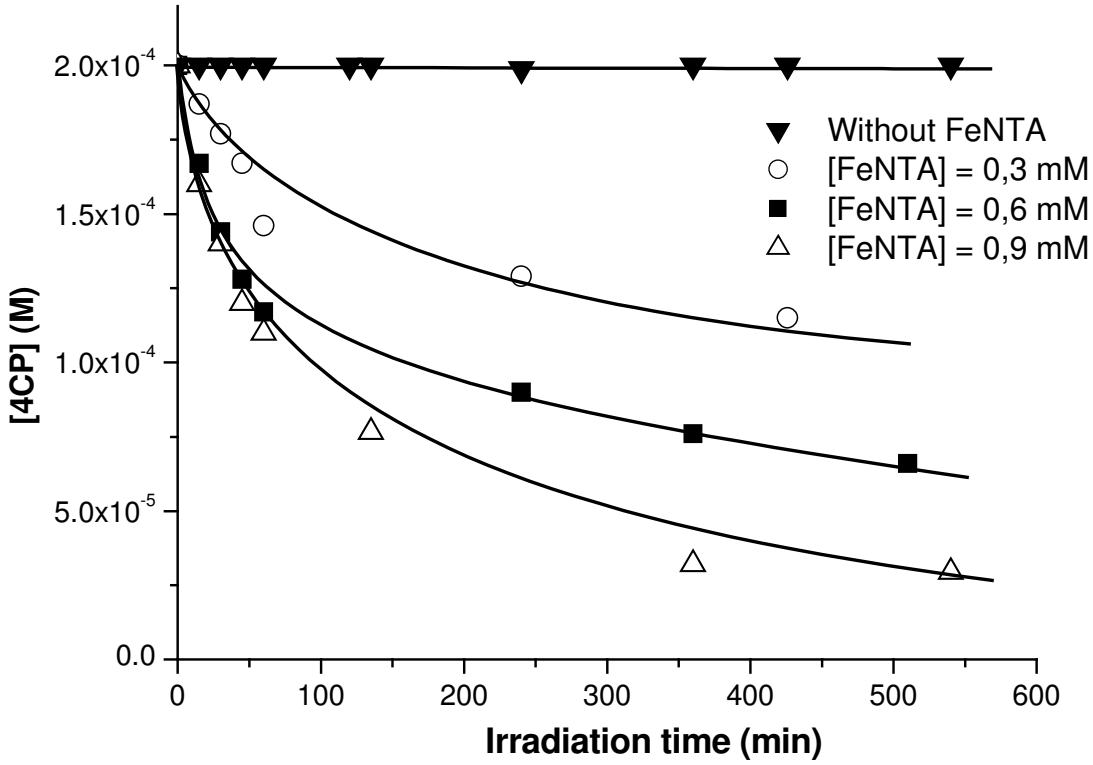
2.0x10-4
1.5x10-4
1.0x10-4
5.0x10-5
0.0
[4CP] (M)
0
100
200
300
400
500
600
Irradiation time (min)
Without FeNTA
[FeNTA] = 0,3 mM
[FeNTA] = 0,6 mM
[FeNTA] = 0,9 mM

Figure 9.9:

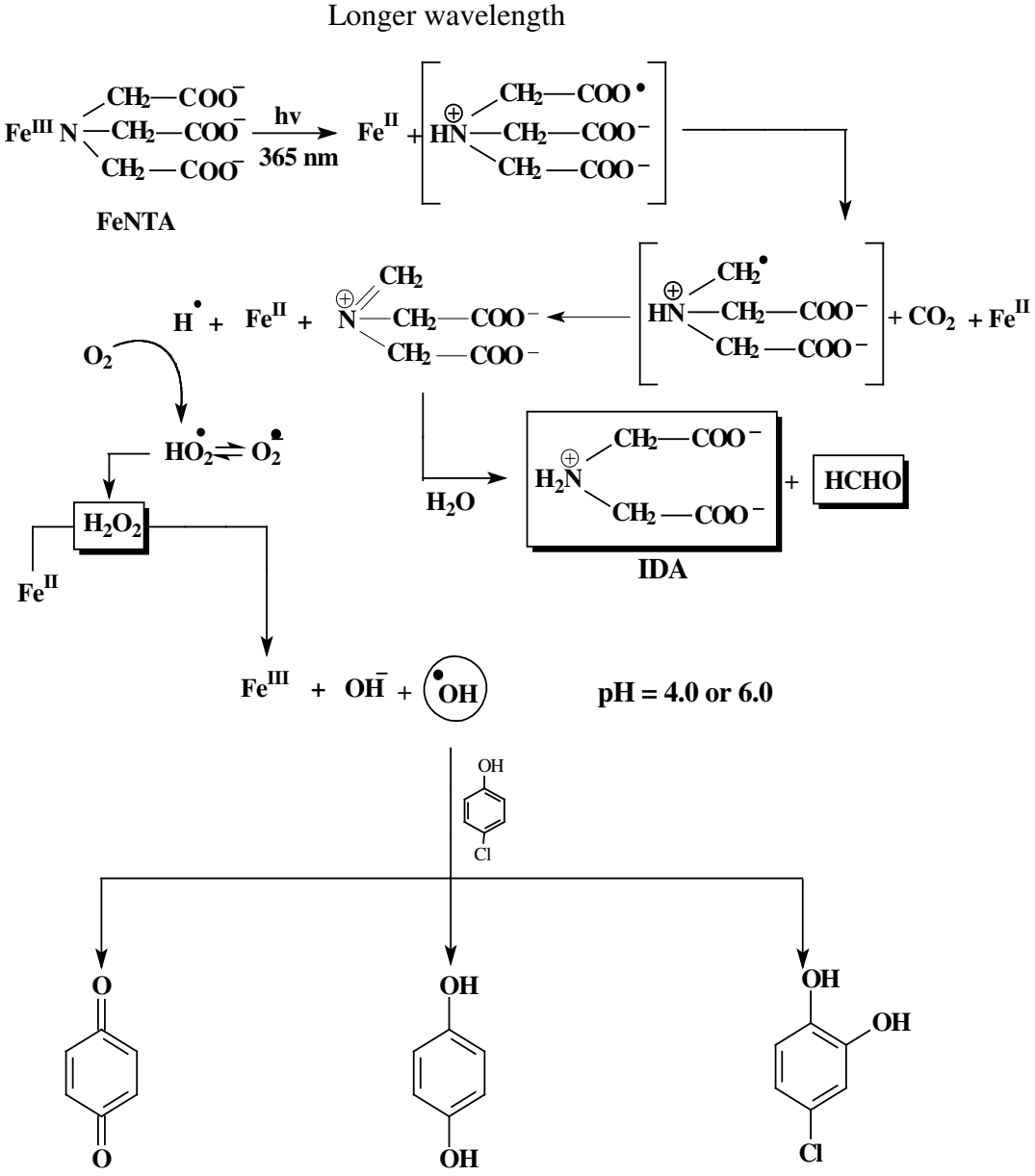
Longer wavelength
FeNTA
hv
365 nm
IDA
HCHO
pH = 4.0 or 6.0
Shorter wavelength

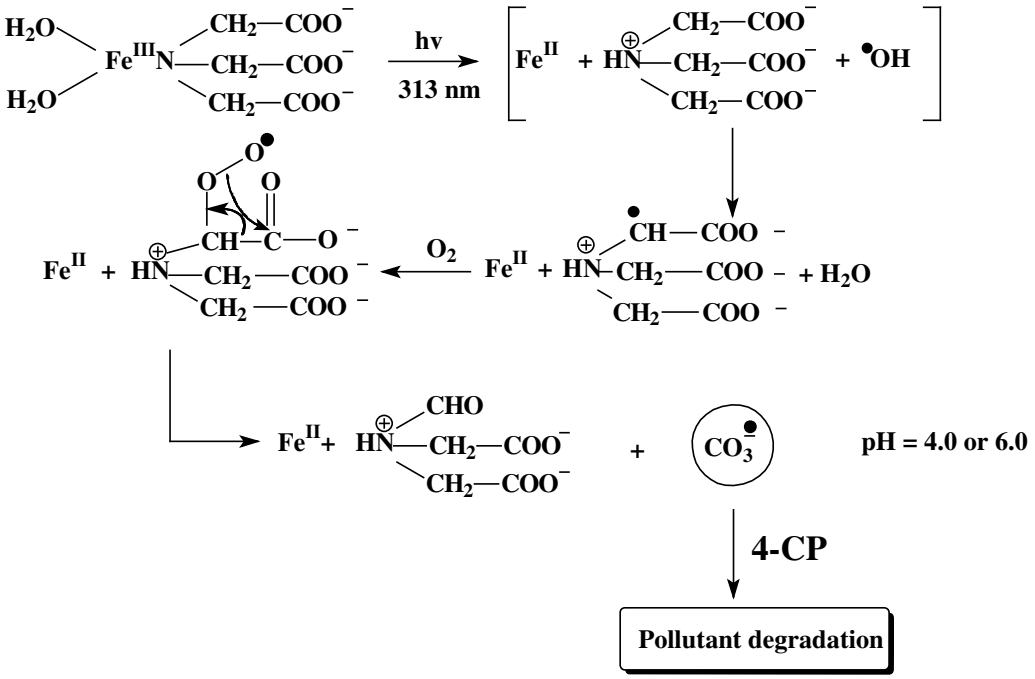
hv
313 nm
O2
pH = 4.0 or 6.0
4-CP
Pollutant degradation

Figure 9.10:

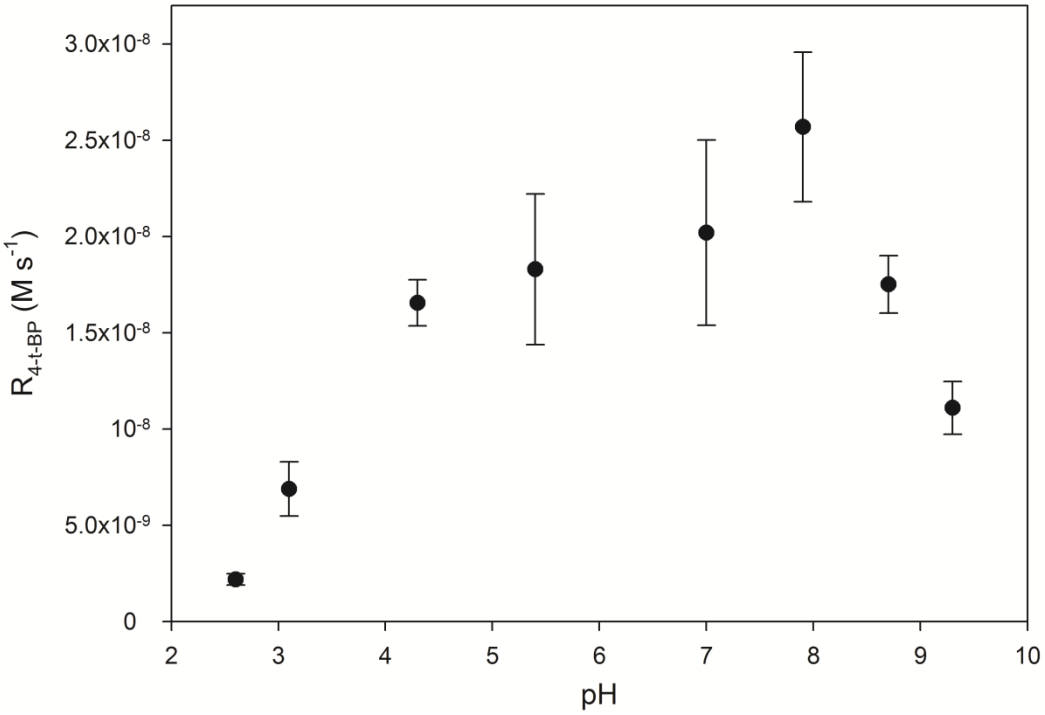
3.0x10-8
2.5x10-8
2.0x10-8
1.5x10-8
10-8
5.0x10-9
0
R4-t-BP (M s-1)
2
3
4
5
6
7
8
9
10
pH

Figure 9.11:

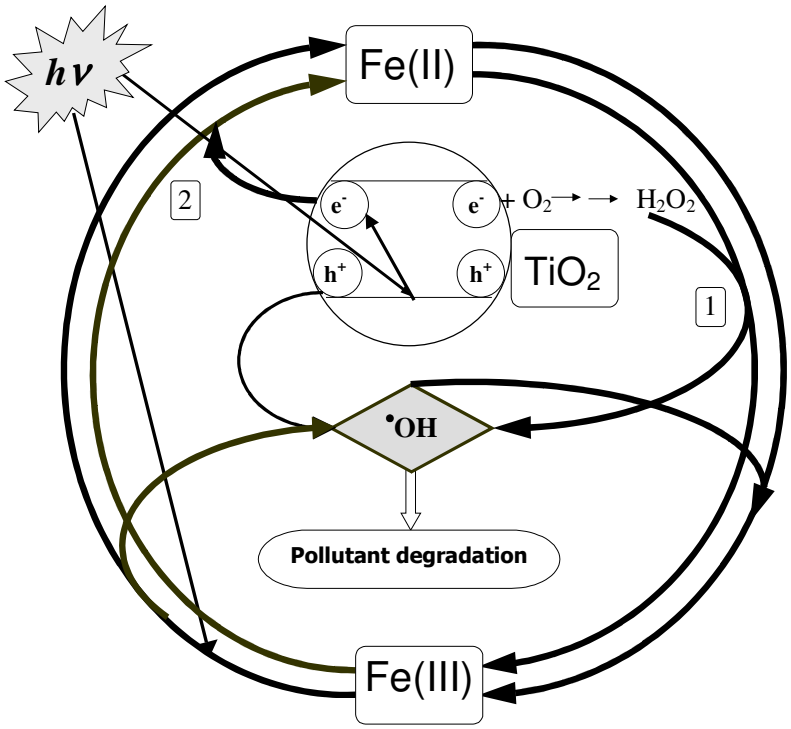

Figure 9.12:

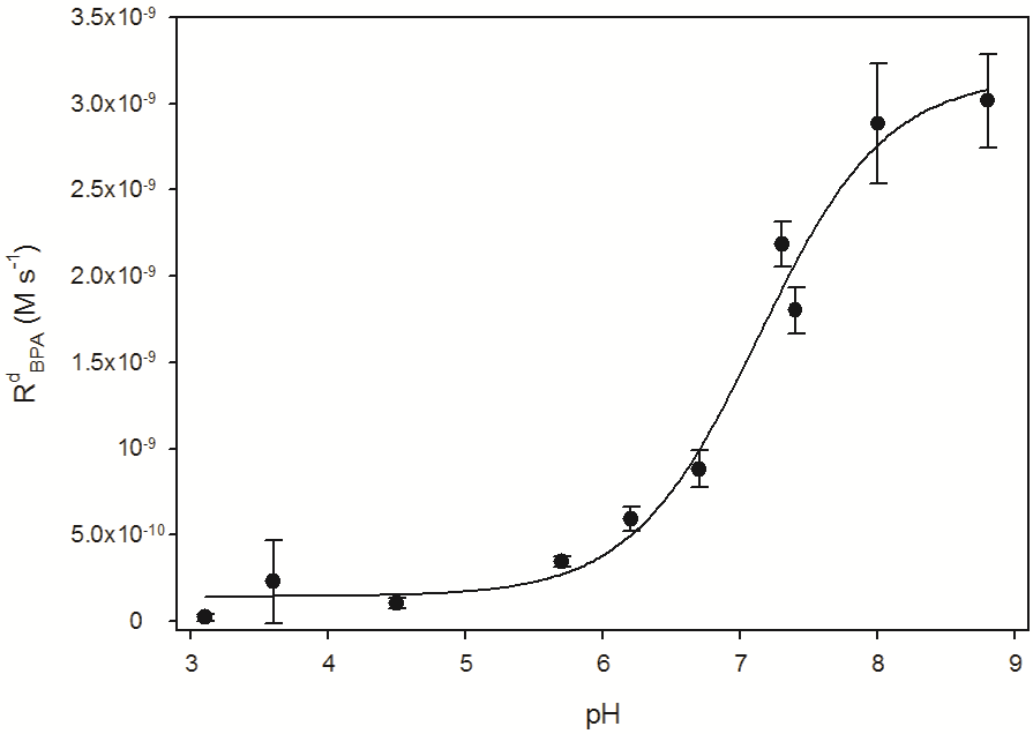
3.5x10-9
3.0x10-9
2.5x10-9
2.0x10-9
1.5x10-9
10-9
5.0x10-10
0
Rd BPA (M s-1)
3
4
5
6
7
8
9
pH

Figure 9.13:

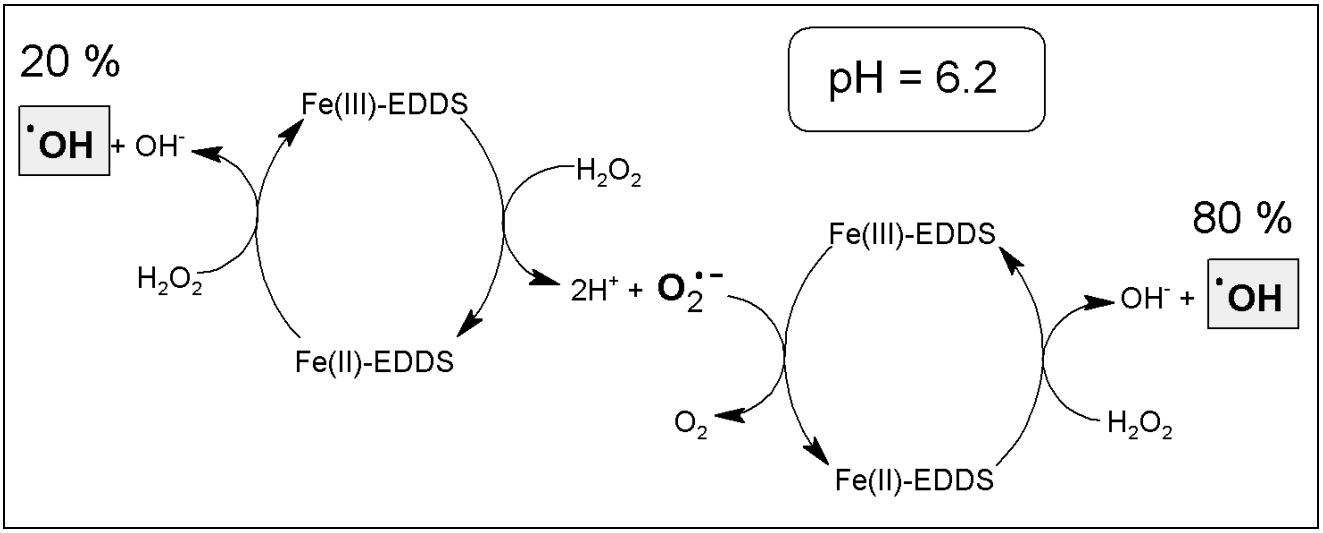
20 %
pH = 6.2
•OH + OH-
Fe(III)-EDDS
H2O2
H2O2
2H+ + O2•-
Fe(II)-EDDS
80 %
Fe(III)-EDDS
OH- + •OH
O2
H2O2
Fe(II)-EDDS

Figure 9.14:

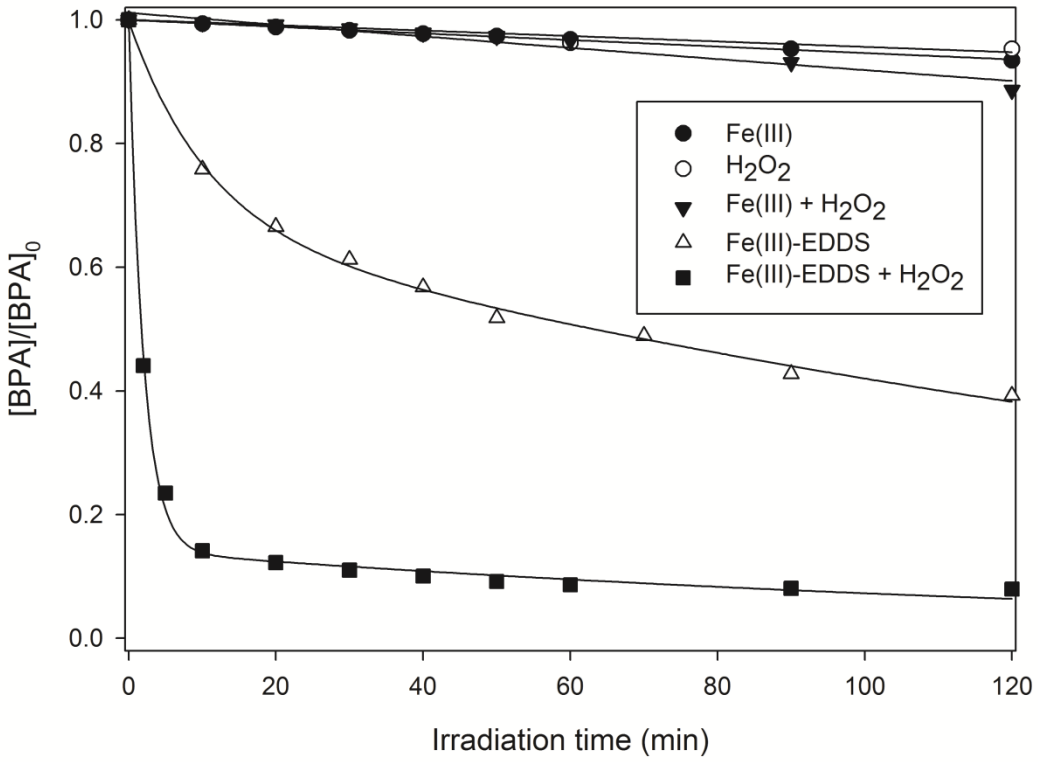
1.0
0.8
0.6
0.4
0.2
0.0
[BPA]/[BPA]0
0
20
40
60
80
100
120
Irradiation time (min)
Fe(III)
H2O2
Fe(III) + H2O2
Fe(III)-EDDS
Fe(III)-EDDS + H2O2

Photochemical reaction kinetics in surface waters

Davide Vione

Department of Chemistry, University of Torino, Via P. Giuria 5, 10125 Torino, Italy.
E-mail: *davide.vione@unito.it* Phone +39-011-6705296

Abstract

The photochemical transformation kinetics of xenobiotics in surface waters can be modelled, based on a number of photochemically significant parameters of the xenobiotic (absorption spectrum, direct photolysis quantum yield, second-order reaction rate constants with $^{\bullet}OH$, $CO_3^{-\bullet}$, $^1O_2$ and ^{3}CDOM*) and on some environmental variables (water depth, DOC, concentration values of nitrate, nitrite, carbonate and bicarbonate). The latter define the ability of the water body to attenuate sunlight in the water column and/or to photochemically produce reactive transient species, while the photochemical parameters of the xenobiotic measure its ability to react *via* the different photochemical reaction pathways. All of the above calculations can be carried out using the APEX software (Aqueous Photochemistry of Environmentally-occurring Xenobiotics). The software is also able to predict the seasonal trends of the phototransformation kinetics and to assess the uncertainty of the model output.

Table of contents

1. Introduction

As seen in previous chapters, xenobiotics can undergo transformation in surface waters because of direct photolysis and indirect photochemistry, where the latter indicates the reactions with transient species that are photochemically generated upon sunlight absorption by the so-called photosensitisers. All such processes depend on water chemistry and depth, which determine the production and consumption of transients as well as the penetration of sunlight in the water column.[1-5]

This chapter will explain how one can model photochemical reactions in surface waters. The model describes the transformation kinetics of a substrate, a generic xenobiotic X, as a function of water chemistry/depth and substrate reactivity, *via* the main photochemical reaction pathways (direct photolysis and reaction with $^{\bullet}OH$, $CO_3^{-\bullet}$, $^1O_2$ and $^3CDOM^*$). The model may use actual data of water absorption spectrum or, in their absence, it can approximate the spectrum from the dissolved organic carbon (DOC) values. The different aspects of the model will be described in detail. First of all the seasonal variation of the sunlight spectrum will be introduced. The effects of the solar zenith angle on the path length of sunlight in water will also be discussed, together with the modelling of the water absorption spectrum. Afterwards, a kinetic treatment of the main photochemical processes in surface waters will be provided, with particular attention to the modelling procedures. Finally, a software will be described (APEX: Aqueous Photochemistry of Environmentally-occurring Xenobiotics) that includes all the reported equations to model the photochemical fate of pollutants in surface-water environments.

2. A photochemical model for surface waters

2.1. Sunlight spectrum at mid latitude

The spectrum of sunlight at the ground undergoes important seasonal variations, not only in total irradiance but also as far as the ratio between its UVB, UVA and visible components is concerned. Indeed, the sunlight spectrum is highly affected by atmospheric absorption and, as a consequence, by the path length of sunlight through the atmosphere.[6-10] If z is the zenith angle of sunlight and h the height of the atmosphere, the path length l is given by $l = h\ (\cos z)^{-1}$ (see Figure 1). Therefore, l is longer if z is higher, which happens in temperate regions in winter when the sun is usually low on the horizon.

During winter, the high solar zenith angle causes the path length of sunlight through the atmosphere to be quite long. A first consequence is that the same sunlight energy is distributed over a surface that is proportional to $(\cos z)^{-2}$. Therefore, the irradiance of sunlight (energy per unit time and surface) is quite low in winter. A second consequence is that the elevated path length of sunlight in winter causes higher atmospheric absorption in the UV region and mostly notably in the UVB, which is absorbed more efficiently by the atmosphere. Therefore, during winter one has both

lower irradiance and a deficit of UVB radiation compared to the other spectral regions.[11] Figure 2 reports the mid-latitude spectra of sunlight in different months of the year. The solar spectrum may also change because of meteorological reasons (e.g. cloudy weather), but these issues cannot usually be taken into account in photochemical models.

2.2. Solar zenith angle and sunlight path length in water

When considering the path length travelled by sunlight in surface water, one should take into account both the solar zenith angle z and the refraction of sunlight at the air-water interface. Light reflection at the interface also takes place, but it is of lesser importance and can be neglected.[12] The geometry of irradiation is reported in Figure 3.

The solar zenith angle z (horizontal system of coordinates) is a function of sun declination δ (geocentric equatorial system of coordinates) and of the hour angle τ. The sun hour angle is defined as the difference between sun's right ascension (geocentric equatorial system of coordinates) and the right ascension of a star on the local meridian. At local noon (when sun is on the local meridian) it is $\tau_{sun} = 0$. Furthermore, every 1 h difference from the local noon gives $\tau \sim 15°$. This means that after 3 h from local noon, the sun has $\tau \sim 45°$. Assume φ as the latitude of the place and (δ,τ) for the sun as above. The following equation holds for the solar zenith angle:[13]

$$\cos z = \cos\delta \cos\tau \cos\varphi + \sin\delta \sin\varphi \qquad (1)$$

Water has refraction index $n \sim 1.34$ that undergoes relatively limited variation with wavelength. It is $\sin z = n \sin\theta$, from which the following relationship can be obtained between the path length l of sunlight and the water column depth d: $d = l \cos\theta = l \sqrt{1-(\sin\theta)^2}$.[12] Therefore, for depth d and solar zenith angle z the optical path length l of sunlight inside the water body would be expressed as follows:[13]

$$l = \frac{d}{\sqrt{1-(\sin\theta)^2}} = \frac{d}{\sqrt{1-(n^{-1}\sin z)^2}} \qquad (2)$$

This means that water depth could be corrected by a factor $\psi = \left(\sqrt{1-(n^{-1}\sin z)^2}\right)^{-1}$ ($\psi > 1$) that depends on latitude, hour and season. Under conditions relevant to a summer sunny day (15 July at 45°N latitude), at the solar noon one has $\psi = 1.05$. At ± 3 h from noon, which makes a reasonable daily average, it is $\psi = 1.17$ (calculations of z were carried out with the *Perseus* software [14]). Therefore, in a water body of depth d, on 15 July at 45°N latitude the path length of sunlight would be $l = 1.17\ d$.

Figure 4 reports the value of ψ at the solar noon, for different months of the year and for different latitudes.

2.3. Surface-water absorption spectrum

It has already been mentioned that photochemical processes are controlled by water chemistry as well as depth. Water absorption spectrum, which depends on the chemical composition, is another key factor that influences photochemical reactions. A key issue here is that, while reasonable values for single chemical parameters can be easily suggested/imagined (e.g. nitrate, organic carbon, bicarbonate), the same cannot be true for a whole absorption spectrum. Considerable help comes from the fact that chromophoric dissolved organic matter (CDOM) is the major radiation absorber among the surface-water components, thus the water absorption spectrum can be approximated very well with the absorption spectrum of CDOM.[15-17] Not surprisingly, it is possible to find a reasonable correlation between the absorption spectrum of surface waters and their content of dissolved organic matter, expressed as NPOC (Non-Purgeable Organic Carbon). The following equation holds for the water spectrum:[18]

$$A_1(\lambda) = (0.45 \pm 0.04) \cdot NPOC \cdot e^{-(0.015 \pm 0.002)\cdot\lambda} \qquad (3)$$

where NPOC has mg C L^{-1} (or ppm C) units, and $A_1(\lambda)$ is the absorbance referred to an optical path length of 1 cm (taken by using a 1 cm cuvette or, more commonly, a longer cuvette and then dividing the measured absorbance data for the cuvette path length; $A_1(\lambda)$ has cm^{-1} units). Equation (3) can be used as the basis for the light-absorption calculations, whenever the actual absorption spectrum of water is not available. Moreover, it allows the water spectrum to be derived from easy guesses of the possible content of dissolved organic matter. This issue is particularly helpful when one wants to get insight into the photochemical fate of a given pollutant under reasonable environmental conditions, but without reference to a definite water body.

Once the absorption spectrum of water ($A_1(\lambda)$) is known, it is possible to address the problem of photochemical reactions in a system where multiple components can simultaneously absorb radiation.

2.4. Modelling of direct photolysis processes in surface waters.

The process of direct photolysis of a xenobiotic X is triggered by the absorption of sunlight by X itself (in fact, compounds that do not absorb sunlight cannot undergo direct photolysis). The rate of photolysis is linked to the photon flux absorbed by X (P_a^X, which has units of Einstein L^{-1} s^{-1}, where 1 Einstein = 1 mole of photons). The value of P_a^X has to be assessed in the presence of other compounds that absorb a considerable fraction of sunlight.[19,20]

The calculation of the photon flux absorbed by X requires taking into account the mutual competition for sunlight irradiance between X itself and the other water components (mostly CDOM, which is the main sunlight absorber in the spectral region of interest, around 300-500 nm).

Moreover, because both the incident sunlight and the absorption spectra are not monochromatic, but they rather span over a wide range of wavelengths, one cannot directly reason on the absorbed photon fluxes. In contrast, one has to consider first the absorbed photon flux densities ($p_a(\lambda)$), with units of Einstein L^{-1} s^{-1} nm^{-1}. Generally speaking, an absorbed photon flux is the integral over wavelength of the absorbed photon flux density. Under the Lambert-Beer approximation, at a given wavelength λ, the ratio of the photon flux densities absorbed by two different species is equal to the ratio of the respective absorbances. The same is also true of the ratio of the photon flux density absorbed by a species to the total photon flux density absorbed by the solution ($p_a^{tot}(\lambda)$).[21] Accordingly, the photon flux absorbed by X over an optical path length l (where l is expressed in cm) can be obtained by the following equations (note that $A_1(\lambda)$ is the specific absorbance of the surface water sample over a 1 cm optical path length, $A_{tot}(\lambda)$ the total absorbance of the water column, $p°(\lambda)$ the spectrum of sunlight, $\varepsilon_X(\lambda)$ the molar absorption coefficient of X, in units of M^{-1} cm^{-1}, and $p_a^X(\lambda)$ its absorbed spectral photon flux density; it is also $p_a^X(\lambda) \ll p_a^{tot}(\lambda)$ and $A_X(\lambda) \ll A_{tot}(\lambda)$ in the very vast majority of environmental cases):[22,23]

$$A_{tot}(\lambda) = A_1(\lambda) \cdot l \quad (4)$$

$$A_X(\lambda) = \varepsilon_X(\lambda) \cdot l \cdot [X] \quad (5)$$

$$p_a^{tot}(\lambda) = p°(\lambda) \cdot (1 - 10^{-A_{tot}(\lambda)}) \quad (6)$$

$$p_a^X(\lambda) = p_a^{tot}(\lambda) \cdot A_X(\lambda) \cdot [A_{tot}(\lambda)]^{-1} \quad (7)$$

Note that the sunlight spectrum $p°(\lambda)$ in the calculations is referred to a UV irradiance of 22 W m^{-2} (see Figure 5).[24] The incident spectral photon flux density $p°(\lambda)$ is computed per unit surface and has units of Einstein s^{-1} nm^{-1} cm^{-2}. Once the $p_a^X(\lambda)$ values are known, the absorbed photon flux P_a^X can be determined as the integral over wavelength of the absorbed photon flux density:[21]

$$P_a^X = \int_\lambda p_a^X(\lambda)\, d\lambda \quad (8)$$

An important issue is that $p°(\lambda)$ is usually reported in units of Einstein cm^{-2} s^{-1} nm^{-1} (see Figure 5 above), thus the absorbed photon flux densities are expressed in the same units. To express the rate of photolysis ($Rate_X$, see later) in M s^{-1}, the absorbed photon flux P_a^X should be expressed in Einstein L^{-1} s^{-1}. However, integration of $p_a^X(\lambda)$ over wavelength gives units of Einstein cm^{-2} s^{-1} for P_a^X, which represent the moles of photons absorbed per unit surface area and unit time. Assuming a cylindrical volume of unit surface area (1 cm^2) and height l (expressed in cm), the rate of photolysis of X, expressed in M s^{-1} (moles per litre per second), can be obtained as follows:

$$Rate_X = 10^3\, \Phi_X\, P_a^X\, l^{-1} \quad (9)$$

where Φ_X is the multi-wavelength, average photolysis quantum yield of X in the relevant wavelength interval, and l is expressed in cm (also note that 1 L = 10^3 cm^3). This approximated expression of $Rate_X$ can be adopted if Φ_X does not vary with wavelength, or if the detailed wavelength trend of Φ_X is not known and only a single average value is available. Such an approximation holds if Φ_X is referred to the same wavelength interval where the spectra of X and sunlight overlap. Once $Rate_X$ is known, the pseudo-first order degradation rate constant of X (k_X) can be obtained as the ratio between $Rate_X$ and the concentration of X. From the pseudo-first order rate constant one can also obtain the lifetime t_X:[21]

$$k_X = Rate_X\,[X]^{-1} \tag{10}$$

$$t_X = ln\ 2\ (k_X)^{-1} \tag{11}$$

The time t_X is expressed in seconds of continuous irradiation under sunlight, at 22 W m^{-2} UV irradiance. It has been shown that the sunlight energy reaching the ground in a summer sunny day (SSD) such as 15 July at 45°N latitude corresponds to 10 h = $3.6\cdot10^4$ s continuous irradiation at 22 W m^{-2} UV irradiance.[25] Accordingly, the half-life time expressed in SSD units would be given by:

$$\begin{aligned}
&\tau^{SSD}_X = (3.6\cdot10^4)^{-1}\ ln\ 2\ (k_X)^{-1} = 1.9\cdot10^{-5}\,[X]\ l\ 10^{-3}\ (\Phi_X\ P_a{}^X)^{-1} = \\
&= 1.9\cdot10^{-5}\,[X]\ l\ 10^{-3}\ (\Phi_X \int_\lambda p_a^X(\lambda)\,d\lambda)^{-1} = \\
&= 1.9\cdot10^{-5}\,[X]\ l\ 10^{-3}\ (\Phi_X \int_\lambda p_a^{tot}(\lambda)\cdot A_X(\lambda)\cdot[A_{tot}(\lambda)]^{-1}\,d\lambda)^{-1} = \\
&= \frac{1.9\times10^{-8}\ l}{\Phi_X \int_\lambda p°(\lambda)\,(1-10^{-A_l(\lambda)\,l})\,\frac{\varepsilon_X(\lambda)}{A_l(\lambda)}\,d\lambda}
\end{aligned} \tag{12}$$

Note that $1.9\cdot10^{-8} = 10^{-3}\ (\ln 2)\ (3.6\cdot10^4)^{-1}$.

If the photolysis quantum yield of X depends on the wavelength ($\Phi_X(\lambda)$), a different approach is to be followed. Instead of equations (8-12), one should apply equations (13,14):[24]

$$Rate_X = 10^3\,l^{-1}\int_\lambda p_a^X(\lambda)\,\Phi_X(\lambda)\,d\lambda \tag{13}$$

$$\tau_X^{SSD} = \frac{1.9\times10^{-8}\ l}{\int_\lambda p°(\lambda)\,(1-10^{-A_l(\lambda)\,l})\,\Phi_X(\lambda)\,\frac{\varepsilon_X(\lambda)}{A_l(\lambda)}\,d\lambda} \tag{14}$$

Note that $\Phi_X(\lambda)$ depends on wavelength and it is to be included in the integral.

2.5. Modelling the formation and reactivity of •OH in surface waters.

The hydroxyl radical (•OH) is a transient that is produced by several photosensitisers and it is consumed by many water components. Because of the fast reactions it undergoes (its lifetime is in the μs range), •OH cannot accumulate in solution and reaches a steady-state concentration that is extremely low when compared to other water components (usually below 10^{-15} M).[26]

In natural surface waters under sunlight illumination, the main •OH sources are (in order of average importance) CDOM, nitrite and nitrate.[25,27] At the present state of knowledge it is reasonable to hypothesise that these three sources generate •OH independently, with no mutual interactions. Therefore, the total formation rate of •OH ($R_{\bullet OH}^{tot}$) is the sum of the contributions of the three species:

$$R_{\bullet OH}^{tot} = R_{\bullet OH}^{CDOM} + R_{\bullet OH}^{NO_2^-} + R_{\bullet OH}^{NO_3^-} \quad (15)$$

Various studies have yielded useful correlation between the formation rate of •OH by the photoactive species and the respective absorbed photon fluxes of sunlight. In particular, it has been found that:[18,28,29]

$$R_{\bullet OH}^{CDOM} = (3.0 \pm 0.4) \cdot 10^{-5} \cdot P_a^{CDOM} \quad (16)$$

$$R_{\bullet OH}^{NO_2^-} = \int_{\lambda} \Phi_{\bullet OH}^{NO_2^-}(\lambda) \; p_a^{NO_2^-}(\lambda) \, d\lambda \quad (17)$$

$$R_{\bullet OH}^{NO_3^-} = (4.3 \pm 0.2) \cdot 10^{-2} \cdot \frac{[IC] + 0.0075}{2.25\,[IC] + 0.0075} \cdot P_a^{NO_3^-} \quad (18)$$

where [IC] = [H_2CO_3] + [HCO_3^-] + [CO_3^{2-}] is the total amount of inorganic carbon. Note that the photolysis quantum yield of •OH by nitrite photolysis, $\Phi_{\bullet OH}^{NO_2^-}(\lambda)$, depends on wavelength. The wavelength-dependent data of $\Phi_{\bullet OH}^{NO_2^-}(\lambda)$ are reported in Table 1.[29]

The calculation of the photon fluxes absorbed by CDOM, nitrate and nitrite requires to take into account the mutual competition for sunlight irradiance, also considering that CDOM is the main absorber in the UV region where also nitrite and nitrate absorb radiation.

Considering that the ratio of the photon flux density absorbed by a species *i* at the wavelength λ ($p_a^i(\lambda)$, where *i* = CDOM, nitrate or nitrite) to the total photon flux density absorbed by the solution ($p_a^{tot}(\lambda)$) is equal to the ratio of the respective absorbances ($A_i(\lambda)$ and $A_{tot}(\lambda)$, respectively),[21] the following equations hold for the different •OH sources:

$$A_{tot}(\lambda) = A_1(\lambda) \cdot l \quad (19)$$

$$A_{NO3-}(\lambda) = \varepsilon_{NO3-}(\lambda) \cdot l \cdot [NO_3^-] \quad (20)$$

$$A_{NO2-}(\lambda) = \varepsilon_{NO2-}(\lambda) \cdot l \cdot [NO_2^-] \quad (21)$$

$$A_{CDOM}(\lambda) = A_{tot}(\lambda) - A_{NO3-}(\lambda) - A_{NO2-}(\lambda) \approx A_{tot}(\lambda) \quad (22)$$

$$p_a^{tot}(\lambda) = p°(\lambda) \cdot (1 - 10^{-A_{tot}(\lambda)}) \quad (23)$$

$$p_a^{CDOM}(\lambda) = p_a^{tot}(\lambda) \cdot A_{CDOM}(\lambda) \cdot [A_{tot}(\lambda)]^{-1} \approx p_a^{tot}(\lambda) \quad (24)$$

$$p_a^{NO2-}(\lambda) = p_a^{tot}(\lambda) \cdot A_{NO2-}(\lambda) \cdot [A_{tot}(\lambda)]^{-1} \quad (25)$$

$$p_a^{NO3-}(\lambda) = p_a^{tot}(\lambda) \cdot A_{NO3-}(\lambda) \cdot [A_{tot}(\lambda)]^{-1} \quad (26)$$

The path length l is related to the water depth d, but it is not equal to d. It also depends on solar zenith angle and on radiation refraction by water, as already shown in section 2.2. The sunlight spectrum $p°(\lambda)$ is referred to a unit surface area (units of Einstein s^{-1} nm^{-1} cm^{-2}, see Figure 5), and the values of $p_a^i(\lambda)$ are expressed in the same units. To avoid problems in rate calculation, the absorbed photon fluxes P_a^i (in Einstein L^{-1} s^{-1} units) should be obtained as follows (note that 1 L = 10^3 cm^3):[30]

$$P_a^{CDOM} = 10^3 \, l^{-1} \int_\lambda p_a^{CDOM}(\lambda) \, d\lambda \quad (27)$$

$$P_a^{NO2-} = 10^3 \, l^{-1} \int_\lambda p_a^{NO2-}(\lambda) \, d\lambda \quad (28)$$

$$P_a^{NO3-} = 10^3 \, l^{-1} \int_\lambda p_a^{NO3-}(\lambda) \, d\lambda \quad (29)$$

Accordingly, having as input data l, $A_1(\lambda)$, $[NO_3^-]$, $[NO_2^-]$ and $p°(\lambda)$ (the latter referred to a 22 W m^{-2} sunlight UV irradiance, see Figure 5), it is possible to model the expected $R_{\bullet OH}^{tot}$ of the sample. The photogenerated $^\bullet$OH radicals could react either with X or with the natural scavengers present in surface water (mainly organic matter, bicarbonate, carbonate and nitrite). The natural scavengers have the following $^\bullet$OH scavenging rate constant:[24]

$$\Sigma_i \, k_{Si} \, [S_i] = 2\times10^4 \, \text{NPOC} + 8.5\times10^6 \, [HCO_3^-] + 3.9\times10^8 \, [CO_3^{2-}] + 1.0\times10^{10} \, [NO_2^-] \quad (30)$$

where the units of $\Sigma_i \, k_{Si} \, [S_i]$ are $[s^{-1}]$, NPOC is expressed in mg C L^{-1}, and the other concentration values are in molarity. By applying the steady-state approximation to [$^\bullet$OH], the reaction rate between X and $^\bullet$OH can be expressed by competition for the hydroxyl radical between X and the other scavengers, as follows:[24]

$$R_X^{\bullet OH} = R_{\bullet OH}^{tot} \frac{k_{X,\bullet OH} \, [X]}{\sum_i k_{Si} \, [S_i]} \quad (31)$$

where $k_{X,\bullet OH}$ is the second-order reaction rate constant between X and $^\bullet$OH and [X] is a molar concentration. Note that, in the vast majority of the environmental cases, one would have $k_{X,\bullet OH}$ [X] « $\Sigma_i \, k_{Si} \, [S_i]$. The pseudo-first order degradation rate constant of X is $k_X^{\bullet OH} = R_X^{\bullet OH} \, [X]^{-1}$, and the half-life time of X for reaction with $^\bullet$OH is $t_X^{\bullet OH} = ln \, 2 \, (k_X^{\bullet OH})^{-1}$. Note that $k_X^{\bullet OH}$ is a pseudo-first order rate constant, while $k_{X,\bullet OH}$ is a second-order one. The time $t_X^{\bullet OH}$ is expressed in seconds of

continuous irradiation under sunlight, at 22 W m^{-2} UV irradiance. As already done in the case of the direct photolysis, it is possible to express the half-life time in SSD (summer sunny day) units, as follows:

$$\tau_{X,^{\bullet}OH}^{SSD} = \frac{\ln 2 \sum_i k_{Si}\,[S_i]}{3.6 \cdot 10^4\; R_{^{\bullet}OH}^{tot}\; k_{X,^{\bullet}OH}} = 1.9 \cdot 10^{-5}\; \frac{\sum_i k_{Si}\,[S_i]}{R_{^{\bullet}OH}^{tot}\; k_{X,^{\bullet}OH}} \qquad (32)$$

2.6. Modelling the formation and reactivity of ^{3}CDOM in surface waters.*

The formation of the excited triplet states of CDOM (^{3}CDOM*) in surface waters is a direct consequence of radiation absorption by CDOM.[31-34] In aerated solution, ^{3}CDOM* could undergo thermal deactivation or reaction with O_2, and a pseudo-first order quenching rate constant $k_{^3CDOM^*}$ = 5×10^5 s^{-1} has been observed.[35] The quenching of ^{3}CDOM* would be in competition with the reaction between ^{3}CDOM* and X:

$$\text{CDOM} + h\nu \rightarrow {}^3\text{CDOM}^* \qquad (33)$$

$$^3\text{CDOM}^* \text{—}(O_2)\rightarrow \text{Deactivation and } {}^1O_2 \text{ production} \qquad (34)$$

$$^3\text{CDOM}^* + X \rightarrow \text{Products} \qquad (35)$$

In the Rhône delta waters it has been found that the formation rate of ^{3}CDOM* is $R_{^3CDOM^*}$ = 1.28×10^{-3} P_a^{CDOM}.[36] Considering the competition between the reaction (35) with X and other processes (reaction 34), and applying the steady-state approximation to [^{3}CDOM*], the following expression for the degradation rate of X by ^{3}CDOM* is obtained:

$$R_X^{^3CDOM^*} = R_{^3CDOM^*} \cdot \frac{k_{X,^3CDOM^*} \cdot [X]}{k_{^3CDOM^*}} \qquad (36)$$

where $k_{X,^3CDOM^*}$ is the second-order reaction rate constant between X and ^{3}CDOM*. In a pseudo-first order approximation, the first-order rate constant is $k_X^{^3CDOM^*} = R_X^{^3CDOM^*}\,[X]^{-1}$ and the half-life time is $t_X^{^3CDOM^*} = ln\ 2\ (k_X^{^3CDOM^*})^{-1}$ (note again that $k_X^{^3CDOM^*}$ is a pseudo-first order reaction rate constant, while $k_{X,^3CDOM^*}$ is a second-order one). Considering the usual conversion (≈ 10 h) between a constant 22 W m^{-2} sunlight UV irradiance and a SSD unit, one gets the following expression for the half-life time of X upon reaction with ^{3}CDOM* (remembering that $P_a^{CDOM} = 10^3\ l^{-1} \int_\lambda p_a^{CDOM}(\lambda)\, d\lambda$):

$$\tau^{SSD}_{X,^3CDOM*} = \frac{7.52 \cdot l}{k_{X,^3CDOM*} \cdot \int_{\lambda} p_a^{CDOM}(\lambda)\, d\lambda} \qquad (37)$$

Note that 7.52 = (ln 2) $k_{^3CDOM*}$ $(1.28{\cdot}10^{-3} \cdot 3.60{\cdot}10^{4} \cdot 10^{3})^{-1}$.

2.7. Modelling the formation and reactivity of $^1O_2$ in surface waters.

The formation of singlet oxygen in surface waters arises from the energy transfer between ground-state molecular oxygen and the excited triplet states of CDOM (^{3}CDOM*). Accordingly, irradiated CDOM is practically the only source of $^1O_2$ in surface waters.[37-39] The main $^1O_2$ sink is the energy loss to ground-state O_2 by collision with the water molecules, with a pseudo-first order rate constant $k_{^1O_2}$ = $2.5{\cdot}10^5$ s^{-1}.[40] The dissolved species, including the dissolved organic matter that is certainly able to react with $^1O_2$, would play a minor to negligible role as sinks of $^1O_2$ in the aquatic systems.[36] The main processes involving $^1O_2$ and X in surface waters would be the following:

$$^3\text{CDOM*} + O_2 \rightarrow \text{CDOM} + {}^1O_2 \qquad (38)$$

$$^1O_2 + H_2O \rightarrow O_2 + H_2O + \text{heat} \qquad (39)$$

$$^1O_2 + X \rightarrow \text{Products} \qquad (40)$$

In the Rhône delta waters it has been found that the formation rate of $^1O_2$ by CDOM is $R^{CDOM}_{^1O_2}$ = $1.25{\cdot}10^{-3}$ P_a^{CDOM}.[36] Considering the competition between the deactivation of $^1O_2$ by collision with the solvent (reaction 39) and the reaction (40) with X, and applying the usual steady-state approximation to [$^1O_2$], one gets the following expression for the degradation rate of X by $^1O_2$:

$$R_X^{^1O_2} = R^{CDOM}_{^1O_2} \cdot \frac{k_{X,^1O_2} \cdot [X]}{k_{^1O_2}} \qquad (41)$$

In a pseudo-first order approximation, the pseudo-first order rate constant is $k_X^{^1O_2}$ = $R_X^{^1O_2}$ $[X]^{-1}$ and the half-life time is $t_X^{^1O_2}$ = *ln 2* $(k_X^{^1O_2})^{-1}$. Considering the usual conversion (≈ 10 h) between a constant 22 W m^{-2} sunlight UV irradiance and a SSD unit, the following expression is obtained for the half-life time of X upon reaction with $^1O_2$ (remembering that $R^{CDOM}_{^1O_2}$ = $1.25{\cdot}10^{-3}$ P_a^{CDOM} and that $P_a^{CDOM} = 10^3\, l^{-1} \int_{\lambda} p_a^{CDOM}(\lambda)\, d\lambda$):

$$\tau^{SSD}_{X,^1O_2} = \frac{4.81}{R^{CDOM}_{^1O_2}\, k_{X,^1O_2}} = \frac{3.85 \cdot l}{k_{X,^1O_2} \cdot \int_{\lambda} p_a^{CDOM}(\lambda)\, d\lambda} \qquad (n.42)$$

Note that 3.85 = (ln 2) $k_{^1O_2}$ $(1.25\cdot10^{-3} \cdot 3.60\cdot10^4 \cdot 10^3)^{-1}$.

2.8. Modelling the formation and reactivity of $CO_3^{-\bullet}$ in surface waters.

The radical $CO_3^{-\bullet}$ can be produced upon oxidation of carbonate and bicarbonate by $^\bullet$OH, upon carbonate oxidation by ^{3}CDOM*, and possibly also from irradiated Fe(III) oxide colloids and carbonate.[41-43] However, as far as the latter process is concerned, there is still insufficient knowledge about the Fe speciation in surface waters to enable a proper modelling. The main sink of the carbonate radical in surface waters is the reaction with DOM, which is considerably slower than that between DOM and $^\bullet$OH.[41,44]

$^\bullet OH + CO_3^{2-} \rightarrow OH^- + CO_3^{-\bullet}$	$[k_{43} = 3.9\times10^8\ M^{-1}\ s^{-1}]$	(43)
$^\bullet OH + HCO_3^- \rightarrow H_2O + CO_3^{-\bullet}$	$[k_{44} = 8.5\times10^6\ M^{-1}\ s^{-1}]$	(44)
$^3CDOM^* + CO_3^{2-} \rightarrow CDOM^{-\bullet} + CO_3^{-\bullet}$	$[k_{45} \approx 1\times10^5\ M^{-1}\ s^{-1}]$	(45)
$DOM + CO_3^{-\bullet} \rightarrow DOM^{+\bullet} + CO_3^{2-}$	$[k_{46} \approx 10^2\ (mg\ C)^{-1}\ s^{-1}]$	(46)

The formation rate of $CO_3^{-\bullet}$ in reactions (43,44) is given by the formation rate of $^\bullet$OH times the fraction of $^\bullet$OH that reacts with carbonate and bicarbonate, as follows:[42]

$$R_{CO_3^{-\bullet}}^{^\bullet OH} = R_{^\bullet OH}^{tot} \cdot \frac{8.5\cdot10^6\cdot[HCO_3^-] + 3.9\cdot10^8\cdot[CO_3^{2-}]}{2.0\cdot10^4\cdot NPOC + 1.0\cdot10^{10}\cdot[NO_2^-] + 8.5\cdot10^6\cdot[HCO_3^-] + 3.9\cdot10^8\cdot[CO_3^{2-}]} \quad (47)$$

The formation of $CO_3^{-\bullet}$ in reaction (45) is given by:

$$R_{CO_3^{-\bullet}}^{CDOM} = 6.5\cdot10^{-3}\cdot[CO_3^{2-}]\cdot P_a^{CDOM} \quad (48)$$

The total formation rate of $CO_3^{-\bullet}$ is $R_{CO_3^{-\bullet}}^{tot} = R_{CO_3^{-\bullet}}^{^\bullet OH} + R_{CO_3^{-\bullet}}^{CDOM}$. The transformation rate of X by $CO_3^{-\bullet}$ is given by the fraction of $CO_3^{-\bullet}$ that reacts with X, in competition with reaction (46) between $CO_3^{-\bullet}$ and DOM (as usual, the steady-state approximation is applied to $[CO_3^{-\bullet}]$):

$$R_X^{CO_3^{-\bullet}} = \frac{R_{CO_3^{-\bullet}}^{tot}\cdot k_{X,CO_3^{-\bullet}}\cdot[X]}{k_{46}\cdot NPOC} \quad (49)$$

where $k_{X,CO_3^{-\bullet}}$ is the second-order reaction rate constant between X and $CO_3^{-\bullet}$. In a pseudo-first order approximation, the first-order rate constant is $k_X^{CO_3^{-\bullet}} = R_X^{CO_3^{-\bullet}}\ [X]^{-1}$ and the half-life time is $t_X^{CO_3^{-\bullet}} = ln\ 2\ (k_X^{CO_3^{-\bullet}})^{-1}$. Considering the usual conversion (≈ 10 h) between a constant 22 W m^{-2} sunlight UV irradiance and a SSD unit, the following expression is obtained for the half-life time of X upon reaction with $CO_3^{-\bullet}$:

$$\tau^{SSD}_{X,CO_3^{-\bullet}} = 1.9 \cdot 10^{-5} \cdot \left(\frac{k_{46} \cdot NPOC}{R^{tot}_{CO_3^{-\bullet}} \cdot k_{X,CO_3^{-\bullet}}} \right) \quad (50)$$

Note that $1.9 \cdot 10^{-5} = ln\ 2\ (3.6 \cdot 10^4)^{-1}$.

2.9. Formation of intermediates from the xenobiotic X

In the photochemical process *ph* (direct photolysis or reaction with $^{\bullet}OH$, $^1O_2$, $CO_3^{-\bullet}$, $^3CDOM^*$), the compound X could produce the intermediate I with yield $y^{ph}_{X \to I}$, experimentally determined as the ratio between the initial formation rate of I and the initial transformation rate of X. The pseudo-first order rate constant of I formation in the process *ph* is $(k^{ph}_{X \to I})' = y^{ph}_{X \to I}\, k^{ph}_X$, where k^{ph}_X is the (model-derived) first-order transformation rate constant of X in the process *ph*. The production of I from X often takes place *via* more than one process. Therefore, the overall rate constant of I formation is:[45]

$$(k_{X \to I})' = \sum_{ph} (k^{ph}_{X \to I})' = \sum_{ph} (y^{ph}_{X \to I}\, k^{ph}_X) \quad (n.51)$$

One can also obtain the overall yield of I formation from X ($y_{X \to I}$), as:

$$y_i = (k_{X \to I})' (k_X)^{-1} = \frac{\sum_{ph} (y^{ph}_{X \to I}\, k^{ph}_X)}{\sum_{ph} k^{ph}_X} \quad (n.52)$$

2.10 The meaning of water depth in the model

An important issue is that the model was not designed to make depth profiles of the transformation kinetics of X or of the formation of intermediates. Therefore, when setting depth (*d*, which defines the sunlight path length *l*) as a variable, one actually compares different water bodies, each with its own depth value. This means that for, *e.g.*, 1 m depth the model returns the average k_X or τ_X in the first 1 m of the water column. It should be underlined that they are the average rate constant and half-life time in the first 1 m of the column and <u>not</u> the point values at 1 m. The transformation kinetics of dissolved species is obtained in the hypothesis of thorough mixing in the water column, because the model applies to well-mixed shallow waters or to the top mixing layer of stratified water bodies. A key issue is that, if one wants to determine the photochemical reaction kinetics in the first 1 m of the water column, the needed value is the average k_X or τ_X (as determined by the model), and not the point value at 1 m (which is only referred to that depth and not to the whole water column).

2.11. Main approximations of the model

Surface waters represent an extremely complex and varied series of environments and the present attempt to describe their photochemical behaviour had to include a number of assumptions and approximations. The main ones are listed below.

- The model considers well-mixed water. Therefore, it applies to shallow water environments and to the well-mixed epilimnion of stratified ones.
- The Lambert-Beer approximation does not take radiation scattering into account. Therefore, the model applies to clear waters rather than to highly turbid ones.
- The data on which the modelling of surface-water absorption spectrum is based (equation 3) were obtained for lake water in NW Italy.[18] There is evidence that applicability is much wider, but one will obtain more accurate results for a particular environment if the actual water spectrum is available.
- The quantum yields for the formation of $^{\bullet}OH$ by CDOM are average values for NW Italian lakes.[18] Those of $^{1}O_2$ and $^{3}CDOM^*$ have been obtained in the Rhône delta (S. France),[36] that of $CO_3^{-\bullet}$ formation from $^{3}CDOM^*$ is from Lake Greifensee (Switzerland).[41,42] In different environments, different values may be found. The best scenario is obviously the availability of data measured in the water environment that one wants to study.
- The scavenging rate constants of $^{\bullet}OH$ and $CO_3^{-\bullet}$ by DOM are average values from the literature.[18,25,41,42] The same consideration as above also applies here.

Despite its approximations, the model could be quite useful for laboratory scientists who measure the photochemical degradation of pollutants, and who would like to have an assessment of the environmental significance of their findings. The possibility to model the water absorption spectrum instead of having to use experimentally measured data could be particularly useful, if one wants to see the significance of different photochemical pathways under variable conditions.

In contrast, if one wants to describe a particular environment, the best way to increase the accuracy of the results is to use measured values from that environment. Such values are water absorption spectrum, formation quantum yields of $^{\bullet}OH$, $^{1}O_2$, $CO_3^{-\bullet}$ and $^{3}CDOM^*$ by CDOM, and scavenging rate constants of $^{\bullet}OH$ and $CO_3^{-\bullet}$ by DOM.

2.12. Seasonal corrections at mid latitude

The standard time unit used in the model output is the SSD, summer sunny day, corresponding to fair-weather 15 July at 45°N latitude.[25] Therefore, half life times are expressed in SSD units and first-order rate constants in SSD^{-1}. As a consequence, the results apply to mid-latitude summertime conditions.

If an (approximated) insight is needed into the behaviour that a compound may have at mid latitude in different seasons, it is possible to take into account the monthly variations of sunlight irradiance. Assume $p°(\lambda)$ as the incident spectral photon flux density of sunlight at mid latitude in a given month of the year (15th day of that month).[11] The incident photon flux P_o can be calculated as the integral over wavelength of $p°(\lambda)$ for different spectral ranges:[21] 290-320 nm (UVB), 320-400 nm (UVA) and 300-450 nm, where most absorption of sunlight by CDOM takes place. The July results are equivalent to a SSD and the results for the other months can be normalised to those of July. Therefore, one can obtain a SSD-normalised photon flux $\wp°$ for the relevant spectral range, which represents the numerical value by which the July rate constants should be multiplied and the July half-life times divided to obtain representative photoreactivity values in a given month. The equations used to calculate $\wp°$ are reported below.

$$[P°]_{month} = \int_{\lambda} [p°(\lambda)]_{month}\, d\lambda \tag{52}$$

$$[\wp°]_{month} = \frac{[P°]_{month}}{[P°]_{July}} \tag{53}$$

The following Table 2 reports the values of $\wp°$ for the different months of the year at mid latitude, for three spectral ranges. Note that $\wp°$ = 1 at 15 July (where 1 day = 1 SSD). The $\wp°$ values reported in Table 2 are referred to different spectral ranges that affect different photosensitisers. In fact, the UVB values can be applied to nitrate photolysis, the UVA ones to nitrite and those at 300-450 nm to CDOM. In the case of reactions induced by $^1O_2$ and ^{3}CDOM* that are produced by CDOM, rate constants should be multiplied by the $\wp°$ values at 300-450 nm (and half-life times divided by the same values). In the case of $^{\bullet}$OH that is produced by nitrate, nitrite and CDOM, the three different contributions should be corrected by the UVB, UVA and 300-450 nm values, respectively. The radical $CO_3^{-\bullet}$ is mostly produced by oxidation of carbonate and bicarbonate by $^{\bullet}$OH, thus the corrections for $CO_3^{-\bullet}$ are the same as for $^{\bullet}$OH. Finally, in the case of direct photolysis the correction would depend on the spectral range where the relevant compound mostly absorbs sunlight (UVB, UVA or extended into the visible). Depending on compound absorption, the most relevant $\wp°$ value should be chosen.

2.13. Model validation

The model described so far has been applied to the photochemical fate of a variety of xenobiotic compounds in surface waters. It was validated by comparison between its predictions and field data of photochemical transformation, when available. Table 3 reports the comparisons that have been carried out so far, which show a good agreement between model predictions and the available field data.

3. The APEX software (Aqueous Photochemistry of Environmentally-occurring Xenobiotics)

APEX is a software tool to model photochemical processes in surface waters. It is based on Octave, an Open Source and freely available mathematics software (http://www.gnu.org/software/octave).[54] APEX is freely available as Electronic Supplementary Information (ESI) of Ref. 24. For using APEX, Octave should be downloaded and installed. It has been developed for Linux, but Windows versions of Octave are also available for free download. After download and installation, one has to launch Octave and run APEX within Octave.

APEX is based on a series of functions: plotgraph.m (data input and 3D graph plot), savetable.m (data input and generation of a table with numerical output data), apex.m (model calculations), Integral.m (numerical integration). In addition, apexvec.m is used to produce the output format by both Plotgraph and Savetable. Finally, part of the input data are contained in a .csv file [24]. Figure 6 gives insight into the flow of information within APEX.

Two additional files (Excel sheets) are provided in the APEX package, namely *Apex_Season.xls* (which computes seasonal data based on the approach reported in section 2.12) and *Apex_Errors.xls* (which computes the model uncertainty). Among the input data, those concerning the photochemical reactivity of the target compound are derived from experiments and they are affected by error. Further uncertainty is related to the experimentally-derived values of quantum yields of photochemical reactions used in model calculations (referred to CDOM, nitrate and nitrite), and to the values of scavenging or deactivation rate constants for $^{\bullet}OH$, $CO_3^{-\bullet}$, $^1O_2$ and ^{3}CDOM*. All the relevant error sources combine to produce an overall uncertainty that can be assessed at the σ level by use of *Apex_Errors.xls*.

3.1. Input data for APEX

Key input data for the software are those describing the photochemical reactivity of the xenobiotic compound of interest: absorption spectrum, photolysis quantum yield and second-order reaction rate constants with $^{\bullet}OH$, $CO_3^{-\bullet}$, $^1O_2$ and ^{3}CDOM*. In some cases the needed data are available from the literature.[32,41,55] To fill up possible gaps, an experimental protocol has been developed for the

experimental determination of all needed parameters.[56] Such a protocol has been applied for instance to all the compounds listed in Table 3 and it is described in the relevant references. It is possible to adapt the protocol to compounds undergoing acid-base equilibria in the environmental pH range, as it is the case for instance of the sunlight filter benzophenone-4 (pK_a ~ 7).[57]

Some input data depend on the wavelength, such as the absorption spectrum (molar absorption coefficients) of the target compound. These data are included in tabular form in an input .csv file, which also contains the molar absorption coefficients of nitrate and nitrite, the wavelength trend of the quantum yield of $^{\bullet}OH$ generation by nitrite, and a standard spectral photon flux density of sunlight (the same of the model, see Figure 5).

In the .csv input file it is also possible to include, if available, the photolysis quantum yield of the target compound (with the possibility to report wavelength-dependent values if applicable or known) and the absorption spectrum of water, expressed as the absorbance over an optical path length of 1 cm. Considering that photochemical reactions are faster near the water surface,[58] the absorption spectrum of a water sample taken from the surface layer should be inserted here, if available. If such a spectrum is not available, the software will model it on the basis of the content of dissolved organic carbon (DOC, also named NPOC, non-purgeable organic carbon). Water spectrum modelling uses equation (3), which predicts an exponential decrease of the absorbance with increasing wavelength, as usually observed.[59] To tell the software that the absorption spectrum is to be modelled instead of taken from the input file, one should insert "-1" overall in the file column related to the water absorbance.

As far as the direct photolysis quantum yield of the xenobiotic compound is concerned, there is the possibility to insert wavelength-dependent values, a constant value throughout, or to define the quantum yield as a variable if its value is not known. Definition of the quantum yield as variable should be made within the *plotgraph* and *savetable* functions. To enable this, one should insert "-1" in the whole quantum yield column of the input .csv file, otherwise the software will read with priority the data contained in that column.

3.2. Plotgraph function

This function is provided as a file (*plotgraph.m*) that can be opened and modified with standard text/notepad applications. Use of word processors is not recommended because they could add text strings when saving the files, which could cause errors when running APEX.

The *plotgraph* function draws a 3D plot, and the X and Y variables have to be chosen among parameters of water chemistry and photochemical reactivity of the target compound. The relevant water parameters are the path length of sunlight (depth dependent, see Figure 4), the molar concentration values of nitrate, nitrite, carbonate and bicarbonate, and the DOC or NPOC value (units of mg C L^{-1}). The reactivity parameters are the photolysis quantum yield (if not already specified in the input .csv file), the second-order reaction rate constants between the target compound and $^{\bullet}OH$, $CO_3^{-\bullet}$, $^1O_2$ and ^{3}CDOM*, and (if available) the formation yields of an

intermediate *via* the relevant photochemical pathways. Note that the reactivity data of the parent compound are needed to calculate intermediate formation kinetics, while the yields of the intermediate are not required to compute the transformation kinetics of the parent compound.

For each of the parameters related to water chemistry, compound photoreactivity or intermediate formation, one should either insert a known (or hypothesised) numerical value, or define the relevant quantity as X or Y variable (the label of the X variable is "-1" for the selected quantity, and "-2" for Y). For X and Y one should also define the range of variation, namely minimum and maximum values as well as step size. The format is *minimum:step:maximum*. The step size defines the grid density of the plot. A smaller step (higher density) enables better resolution but it also requires longer computational time. Indeed, if the step size of both X and Y is decreased by a factor of 10, the number of calculations (and time as a consequence) is multiplied by 100.

The Z variable to be plotted as a function of X and Y can be chosen within a list of 36 possible options (half-life times, pseudo-first order decay constants, fractions of degradation accounted for by a particular photochemical pathway, rate constants and yields of intermediate formation), which are referred to either a single photochemical pathway (*e.g.* $^{\bullet}OH$ or $^{1}O_2$) or to the overall photochemical behaviour of the substrate or intermediate. Note that the time unit of APEX is the summer sunny day (SSD).

Within *plotgraph* one should also specify the name of the input .csv file. At this point, in most cases the procedure is over. However, the file also contains values of the quantum yields of $^{\bullet}OH$, $CO_3^{-\bullet}$, $^{1}O_2$ and ^{3}CDOM* generation by irradiated CDOM. They have been derived from studies dealing with irradiation of natural water samples,[36,41,60] but the relevant values could change in different environments. Therefore, if one needs to use CDOM-related quantum yields that have been measured in a particular environment, the existing data can be modified.

3.3. Savetable function

This function is intended to produce a table instead of a plot, out of the same calculations. Many issues already cited in the case of *plotgraph* hold here as well: choice of the X and Y variables and definition of their range and step size; introduction of numerical values for the additional parameters related to water chemistry and substrate photoreactivity/intermediate formation; definition of the name of the input .csv file. The *savetable.m* file can be opened, modified and saved with the same applications used for *plotgraph.m*.

The main difference is that here one has not to choose the Z variable, because all the possible output quantities (half-life times, pseudo-first order rate constants, steady-state concentrations and so on) will appear in the output table. An advantage that can be connected with the use of *savetable* compared to *plotgraph* is the availability of the actual numerical values. These values allow further calculations to be carried out, including model errors and seasonal trends as well as the possible photochemical formation and reactivity of additional transient species not included in the original

model (*e.g.* $^{\bullet}NO_2$, $Br_2^{-\bullet}$ and $Cl_2^{-\bullet}$).[57,61-63]

A further similarity with *plotgraph* is that the formation quantum yields of $^{\bullet}OH$, $CO_3^{-\bullet}$, $^1O_2$ and $^3CDOM^*$ by CDOM are also reported in *savetable*. If needed, the existing values can be modified with new ones, derived for instance by irradiation of water samples from a definite environment. This will improve the accuracy of model predictions for photochemical processes taking place in that environment.

3.4. Application of APEX to the phototransformation of atrazine

Atrazine is transformed in surface waters mainly by direct photolysis (quantum yield of $(1.6\pm0.2)\cdot10^{-2}$) and reactions with $^{\bullet}OH$ (second-order rate constant of $(2.7\pm0.3)\cdot10^9$ M^{-1} s^{-1}) and $^3CDOM^*$ ($(1.4\pm0.1)\cdot10^9$ M^{-1} s^{-1}). The intermediate DEAOH (4-amino-2-hydroxy-6-isopropylamino-1,3,5-triazine) is formed from ATZ by direct photolysis (yield 0.10±0.01) and reaction with $^{\bullet}OH$ (yield $(8.6\pm4.6)\cdot10^{-2}$). The DEAOH yields of other processes are negligible.[53]

Figure 7 shows the modelling of atrazine transformation and DEAOH formation, as a function of nitrate concentration and DOC. The plots were obtained by applying the *plotgraph* function, with the above photochemical parameters and the atrazine absorption spectrum. The pseudo-first order rate constant of ATZ transformation (Figure 7a) has a minimum as a function of DOC, because of the prevalence of direct photolysis and $^{\bullet}OH$ reaction at low DOC and of $^3CDOM^*$ at high DOC. Indeed, organic matter inhibits both direct photolysis and reaction with $^{\bullet}OH$, the former because of competition for irradiance between ATZ and CDOM and the latter because of $^{\bullet}OH$ scavenging by DOM. Furthermore, high DOC also implies high CDOM that understandably enhances the $^3CDOM^*$-mediated processes. The fact that $^3CDOM^*$ is not involved in DEAOH formation explains why, differently from ATZ, the DEAOH rate constant steadily decreases with increasing DOC (Figure 7b).

The used time unit (SSD) is referred to mid-latitude summertime conditions. The photodegradation kinetics in different seasons is understandably slower,[64,65] and it can be approximately assessed by using the file *Apex_Season.xls*. An example of the results that can be obtained by use of the *Apex_Season.xls* file is reported in Figure 8 for atrazine, where the half-life time is plotted in the different months (the ±σ error bars are obtained by using the *Apex_Errors.xls* file for each monthly value of the half-life time).

4. Conclusions

This chapter has shown that is it possible to model the photochemical transformation kinetics of xenobiotics in surface waters, based on a number of photochemically significant parameters concerning the xenobiotic itself (absorption spectrum, direct photolysis quantum yield, second-order reaction rate constants with $^{\bullet}OH$, $CO_3^{-\bullet}$, $^1O_2$ and $^3CDOM^*$) and on environmental variables (water depth, DOC, concentration values of nitrate, nitrite, carbonate and bicarbonate). The environmental variables define the ability of the water body to attenuate sunlight in the water column and/or to photochemically produce reactive transient species, while the photochemical parameters of the xenobiotic compound measure its ability to react *via* the different photochemical reaction pathways. Furthermore, if the formation yields of an intermediate of interest through the various photochemical processes are known, it is possible to predict its formation kinetics in the same environment.

All of the above calculations can be carried out using the APEX software (Aqueous Photochemistry of Environmentally-occurring Xenobiotics). The software is also able to predict the seasonal trends of the phototransformation kinetics and to assess the uncertainty of the model output.

References

1. S. Bahnmueller, U. von Gunten and S. Canonica, *Wat. Res.*, 2014, **57**, 183-192.
2. P. Sun, S. G. Pavlostathis and C. H. Huang, *Environ. Sci. Technol.*, 2014, **48**, 13188-13196.
3. C. K. Remucal, *Environ. Sci.: Processes Impacts*, 2014, **16**, 628-653.
4. S. R. Batchu, V. R. Panditi, K. E. O'Shea and P. R. Gardinali, *Sci. Total Environ.*, 2014, **470**, 299-310.
5. A. Y. C. Lin, X. H. Wang and W. N. Lee, *Environ. Sci. Technol.*, 2013, **47**, 4104-4112.
6. M. Drame, B. O. Bilal, M. Camara, V. Sambou and A. Gaye, *J. Renew. Sustain. Energy*, 2012, **4**, 013105.
7. G. F. Clark, J. S. Stark, E. L. Johnston, J. W. Runcie, P. M. Goldsworthy, B. Raymond and M. J. Riddle, *Glob. Change Biol.*, 2013, **19**, 3749-3761.
8. M. Kuivikko, T. Kotiaho, K. Hartonen, A. Tanskanen and A. V. Vahatalo, *Environ. Sci. Technol.*, 2007, **41**, 7016-7021.
9. J. E. Frederick and Y. X. Liao, *Photochem. Photobiol.*, 2005, **81**, 603-608.
10. M. Sasaki, S. Takeshita, M. Sugiura, N. Sudo, Y. Miyake, Y. Furusawa and T. Sakata, *J. Geomagn. Geoelectr.*, 1993, **45**, 473-485.
11. R. Frank and W. Klöpffer, *Chemosphere*, 1988, **17**, 985-994.
12. R. G. Zepp and D. M. Cline, *Environ. Sci. Technol.*, 1977, **11**, 359-366.
13. O. Montenbruck and T. Pfleger, *Astronomy on the Personal Computer*, 2nd Edition. Springer, Berlin, 1994.
14. F. Riccio, 2009. http://www.perseus.it.
15. G. J. Jiang, R. H. MA, S. A. Loiselle and H. T. Duan, *Environ. Res. Lett.*, 2012, **7**, 034014.
16. L. Bracchini, A. M. Dattilo, M. Falcucci, V. Hull, A. Tognazzi, C. Rossi and S. A. Loiselle, *Photochem. Photobiol. Sci.*, 2011, **10**, 1000-1013.
17. S. A. Loiselle, L. Bracchini, A. M. Dattilo, M. Ricci, A. Tognazzi, A. Cozar and C. Rossi, *Limnol. Oceanogr.*, 2009, **54**, 590-597.
18. D. Vione, R. Das, F. Rubertelli, V. Maurino, C. Minero, S. Barbati and S. Chiron, *Intern. J. Environ. Anal. Chem.*, 2010, **90**, 258-273.
19. P. G. Carbajo, S. C. Smith, A. L. Holloway, C. A. Smith, F. D. Pope, D. E. Shallcross and A. J. Orr-Ewing, *J. Phys. Chem. A*, 2008, **112**, 12437-12448.
20. C. I. Koh, S. J. Lee and J. W. Kang, *Ozone-Sci. Eng.*, 2001, **23**, 245-253.
21. S. E. Braslavsky, *Pure Appl. Chem.*, 2007, **79**, 293-465.
22. D. Vione, J. Feitosa-Felizzola, C. Minero and S. Chiron, *Wat. Res.*, 2009, **43**, 1959-1967.
23. D. Vione, M. Minella, C. Minero, V. Maurino, P. Picco, A. Marchetto and G. Tartari, *Environ. Chem.*, 2009, **6**, 407-415.
24. M. Bodrato and D. Vione, *Environ. Sci.: Processes Impacts*, 2014, **16**, 732-740.
25. C. Minero, S. Chiron, G. Falletti, V. Maurino, E. Pelizzetti, R. Ajassa, M. E. Carlotti and D. Vione, *Aquat. Sci.*, 2007, **69**, 71-85.

26. S. E. Page, J. R. Logan, R. M. Cory and K. McNeill, *Environ. Sci.: Processes Impacts*, 2014, **16**, 807-822.
27. E. Lee, C. M. Glover and F. L. Rosario-Ortiz, *Environ. Sci. Technol.*, 2013, **47**, 12073-12080.
28. D. Vione, S. Khanra, S. Cucu Man, P. R. Maddigapu, R. Das, C. Arsene, R. I. Olariu, V. Maurino and C. Minero, *Wat. Res.*, 2009, **43**, 4718-4728.
29. J. Mack and J. R. Bolton, *J. Photochem. Photobiol. A: Chem.*, 1999, **128**, 1-13.
30. D. Vione, M. Minella, V. Maurino and C. Minero, *Chemistry Eur. J.*, 2014, **20**, 10590-10606.
31. S. Canonica, U. Jans, K. Stemmler and J. Hoigné, *Environ. Sci. Technol.*, 1995, **29**, 1822-1831.
32. S. Canonica, B. Hellrung, P. Muller and J. Wirz, *Environ. Sci. Technol.*, 2006, **40**, 6636-6641.
33. S. Canonica, *Chimia*, 2007, **61**, 641-644.
34. S. Halladja, A. Ter Halle, J. P. Aguer, A. Boulkamh and C. Richard, *Environ. Sci. Technol.*, 2007, **41**, 6066-6073.
35. S. Canonica and M. Freiburghaus, *Environ. Sci. Technol.*, 2001, 35, 690-695.
36. F. Al-Housari, D. Vione, S. Chiron and S. Barbati, *Photochem. Photobiol. Sci.* 2010, **9**, 78-86.
37. A. Pace and S. Barreca, *Curr. Org. Chem.*, 2013, **17**, 3032-3041.
38. S. Rayne, K. Forest and K. J. Friesen, *Environ. Intern.*, 2009, **35**, 425-437.
39. A. L. Boreen, W. A. Arnold and K. McNeill, *Aquat. Sci.*, 2003, **65**, 320-341.
40. M. A. J. Rodgers and P. T. Snowden, *J. Am. Chem. Soc.*, 1982, **104**, 5541-5543.
41. S. Canonica, T. Kohn, M. Mac, F. J. Real, J. Wirz and U. Von Gunten, *Environ. Sci. Technol.*, 2005, **39**, 9182-9188.
42. D. Vione, V. Maurino, C. Minero, M.E. Carlotti, S. Chiron and S. Barbati, *C. R. Chimie*, 2009, **12**, 865-871.
43. S. Chiron, S. Barbati, S. Khanra, B. K. Dutta, M. Minella, C. Minero, V. Maurino, E. Pelizzetti and D. Vione, Photochem. Photobiol. Sci., 2009, 8, 91-100.
44. G. V. Buxton, C. L. Greenstock, W. P. Helman and A. B. Ross, *J. Phys. Chem. Ref. Data*, 1988, **17**, 1027-1284.
45. E. De Laurentiis, S. Chiron, S. Kouras, C. Richard, M. Minella, V. Maurino, C. Minero and D. Vione, *Environ. Sci. Technol.*, 2012, **46**, 8164-8173.
46. P. R. Maddigapu, M. Minella, D. Vione, V. Maurino and C. Minero, *Environ. Sci. Technol.*, 2011, **45**, 209-214.
47. D. Vione, P. R. Maddigapu, E. De Laurentiis, M. Minella, M. Pazzi, V. Maurino, C. Minero, S. Kouras and C. Richard, *Wat. Res.*, 2011, **45**, 6725-6736.
48. C. Tixier, H. P. Singer, S. Oellers and S. R. Müller, *Environ. Sci. Technol.*, 2003, **37**, 1061-1068.
49. P. R. Maddigapu, D. Vione, B. Ravizzoli, C. Minero, V. Maurino, L. Comoretto and S. Chiron, *Environ. Sci. Pollut. Res.*, 2010, **17**, 1063-1069.
50. B. Sur, E. De Laurentiis, M. Minella, V. Maurino, C. Minero and D. Vione, *Sci. Total Environ.*, 2012, **426**, 296-303.

51. E. De Laurentiis, M. Minella, M. Bodrato, V. Maurino, C. Minero and D. Vione, *Aquat. Ecosyst. Health Manag.*, 2013, **16**, 216-221.
52. L. L. McConnell, J. A. Harman-Fetcho and J. D. Hagy, *J. Environ. Qual.*, 2004, **33**, 594-604.
53. G. Marchetti, M. Minella, V. Maurino, C. Minero and D. Vione, *Wat. Res.*, 2013, **47**, 6211-6222.
54. D. Eddelbuettel, *J. Appl. Econom.*, 2000, **15**, 531-542.
55. J. Wenk and S. Canonica, *Environ. Sci. Technol.*, 2012, **46**, 5455-5462.
56. G. Ruggeri, G. Ghigo, V. Maurino, C. Minero and D. Vione, *Wat. Res.*, 2013, **47**, 6109-6121.
57. E. De Laurentiis, M. Minella, M. Sarakha, A. Marrese, C. Minero, G. Mailhot, M. Brigante and D. Vione, *Wat. Res.*, 2013, **47**, 5943-5953.
58. P. L. Brezonik and J. Fulkerson-Brekken, *Environ. Sci. Technol.*, 1998, **32**, 3004-3010.
59. R. Del Vecchio and N. V. Blough, *Environ. Sci. Technol.*, 2004, **38**, 3885-3891.
60. D. Vione, G. Falletti, V. Maurino, C. Minero, E. Pelizzetti, M. Malandrino, R. Ajassa, R. I. Olariu and C. Arsene, Environ. Sci. Technol., 2006, **40**, 3775-3781.
61. P. R. Maddigapu, C. Minero, V. Maurino, D. Vione, M. Brigante and G. Mailhot, *Chemosphere*, 2010, **81**, 1401–1406.
62. E. De Laurentiis, M. Minella, V. Maurino, C. Minero, G. Mailhot, M. Sarakha, M. Brigante and D. Vione, *Sci. Total Environ.*, 2012, **439**, 299-306.
63. M. Brigante, M. Minella, G. Mailhot, V. Maurino, C. Minero and D. Vione, *Chemosphere*, 29014, **95**, 464-469.
64. S. Huntscha, H. Singer, S. Canonica, R. P. Schwarzenbach and K. Fenner, *Environ. Sci. Technol.*, 2008, **42**, 5507-5513.
65. S. W. Chung and R. R. Gu, *Environ. Manag.*, 2009, **44**, 46-61.

Table 1. Values of the quantum yield of $^{\bullet}OH$ photoproduction by nitrite, for different wavelengths of environmental significance.

λ, nm	$\Phi_{^{\bullet}OH}^{NO_2^-}(\lambda)$	λ, nm	$\Phi_{^{\bullet}OH}^{NO_2^-}(\lambda)$	λ, nm	$\Phi_{^{\bullet}OH}^{NO_2^-}(\lambda)$
292.5	0.0680	315.0	0.061	350	0.025
295.0	0.0680	317.5	0.058	360	0.025
297.5	0.0680	320.0	0.054	370	0.025
300.0	0.0678	322.5	0.051	380	0.025
302.5	0.0674	325.0	0.047	390	0.025
305.0	0.0668	327.5	0.043	400	0.025
307.5	0.066	330.0	0.038	410	0.025
310.0	0.065	333.3	0.031	420	0.025
312.5	0.063	340.0	0.026	430	0.025

Table 2. Values of $\wp^{\circ}$ (SSD-normalised photon flux) for different spectral ranges and different months.

Month	**SSD-normalised photon flux $\wp^{\circ}$ (mid latitude)**		
	UVB (300-320 nm)	**UVA (320-400 nm)**	**300-450 nm**
January	0.0673	0.197	0.214
February	0.168	0.352	0.370
March	0.389	0.596	0.604
April	0.720	0.862	0.860
May	0.924	0.979	0.966
June	1.05	1.03	1.01
July	1.00	1.00	1.00
August	0.985	0.934	0.928
September	0.596	0.664	0.671
October	0.303	0.421	0.439
November	0.101	0.220	0.238
December	0.040	0.129	0.143

Table 3. Comparison between model predictions and field data, for different compounds and different locations.

Substrate	$t_{½}$, model (days)	$t_{½}$, field (days)	Location	Reference
2,4-Dichloro-6-nitrophenolate	6.3±2.3	8.4±0.5	Rhône delta (S. France)	46
Ibuprofen	58±9	60-110	Greifensee (Switzerland)	47, 48
4-Chloro-2-nitrophenolate	5.5±1.5	6.4±0.3	Rhône delta (S. France)	49, 50
Carbamazepine	115±40	140±50	Greifensee (Switzerland)	45, 48
MCPA	12±1	10±2	Rhône delta (S. France)	51
Atrazine	17±4 64±18	20-21 67-100	Chesapeake Bay, MD, USA (2 sites)	52, 53

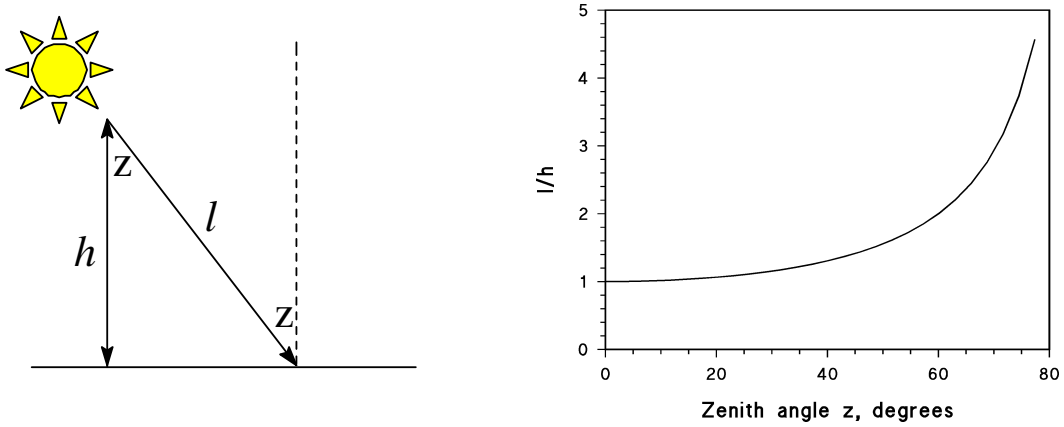

Figure 1. *Left*: schematic of the sunlight path length in the atmosphere. *Right*: dependence of the *l*/*h* ratio on the solar zenith angle *z*.

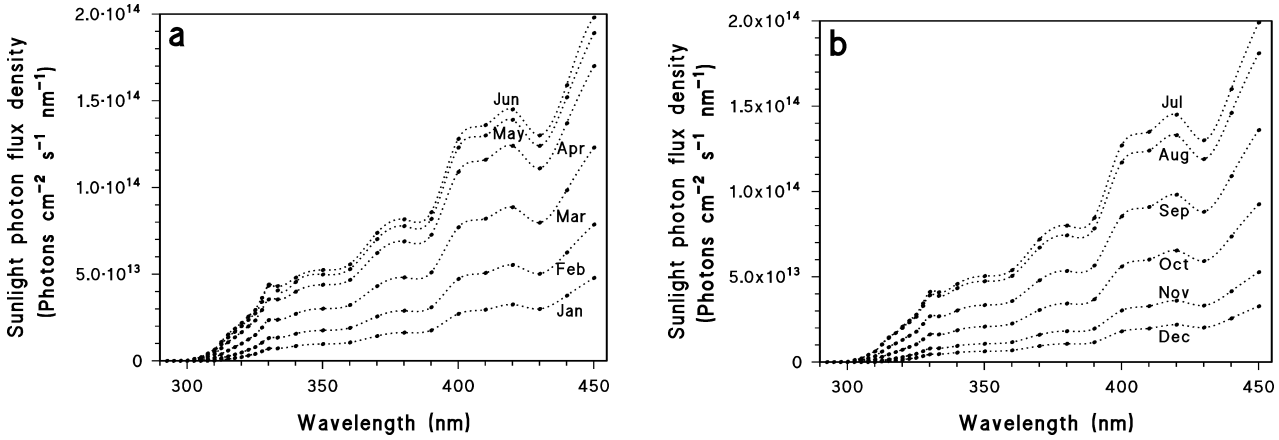

Figure 2. Sunlight irradiance at the ground in different months of the year (50°N latitude).

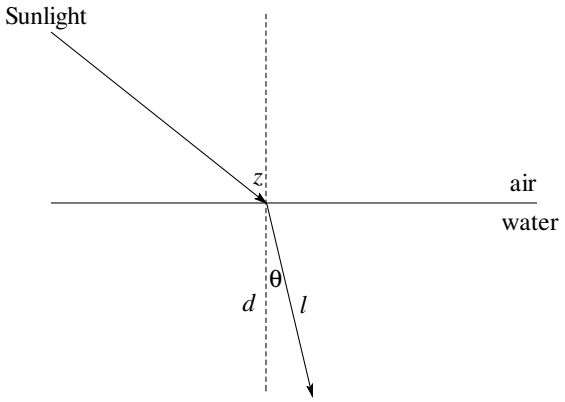

Figure 3. Refraction of sunlight at the air-water interface. *z*: solar zenith angle; *θ*: refraction angle; *d*: water depth; l: path length of sunlight in water.

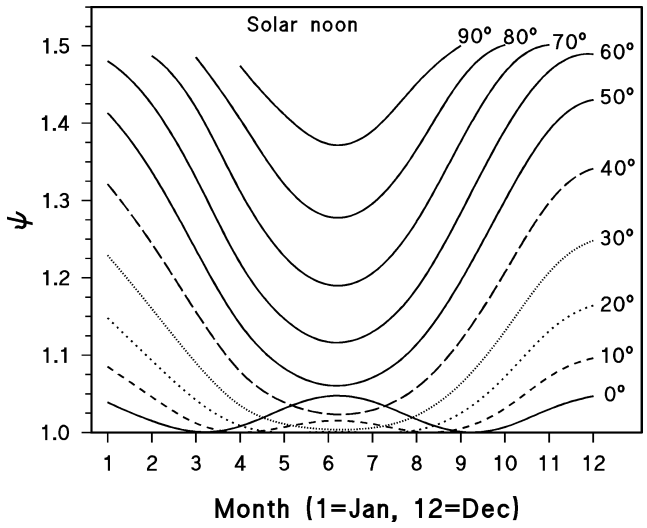

Figure 4. Values of ψ as a function of month and latitude, for the local solar noon. The latitude value (northern hemisphere) is specified near each curve.

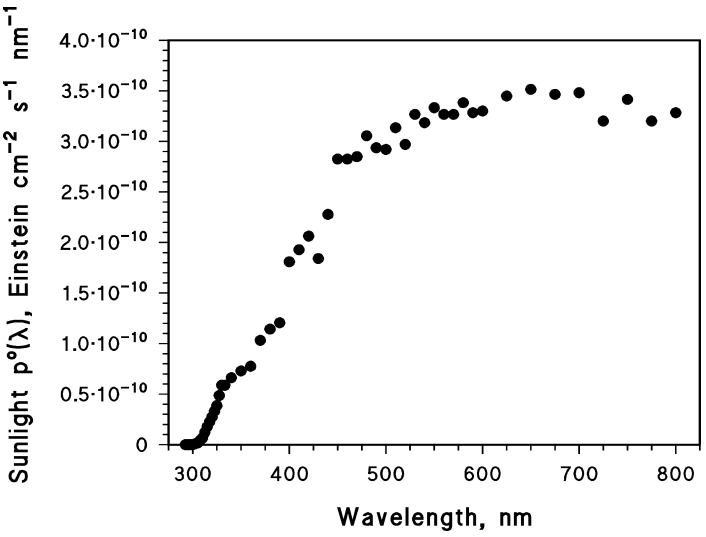

Figure 5. Sunlight spectral photon flux density at the water surface per unit area. The corresponding UV irradiance is 22 W m^{-2}.

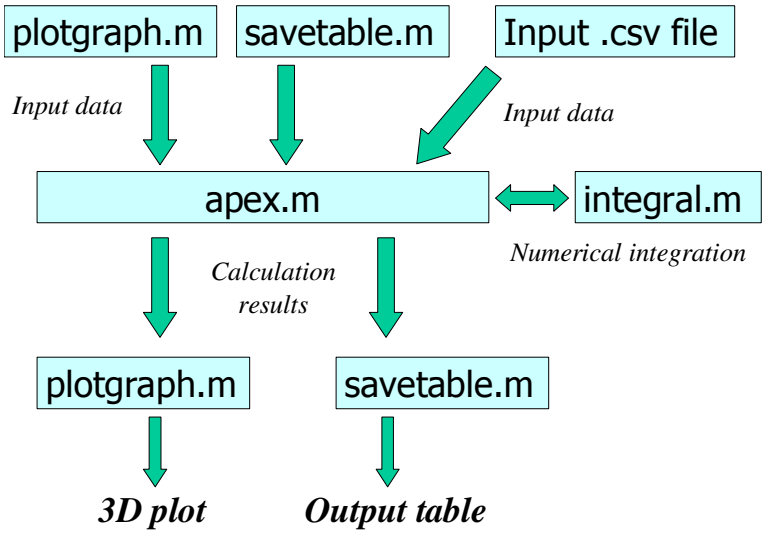

Figure 6. Structure of the APEX software.

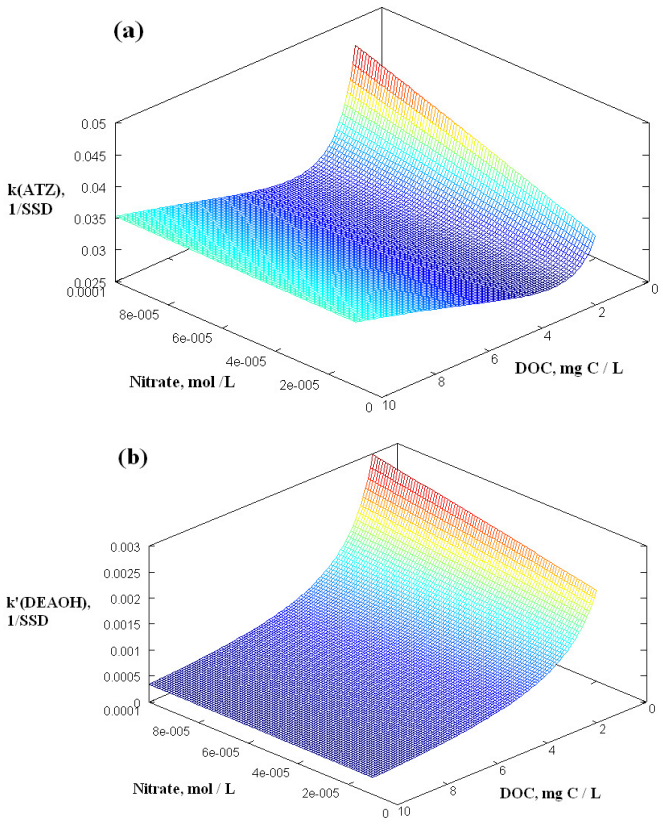

Figure 7. **(a)** Pseudo-first order degradation rate constant of atrazine (ATZ) as a function of nitrate concentration and of DOC. Other conditions: 2 m path length, 1 µM nitrite, 1 mM bicarbonate, 10 µM carbonate.

(b) Pseudo-first order formation rate constant of 4-amino-2-hydroxy-6-isopropylamino-1,3,5-triazine (DEAOH) as a function of nitrate and DOC. Other conditions are as above.

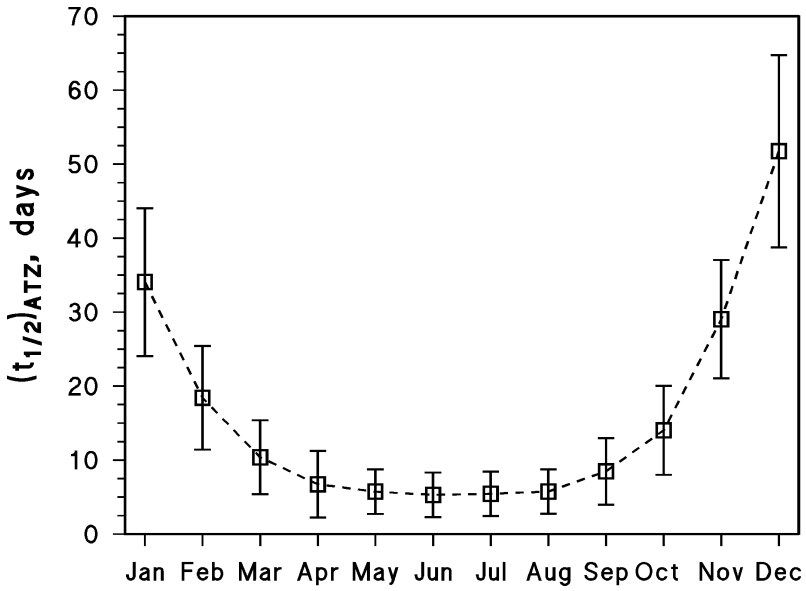

Figure 8. Modelled half-life time of atrazine in different months of the year. Water conditions: 2 mM nitrate, 20 µM nitrite, 1 mg C L^{-1} DOC, 1 mM bicarbonate, 10 µM carbonate, 4.3 m path length of sunlight.

11.1. Introduction

Photoalteration processes are known to play an important role in regards AQ:2 to the abiotic transformation of organic micro-pollutants. Numerous studies have documented the photochemical fate of a wide array of micro-pollutants, such as pesticides, pharmaceuticals, sunscreens, UV-filters, *via* direct and/or indirect pathways.

Direct photolysis occurs when a contaminant directly absorbs light and undergoes a chemical reaction depending on its chemical structure. The presence of aromatic rings and conjugated π systems, as well as various functional groups and heteroatoms, facilitate the direct absorption of solar radiation.[1] Indirect photolysis proceeds when chemical species (photosensitizers) absorb light and become electronically excited and either react directly with the contaminant or form reactive intermediates which further transform the micro-pollutant. Indirect photolysis mechanisms play an important role in the overall photolytic fate of organic contaminants, especially for those that do not appreciably absorb light above 290 nm.[2] It is apparent that indirect processes in natural waters are more complicated and are much harder to predict, as contaminants can react *via* multiple pathways through interaction with naturally occurring photo-generated transient species. Many studies have shown that dissolved organic matter (DOM), nitrate/nitrite, iron ions, as well as bi/carbonate and halide ions, play an important role in the photolytic behavior of organic micro-pollutants and may either enhance or inhibit their phototransformation.[3–5]

In this context, studies regarding indirect photolysis of a molecule are rather difficult, and usually the methods utilized to study the photochemical fate were based on univariate analysis. In order to provide a more realistic description of real-life photoinduced transformations in natural waters, multivariate methods have been set forth based on response surface methodology (RSM) and experimental design (chemometric methods).[6,7] Such statistical analyses are more efficient, since they account for interaction effects between the studied variables and may explain more accurately the relevant environmental data to understand and/or predict photolytic fate processes of organic micro-pollutants in natural systems.

Recently, studies on organic micro-pollutant degradation in real or simulated natural waters have been carried out to examine the interactions between organic micro-pollutants and natural components in water.[8–12]

To this end, in the present chapter the sequential steps of RSM are highlighted and an attempt was made to emphasize the study of diuron phototransformation in natural waters, capitalizing on the potency of chemometrics. Diuron, *N*′-(3,4-dichlorophenyl)-*N*,*N*-dimethylurea (DCMU) is a herbicide derived from urea and is considered a priority hazardous substance by the European Commission.[13] Diuron, is also used as an organic booster biocide in some antifouling paint formulations and is reported to be persistent in seawater, with reported half-lives ranging from 43 to 2180 days.[14]

11.2. Building a Response Surface Methodology

11.2.1. Selection of Response Variables and Screening Experiments

A variable that can provide the necessary information in the assessment of the performance of the process must be selected to be subjected to the optimization procedure.

In experiments where photodegradation/phototransformation processes are investigated, possible response(s) – dependent variable(s) – could be percent of degradation, photodegradation rate constant or half-life ($t_{1/2}$). On the other hand, variables that affect the response – independent variables – could be aqueous matrix (*e.g.* tap water, distilled, natural waters), photosensitizers such as DOM, nitrate/nitrite, iron ions, as well as bi/carbonate and halide ions. Among a multitude of parameters, it is important to select the most important, whose effect on the process is most significant (screening design). For this purpose, fractional factorial and Plackett–Burman designs, all of them at two levels for each factor (k), are the most widely used in the step of selection of variables.[15]

11.2.2. Choice of Optimization Design for Response Surface Methodology

The most important part, before applying the RSM methodology, is the selection of an appropriate design of experiment (DOE). Several design methods have been applied for optimization processes including photolysis, among them full factorial at three levels, central composite and Box–Behnken. The main features of these DOEs used in RSM are presented.

11.2.2.1. Full Three Level Factorial Design

Three level full factorial design is a common experimental design where input variables are set at three levels: low (−), medium or center (0) and high (+). However, the bottleneck of the 3^k design (3 levels, k parameters) is the need for a large number of experimental runs, which may produce unwanted high order interactions. Therefore 3^k full factorial design is suggested to be more appropriate if factors are less than five.

11.2.2.2. Central Composite Design

The central composite design (CCD) yields as much information as the 3^k full factorial design with a smaller number of experimental runs, and therefore CCD is the most frequently used fractional factorial design for the construction of a second-order response surface model. CCD consists of three types of points: cube points that come from factorial design, axial points and center points; therefore, the total number of experiments (N) needed can be determined by $N = 2^k + 2k + C_0$, where k is the number of factors, 2^k cubic runs, $2k$ axial runs and C_0 center point runs. The center point of CCD is often used to calculate experimental error. The main

drawback of using CCD is time consuming design with large numbers of factors.

11.2.2.3. Box–Behnken Design

Box–Behnken (BBD) design is for three levels of variables that are evenly spaced. The number of experiments required (N) is given by $N = 2k(k-1) + C_0$, where k is the number of variables and C_0 is the number of center points. The main advantage of using BBD is that this design avoids extreme conditions of experiments. BBD is slightly more labor efficient compared to CCD, however, it is restricted by the fact that the number of experimental variables has to be equal to or higher than three, and it could not be employed for fitting equations other than second-order polynomial.

11.2.3. Model Fitting

It is important to fit a mathematical model equation in order to describe the behavior of the response in the experimental domain by selected DOE. As RSM is mainly based on a second-order polynomial model, the experimenters should sequentially fit the first-order model to a second-order polynomial model. The first-order model will be applicable when the approximation of true functional relationship between response and the set of independent variables has a relatively small region of interest. In another sense, a first-order model uses a low-order polynomial model to divulge some part of the response surface. Generally, this model is appropriate for describing a flat surface, according to the equation:

AQ:3

$$R = \beta_0 + \Sigma\ \beta_i X_i + \varepsilon \tag{11.1}$$

In eqn (11.1), R is the response, β_o is the constant term, β_i represents the coefficients of the linear parameters, X_i represents the variables and ε is the random error or noise to the response. Sometimes, it is called main-effects model because it includes only the main effects of the variables.

If interaction terms are included, the first-order model can then be represented as follows:

$$R = \beta_0 + \Sigma\beta_i X_i + \Sigma\beta_{ij} X_i X_j + \varepsilon \tag{11.2}$$

where β_{ij} represents the coefficients of the interaction parameters X_i and X_j and $i<j$.

If first-order or factor interaction models are not adequate for the representation of true functional relationships with independent variables, then a more highly structured, flexible and diversified functional forms model, such as a second-order model, may be studied in order to locate the optimum point. The second-order model can be expressed as follows:

$$R = \beta_0 + \Sigma\beta_i X_i + \Sigma\beta_{ij} X_i X_j + \Sigma\beta_{ii} X_i^2 + \varepsilon \tag{11.3}$$

where β_{ii} represents the coefficients of the quadratic parameter and $i<j$.

However, obtaining a significant model does not necessarily mean that it explains correctly the variation in the data. Therefore, in order to determine the adequacy of the model, analysis of variance (ANOVA) statistics, such as residual analysis, *F*-test, *t*-test, R^2, adjusted-R^2, lack of fit, should be evaluated.

11.2.4. Optimization

The traditional ''trial-and-error'' or univariate approach for optimization has lots of drawbacks in relation to the absence of interaction effects, as well as the efficiency to predict the true optimum.

The RSM is mainly based on second-order models; so a suitable way to find the optimal location is through the graphical representation of the model. The optimal value may correspond to a maximum, a minimum or a value that can be determined by visual inspection of the predicted model by either the three dimensional space graph or the two dimensional contour plot.

However, this approach is more complicated when more than one response is involved during the optimization process since the optimal values for each response may be localized in different experimental regions. In such cases, the desirability function is employed for optimization of multiple responses. Harrington[16] first developed the desirability function, which was later modified by Derringer and Suich[17] for specifying the relationship between predicted responses on a dependent variable and the desirability of the responses.

The desirability is an objective function (D) that ranges from zero (low) outside of the limits to one (maximum) at the goal. The numerical optimization finds a point that maximizes the desirability function. The characteristics of a goal may be altered by adjusting the weight or importance of the factors based on experimenter desire. For several responses and factors, all goals are transformed into one desirability function:

$$D = (d_1 \times d_2 \times d_3 \ldots d_n)^{1/n} = \left(\prod_{i=1}^{n} d_i \right)^{1/n} \tag{11.4}$$

where d_i indicates the desirability of the response and n is the number of responses in the measure. According to this, eqn (11.4) can be extended to

$$D = \left[d_1^{v1} \times d_2^{v2} \times \ldots\ldots \times d_n^{vn} \right]^{1/n}, \quad 0 \le v_i \le 1 (i = 1, 2 \ldots\ldots n), \quad \sum_{i=1}^{n} v_i = 1 \tag{11.5}$$

where d_i indicates the desirability of the response y_i ($i = 1, 2, 3 \ldots n$) and v_i represents the importance of responses that varies from the least important ($v_i = 1$) to the most important ($v_i = 5$). So, the maximum overall desirability function, D, depends on the v_i value.

11.3. Photolytic Degradation of Diuron

11.3.1. Experimental

An analytical grade standard of diuron of high purity was obtained from Riedel-de-Häen, (Seelze-Hannover, Germany) and was used without further purification. A stock standard solution was prepared at 2000 mg L^{-1} in methanol (HPLC grade). Sodium hydrogencarbonate ($NaHCO_3$) and sodium nitrate ($NaNO_3$) were purchased from Riedel-de-Häen, while DOM was isolated from Pamvotis Lake using the IHSS isolation method pre-established by Thurman and Malcolm in 1981, by the so-called XAD technique.[18] HPLC analysis grade solvents were obtained from Merck (Darmstadt, Germany). $NaNO_3$, HCO_3^- and DOM stock solutions were diluted to achieve the respective concentrations outlined in the experimental section. Natural water samples used in the experiments were collected from the Epirus region of NW Greece with the following physicochemical characteristics: Louros River, DOM = 2.9 mg L^{-1}, nitrate = 3.3 mg L^{-1}, bicarbonate = 3.5 mM; Pamvotis Lake, DOM = 10.3 mg L^{-1}, nitrate = 11.1 mg L^{-1}, bicarbonate = 4.4 mM.

11.3.2. Analysis

The LC system comprised a Shimadzu online DGU-14A degassing system coupled to an FCV-10AL controller unit and an LC-10AD high-pressure solvent delivery pump, with a 20 μL sample loop injector and a Shimadzu SPD-M10A UV/diode-array detector (used at 250 nm). The column material was a Discovery C18 (Supelco), with 5 μm particles (25 cm – 4.6 mm i.d.) with a guard column of the same material (8 mm – 3 mm). The mobile phase consisted of acetonitrile : water (HPLC-grade) 40 : 60% mixture. The flow rate was 1 mL min^{-1} and the volume injected 20 μL. The oven temperature was set to 40 °C.

11.3.3. Photolysis in Aqueous Solutions Under Simulated Solar Irradiation

The photochemical stability of diuron was tested using a Suntest CPS + photosimulator from Heraeus (Hanau, Germany), equipped with a xenon arc lamp (1500 W) and special glass filters restricting the transmission of wavelengths below 290 nm. The light source was on the top of the reactor and an average irradiation intensity of 750 W m^{-2} was maintained throughout the experiments, measured by an internal radiometer. Chamber and black panel temperatures were regulated by a pressurized air-cooling circuit and monitored using thermocouples supplied by the manufacturer. The temperature of samples did not exceed 25 °C, using a tap water cooling circuit for the photo-reactor.

Irradiation experiments were carried out by exposing 50 mL of the aqueous solutions of diuron (10 mg L^{-1}) under artificial solar irradiation (Table 11.1). A dark control experiment was also conducted in this series of experiments.

Table 11.1. Design matrix for three test variables in coded and natural units along with the observed and the predicted responses of diuron photodegradation after 48 h of simulated solar irradiation.

Bicarbonate (x_1) mM	Nitrate (x_2) mg L^{-1}	DOM (x_3) mg L^{-1}	Degradation% (Y_{obs})	Degradation% (Y_{calc})
1 (−1)	4.1 (−1)	2.1 (−1)	22	24
4 (+1)	4.1 (−1)	2.1 (−1)	28	33
1 (−1)	15.9 (+1)	2.1 (−1)	35	32
4 (+1)	15.9 (+1)	2.1 (−1)	53	61
1 (−1)	4.1 (−1)	7.9 (+1)	60	55
4 (+1)	4.1 (−1)	7.9 (+1)	46	52
1 (−1)	15.9 (+1)	7.9 (+1)	75	73
4 (+1)	15.9 (+1)	7.9 (+1)	90	91
2.5 (0)	10.0 (0)	5.0 (0)	53	53
2.5 (0)	10.0 (0)	5.0 (0)	55	53
0.8 (−1.68)	10.0 (0)	5.0 (0)	37	43
4.2 (+1.68)	10.0 (0)	5.0 (0)	75	65
2.5 (0)	0.08 (−1.68)	5.0 (0)	25	22
2.5 (0)	19.9 (+1.68)	5.0 (0)	62	61
2.5 (0)	10.0 (0)	0.1 (−1.68)	44	38
2.5 (0)	10.0 (0)	9.9 (+1.68)	86	88
2.5 (0)	10.0 (0)	5.0 (0)	50	53

11.3.4. Design of Experiment

An experimental factorial design of the reaction system was performed for the photolytic transformation of diuron to assess the effect of natural water constituents, namely nitrate, bicarbonate and DOM, on the photolytic degradation rate. Multivariate design was performed according to the methodology of response surface following the methodology described by Fernandez *et al.*[19] The initial concentrations of the photoreactants were considered as the experimental variables and their actual and coded values taken for the calculations appear in Table 11.1. DOM concentration range was considered between 0.1 and 9.9 mg L^{-1}, nitrate concentration range varied from 0.1 to 19.9 mg L^{-1}, while bicarbonate was selected between 0.8 and 4.2 mM. The above concentrations of photosensitizers were chosen in order to resemble those commonly present in surface waters. Dark control experiments showed no loss of diuron as it does not react with nitrate, bicarbonate or DOM and there is no biodegradation.

The modeled response (Y) was the degradation percentage (%) of diuron calculated after 48 h of simulated solar irradiation. The generation of the experimental design, as well as the statistical evaluation of the results, was performed by the STATISTICA 7.0 (StatSoft Inc., Tulsa, OK, USA) statistical package.

The main effects – interaction effects as well as quadratic effects – were evaluated through analysis of variance (ANOVA). p-values were used to identify the significance of each variable on the photolytic degradation of diuron. An effect was considered significant when it was above the standard

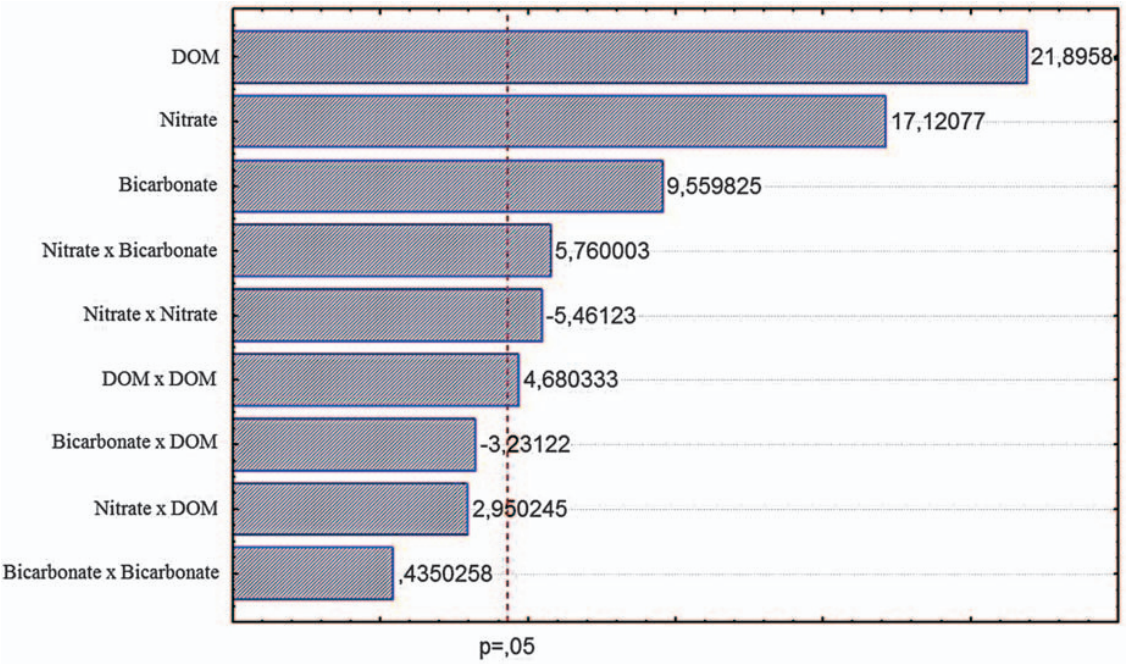

Figure 11.1. Pareto Chart of Standardized Effects of the main effects for diuron degradation% after 48 h of simulated solar irradiation. The vertical dashed line indicates the level of significance at $p = 0.05$.

error at the 95% confidence level, which is denoted by the vertical line on the Pareto chart (Figure 11.1). A low p value ($p < 0.05$) indicated a high significance. The results of statistical analysis showed that all three linear terms ($x_{1\text{-bicarbonate}}$: $p = 0.0108$, $x_{2\text{-nitrate}}$: $p = 0.0034$, $x_{3\text{-DOM}}$: $p = 0.0021$) are significant ($p < 0.05$). With regards to the interaction effects, the results have shown that simultaneous changes of bicarbonate and nitrate concentrations (x_1x_2, $p = 0.0288$) have a significant effect on the photolytic degradation of diuron, while DOM (x_3) and nitrate (x_2) displayed significant quadratic effects.

Table 11.1 shows the experimental results for the response factor (Y) corresponding to diuron degradation (%) after 48 h of irradiation, varying the bicarbonate (x_1), nitrate (x_2) and DOM (x_3) concentration in a defined range of realistic environmental concentrations. The fourth column in Table 11.1 presents the observed values obtained for the response factor (Y_{obs}) and the last column presents the calculated values by way of the modeling procedure (Y_{calc}).

Solving the matrix of data presented in Table 11.1, a second grade polynomial was obtained in terms of significant coded variables [eqn (11.6)] that describes the photolytic degradation of diuron under given conditions. The coefficients in the polynomial represent the weight of each coded variable (x_1, x_2, x_3) – corresponding to bicarbonate, nitrate and DOM concentration, respectively, as well as the interaction between them.

$$Y = 52.91 + 6.51\ x_1 + 11.66\ x_2 + 14.91\ x_3 - 4.09\ x_2^{\,2} + 3.51\ x_3^{\,2} + 5.12\ x_1x_2 \quad (11.6)$$

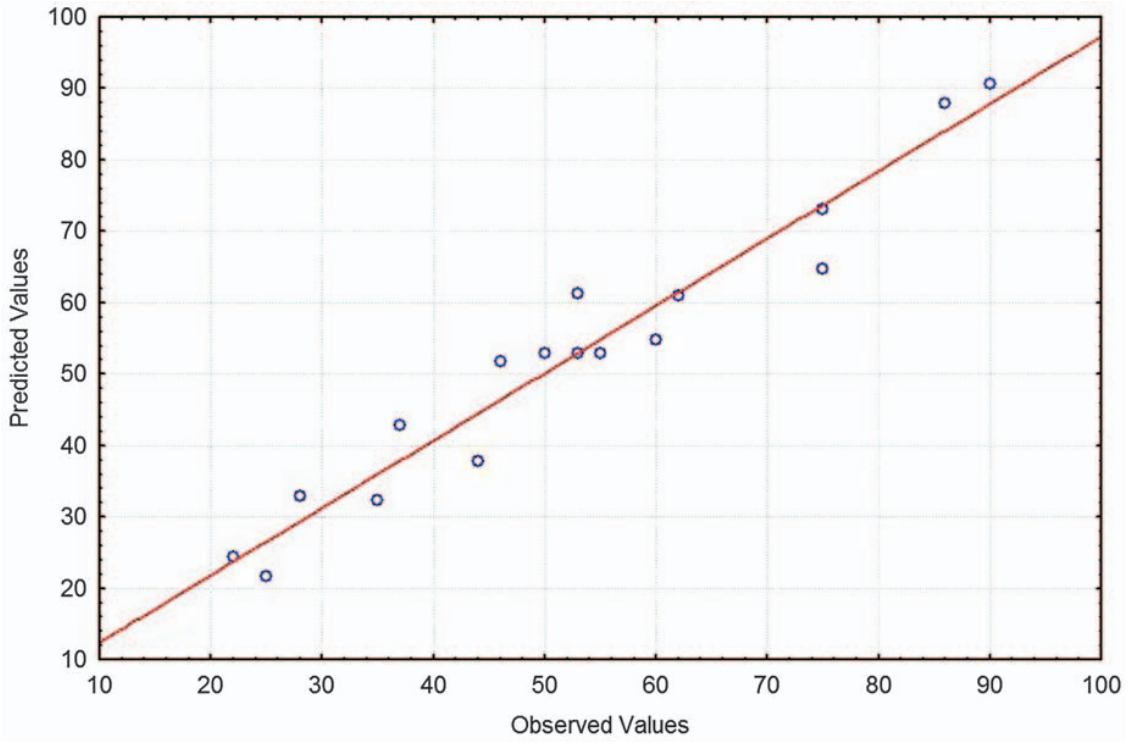

AQ:8 **Figure 11.2.** Actual *vs.* predicted plot.

Lack of Fit, which measures the failure of the model to represent data in the experimental domain at points that are not included in the regression,[16] was also checked and was shown to be not significant relative to the pure error, indicating good response to the model. The model coefficient of determination ($R^2 = 0.94$) is in reasonable agreement with the experimental results. As well, the adjusted determination coefficient (adjusted $R^2 = 0.87$) also advocates for a high significance of the model. The values obtained by the model (Y_{calc}, Table 11.1, last column) are compared with those of experimental data (Y_{obs}, Table 11.1, 4th column). These values were in good agreement, indicating a correspondence between the mathematical model and experiment (Figure 11.2).

Analyzing eqn (11.6) and taking into consideration only the first-order effect, the experimental parameters for the highest photolytic degradation of diuron seemed to be when DOM (x_3), nitrate (x_2) and bicarbonate (x_1) have a high value, since the highest numerical value of diuron degradation% (Y) corresponds to such conditions. The accelerated degradation of the model compound in such conditions could be attributed to oxidation reactions triggered by reactive species such as singlet oxygen ($^1O_2$), peroxyl radicals ($ROO^\bullet$), hydroxyl radicals ($^\bullet OH$) and carbonate radicals ($CO_3^{\bullet -}$).[3] It is well known that DOM (humic and fulvic acids) present in natural waters can act as sensitizers, giving rise to highly reactive molecules promoting indirect photolysis.[4] On the other hand, DOM can also react with, and serve as the sink for, these excited species[3] and/or exert an optical filter effect, thereby attenuating the direct photolysis. In our study, when low amounts of DOM were introduced, the photodegradation rate of diuron was increased;

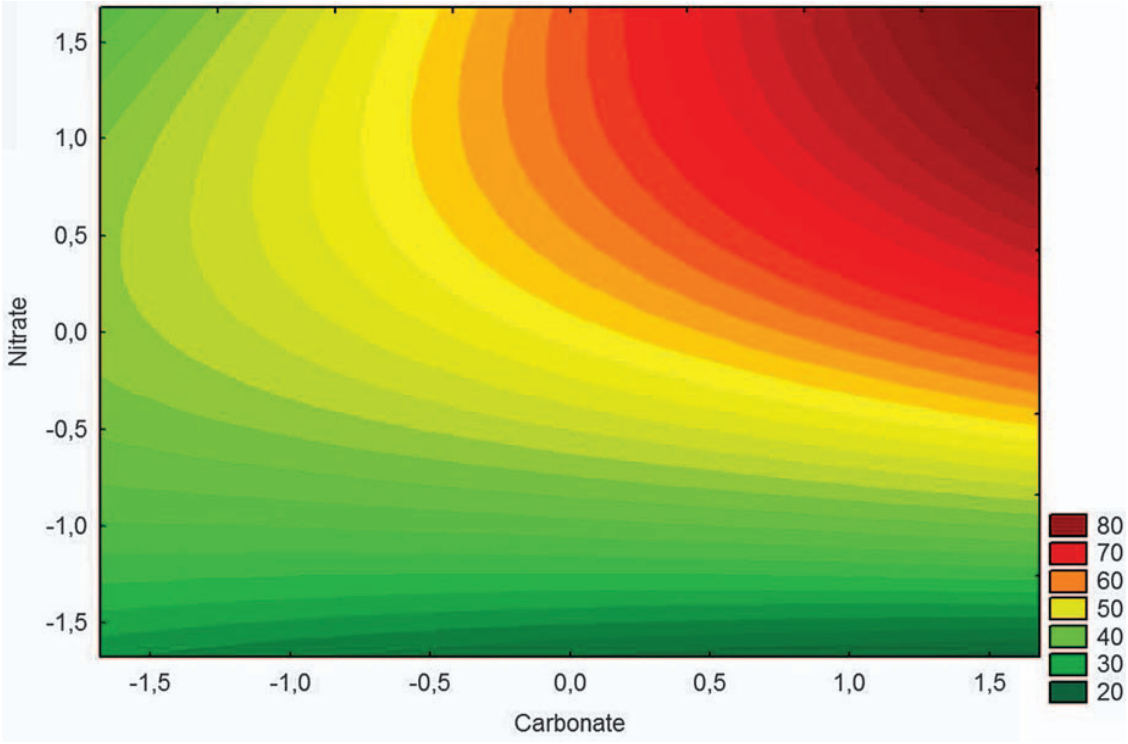

Figure 11.3. Contour plot of simulated 2-parameter interaction – bicarbonate *vs.* nitrate in terms of coded values (Table 11.1). The fitted surface represents the photolytic degradation efficiency of diuron after 48 h of simulated solar irradiation.

however, at higher concentrations this effect tends to level off, as indicated by the low coefficient of the quadratic term [x_3, eqn (11.6)], suggesting that light attenuation is important at high DOM concentrations. This observation is in agreement with the findings of Shankar *et al.* (2008),[5] who reported an inhibition effect of humic acids (HA) during diuron photodegradation, attributed to a screening effect and/or radical scavenging, at HA concentrations higher than those commonly found in natural waters.

Concerning the interaction effects, ANOVA indicated a significant effect between bicarbonate and nitrate that is illustrated as a 2D contour plot in Figure 11.3. When the reaction was performed at very low concentrations of photoreactants, the photolytic reaction was significantly diminished (degradation% $<$ 30%). A sensitization effect in the nitrate–bicarbonate system (at fixed DOM concentration of 5 mg L^{-1}) was observed at higher concentrations of both reactants and is attributed to the fact that bicarbonate acts as a $^{\bullet}OH$ scavenger, and the reaction of $^{\bullet}OH$ with bicarbonate is considered to be a major source of carbonate radical in aquatic systems.[20] The latter is a highly selective oxidizing agent, particularly for N-containing compounds.[3,4] The explanation for the bicarbonate-enhanced nitrate system is not straightforward, and it is believed that scavenging of $^{\bullet}OH$ by bicarbonate prevents $^{\bullet}OH + {}^{\bullet}NO_2$ recombination, resulting in a higher generation rate of $^{\bullet}OH$ and carbonate radical in the presence of bicarbonate than for $^{\bullet}OH$ alone.[3] However, it should be noted that, for

compounds that are not sufficiently reactive toward carbonate radicals, their photodegradation rate may be inhibited by carbonate and bicarbonate because of the scavenging of hydroxyl radicals.[20]

With the aid of the desirability function, the model predicted the concentrations of the photoreactants for which the highest photolytic degradation rate would be observed: carbonate 3.8 mM, nitrate 16.1 mg L^{-1} and DOM 9.8 mg L^{-1}.

The above observations were confirmed by the results of diuron photodegradation in distilled water, as well as natural waters such as the Louros River and Pamvotis Lake (Figure 11.4). Photolysis in distilled water generally proceeded much slower than photolysis in other natural aqueous solutions. In particular, while the degradation of diuron alone (distilled water) after 48 h of simulated solar irradiation was 22%, in natural waters it was 4-fold faster (87%) for lake, and 1.6-fold faster (35%) for river, respectively, over the same irradiation period. This acceleration effect was more pronounced at higher concentrations of these naturally occurring components (Pamvotis Lake) suggesting that, in natural surface waters, NO_3^-, HCO_3^- and DOM all contribute to indirect photodegradation of the parent molecule, showing the importance of these constituents when considering indirect photodegradation processes and the fate of organic micro-pollutants.

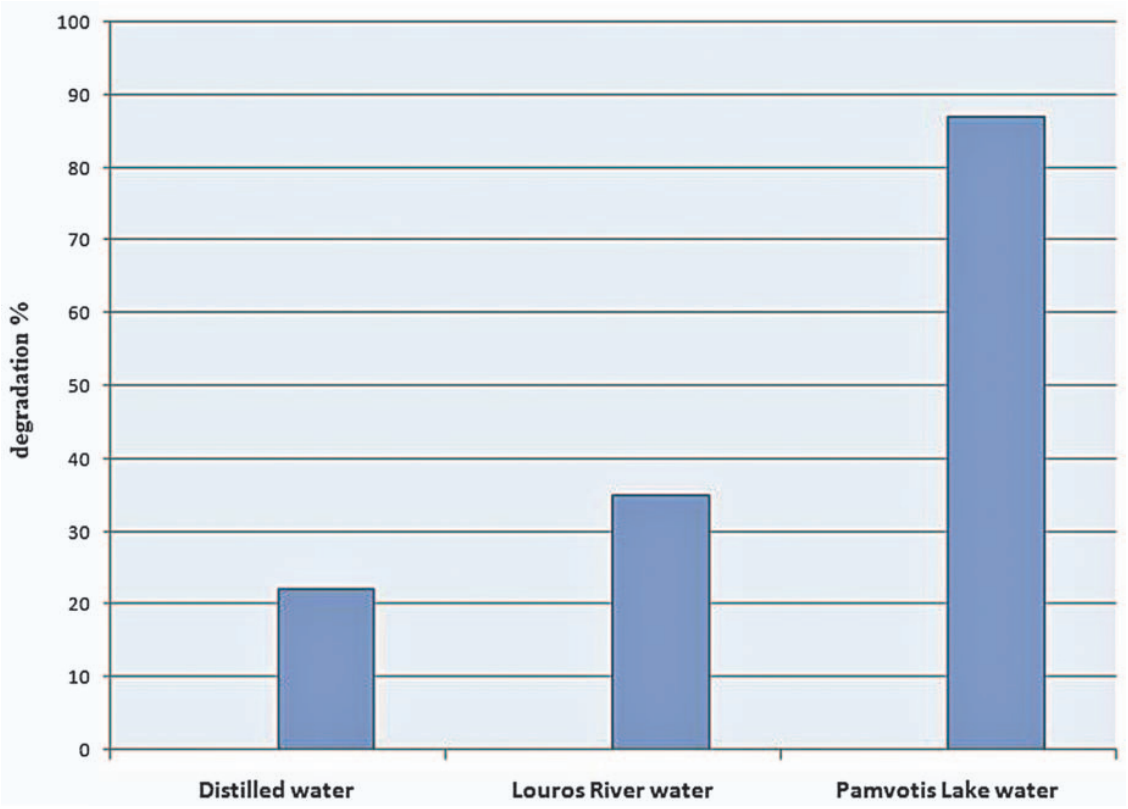

AQ:11 **Figure 11.4.** Photolytic degradation% of diuron in distilled water and natural waters under simulated solar irradiation (48 h).

11.4. Conclusion

Experimental design followed by response surface methodology (RSM) play an important role for multivariate optimization of processes, including the photolytic ones. The use of chemometrics as a tool to assess photoreaction photodegradation is still scarce. Therefore, besides the basic theory of chemometric tools, an example of diuron phototransformation in the presence of photosensitizers is presented, with the belief that the new trends in photolytic processes will be focused towards RSM optimizations based on factorial design.

References

1. A. L. Boreen, W. A. Arnold and K. McNeill, *Aquat. Sci.*, 2003, **65**, 320.
2. J. K. Challis, M. L. Hanson, K. J. Friesen and C. S. Wong, *Environ. Sci.: Processes Impacts*, 2014, **16**, 672.
3. X.-H. Wang and A. Y.-C. Lin, *Environ. Sci. Technol.*, 2012, **46**, 12417.
4. C. Goncalves, S. Perez, V. Osorio, M. Petrovic, M. F. Alpendurada and D. Barcelo, *Environ. Sci. Technol.*, 2011, **45**, 4307.
5. M. V. Shankar, S. Nelieu, L. Kerhoas and J. Einhorn, *Chemosphere*, 2008, **71**, 1461.
6. D. L. Giokas and A. G. Vlessidis, *Talanta*, 2007, **71**, 288.
7. V. A. Sakkas, K. Shibata, Y. Yamaguchi, S. Sugasawa and T. Albanis, *J. Chromatogr. A*, 2007, **1144**, 175.
8. J.-K. Im, Y. Yoon and K.-D. Zoh, *J. Environ. Sci. Health, Part A: Toxic/Hazard. Subst. Environ. Eng.*, 2014, **49**(4), 422.
9. S. S. Walse, S. L. Morgan, L. Kong and J. L. Ferry, *Environ. Sci. Technol.*, 2004, **38**, 3908.
10. L. A. Tercero Espinoza, M. Neamtu and F. H. Frimmel, *Water Res.*, 2007, **41**, 4479.
11. J. Huang and S. A. Mabury, *Environ. Toxicol. Chem.*, 2000, **19**, 2181.
12. S. Lofts, E. Tipping and J. Hamilton-Taylor, *Aquat. Geochem.*, 2008, **14**, 337.
13. S. Malato, J. Blanco, C. Richter and M. I. Maldonado, *Appl. Catal., B*, 2000, **25**, 31.
14. A. Moncada, 2004. DPR report: environmental fate of diuron. DPR pesticide chemistry database. Environmental Monitoring Branch, Department of Pesticide Regulation, 2003 <http://www.cdpr.ca.gov/docs/empm/pubs/fatememo/diuron.pdf>.
15. G. E. P. Box, J. S. Hunter and W. G. Hunter, *Statistics for Experimenters: Design, Innovation, and Discovery*, 2nd edn, Wiley Interscience, New Jersey, 2005.
16. E. C. Harrington, *Ind. Qual. Cont.*, 1965, **21**, 494.
17. G. Derringer and R. Suich, *J. Qual. Technol.*, 1980, **12**, 214.
18. E. M. Thurman and R. L. Malcolm, *Environ. Sci. Technol.*, 1981, **15**, 463.
19. J. Fernandez, J. Kiwi, C. Lizama, J. Freer, J. Baeza and H. D. Mansilla, *J. Photochem. Photobiol., A*, 2002, **151**, 213.
20. D. Vione, S. Khanra, S. Cucu Man, P. Reddy Maddigapu, R. Das, C. Arsene, R.-I. Olariu, V. Maurino and C. Minero, *Water Res.*, 2009, **43**, 4718.

12.1. Introduction

AQ:2 The identification of potential water pollutants is essential for maintaining a safe drinking water supply and a healthy aquatic habitat/environment. Approximately 2.6 billion people worldwide do not have access to safe drinking water.[1] Water pollution occurs when waste or hazardous material of some kind is discharged directly into a natural body of water without satisfactory remediation. Potential pollutants that lead to adverse health effects are classified into two general groups: chemicals, and pathogens. Pathogens are removed from polluted water by filtration and disinfection by chlorine, hypochlorite, or ozone. Water disinfection with chlorine was carried out in North America as early as 1908.[2] Chemical contamination did not become a major public health concern in the United States until 1970, AQ:3 culminating in the passage of the Safe Drinking Water Act of 1974.[3] The determination of new water pollutants is perhaps one of the greatest challenges we face currently, given that there are more than 91 million compounds currently listed in the Chemical Abstracts registry with approximately 15 000 being added per day.[4] When compounds enter the environment they may transformed into species with truly unknown, unanticipated structures. Here, we describe a new analytical approach based on full scan tandem mass spectrometry for the detection of unknown pollutants, based on structural features that suggest their possible toxicity.

12.1.1. Current Analytical Strategies for the Analysis of Water Pollutants

Analytical strategies used presently for the analysis of water pollutants are classified as either targeted or untargeted compound analysis. Targeted analyses are carried out by tandem mass spectrometry based on detection of two fragmentation reactions, one for quantification and the second transition for verification.[5] A known amount of an isotopically-labeled standard having the same structure as the analyte is analyzed simultaneously with the target compound to provide quantification. A second analytical strategy is focused on the determination of ''known unknowns''.[6] In this non-target screening approach, wastewater and/or natural water extracts are analyzed by full scan techniques that provide accurate mass data for potential pollutants that can be verified by database matching. The empirical formulas suggested by the m/z values of the ions detected are searched in databases to determine the identities of the compounds detected. Average molecular weights may be used to search the Chemical Abstracts Service Registry using the web-based version of SciFinder Scholar and the ChemSpider database.[7] Smaller databases that are routinely queried for molecular formulas include the NIST, Merck, and PubChem databases.[8] User-defined libraries containing compounds of environmental relevance have been created often for the purpose of identifying pollutants of a particular compound class. These libraries often contain retention time and fragmentation data to help differentiate isomers.[9] The most common mass spectrometer

used for the analysis of ''known unknowns'' is a quadrupole time-of-flight mass spectrometer (Q-TOF MS)[10,11] because it combines high mass resolution ($m/\Delta m = 30\,000$) with fast-scanning to yield well-resolved chromatograms.

These untargeted analyses are often carried out to detect pollutants that are regarded as ''emerging contaminants''.[12] Emerging contaminants are pollutants that have only recently been detected in the environment and no standard methods exist to quantify them presently. Data regarding their environmental or human health effects are yet unknown.[13] Wastewater effluent (treated wastewater that is released back into the environment) is frequently screened in non-target analyses to gain insight into how effective water treatment facilities are in removing these compounds.[14,15]

Despite the growth of databases for the identification of water pollutants by mass spectrometry methods, there is evidence to suggest that a large number of potential pollutants remain unidentified in untargeted analyses. One of the most extensive examples of non-targeted pollutant identification with a user defined database was carried out with an effluent water sample (treated wastewater that will be released into a river or stream) using high resolution Q-TOF analysis.[15] A user-defined database was assembled with accurate mass data, molecule ion isotopic pattern data, product ion data, and retention times of over 3000 pesticides and 87 pharmaceuticals. When retention time data were considered with the accurate mass data to identify potential pollutants, 51 compounds were identified.

12.1.2. New Strategy for the Analysis of Unknown Water Pollutants Based on Full Scan Tandem MS Over Short, Consecutive Mass Ranges

We are postulating that many, potentially harmful water pollutants, whose chemical and physical properties are not present in a database and perhaps have unknown chemical structures, may be present in natural water (lakes, rivers, *etc*.). We wish to identify the most persistent of these unknown pollutants so that fundamental questions regarding their potential toxicity may be addressed. We are suggesting that full scan tandem mass spectrometry may be used to detect unknown pollutants (m/z value and corresponding retention time) based on structural features that suggest their potential toxicity. Once a potential water pollutant is detected, possible structures may be inferred from accurate mass and product ion analysis. Ultimately, the structure of an unknown pollutant can be determined by comparing its chromatographic and spectroscopic properties with a set of synthetic standards.

The key feature of this strategy is the use of precursor ion scanning (based on the detection of chloride ion at m/z 35) over narrow, consecutive mass ranges (m/z 200 to 205, m/z 205 to 210, *etc*.) with sequential injections of sample. Such a strategy allows the determination of the molecular weights and retention times of potentially all (and only) chloride-containing

compounds with sensitivity approaching most multiple reaction monitoring experiments carried out with a triple quadrupole mass spectrometer. Tandem MS applications such as constant neutral loss, precursor ion scanning are well-known, but applications of such methods have been limited due to lack of sensitivity associated will full scan analyses conducted with triple quadrupole instruments. Sensitivity is less of a concern in our application because we are able to acquire sufficiently large volumes of water when a particular location is sampled (wastewater treatment plant, Chicago River, or Lake Michigan) to analyze all chlorinated species over a large mass (m/z) range. We currently extract four liters of water to analyze all ions that fragment to give a chloride ion over a 400 dalton mass range (typically m/z 200–600) using 80 individual injections.

We have chosen to focus our studies on chlorinated compounds for two principal reasons. One, there is substantial historical evidence to suggest that the chlorinated compounds we detect may degrade aquatic ecosystems or pose human health risks. Organochlorine compounds known to be toxic include chlorophenols, polychlorinated biphenyls (PCBs), dioxins, organochlorine pesticides such as DDT (dichlorodiphenyltrichloroethanes) and HCH (hexachlorocyclohexanes).[16] The risks of these types of chlorinated compounds may be intensified because many are known to accumulate in the environment due to the stability of the carbon–chlorine bond. The EPA still monitors many of these compounds despite the fact that their manufacture was halted over 40 years ago. There are two relatively new sources of chlorinated compounds that are now of environmental concern. These include pharmaceuticals and water disinfection by-products (DBPs). Chlorine atoms are often incorporated in pharmaceuticals because the lipophilicity and polarizability they impart to these molecules often encourages receptor binding in the targeted tissues that facilitates pharmacological function and also because chlorine atoms block metabolism. Eight of the top 40 selling drugs worldwide contain at least one chlorine atom.[17] In addition, many water DBPs contain chlorine atoms. Chlorinated DBPs can form when water is chlorinated to destroy disease-causing pathogens and microorganisms. Six hundred different disinfection products have been identified thus far and many are regarded as carcinogenic.[18] It is anticipated that the number of DBPs will increase as different methods of disinfection involving chlorine (*i.e.*, chloroamine) are implemented.[19]

The second reason we chose to study chlorinated compounds is that the formation of an m/z 35 or 37 ion during a fragmentation reaction is specific for the chloride ion. Neutral losses of 36 daltons during a fragmentation reaction are specific for HCl. These are the only logical elemental compositions corresponding to these masses. Therefore, our precursor ion studies are truly specific for chlorine-containing compounds.[20] Accurate mass analysis is not necessary to verify the presence of a chloride ion in a precursor ion scan or the loss of HCl in a constant neutral loss analysis.

12.2. Experimental

12.2.1. Extraction of Chlorinated Compounds

Chlorinated compounds are isolated by solid phase extraction (SPE) immediately after collection. Water samples are filtered through Whatman 1.6 μm glass fiber filter papers to remove particulate matter. Typically, 250 mL of filtered water are passed through a single 200 mg Oasis HLB cartridge (Waters Corp., Milford, MA, USA), as described previously for the analysis of targeted chlorinated compounds.[21] The eluate from the cartridge is evaporated to near dryness after elution with methanol. The residue is reconstituted in a 200 μL autosampler vial for analysis by LC/MS/MS.

12.2.2. LC/MS/MS Analyses

Precursor ion and constant neutral loss scans are carried out over consecutive, 5.0 dalton mass ranges per 15 μL injection on an Agilent 6460 triple quadrupole mass spectrometer interfaced to an Agilent 1290 Infinity UPLC system (Santa Clara, CA, USA). Eighty individual injections are required to analyze a 400 dalton mass range. Typically, eight cartridges are prepared from 2–4 liters of treated effluent wastewater or natural water to analyze chlorine-containing compounds over a 400 dalton mass range. LC/MS/MS analyses have been carried out using a 30 minute water/methanol gradient with a 2.1×100 mm (5 μm) C18 column that is preceded with a guard column (Phenemonex Inc., Torrance, CA., USA). Accurate mass molecular weight (and accurate mass product ion spectra) are acquired with a Waters Synapt Quadrupole Time-of-Flight mass spectrometer interfaced to a Waters 2690 HPLC at the University of Illinois-Chicago's Research Resource Center (RRC). Sucralose (early eluting, retention time 10.5 minutes) and Triclosan (late eluting, retention time of 23.5 minutes) are used as retention time markers (and as MS tuning compounds) to compare elution profiles of different ions analyzed with the triple quadrupole and Q-TOF MS.

12.2.3. Synthesis of Dichlorohydroxybenzene Sulfonic Acid Standards

All six isomeric dichlorophenols were purchased from Sigma Aldrich Chemical (St. Louis, MO, USA) and used without further purification. The dichlorophenols were sulfonated using a modification of the methods of De Wit and Cerfontain.[22] Dichlorophenol (1 mmol) was treated with sulfonating reagent (per Method A, B, or C) at room temperature for 18 hours. The reaction mixture was cooled to <5 °C and ice-cold deionized water (0.5 mL) was added. The resulting slurries were filtered; the wet cake solids were washed with cold deionized water (2×0.5 mL) and dried *in vacuo* at 40 °C to afford the dichlorohydroxybenzene sulfonic acid. Each of the three methods may be summarized as follows. One millimole of dichlorophenol was treated with 2 mL of (Method A) 95–98% sulfuric acid or 2 mL of (Method B) a 1 : 1

mixture of fuming sulfuric acid (20% SO_3) and 95–98% sulfuric acid. Method C involved treating 1 mmol of dichlorophenol with 1 mL of fuming sulfuric acid (20% SO_3). Individual reaction products were isolated by Agilent 1200 HPLC using a 10 mM K_3PO_4 water/acetonitrile gradient using a 4.6 $\times$100 mm C18 (5 μm) Waters Symmetry shield column. Proton NMR spectra of isolated reaction products were acquired to verify structures using a Bruker 400 MHz Avance NMR.

Standard compounds were analyzed in conjunction with environmental samples to enable the determination of the structure(s) of the compound(s) indicated to be dichlorohydroxybenzene sulfonic acids by accurate mass and product ion analysis. Cochromatographic analyses were carried out under isocratic conditions (98% water/2% methanol) to differentiate the structures of standard compounds and compounds isolated from different water samples.

12.2.4. Sampling Strategy

Water samples were acquired at different times from ten different locations around the Chicago, IL, USA metropolitan area. Effluent water samples were acquired from the Stickney, IL wastewater treatment plant. The Chicago metropolitan area within Cook County, IL has an estimated population of 5.2 million people.[23] The sampling sites were selected with the help of Mr David Treering, a geographic information specialist in Loyola University's Institute of Environmental Studies. Sampling sites were selected based, in part, on the population density around the immediate area and ease of access to the shoreline (Figure 12.1). An individual ''pooled'' sample is composed of many combined discreet samples taken over 100 meters of shoreline around a Lake Michigan pier or coast area along one of the rivers in the area. Normally six liters of water are acquired and combined at the time of collection.

AQ:5

The flow of the Chicago and Calumet Rivers (Figure 12.1) was diverted to the Illinois River and away from Lake Michigan in the early part of the 20th Century to prevent sewage from contaminating drinking water intake cribs in Lake Michigan. However, raw sewage may be released into Lake Michigan or natural waterways when sewers overflow during a rainstorm. A large part of the sewer system in the Chicago area was built well over a hundred years ago, before the age of wastewater treatment. These sewers originally carried waste and runoff directly into the rivers running through the Chicago area.

As wastewater treatment plants were built, a new sewer system was put in place (referred to as an intercepting sewer) to drain the flow from the old sewage line and direct it to the water treatment plant. Sewer configurations like the one in Chicago are common in older cities around the world.[24] If the intercepting sewers reach capacity during a heavy rainfall, then the local sewer may drain into a waterway or Lake Michigan. Therefore, it is possible that potentially harmful pollutants can bypass the water treatment system en route to natural water sources.

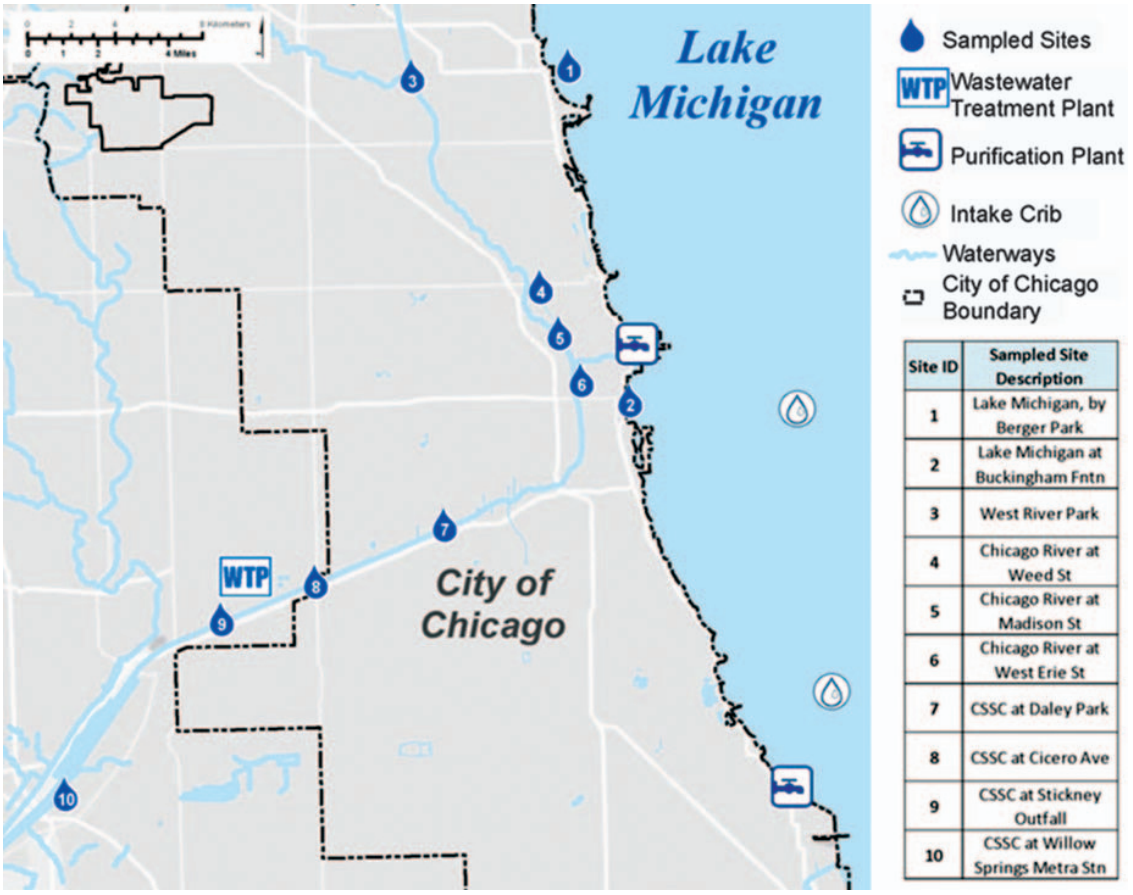

Site ID	Sampled Site Description
1	Lake Michigan, by Berger Park
2	Lake Michigan at Buckingham Fntn
3	West River Park
4	Chicago River at Weed St
5	Chicago River at Madison St
6	Chicago River at West Erie St
7	CSSC at Daley Park
8	CSSC at Cicero Ave
9	CSSC at Stickney Outfall
10	CSSC at Willow Springs Metra Stn

AQ:6 **Figure 12.1.** Map of Chicago area Lake Michigan shoreline and waterways. Sampling sites are indicated by drops (CSSC = Chicago Sanitary and Shipping Canal).

12.3. Results and Discussion

12.3.1. Precursor Ion Scanning of Water Extracts

We have analyzed wastewater effluent and water samples acquired from a number of different natural water sources for the presence of chlorinated compounds. Water sample extracts were analyzed by precursor ion scans carried out over consecutive, five dalton mass ranges for the presence of *m*/*z* 35. Thus far, water samples have been analyzed for chlorine-containing compounds over an *m*/*z* 200 to *m*/*z* 600 mass range. The ions most frequently detected (based on *m*/*z* value and retention time) at different sampling sites are analyzed further to determine their structures in order that questions regarding their potential human or environmental toxicity may be addressed. The following discussion concerns the structure determination of a dichlorohydroxybenzene sulfonic acid that has been detected in natural water and wastewater effluent and the Chicago River over the period from April 2011 through July 2014.

Figure 12.2 shows extracted ion chromatograms derived from a typical precursor ion scan for *m*/*z* 35 ions, conducted over an *m*/*z* 240–245 mass range in the analysis of an effluent wastewater sample.

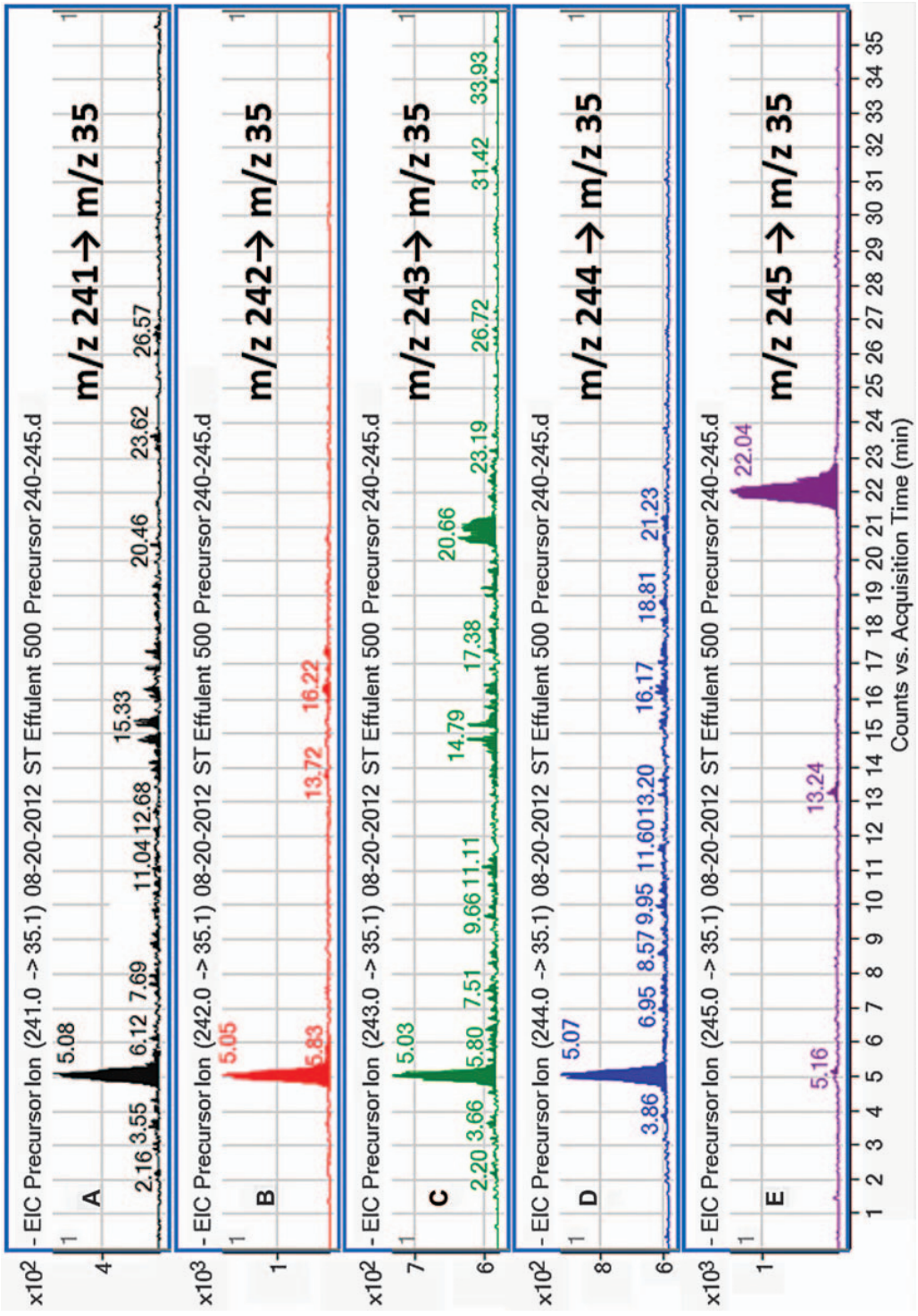

Figure 12.2. Extracted ion chromatograms associated with "full-scan" precursor ion scanning for *m/z* 35 over the mass range *m/z* 240–245.

The extracted ion chromatograms (Figures 12.2A–C) taken together suggest the presence of a compound with two chlorine atoms. Three transitions involving *m/z* 241–244 to *m/z* 35 are suggested to have the same retention time. The ions at *m/z* 241 and *m/z* 242 (C13 peak) have two chlorine-35 atoms (Figures 12.2A and B), while the ion at *m/z* 243 and *m/z* 244 (C13 peak) has one chlorine-35 and one chlorine-37 atom (Figures 12.2C and D). The ion at *m/z* 245, contains only chlorine-37 atoms, so it is not observed in this experiment. This dichlorinated species, eluting with a retention time of five minutes in the initial precursor ion analyses, has been detected in water samples acquired at Stickney wastewater treatment plant (effluent), the Chicago River at Erie street and the Chicago Sanitary and Shipping Canals (CSSC-Figure 12.1) at Daley Park and Cicero on three separate occasions and once at Willow Springs SSC over the last three years. We have not detected the dichlorinated species at the two Lake Michigan sampling sites along the coast, specified in Figure 12.1, to date.

12.3.2. Accurate Mass and Product Ion Analyses of Dichlorinated Compounds

Accurate mass data were acquired to determine the empirical formula of this particular chlorinated compound. The high resolution LC-Time-of-Flight mass spectrum is shown in Figure 12.3 for a wastewater effluent sample. The exact masses (and errors) of the ions observed at *m/z* 241.9135 (2.4 ppm), 243.9110 (0.0 ppm), and 245.9081 (4.1 ppm) are consistent with the empirical formula $C_6H_3Cl_2SO_4$. The relative abundances of these three ions

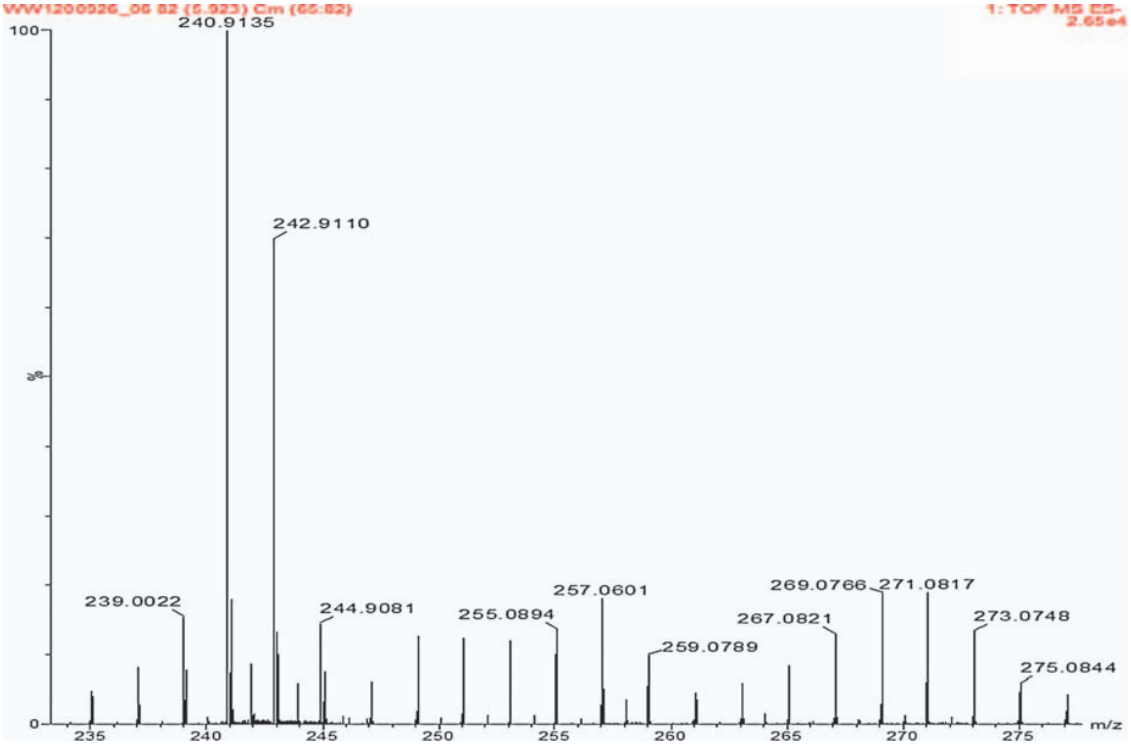

Figure 12.3. Q-TOF mass spectrum of chlorinated ions at *m/z* 241 and *m/z* 243 indicated by accurate mass analysis to contain two chlorine atoms.

strongly suggest the presence of two chlorine atoms in this compound as well. The valences of the atoms in the empirical formula (rings-plus-double bonds analysis) suggest that these ions are $(M–H)^-$ ions derived from a compound with the empirical formula $C_6H_4Cl_2SO_4$ containing four elements of unsaturation.

Product ion spectra of the *m*/*z* 240.9 ion acquired on the triple quadrupole mass spectrometer suggest that this ion is an aromatic sulfonic acid (Figure 12.4). The major ion formation processes of the main *m*/*z* values observed in this spectrum are indicated in Figures 12.4A and 12.4B. Product ion spectra are shown for the *m*/*z* 241 ion extracted from the wastewater effluent sample (Figure 12.4A) and a sample taken from Daley Park Sanitary and Shipping Canal (Figure 12.4B). Product ion spectra from these two samples were chosen for Figure 12.3 because these samples provided the most abundant *m*/*z* 241 ions in the original precursor ion scans (scanning in

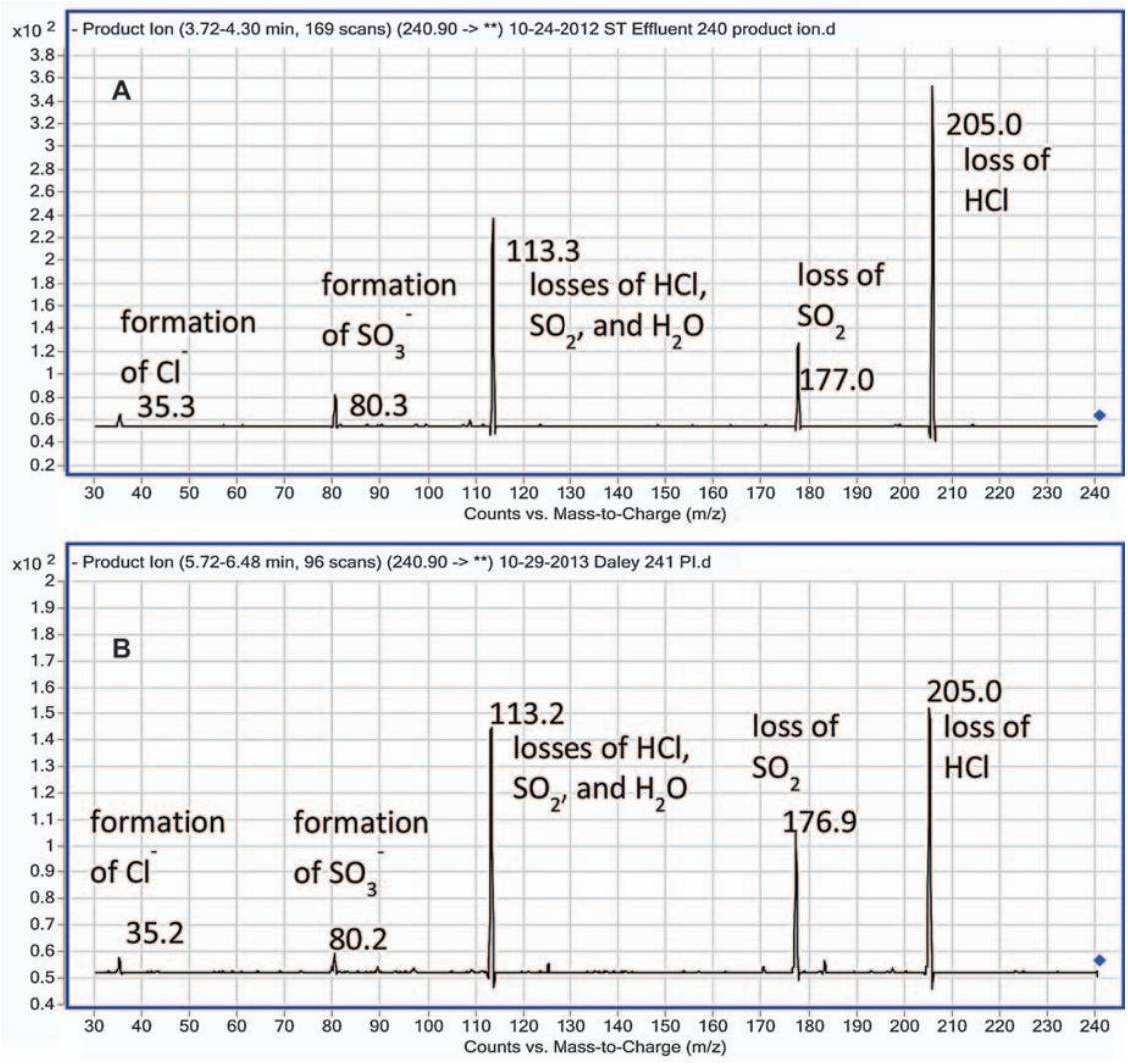

Figure 12.4. Product ion mass spectra of *m*/*z* 240.9 ion from a wastewater effluent sample eluting at 6.3 minutes acquired on a triple quadrupole mass spectrometer (**A**) extracted from wastewater treatment plant effluent and (**B**) a Chicago river water sample taken from the Daley Park Sanitary and Shipping Canal.

the *m*/*z* 240 to *m*/*z* 245 mass range). Both product ion spectra show the same five major fragment ions at similar relative abundances, suggesting that the compounds extracted from the two different water samples may have the same chemical structure. The neutral losses and/or the identities of the fragment ions formed in the collision process are labeled in the Figure 12.4 product ion spectra.

These five fragment ions are *m*/*z* 35 (chloride ion), *m*/*z* 80 (the SO_3^- ion), *m*/*z* 113 (formed by neutral losses of H_2O, HCl, and SO_2), *m*/*z* 177 (formed by the neutral loss of SO_2), and *m*/*z* 205 (formed by the loss of HCl). There is no apparent fragmentation pathway that involves the breaking of a carbon–carbon bond, suggesting the presence of a benzene ring. This observation, taken with the fragmentation pathways specified in the Figure 12.4 product ion spectra, suggest a substituted benzene ring structure. The product ion mass at *m*/*z* 80 is consistent with an SO_3^- ion, which is a signature for a sulfonic acid group. The loss of water is consistent with the presence of a phenol. The Figure 12.4 product ion spectrum suggests that this compound is a dichlorobenzene phenol sulfonic acid. We then proceeded to identify this chlorinated sulfonic acid using synthetic standards.

AQ:8

12.3.3. Product Ion Analyses of Dichlorohydroxybenzene Sulfonic Acid Standards

We set out to identify the unknown dichlorinated compound by comparing retention time and spectroscopic properties with a set of synthetic standards. The implicit assumption here is that the correct standard compound will have the same structure as the unknown pollutant detected in natural and/or effluent wastewater. If one simply considers the number of different permutations of four groups (two chlorines, one hydroxyl, and one sulfate), there are 16 possible isomers for all possible dichlorohydroxybenzene sulfonic acids. Four structures are 1,4-phenolsulfonic acids (*para*-substituted), six are 1,3-phenolsulfonic acids (*meta*-substituted), and another six are 1,2-phenolsulfonic acids (*ortho*-substituted). Three of the four possible *para*-substituted compounds were generated by sulfonation. Sulfonation of 3,5-dichlorophenol to prepare 2,6-dichloro-4-hydroxybenzene sulfonic acid (the fourth *para*-substituted isomer) was unsuccessful due to the high *ortho* deactivating effect of the chlorine atoms of 3,5-dichlorophenol. No *meta* isomers were generated (phenol groups are *ortho*,*para*-directing). All six *ortho*-substituted isomers were formed in varying amounts.

We first acquired product ion spectra and retention times of the standard compounds with the same gradient used for discovery of unknown chlorinated pollutants. All six of the *ortho*-phenol, substituted sulfonic acids eluted at much longer retention times (between 11.5 and 17.5 minutes) than the environmental samples (*ca*. five minutes) when analyzed with the 30 minute water/methanol gradient. Also, the product ion spectra of the *ortho*-substituted isomers are distinctly different than the product ion spectra of the *m*/*z* 240.9 derived from the natural water samples. The product

ion spectra of the *ortho*-substituted hydroxybenzene sulfonic acids are dominated by an ion at *m/z* 161, which is formed by the inductive cleavage of the SO_3 from the benzene ring. The product ion spectra of 3,5-dichloro-2-hydroxybenzene sulfonate are shown in Figure 12.5.

This compound is used as a colorimetric indicator compound in different over-the-counter test kits for glucose and lactose.[25] No *m/z* 161 is observed in the product ion spectra of the *m/z* 240.9 ion suggested to be a hydroxybenzene sulfonic acid in the extracted water samples (Figure 12.4) analyzed or in the product ion spectra of the *para*-substituted hydroxybenzene sulfonates. Therefore, the sulfonic acids detected in natural water or treatment plant effluent are suggested to be *ortho*-substituted hydroxybenzene sulfonic acids. The *m/z* values and relative abundances of the product ions observed in Figure 12.5B (m/z 113 > m/z 205 > m/z 177 > m/z 80 = m/z 35) are

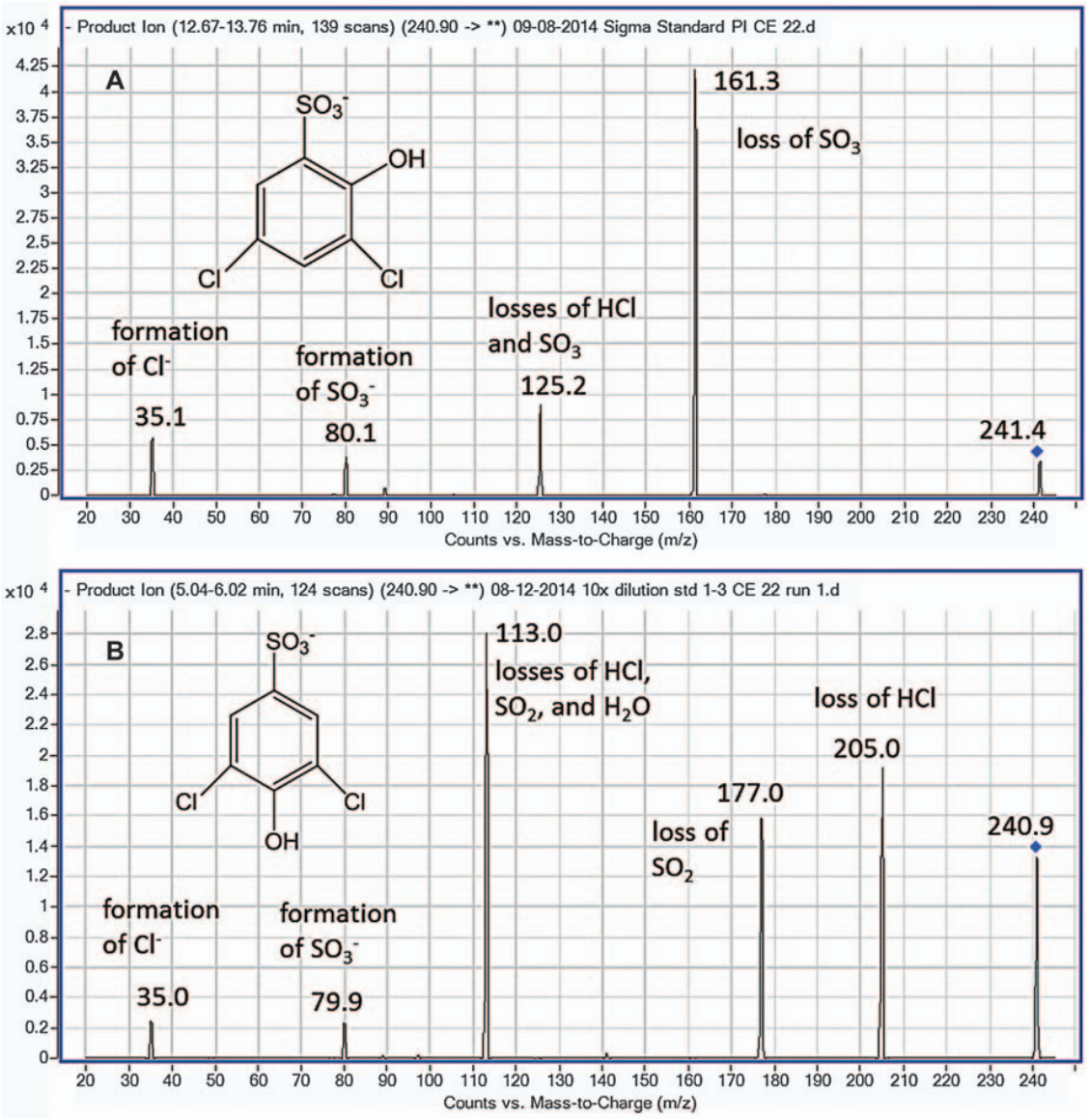

Figure 12.5. Product ion spectra of the $(M–H)^-$ ion derived from *m/z* 241 for (**A**) 3,5-dichloro-2-phenolsulfonic acid and (**B**) synthesized 3,5-dichloro-4-hydroxybenzene sulfonic acid.

consistent with the product ion spectra of the *m/z* 241 ion isolated from effluent wastewater and the Chicago River shown in Figure 12.4.

12.3.4. Cochromatography Analyses of Dichlorinated Ions Isolated from Water Samples and para*-Hydroxysulfonic Acid Standards*

Our next set of experiments was carried out to identify the dichlorohydroxybenzene sulfonic acid detected in these different water samples by comparing the retention times of the unknown dichlorinated species in different water samples with those of the three *para*-hydroxybenzene sulfonic acids. The composition of the gradient was adjusted to lengthen the retention times and to separate the dichlorinated compounds with different structures. Chromatograms showing the retention times of the *m/z* 241 ions isolated from three different water samples are shown in Figure 12.6.

AQ:9

Figure 12.7 shows the retention times of the three 1,4-hydroxybenzene sulfonic acid standard compounds. The chromatograms in Figures 12.6 and

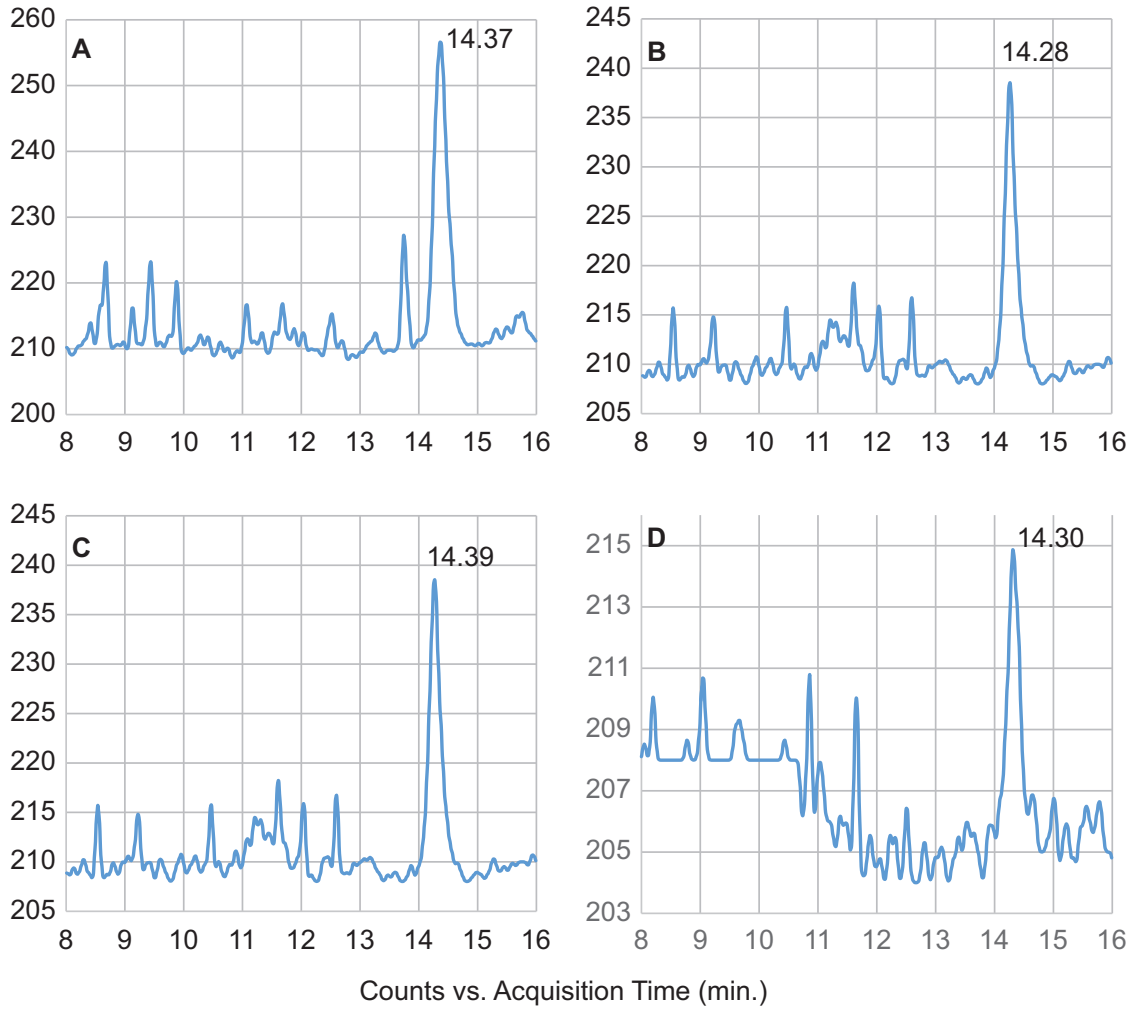

Figure 12.6. Chromatograms of dichlorinated *m/z* 241 ion isolated from water samples taken from (**A**) Stickney wastewater effluent, (**B**) Cicero SSC, (**C**) Erie SSC, and (**D**) Daley SSC. The standard deviation associated with the retention times ($N = 3$) is ± 0.06 minutes.

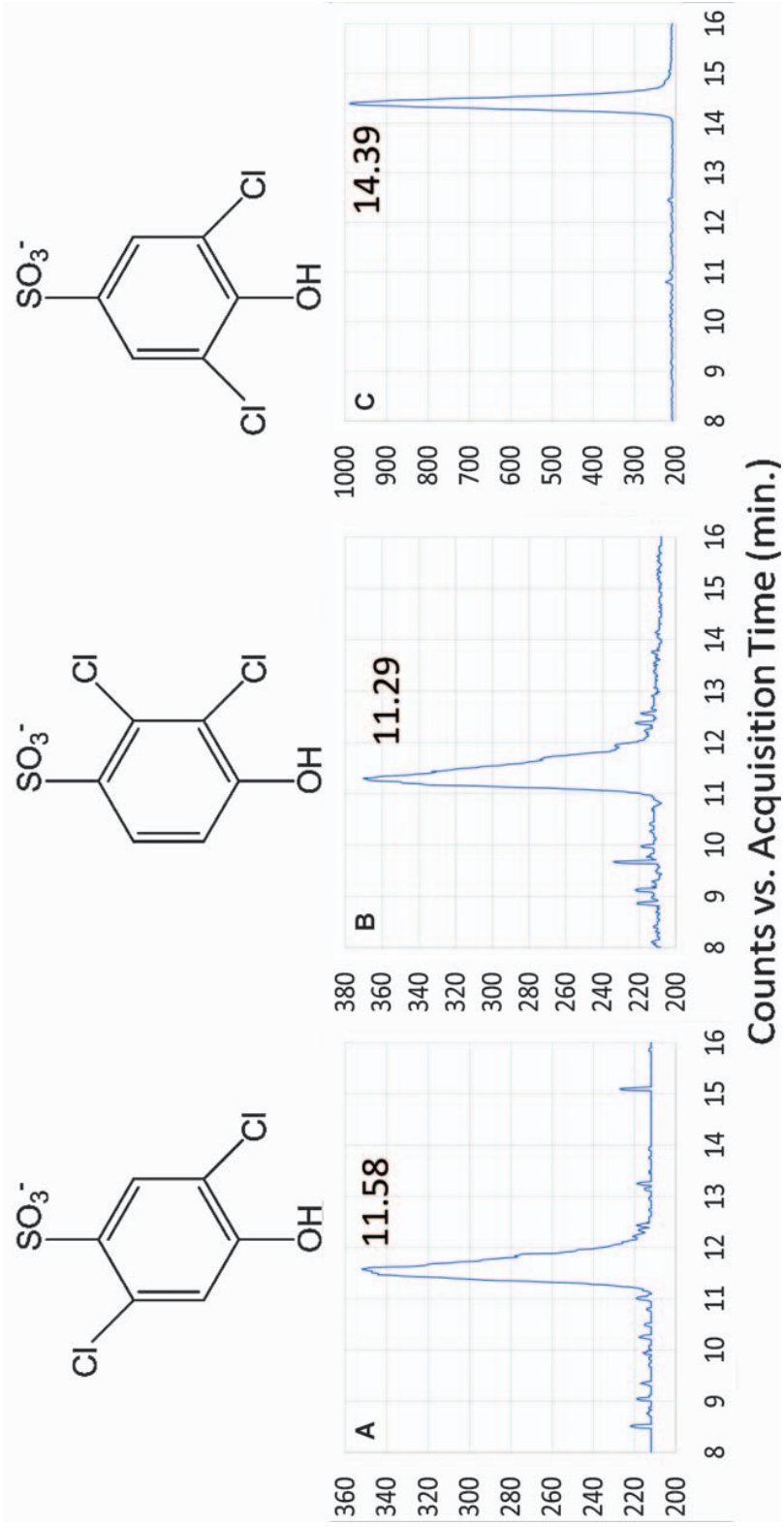

Figure 12.7. Chromatograms of (**A**) 3,6-dichloro- (**B**) 2,3-dichloro, and (**C**) 3,5-dichloro-4-hydroxybenzene sulfonic acid standards.

AQ:10 12.7 suggest that the dichlorinated hydroxyl-benzene sulfonic acids isolated from water samples taken from different places around Chicago have retention times similar to 3,5-dichloro-4-hydroxybenzene sulfonic acid with a retention time of *ca.* 14.4 minutes. The other two standards, 2,5-dichloro- and 2,3-dichloro-4-hydroxybenzene sulfonic acid eluted with retention times of 11.3 and 11.6 minutes under these conditions. Therefore, we conclude that the dichlorohydroxybenzene sulfonic acid detected in the effluent wastewater and natural water samples is 3,5-dichloro-4-hydroxybenzene sulfonic acid.

There is evidence to suggest that 3,5-dichloro-4-hydroxybenzene sulfonic acid is a by-product of the dye industry.[26,27] This compound may be attached to a dye molecule or some other intermediate as a phenol ester. This phenol ester functions as a leaving group when the dye is attached to another substrate. Another possibility is that 3,5-dichlorophenol-4-sulfonic acid may be formed during the water treatment process. 4-Hydroxybenzene sulfonic acid is a by-product of the electroplating industry.[28] The 3,5-dichloro-hydroxybenzene sulfonic acid would be the favored dichlorination product based on the activating/deactivating directing properties of the hydroxyl and sulfonic acid groups attached to the benzene ring. If chlorination of the 4-phenolsulfonic acid was a significant source of 3,5-dichlorophenol-4-sulfonic acid, one might expect to find the monochloro product as well. We have not observed any ion suggested to be a monochlorophenol sulfonic acid in any single reaction monitoring analysis of extracted natural or effluent wastewater samples to date.

The six 1,3-hydroxybenzene sulfonic acids and 3,5-dichloro-4-benzene sulfonic acids were not included in this study as standard compounds because there are no published synthetic methods or commercial sources for any of these compounds to date. Therefore, we cannot state with absolute certainty that they are not present in any of the water samples analyzed; however, the difficulty and expense of generating the 1,3 isomers would suggest that they are not present in the environment as pollutants. The synthesis of these *meta*-substituted isomers would require more individual synthetic steps than the preparation of the *ortho*- and *para*-hydroxybenzene sulfonic acids, given that phenols are *ortho*- and *para*-directing, again significantly decreasing the likelihood that they would be used industrially on such a scale to be detected in the environment. The production of the *meta*-substituted isomers would be precluded in wastewater treatment, in consideration of well-known patterns of electrophilic aromatic substitution. 1,3-Hydroxybenzene sulfonic acid as a starting material for the production of the dichloro-1,3-hydroxybenzene sulfonic acids is relatively expensive (*ca.* $2,950 per gram),[29] therefore it is not likely that large quantities of this material would be released into the environment on a large scale as a manufacturing by-product. The generation of 3,5-dichloro-4-hydroxybenzene sulfonic acid as a synthetic product with any starting material is unlikely because it requires two chlorine atoms be adjacent to the sulfonic acid group on the benzene ring.

12.4. Conclusion

We have demonstrated an analytical method based on full scan tandem mass spectrometry for the detection of potential pollutants in different water sources. The key feature of this strategy is the use of precursor ion scanning over narrow, consecutive mass ranges with sequential injections of sample. Such a strategy allows the determination of the molecular weights and retention times of all chlorine-containing compounds with sensitivity approaching most multiple reaction monitoring experiments carried out with a triple quadrupole mass spectrometer. Potential pollutants detected by full scan tandem mass spectrometry analysis may then be subjected to accurate mass and product ion analysis to determine their empirical formulas and primary structural characteristics. Identification is ultimately achieved by comparing retention time and spectroscopic characteristics of the compounds isolated from water samples to those of synthetic standards. This approach to unknown analysis is demonstrated by the identification of 3,5-dichloro-4-hydroxybenzene sulfonic acid in wastewater effluent and the Chicago River. Once potential pollutants have been identified, their toxicity may be assessed and their persistence in the environment quantified using isotopically-labeled standard compounds. The success of this full scan tandem mass spectrometry method that we are using for the analysis of chlorinated molecules may eventually be extended to other compounds with functional groups that make them well-suited for constant neutral loss or precursor ion studies, including glucuronides (176 dalton neutral loss), bromine-containing compounds (precursor ion scans for bromides ions at m/z 79 or 81), as well as molecules that contain nitroso/nitro groups (m/z 30, m/z 46), sulfates (m/z 80), or cyano groups (m/z 26).

References

1. http://www.who.int/water_sanitation_health/mdg1/en/ Accessed January 26, 2015.
2. http://water.epa.gov/aboutow/ogwdw/upload/2001_11_15_consumer_hist.pdf, Accessed March 14, 2015.
3. J. A. Roberson, *Environ. Sci. Technol.*, 2011, **45**(1), 154.
4. http://www.cas.org/content/at-a-glance accessed March 14, 2015.
5. P. C. von der Ohe, V. Dulio, J. Slobodnik, E. De Deckere, R. Kuhne, R.-U. Ebert, A. Ginebreda, W. De Cooman, G. Schuurmann and W. Brack, *Sci. Total Environ*, 2011, **409**, 2064.
6. M. Zedda and C. Zwiener, *Anal. Bioanal. Chem.*, 2012, **403**, 2493.
7. J. L. Little, C. D. Cleven and S. D. Brown, *J. Am. Soc. Mass Spectrom*, 2011, **22**, 348.
8. J. L. Little, A. J. Williams, A. Pshenichnov and V. Tkachenko, *J. Am. Soc. Mass Spectrom*, 2012, **23**, 179.
9. I. Ferrer and E. M. Thurman, *TrAC, Trends Anal. Chem.*, 2003, **22**, 750.
10. M. Petrovic and D. Barcelo, *Anal. Bioanal. Chem.*, 2006, **385**(3), 422.
11. F. Hernandez, J. V. Sancho, M. Ibanez, E. Abad, T. Portoles and L. Mattioli, *Anal. Bioanal. Chem.*, 2012, **403**, 1251.

12. S. D. Richardson and T. A. Ternes, *Anal. Chem.*, 2014, **86**(6), 2813.
13. A. Joss, H. Siegrist and T. A. Ternes, *Water Sci. Technol.*, 2008, **57**(2), 251.
14. J. H. Writer, S. K. Keefe, J. N. Ryan, I. Ferrer, E. M. Thurman and L. B. Barber, *Appl. Geochem.*, 2011, **26**(Suppl.), S344.
15. M. J. Gomez, M. M. Gomez-Ramos, O. Malato, M. Mezcua and A. R. Fernandez-Alba, *J. Chromatogr. A*, 2010, **1217**, 7038.
16. C. Baird, *Environmental Chemistry*, W.H. Freeman and Company, New York, NY, USA, 2nd edn, 1999, vol. 293–309, pp. 337–353.
17. N. A. McGrath, M. Brichacek and J. T. Njardarson, *J. Chem. Educ.*, 2010, **87**(12), 1348.
18. S. D. Richardson, M. J. Plewa, E. D. Wagner, R. Schoeny and D. M. DeMarini, *Mutat. Res., Rev. Mutat. Res.*, 2007, **636**, 178.
19. A. D. Shah and W. A. Mitch, *Environ. Sci. Technol.*, 2012, **46**, 119.
20. F. W. McLafferty and F. Turecek, *Interpretation of Mass Spectra*, University Science Books, Sausalito, CA. USA , 4th edn, 1993, p. 39.
21. Y. Zhao, F. Qin, J. M. Boyd, J. Anichina and X.-F. Li, *Anal. Chem.*, 2010, **82**, 4599.
22. P. De Wit and H. Cerfontain, *Recl. Trav. Chim. Pays–Bas*, 1988, **107**(3), 121.
23. <http://en.wikipedia.org/wiki/Cook_County,_Illinois> accessed March 15, 2015.
24. https://www.mwrd.org/pv_obj_cache/pv_obj_id_E74696A306E382BCCC0C324661BA1489BB6E1000/filename/Understanding_Your_Sewer.pdf accessed March 15, 2015.
25. W. Dungchai, O. Chailapakul and C. S. Henry, *Anal. Chim. Acta*, 2010, **674**, 227.
26. E. Antoulinakis, D. M. Witczak, K. Gee and A. Rukavishnikov, *Preparation of reactive dyes as labeling reagents* U.S. Pat. Appl. Publ. (2009), US 20090004753 A1 20090101.
27. K. Gee, A. Chen and H. C. Kang, *Heterobifunctional esters for use in labeling target molecules* PCT Int. Appl. (2012), WO 2012134925 A1 20121004.
28. http://pubchem.ncbi.nlm.nih.gov/summary/summary.cgi?sid=87574361 accessed March 15, 2015.
29. Price quote from American Custom Chemical Corporation, San Diego, CA, USA, provided 8/28/2014.

13.1. Introduction

Environmental studies on the fate of organic compounds generally refer to different compartments with distinct physicochemical properties, whose AQ:2 interactions and movements (between river, estuary, sea, atmosphere, groundwater and land) are studied through mathematical models.[1,2] In each compartment, and also in diverse sites of a single compartment, different chemical reactions could take place due to changeable conditions (pH, pE, temperature, light, *etc*.). Risk management associated with hazardous organic compounds in the environment requires detailed knowledge of the extent of their degradation. An evaluation of the contribution of natural biodegradation or abiotic transformation processes in different environmental matrices, such as surface or groundwater, soil and sediments, is critical for the legislation and registration of man-made chemicals. Since the 1990s, increasing attention has been focused on the micropollutant class of AQ:3 so-called ''*emerging pollutants*'' (ECs), defined as natural or synthetically occurring substances that are not commonly monitored in the environment but that can induce known or suspected undesirable effects on humans and ecosystems,[3–6] and on their introduction to and transformation within the environment.[7–9] Their concentrations have been assessed in many countries at parts-per-billion (ppb) and parts-per-trillion (ppt) in wastewater, surface water, as well as drinking water.[10,11] Although these levels are much lower than those used in human applications, the related potential toxic effects are still poorly known and cannot be discarded. Some of these compounds show long environmental persistence, being only partially or slowly biodegradable. Other compounds have rather less persistence but, due to their continuous release into the environment or to the formation of transformation products (TPs) arising from their degradation, they may impact on the aquatic ecosystem and human health.

The growing awareness of this new form of environmental contamination led the scientific community to address an increased interest particularly in pharmaceutical products; their presence (and fate) is of great concern, as they are ubiquitous environmental pollutants that contaminate the environment through a number of point sources.[12,13] Even if the concentration of these residues in the aquatic environment is too low to pose a very acute risk, it is unknown whether other receptors in non-target organisms are susceptible to individual residues or if the combination of drugs sharing a common mechanism of action could exhibit synergistic effects.[14] As a consequence of the discharge of substances subjected to human consumption, products formed through metabolic, abiotic processes and abiotic transformation of products formed through a metabolic process could be found in the environment. Metabolic pathways include phase I and phase II reactions, and both classes of reaction often occur in parallel. Abiotic degradation includes hydrolysis, oxidation, reduction and photolysis pathways, while biotic degradation is defined as the transformation of substances caused by microorganisms (predominantly by bacteria).

A thorough understanding of the pollutant fate therefore requires a comprehensive evaluation of all pathways. However, the information available about the fate of these ECs in aquatic systems appears rather limited.[15,16] At present, systematic data are scarce and insufficient for an environmental risk assessment.[15] This goal is particularly hard to reach and could be achieved only by employing a combined theoretical and experimental approach. In this chapter, an overview of the strategies adopted to overcome this limit, trying to recognize the possible transformation routes occurring in the environment, is presented.

13.2. Strategies to Simulate the Overall Transformations

The main difficulty associated with conducting degradation studies in environmental matrices, in general, is linked with the very low concentrations of the pollutants, which require very sensitive analytical instrumentation. Another important issue is related to the complexity (*i.e.* wastewater) of the matrices, which can affect analytical performance and degradation kinetics of the pollutants.

To predict the fate of persistent organic pollutants in the environment, several aspects have to be considered carefully: their basic physical and chemical properties, distribution, transport within and among compartments, biotic and abiotic transformation processes, as well as effects on living organisms, including humans. Several methodologies have, at present, been explored to comprehend the fate of this new generation of pollutants.

Laboratory simulation of the processes that control the chemical behavior of organic compounds in the environment is often desirable for deeper understanding, as well as for determination of the basic characteristics required for successful environmental modeling.

An experimental methodology could be applied by combining a laboratory study followed by in-field analyses. Several studies were aimed at enlightening the fate of selected drugs, focusing on the identification of their TPs and trying to recognize the main transformation routes followed by these drugs when discharged in the environment. In most cases, the identification of TPs was done by high performance liquid chromatography/high resolution mass spectrometry (HPLC/HRMS). The goal can be attained in two steps. Firstly, laboratory experiments can be performed by using heterogeneous photocatalysis and/or river water spiked with drug(s) under dark or simulated solar light. Secondly, all the possible main and secondary TPs have to be searched for in natural samples. Another approach to simulate the fate of compounds in the environment may consist of the use of the quantitative structure–activity relationship (QSAR) method. The father of the concept of the QSAR is Hansch, who published a free-energy related model to correlate biological activities with physicochemical properties.[17] A QSAR is a statistical model that relates a set of structural descriptors of a chemical compound to its biological activity.

The principal purposes of the QSAR include:

- to predict biological activity and physicochemical properties by rational means;
- to comprehend and rationalize the mechanisms of action within a series of chemicals;
- to provide savings in the cost of product development;
- to reduce the requirement for lengthy and expensive animal tests.

AQ:6 The QSAR modeling process consists of five main steps that are reported in Figure 13.1.

There are a large number of applications of these models within industry, academia and governmental (regulatory) agencies, which comprise:

(1) the estimation of physicochemical properties, biological activities and understanding the physicochemical features behind a biological response in drug design;
(2) the rational design of numerous other products such as surface-active agents, perfumes, dyes and fine chemicals;
(3) the prediction of a variety of physicochemical properties of molecules;
(4) the prediction of the fate of molecules that are released into the environment;
(5) the identification of hazardous compounds at early stages of product development, the prediction of toxicity to humans and the environment.

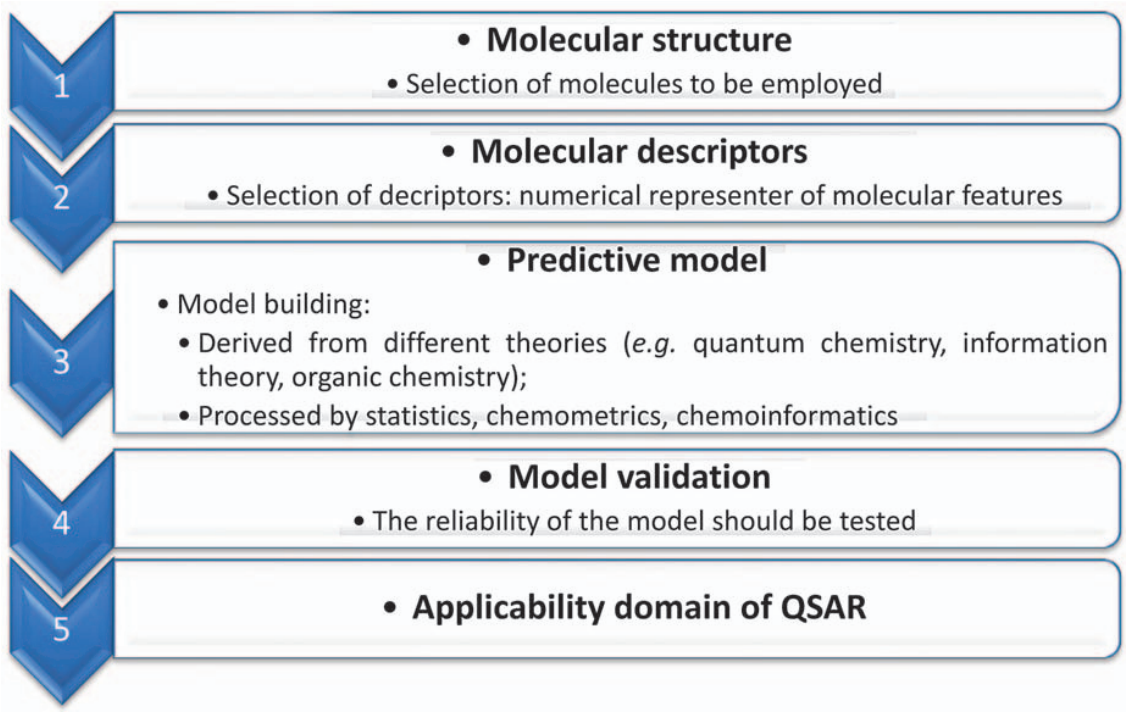

Figure 13.1. QSAR modeling process.

13.2.1. QSAR

The primary source of information about the degradability or persistency of chemicals in different compartments is data arising from contaminated sites as a result of industrial and agricultural activities, discharge of wastewater, accidents, firefighting, military operations, *etc*. Although these field data truly reflect the fate of contaminants, the environmental conditions are very different from each other in terms of the physical or/and chemical conditions (temperature, salinity, pH, radiation, oxygen concentration, presence of nutrients), media (surface or ground water, soil, sediments) and microbial consortia.

In order to approach a systematic assessment of chemicals' biodegradation, predictive test methods have been developed by different organizations such as the Organisation for Economic Co-operation and Development (OECD), International Standards Organization (ISO), Ministry of Economy, Trade and Industry (MITI) Japan, EU, US Environmental Protection Agency (US EPA) and ASTM (formerly the American Society for Testing and Materials). These methods can be classified into three groups:[18]

(1) **Ready biodegradability tests**: stringent screening tests, conducted under aerobic conditions, in which a high concentration of the test substance (in the range of 2 to 100 mg L^{-1}) is used and biodegradation is measured by non-specific parameters like dissolved organic carbon (DOC), biochemical oxygen demand (BOD) and CO_2 production;
(2) **Inherent biodegradation tests**: aerobic tests that possess a high capacity for degradation to take place and in which biodegradation rate or extent is measured. The test procedures allow prolonged exposure of the test substance to microorganisms at a low ratio of test substance to biomass;
(3) **Simulation tests**: aerobic and anaerobic tests that provide data for biodegradation under specified environmentally relevant conditions. These tests simulate the degradation in a specific environment by using indigenous biomass, media, relevant solids (*i.e.* soil, sediment, activated sludge or other surfaces) to allow sorption of the chemical and a typical temperature which represents the particular environment. A low concentration of test substance is used in tests designed to determine the biodegradation rate constant, whereas higher concentrations are normally used for identification and quantification of more abundant TPs.

In these tests, the experimental conditions mimic quite realistically the environmental compartments such as surface water, sediments and soil. Obviously, the complexity of and cost to perform these tests limit their use.

A time and cost-effective alternative to assess the degradation potential of substances is represented by (quantitative) structure–activity relationships ((Q)SARs).

The first attempts to predict the biodegradability of substances on the basis of their chemical structures were developed in the 1980s[19] with a series of statistical correlations named quantitative structural–biodegradation relationships (QSBRs). The use of molecular descriptors such as connectivity indexes, physical/chemical descriptors and descriptors generated from quantum mechanical procedures allowed a very large number of chemicals to be dissected into a few hundred functional groups.

Multiple regression analysis, principal component analysis, partial least squares and different variants of artificial neural networks were used in the computational approaches to derive these QSBRs.[20]

Nowadays, the most popular models are those based on the group contribution approach.[21] Here, the presence or absence of specific 'degradable' groups (linear methanedyl, aliphatic alcohol, ester, *etc*.) and 'non-degradable' groups (chlorine or fluorine atoms, aromatic nitro group, quaternary carbon atom, quaternary amine, *etc*.) are used to estimate the susceptibility of a target compound to undergo abiotic or microbial degradation. This approach takes into account the effect of molecular weight and the frequency of appearance of these groups on the degradation process.

However, these models are thus unable to provide any detail about the formation of persistent or reactive TPs.

The first system attempting to combine in a single model the simulation of metabolism with quantitative assessment of chemical biodegradability and toxicity of chemicals based on simulated metabolism was CATABOL.[22,23]

CATABOL, from the simulation of metabolism, generates a single 'preferred' transformation pathway which was explicitly implemented in the models to predict biodegradation.

In this case, the use of pairs of fragments (source fragments and product(s)) in rule-based models preserves all the advantages of group contribution methods and allows the identification of TPs of the target chemical. A simulation of metabolism and the generation of the metabolic tree can be obtained from recursive application of the transformations.

The common parts of metabolism simulators are a set of transformations and a system of rules that control the application of these transformations. Transformations are more oriented to represent the chemistry, while the rules are focused to reflex the logic of application of these rules.

In the CATALOGIC approach, each transformation consists of a reaction center and corresponding products, which are described by chemical fragments that contain atoms and bonds.

Compared with CATABOL, the stochastic nature of metabolism simulation is replaced in the CATALOGIC approach with a well-organized dynamic chemical specific system of rules and options reflecting the current theoretical and empirical knowledge about the control and goal of the metabolism.

Atom type, hybridization, valence, attached hydrogen or heavy atoms, charge and bond type (*i.e.* single, double, aromatic, ionic, *etc*.) are part of the atomic and bond characteristics used to define the reaction center and the corresponding products. In order to better simulate the metabolic process, a

series of implemented information, empirical or theoretical, was added to each transformation (type of transformation, reaction center, products, local and global forbidden fragments, intrinsic probability of occurrence, list of impossible transformations, list of only possible transformations, list of enzymes associated with the transformation and transformation reliability).

The transformations are separated into two major classes: non-rate determining and rate determining reactions. The first class includes abiotic and biologically mediated transformations, which occur at very high rate compared with the duration of the biodegradation tests.

The generation of the metabolic tree depends on the hierarchy of transformations: the highest hierarchy is ascribed to non-rate determining transformations, the second level of hierarchy depends on the intrinsic transformation probabilities. By a set of the ''general and local options'' in combination with the transformation hierarchy, CATALOGIC controls the application of transformation and mimics the logic of metabolism.

Based on the available theoretical and empirical knowledge, this method, with a mechanistic background and mathematical formalism, allows as much information as possible to be extracted for the degradation potential of chemicals, *i.e.* biodegradability (BOD or CO_2 production), primary and ultimate half-lives, biodegradability within a 10 day window, and quantities of TPs.

13.2.1.1. Some Case Studies

Mahmoud *et al.*[24] carried out a study about the environmental fate of thalidomide (TD), a sedative, hypnotic, immune-modulating and anti-inflammatory pharmaceutical compound. The new increased use of this substance in the treatment of some types of cancer and inflammatory diseases poses a risk to the aquatic environment due to the pharmacological activity of TD and unknown chemical properties of its TPs.

This study investigated the photolytic degradation employing two different light sources and the aerobic biodegradability using two tests from the Organization for Economic Co-operation and Development guidelines (OECD).[25]

In order to investigate the degradation pathway of TD, the detection, quantification and elucidation of structures of its photo-abiotic and biodegradation products were performed by HPLC-UV–Fluorescence-MS^n.

The experimental data were compared with the results obtained from five silicon prediction programs (QSAR MODELS): the EPI Suite Software (EPIWEB 4.1) from US Environmental Protection Agency (US EPA, 2004),[26] two models of Oasis Catalogic software V.5.11.6TB from the Laboratory of Mathematical Chemistry, University Bourgas, Bulgaria (Laboratory of Mathematical Chemistry U'AZBB)[27] and Case Ultra V 1.4.5.1 (MultiCASE Inc.).[28]

In good accordance with QSAR data, the biodegradation results showed that TD and its stable dead-end TPs are not readily degraded, indicating that *silico* prediction programs can be helpful to assess the biodegradability potential in the environment.

In the study of Ioele *et al.*,[29] a quantitative structure–property relationship (QSPR) model was built correlating the photostability of the 1,4-dihydropyridine (1,4-DHP) drugs with global and structural fragment descriptors.

The photodegradation rates, obtained by exposing the drugs to a xenon lamp, combined with a series of descriptors related to the chemical structures, were computed by partial least squares (PLS) multivariate analysis. The influence of different substituents on both benzene and pyridinic rings has been evaluated in terms of hydrophobic, electronic and steric parameters.

The QSPR model was fully cross-validated and then optimized with an external set of novel 1,4-dihydropyridine drugs. The good agreement between predicted and measured photodegradation rate demonstrated the high predictive ability and robustness accuracy of the QSPR model for estimating the photosensitivity of the drugs belonging to this class.

The model was finally proposed as an effective tool to design new congeneric molecules characterized by high photostability.

UV-Vis degradation of iprodione, a pesticide, and the estimation of the acute toxicity related to its photodegradation products were carried out by Lassalle *et al.*[30]

In silico QSAR toxicity predictions, conducted with the Toxicity Estimation Software Tool (T.E.S.T.), revealed that all photoproducts were potentially more toxic and mutagenic than iprodione. An *in vitro* assay on *Vibrio fischeri* confirmed the increase of toxicity of an aqueous iprodione solution after irradiation, in particular due to the formation of phenolic compounds.

13.2.2. Laboratory Simulations and In-field Analysis Based on Laboratory Simulations

Laboratory simulations may involve the use of heterogeneous photocatalysis, employing TiO_2[31,32] or MnO_2[33] as photocatalysts, as it is known to be used to artificially produce degradation compounds similar to those formed through oxido/reductive metabolic and environmental pathways.[34–36] Key reactions occurring at the catalyst surface are schematized in Figure 13.2.

AQ:11 Following irradiation with proper light, holes and electrons are generated and can migrate at the oxide surface or directly react with oxygen or organic compounds; thus, a combination of oxido/reductive reactions occur and AQ:12 promote the transformation of organic compounds. Such a photocatalytic process was employed in several studies as a model system. Typical reactions involve hydroxylation, dealkylation, dehalogenation and molecule breakage. It has to be underlined that the employment of different semiconductor oxides, characterized by a diverse position of the valence and conductive bands, may promote different reactions.

MnO_2-mediated abiotic transformation may be an important chemical process, helpful in understanding what is occurring at the soil–water interface. MnO_2 is typically present in soils and sediments and is among the most important naturally occurring reactant or catalyst in the organic transformation of soil and sediments. It has a high reaction potency with

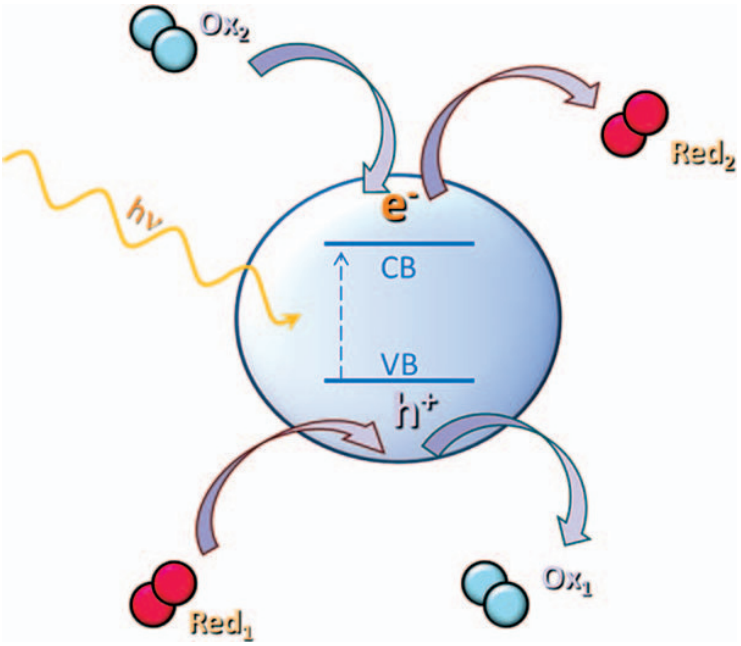

Figure 13.2. Main reactions occurring at the surface of a semiconductor oxide.

several organic pollutants, including anilines, phenols, antibacterial agents, atrazine and acetaminophen.[37–42] These works tried to achieve an AQ:13 understanding of the transformation processes of pollutants in the MnO_2 system and to evaluate the factors influencing their transformation by MnO_2. The mechanistic information helps as a useful foundation for predicting the reactivity of selected pollutants in the soil–water environment and the potential fate and impact of their TPs.

AQ:14 Several studies reported the use of TiO_2 to simulate abiotic transformation of AQ:15 pollutants in surface as well. Extensive use of TiO_2 as a photocatalyst is due to the favorable position of the valence and conduction band on the energy scale (the holes are powerful oxidants, reducing the conduction electrons well), which allows the oxidation of most organic compounds in the presence of AQ:16 dissolved oxygen. In order to characterize the overall TPs and the role of biotic and abiotic processes, a possible approach may entail a sequence of experiments aimed at discriminating the role of photoinduced reactions from those AQ:17 involving biotic processes occurring in the dark. In several cases, laboratory experiments were performed by using river water spiked with the selected pollutant under dark or simulated solar light, in the presence or absence of a photocatalyst. We focus here on key examples where TiO_2 was used to simulate the fate of some drugs included in the priority list of pharmaceutical products and of a ubiquitous pollutant, *N*,*N*-diethyl-*m*-toluamide (DEET).

13.2.2.1. DEET

The use of a TiO_2-mediated process permitted a total of 51 unknown TPs to be produced following DEET degradation, all identified and characterized *via* HPLC-HRMS,[43] and TPs' structural attributions were done by taking into account their MS spectrum, product ions and retention time. These

compounds could be similarly formed in aquatic systems and consequently their presence was monitored firstly in river waters enriched with DEET just after sampling and then verified in the field on river water sampled at several sampling points along the Po River tract (Northern Italy).

Under illumination in spiked river water, DEET was degraded and transformed into numerous organic intermediate compounds, 37 of which could be identified; then, 14 of them were also found in natural river water.[36] It is worth noting that these detected compounds coincide with TPs formed at a higher rate (and amount) in the laboratory experiments. Conversely, TPs formed in low amounts in the laboratory simulation were not detected in the natural samples, even if their evolution profiles are compatible with those followed by the detected species, suggesting their formation was below the detection limit.

DEET environmental transformation involved dealkylation, mono- and poly-hydroxylation followed by oxidation of the hydroxyl groups and cleavage of the alkyl chains; all the recognized TPs may be linked through the transformation pathways summarized in Scheme 13.1. Their formation

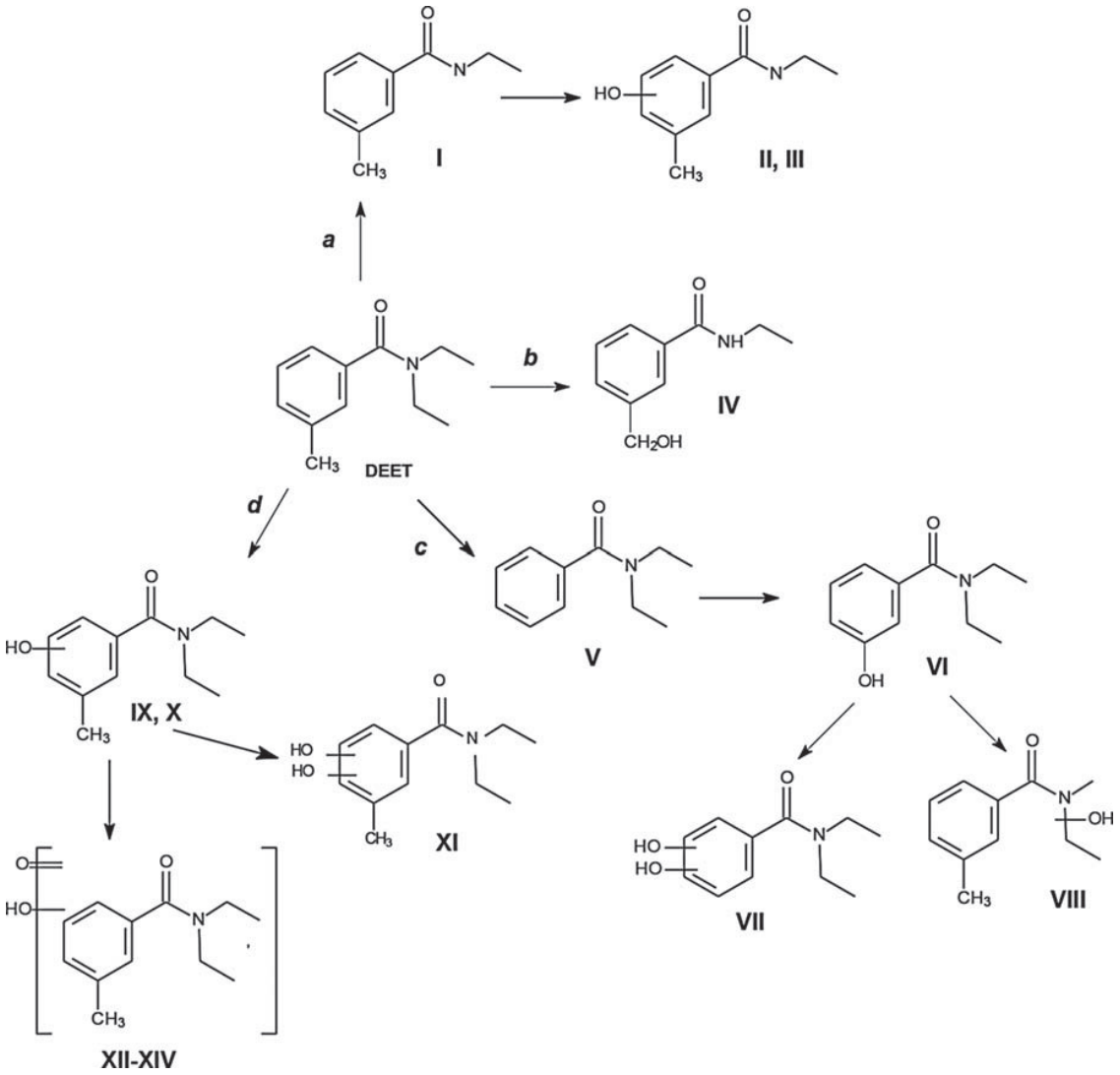

Scheme 13.1 Transformation products formed from DEET in Po river water (scheme adapted from ref. 36).

could occur through a combination of biotic and abiotic pathways; two TPs, namely **I** and **V**, were mainly formed in dark conditions, while the others are chiefly produced through indirect photolysis processes mediated by natural photosensitizers such as dissolved organic matter, nitrite and nitrate ions, H_2O_2 and iron species.[44]

13.2.2.2. Pharmaceuticals

The aqueous environmental fate of three antibiotics, spiramycin, lincomycin and clarithromycin, and an antiepileptic drug, carbamazepine, is discussed.

Clarithromycin, lincomycin and carbamazepine were detected in river samples, together with a number of degradation compounds previously characterized through a photocatalytic process coupled with HPLC/HRMS analysis,[45,46] allowing the monitoring of the drug presence and its TPs in environmental analysis. Interestingly, carbamazepine appears at higher concentrations than the other two drugs: this is consistent with the degradation tests conducted in the laboratory that have shown how carbamazepine has longer persistence in the aquatic compartment.

Eight TPs identified in the laboratory simulation were also found in natural river water from carbamazepine degradation, three from clarithromycin and two from lincomycin. Their transformation mainly involved mono- and poly-hydroxylation followed by oxidation of the hydroxyl groups.

Considering carbamazepine, TPs could be formed following three initial pathways, summarized in Scheme 13.2,[47] and involving hydroxylation (pathway A), hydroxylation and ring contraction (pathway B) and hydration on the double bond (pathway C). A qualitative assessment can highlight that the main TPs were those arising from hydration on the C_{10}–C_{11} double bond and monohydroxylation.

Based on the peak areas, the sum of all TPs found was roughly 50% of the drug amount, underlining that almost 50% of the drug was degraded. The temporal profiles show similar kinetics of formation/disappearance for all the detected TPs, such that, by analysing their relative ratios, it is possible to understand which are the predominant transformation pathways followed in river water. Compounds **253**, **269** and **285** are closely related through a hydroxylation mechanism that involves a sequence of hydroxyl addition; the lower amount detected is due to the consecutive pathways depicted in Scheme 13.2. Compounds **271** and **287** could be formed through human metabolism[9,16] or photolysis as well. Analysis of the relative TP ratios obtained in laboratory and in-field samples show that the ratio **253**/**271** passed from 1.33 (laboratory data) to 0.7 for field samples. This could be the expression of a remarkable effect of human metabolism in the drug transformation, particularly for pathway C. Nevertheless, even if compound **253-B**, formed through pathway A, could be formed as a human metabolite, di and tri-hydroxy-carbamazepine formation should be attributed to a photochemical process, in agreement with the carbamazepine modeled fate.[48] This permits these compounds to be considered as markers of a photoinitiated carbamazepine transformation in the aquatic environment.

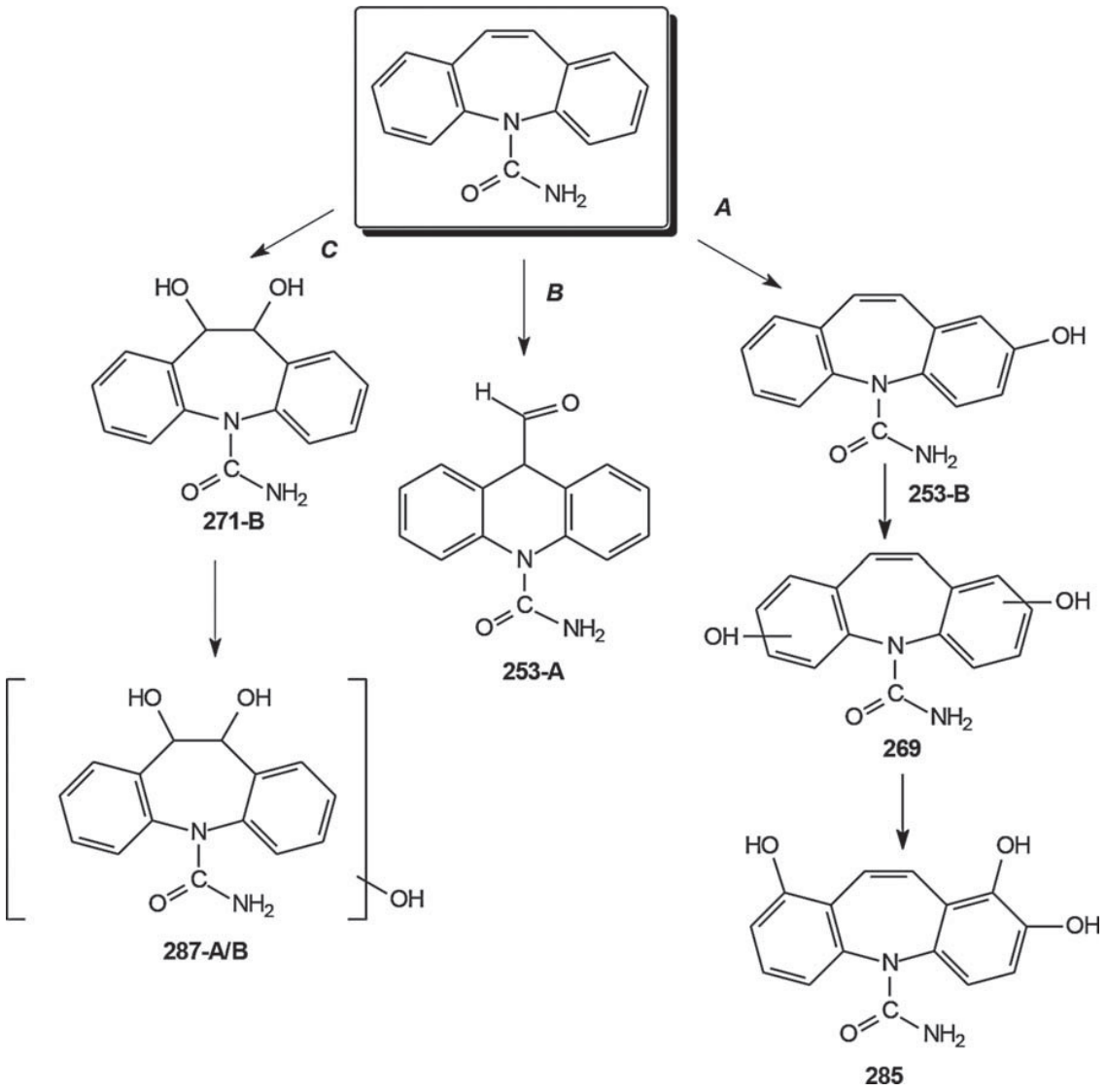

Scheme 13.2 Transformation products formed from carbamazepine in Po river water.

Considering the case of spiramycin, a widely used veterinary macrolide antibiotic, the aqueous environmental fate of this antibiotic compound in the first stage was studied through laboratory simulation performed on river water spiked with the drug, where drug decomposition and the identification of the main and secondary TPs were monitored by HPLC/HRMS.[35] Laboratory experiments permitted assessment that, even if biotic degradation contributed to the drug's disappearance, aqueous photolysis is rapid and will be the main route of degradation in aquatic systems exposed to sunlight. Furthermore, both direct and indirect photolysis processes took part in spiramycin degradation. Under illumination, spiramycin was degraded rapidly and transformed into numerous intermediate compounds, of which 11 could be identified; these TPs could be formed through five initial transformation routes, collected in Scheme 13.3.

These laboratory simulation experiments were then verified in-field in Po River water (N-Italy) at several sampling points. Spiramycin was found at

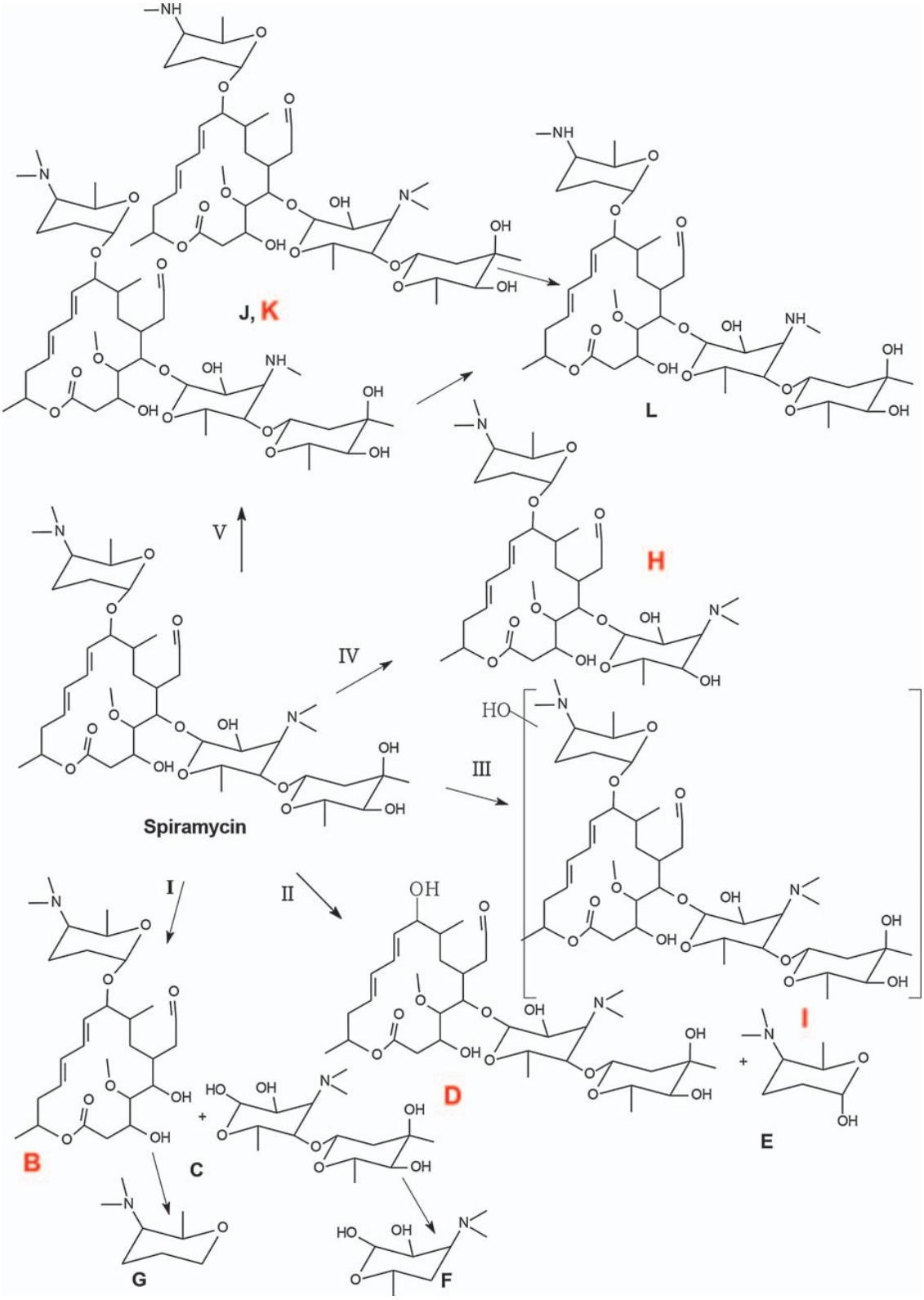

Scheme 13.3 Transformation products formed from spiramycin under different conditions.

traceable levels (ng L^{-1} range), together with five previously identified TPs, marked in red in Scheme 13.3. Again, it is worth noting that these compounds coincide with the TPs formed at a higher rate (and amount) in the

laboratory experiments. The transformation occurring in the aquatic system involved hydroxylation, demethylation and the detachment of forosamine or mycarose sugars. Three of them seem to be formed through a direct photolysis process and involve detachment of mycarose/mycaminose (namely **B**), detachment of forosamine (namely **D**) and demethylation (namely **K**). The other two TPs, hydroxyl-spiramycin, namely **I**, and neospiramycin, namely **H**, had already been detected during photocatalytic experiments, but not through direct photolysis, so their formation in the Po River samples could be attributed to indirect photolysis processes mediated by natural species.[44]

13.3. Conclusions

From decades ago to recent research, QSAR methods have been applied in the development of the relationship between properties of chemical substances and their biological activities to obtain a reliable statistical model for prediction of the activities of new chemical compounds.

Moreover, several publications described development of QSAR/QSPR models to rapidly assess a substance's environmental fate, toxicity and biodegradation. The results of the predictions, in many cases in very good agreement with the experimental evidence, suggest that these approaches can be employed as a highly promising tool for the fast and efficient assessment of the environmental fate of different compound classes.

On the other hand, the photocatalytic process demonstrated itself as helpful to produce a number of degradation compounds, identified by HRMS combined with HPLC, whose measurement gives a useful tool to monitor drug presence and transformation in environmental analysis.

This approach has not only permitted assessment of the selected drug's presence in natural waters but also identification of which of the transformation routes recognized in simulation experiments also occurred in the aquatic environment. Some of them seem to be formed through a biotic or abiotic process. Specifically for the case of carbamazepine, it was possible to find some key TPs that could be considered as markers for its photochemical environmental transformation in the aquatic environment.

References

1. V. Petit, R. Cabridenc, R. P. J. Swannell and R. S. Sokhi, *Environ. Int.*, 1995, **21**, 167.
2. R. A. Larson and E. J. Weber, *Reaction Mechanisms in Environmental Organic Chemistry, CRC press*, Lewis Publishers, Boca Raton, FL, 1994.
3. M. Stuart, D. Lapworth, E. Crane and A. Hart, *Sci. Total Environ.*, 2012, **416**, 1.
4. S. D. Richardson and T. A. Ternes, *Anal. Chem.*, 2011, **83**, 4614.
5. S. D. Richardson and T. A. Ternes, *Anal. Chem.*, 2014, **86**, 2813.
6. C. G. Daughton, *J. Am. Soc. Mass Spectrom.*, 2001, **12**, 1067.
7. C. Zwiener, *Anal. Bioanal. Chem.*, 2007, **387**, 1159.

8. S. K. Khetan and T. J. Collins, *Chem. Rev.*, 2007, **107**, 2319–2364.
9. D. Barceló and M. Petrovic, *Anal. Bioanal. Chem.*, 2007, **387**, 1141.
10. T. Heberer, *Toxicol. Lett.*, 2002, **131**, 5.
11. S. D. Costanzo, J. Murby and J. Bates, *Mar. Pollut. Bull.*, 2005, **51**, 218.
12. S. K. Khetan and T. J. Collins, *Chem. Rev.*, 2007, **107**, 2319.
13. C. G. Daughton and T. Ternes, *Environ. Health Perspect.*, 1999, **107**, 907.
14. C. Hao, X. Zhao and P. Yang, *TrAC, Trends Anal. Chem.*, 2007, **26**, 569.
15. E. Zuccato, S. Castiglioni, R. Bagnati, M. Melis and R. Fanelli, *J. Hazard. Mater.*, 2010, **179**, 1042.
16. X. S. Miao, J. J. Yang and C. D. Metcalfe, *Anal. Chem.*, 2003, **75**, 3731.
17. C. Hansch, *Acc. Chem. Res.*, 1969, **2**, 232.
18. S. Dimitrov, T. Pavlov, N. Dimitrova, D. Georfieva, D. Nedelcheva, A. Kesova, R. Vailev and O. Mekenyan, *SAR QSAR Environ. Res.*, 2011, **22**, 719.
19. J. Hermens, S. Balaz, J. Damborsky, W. Karcher, M. Müller, W. Peijnenburg, A. Sabljic and M. Sjöström, *SAR QSAR Environ. Res.*, 1995, **3**, 223.
20. E. Rorije, M. C. van Wezel and W. Peijnenburg, *SAR QSAR Environ. Res.*, 1995, **4**, 219.
21. J. Tunkel, P. H. Howard, R. S. Boethling, W. Stiteler and H. Loonen, *Environ. Toxicol. Chem.*, 2000, **19**, 2478.
22. S. D. Dimitrov, J. S. Jaworska, N. Nikolova and O. G. Mekenyan, *9th International Workshop on Quantitative Structure– Activity Relationships in Environmental Sciences* (QSAR'2000), Bourgas, 2000.
23. J. Jaworska, S. Dimitrov, N. Nikolova and O. Mekenyan, *SAR QSAR Environ. Res.*, 2002, **13**, 307.
24. W. M. M. Mahmoud, C. Trautwein, C. Leder and K. Kummerer, *Sci. Total Environ.*, 2013, **463–464**, 140.
25. Organization for Economic Co-operation and Development. OECD guidelines for the testing of chemicals 310D: ready biodegradability. Closed bottle test. Paris OECD Publishing, 1992.
26. US EPA United States Environmental Protection Agency. EPA/OPPT/Exposure Assessment Tools and Models/Estimation Program Interface (EPI) suite version 3.12 (August 17, 2004). http://www.epa.gov/oppt/exposure/pubs/episuite.htm, 2004. [accessed November 28, 2012].
27. Laboratory of Mathematical Chemistry. ''Prof. Dr. Assen Zlatarov'' University, Bourgas, Bulgaria. Oasis Catalogic software V.5.11.6TB; 2012.
28. S. K. Chakravarti, R. D. Saiakhov and G. Klopman, *J. Chem. Inf. Model.*, 2012, **52**, 2609.
29. G. Ioele, M. De Luca, F. Olivierio and G. Ragno, *Talanta*, 2009, **79**, 1418.
30. Y. Lassalle, H. Jellouli, L. Ballerini, Y. Souissi, E. Nicol, S. Bourcier and S. Bouchonnet, *J. Chromatogr. A*, 2014, **1371**, 146.
31. V. A. Sakkas, P. Calza, C. Medana, A. E. Villioti, C. Baiocchi, E. Pelizzetti and T. Albanis, *Appl. Catal., B*, 2007, **77**, 135.
32. C. Medana, P. Calza, F. Carbone, E. Pelizzetti, H. Hidaka and C. Baiocchi, *Rapid Commun. Mass Spectrom.*, 2008, **22**, 301.
33. H. Xiao, H. Song, H. Xie, W. Huang, J. Tan and J. Wu, *J. Hazard. Mater.*, 2013, **250–251**, 138.
34. P. Calza, C. Medana, M. Pazzi, C. Baiocchi and E. Pelizzetti, *J. Pharm. Biomed. Anal.*, 2004, **35**, 9.
35. P. Calza, S. Marchisio, C. Medana and C. Baiocchi, *Anal. Bioanal. Chem.*, 2010, **396**, 1539.

36. P. Calza, C. Medana, E. Raso, V. Giancotti and C. Minero, *Sci. Total Environ.*, 2011, **409**, 3894.
37. J. Y. Shin and M. A. Cheney, *Colloids Surf., A*, 2004, **242**, 85.
38. H. Zhang, W. R. Chen and C. H. Huang, *Environ. Sci. Technol.*, 2008, **42**, 5548.
39. G. Chen, L. Zhao and Y. H. Dong, *J. Hazard. Mater.*, 2011, **193**, 128.
40. W. R. Chen and C. H. Huang, *Environ. Pollut.*, 2011, **159**, 1092.
41. H. Selig, T. M. Keinath and W. J. Weber Jr., *Environ. Sci. Technol.*, 2003, **37**, 4122.
42. H. Xiao, H. Song, H. Xie, W. Huang, J. Tan and J. Wu, *J. Hazard. Mater.*, 2013, **250–251**, 138.
43. C. Medana, P. Calza, F. Del Bello, E. Raso, C. Minero and C. Baiocchi, *J. Mass Spectrom.*, 2011, **46**, 24.
44. P. Boule, D. W. Bahenmann, D. W. Robertson and P. K. J. Robertson, *The handbook of environmental Chemistry*, Springer, Berlin, 2005.
45. P. Calza, C. Medana, E. Padovano, F. Dal Bello and C. Baiocchi, *J. Mass Spectrom.*, 2012, **47**, 751.
46. P. Calza, C. Medana, E. Padovano, V. Giancotti and C. Baiocchi, *Rapid Commun. Mass Spectrom.*, 2012, **26**, 1687.
47. P. Calza, C. Medana, E. Padovano, V. Giancotti and C. Minero, *Environ. Sci. Pollut. Res.*, 2013, **20**(4), 2262–2270.
48. E. De Laurentiis, S. Chiron, S. Kouras-Hadef, C. Richard, M. Minella, V. Maurino, C. Minero and D. Vione, *Environ. Sci. Technol.*, 2012, **46**, 8164.

Photocatalytic degradation of Irgarol in water by photo-Fenton reactions

Fawzy Eissa[a,c], Nour El-Hoda Zidan[b,c], Hiroshi Sakugawa[*c]

[a] Environment and Bio-Agriculture Department, Faculty of Agriculture, Al-Azhar University, 11884, Nasr City, Cairo, Egypt.

[b] Pesticides Chemistry and Toxicology Department, Faculty of Agriculture, 33516, Kafrelsheikh University, Kafr El-Sheikh, Egypt.

[c] Department of Environmental Dynamics and Management, Graduate School of Biosphere Science, Hiroshima University, 1-7-1 Kagamiyama, Higashi, Hiroshima 739-8521, Japan.

*Corresponding author email: hsakuga@hiroshima-u.ac.jp;

Abstract

The degradation behavior of the pesticide Irgarol 1051 in pure (Milli-Q) and river water samples in response to photolysis and Fenton reactions was investigated and the hydroxyl radical ($^{\bullet}OH$) formation rate was determined. Irgarol photolysis was found to occur at a much slower rate in both types of water in terms of the half-life ($t_{1/2}$) and degradation rate constant (k). Prolongation of photolysis did not lead to complete degradation, even after 480 min. Conversely, Irgarol was rapidly degraded in pure water at pH 3 after 12 and 16 min of irradiation via the photo-Fenton reaction (Fe^{2+}/H_2O_2/UV-Vis) and photo-Fenton-like reaction (Fe^{3+}/H_2O_2/UV-Vis), respectively, because of the generation of additional $^{\bullet}OH$. Irgarol was also completely degraded by the Fe^{2+}/H_2O_2/UV-Vis and Fe^{3+}/H_2O_2/UV-Vis reactions in river water at pH 3 after 60 min, while it disappeared after 180 min of irradiation by the Fe^{2+}/H_2O_2/UV-Vis reaction at pH 5. The photodegradation rates of Irgarol in pure and river water were consistent with the $^{\bullet}OH$ generation rates in both types of water. Mineralization of 96.9 and 92.9% of the Irgarol was achieved in pure water at pH 3 after 16 h of irradiation by the Fe^{3+}/H_2O_2/UV-Vis and Fe^{2+}/H_2O_2/UV-Vis systems, respectively. Overall, these results indicate that photo-Fenton reactions are useful for treating Irgarol-contaminated water.

Keywords**:** Fenton reactions, pesticide, $^{\bullet}OH$, mineralization, water**.**

Table of Contents

1. Introduction

The s-triazine herbicide Irgarol 1051 (N'-tert-butyl-N-cyclopropyl-6-(methylthio)-1,3,5-triazine-2,4-diamine) was introduced as an alternative antifouling paint booster biocide to tributyltin (TBT) compounds, which were banned in 2003 (IMO, 2001) because of their adverse effects on non-target species (Alzieu, 2000). The Anti-Fouling System Treaty of the International Maritime Organization (IMO), which entered into force in 2008, completely prohibited the use of organotin-based antifouling paints on ships of any size (Dafforn et al., 2011). Antifouling paints are applied to the hulls of boats and ships, as well as to submerged structures such as oil rig supports, pipes, buoys and fish cages to prevent adhesion and colonization by aquatic organisms, especially mollusks and algae (Evans et al., 2000; Koutsaftis and Aoyama, 2007). Irgarol is highly effective against freshwater and marine algal fouling because it inhibits photosynthetic electron transport within the chloroplasts of photosystem II (Hall and Gardinali, 2004).

Irgarol 1051 is currently one of the most widely applied booster algicides in copper-based antifouling paint formulations (Sapozhnikova et al., 2013). Accordingly, it is the antifouling paint booster biocide most often found in aquatic environments because of permanent leaching from painted ship hulls (Carbery et al., 2006; Zhou, 2008; Sapozhnikova et al., 2013; Kim et al., 2014; Saleh et al., 2014) Irgarol 1051 is highly toxic to macrophytes, phytoplankton and periphyton (Okamura et al., 2003; Mohr et al., 2008), and is also relatively persistent, with a half-life in seawater of 24 to 100 days (Liu et al., 1999; Konstantinou and Albanis, 2004). Owing to its toxic and persistent nature, Denmark, the Netherlands, Sweden, and the UK, have restricted its use (Thomas and Brooks, 2010).

The existence of persistent pesticides in water should be investigated to enable their elimination. While many traditional technologies are effective, they are often costly and time-

consuming (Schwarzenbach et al., 2006). Advanced oxidation processes (AOPs) have received increased attention as potential alternatives because of their ability to degrade a wide range of refractory contaminants found in the environment (Doria et al., 2013). According to Pirkanniemi and Sillanpää (2002), homogeneous AOPs such as the Fenton reaction have the potential for use in water treatment and remediation processes. The Fenton reaction, which involves H_2O_2 and ferrous iron (Fe^{2+}), has been shown to be effective at degrading a wide spectrum of organic and inorganic pollutants via the formation of hydroxyl radicals (Pignatello et al., 2006). If ferrous iron is replaced by ferric iron (Fe^{3+}), it is called a Fenton-like reaction, while it is referred to as a photo-Fenton reaction when complemented with UV/visible radiation. Hydroxyl radical ($^{\bullet}OH$) is capable of oxidizing and mineralizing almost any organic molecule to yield CO_2, H_2O, and corresponding mineral acids (Macounova et al., 2003). However, little information is available regarding the photodegradation of Irgarol by Fenton reactions.

Accordingly, this study was conducted to compare the efficiency of different Fenton systems and extend their optimal pH toward neutral conditions, to enable the greatest degradation and mineralization of Irgarol from water. Moreover, the rate of $^{\bullet}OH$ formation under different Fenton systems was determined to evaluate the role of this radical in the degradation of Irgarol.

2. Materials and methods

2.1. Chemicals

Irgarol 99% and commercial phenol standard stock solution (100 mg L^{-1} of phenol) were purchased from Sigma-Aldrich, Japan. Hydrogen peroxide (30%) was obtained from Cica-reagent, Kanto Chemical Co., Inc., Japan. Acetonitrile, benzene (HPLC grade, >99.5%) and

ferrous sulfate ($FeSO_4 \cdot 7H_2O$) (99%) were obtained from Nacalai Tesque Inc., Japan. Ferric chloride ($FeCl_3 \cdot 6H_2O$) (99%) was acquired from Katayama Chemicals, Japan. 2-Nitrobenzaldehyde was purchased from Tokyo Kasei Kogyo. All solutions were prepared with ultra-pure water obtained from a Milli-Q Plus system, Japan (Millipore; ≥ 18 MΩ cm).

2.2. River water analysis

Surface river water samples were collected from the Kurose River at the Ochiai bridge site, next to the water treatment facility that serves the City of Higashi Hiroshima, Japan (34°23′10.8″ N, 132°43′24.5″E). The water samples were filtered through a glass fiber filter (GC-50, 47 mm diameter, 0.5 µm pore size, Advantec), after which the anions (Cl^-, NO_2^-, NO_3^- and SO_4^{2-}) and cations (Na^+, NH_4^+, K^+, Mg^{2+} and Ca^{2+}) were analyzed using a Dionex ion chromatography (Dionex ICS-1600, Japan). In addition, dissolved organic carbon (DOC) and conductivity were measured using a total organic carbon analyzer (TOC analyzer, TOC-V_{CSH}, Shimadzu Co., Kyoto, Japan) and a pH meter (Model D-51, Horiba Co., Japan), respectively. The chemical composition of river water is given in Table (1). It was also confirmed that the river water samples contained no detectable Irgarol.

2.3. Photodegradation experiments

For the irradiation experiments, Irgarol was added to pure and river water (50 mL aliquot volume) at an initial concentration of 0.1 mg L^{-1}, after which Fe^{2+} or Fe^{3+} and H_2O_2 were added at specific concentrations. The pH of the reaction mixture was then adjusted by the addition of dilute aqueous HCl or NaOH. Next, samples were transferred to a quartz cell and irradiated using

a solar simulator (Oriel model 81160-1000, Oriel Corp.) equipped with a 300-W Xenon lamp (ozone free, model 6258, Oriel Corp.) and special glass filters restricting the transmission of wavelengths below 300 nm. The emission wavelengths of the xenon lamp range from 300 to 800 nm, which is very close to that of natural sunlight (Durand et al., 1991).

During irradiation, the sample solution was well mixed with a stirring bar and the temperature was kept at 20°C. Aliquots of the irradiated samples were removed at regular intervals and filtered through a 0.45-μm Ekicrodisc syringe filter, after which samples were subjected to HPLC analysis using a system composed of a PU-2089 plus pump (Jasco, Japan) and a Rheodyne injection valve (Cotati, California, USA) with a 50-μL sample loop. The column was an Ultron VX-ODS (Supelcosil LC-18, particle size 5 μm; Supelco) with a length of 250 mm and an inner diameter (ID) of 4.6 mm. A guard column (Supelcosil LC-18, 5 μm, 10 mm × 4.6 mm ID) was fitted in the front of the analytical column. A mixture of acetonitrile and pure water (60/40, v/v) was applied as the mobile phase at a flow rate of 1 ml min^{-1} and samples were detected at 223 nm using a UV-VIS detector (SPD-10A, Shimadzu). The Irgarol retention time under the aforementioned conditions was 10.97 min. Calibration was conducted based on the peak areas of standard samples, analyzed under the same HPLC conditions.

Similar procedures were followed for dark Fenton reactions. The detection and quantification limits for Irgarol were 0.496 and 0.827 μg L^{-1} in water samples, respectively. The degradation of Irgarol followed first-order kinetics, and the half-life values ($t_{1/2}$) were calculated using the equation $t_{1/2} = \ln 2/k$ (Moye et al., 1987), where k is the degradation rate constant.

2.4. Determination of •OH radical formation rate

Hydroxyl radical formation rates under different Fenton systems (Fe^{2+}/H_2O_2/UV-Vis, Fe^{3+}/H_2O_2/UV-Vis, Fe^{2+}/H_2O_2/Dark and Fe^{3+}/H_2O_2/Dark) in both pure and river water were determined after the addition of benzene as a chemical probe to water in a reaction cell. Phenol produced by the reaction between •OH and the benzene added to the water sample was determined by HPLC as a function of time to quantify the •OH formation rate in the presence and absence of simulated sunlight. At the beginning of each experiment, an aliquot of aqueous benzene stock solution (2×10^{-2} M) was added to water to give an initial benzene concentration of 1.2 mM. The solution was then spiked with Fenton's reagent (Fe^{2+} or Fe^{3+} and H_2O_2), stirred to mix the solution, transferred to a quartz cell (60 mL) and irradiated (if applicable) using the solar simulator.

The initial pH of the diluted solution was adjusted to 3 with HCl in all experiments (Huston and Pignatello, 1999). During irradiation, the solution in the quartz cell was mixed well with a stirring bar and the temperature was kept at 20°C. Aliquots were removed from the irradiated samples at regular intervals for HPLC analysis. All experimental conditions were the same both in the presence and in the absence of simulated sunlight.

Phenol was analyzed by HPLC using a system with a fluorescence detector (Shimadzu, RF-10AXL) operated at 270 and 298 nm for excitation and emission, respectively. Analytical signals were recorded by an integrator (Shimadzu, CR-6A). The detection limit of phenol using this HPLC system was 2×10^{-9} M. The •OH formation rate (R_{OH}) was determined as follows:

$$R_{OH} = \frac{R_{phenol}}{Y_{phenol} \times F_{benzene,OH}}$$

where R_{phenol} is the photoformation rate of phenol in water samples (M s^{-1}), Y_{phenol} is the yield of phenol formed per benzene oxidized by •OH (mean ± standard deviation = 0.75 ± 0.07, Arakaki and Faust, 1998), and $F_{benzene,OH}$ is the fraction of •OH that reacts with benzene, which was assumed to be 1.00 in the present study. It should be noted that the actual $F_{benzene,OH}$ value may be slightly lower than 1.00 because of possible reactions of •OH with other scavengers such as H_2O_2 and Fe used for the Fenton reagent. In contrast, the effects on •OH scavenging of other chemical species present in the experimental aquatic systems (*e.g.*, river water) used for the Fenton reactions in the present study were very limited, compared to benzene. For these reasons, it can be assumed that $F_{benzene,OH}$ = 1.00 with excellent approximation.

2.5. Light intensity determination

The irradiation light intensity for each day of the photochemical experiments was determined using 2-nitrobenzaldehyde (2-NB) as chemical actinometer (Kuhn et al., 2004), in the same reaction cell that was used to quantify •OH. The 2-NB photolysis rate constant ($J_{2\text{-NB}}$) was determined by HPLC with a UV detector set to a wavelength of 260 nm. The column, mobile phase and flow rate were the same as for the determination of Irgarol and •OH. The value of $J_{2\text{-NB}}$ obtained in the present study was 0.0058 s^{-1}. For this study, the •OH photoformation rates were normalized to $J_{2\text{-NB}}$ = 0.0093 s^{-1}, which was determined at noon, under clear-sky conditions in Higashi Hiroshima (34°N) on October 7th, 2002 (Takeda et al., 2005). It is important to note that the photochemical reaction depends on both the light intensity and the wavelength of the light source. However, this normalization using the 2-NB photolysis rate constant enables a comparison to be made between datasets, as well as a quantitative discussion on the contribution from each •OH source.

2.6. Mineralization

The trend of mineralization in the irradiated solutions, with an initial Irgarol concentration of 2.5 mg carbon L^{-1}, was monitored by measuring the TOC concentration at regular intervals after Ekicrodisc filtration. It was used a Shimadzu TOC-V_{CSH} analyzer, which works according to the thermal catalytic oxidation principle. Platinum was used as a catalyst to carry out the combustion reaction at 680°C, while oxygen was applied as the carrier gas at a flow rate of 150 mL min^{-1}. The detection was carried out using a non-dispersive infrared (NDIR) detector. Calibration of the analyzer was carried out using potassium hydrogen phthalate standards.

All experiments were conducted in triplicate, and data are reported as the average ± the standard deviation (SD). Analyses were conducted using SPSS (Statistical Package for the Social Sciences, version 16.0; SPSS Inc., Chicago, IL, USA).

3. Results and discussion

3.1. Photolysis of Irgarol

In this study, direct photolysis experiments were carried out using both pure and river water at pH 3, 5 and 7. As shown in Fig. (1), Irgarol showed greater degradation in pure water than in river water, as well as at pH 3 than at pH 5 or 7 in both types of water. Irgarol completely disappeared after 6 h in pure water at pH 3 ($t_{1/2}$ = 86.6 min; k = 0.008 min^{-1}), while it was not completely degraded in river water at the same pH, even after 8 h of irradiation ($t_{1/2}$ = 93.7 min; k = 0.0074 min^{-1}). These findings indicate that the water type plays an important role in the

photolysis of Irgarol. Conversely, 10.6 and 75.7% of the parent compound remained after 8 h of irradiation at pH 7 in pure water ($t_{1/2}$ = 217 min; k = 0.0032 min^{-1}) and river water ($t_{1/2}$ = 1200 min; k = 0.00058 min^{-1}), respectively. Interestingly, no noticeable hydrolysis of Irgarol occurred at 20°C in aqueous solutions at pH 3, 5 and 7 in both pure and river water over a period of 30 d (data not shown). These findings indicate that the hydrolytic processes of Irgarol during the course of the photolysis experiments can be ignored. Photolysis is one of the major transformation processes that influence the fate of pesticides in the aquatic environment (Durand et al., 1992). These results agree with those obtained by Okamura et al. (1999), who found that Irgarol is rather stable toward hydrolysis, but undergoes sunlight-induced photodegradation in aqueous solution. Similar results were also observed by Zamy et al. (2004), who demonstrated that the photolysis of profenofos and isofenfos in water from the Capot River occurred more slowly than in purified water. However, shorter photolysis half-lives were obtained in this study for Irgarol than it has been previously reported. Sakkas et al. (2002) indicated that the half-life of Irgarol was 29 h in distilled water. Under irradiation within the range of 300 to 450 nm, less than 50% of Irgarol (10^{-5} M) in MilliQ water (pH 6.5) was transformed after 48 h (Amine-Khodja et al., 2006). It is possible that such differences are accounted for by the different irradiation intensities of the used lamps.

3.2. Optimization of Fe^{2+}, Fe^{3+} and H_2O_2 concentrations for the removal of Irgarol from pure water using the photo-Fenton systems

The photodegradation kinetics of Irgarol (0.1 mg L^{-1}) at various concentrations of Fe^{2+} (0.0032, 0.0063 and 0.013 mM) and H_2O_2 (0.064, 0.13 and 0.25 mM) were studied in pure water at pH 3 to evaluate the effects of reactants concentration on the degradation rate. The Fenton reagent was

also applied to degrade Irgarol at three concentrations of Fe^{3+} (0.025, 0.05 and 0.1 mM) and H_2O_2 (0.126, 0.5 and 1.0 mM), to examine the oxidation rates in pure water at pH 3. As shown in Fig. (2a), Irgarol photodegradation at the highest concentrations of Fe^{2+} and H_2O_2 ($t_{1/2}$ = 0.61 min; k = 1.13 min^{-1}) was better than that at the middle concentration levels ($t_{1/2}$ = 1.06 min; k = 0.651 min^{-1}), while photodegradation at the lowest concentrations was far slower compared to the other two cases ($t_{1/2}$ = 4.15 min; k = 0.167 min^{-1}). As shown in Fig. (2b), similar results were observed for the photo-Fenton-like reaction (Fe^{3+} + H_2O_2). Overall, complete disappearance of Irgarol was achieved after 8, 16 and 32 min at the highest, middle and lowest concentrations of Fe^{3+} and H_2O_2, respectively.

The middle concentrations of Fe^{2+}, Fe^{3+} and H_2O_2 were used hereafter in this study for economic and practical reasons, and because higher concentrations of Fe and H_2O_2 have been shown to lead to less effective degradation of organic pollutants through self-scavenging of $^{\bullet}OH$ (Catastini et al., 2002; El-Morsi et al., 2002). Moreover, the use of a much higher concentration of Fe results in the need for its removal after treatment, which should be avoided.

3.3. Irgarol degradation using Fenton reactions

As shown in Fig. (3), Irgarol was rapidly degraded in pure water at pH 3 after 12 ($t_{1/2}$ = 1.06 min; k = 0.65 min^{-1}) and 16 ($t_{1/2}$ = 1.86 min; k = 0.37 min^{-1}) min irradiation by photo-Fenton reaction [Fe^{2+} (0.0063 mM)/H_2O_2 (0.126 mM)/UV-Vis] and photo-Fenton-like reaction [Fe^{3+} (0.05 mM)/H_2O_2 (1 mM)/UV-Vis], respectively. Moreover, it was fully decomposed by the same reactions after 315 ($t_{1/2}$ = 61.9 min; k = 0.011 min^{-1}) and 405 ($t_{1/2}$ = 83.5 min; k = 0.0083 min^{-1}) min in the dark, respectively. Degradation of Irgarol in pure water under simulated solar light by photo-Fenton reactions was significantly faster than under dark conditions. The great

enhancement in degradation under light conditions was due to the higher rate of $^{\bullet}OH$ generation (*vide infra*), as well as to photochemical reactions.

As shown in Fig. 3, the degradation of Irgarol was faster during the photo-Fenton reaction than in the photo-Fenton-like reaction at lower molar concentrations of iron and H_2O_2. When ferrous salts are used in the Fenton reaction, hydroxyl radicals are produced immediately by the rapid reaction between ferrous iron and hydrogen peroxide (Eq. 1; Walling, 1975). With ferric salts, the hydroxyl radical is produced in a two-stage process. Specifically, there is a slow reaction between ferric ion and hydrogen peroxide (Eq. 2), followed by a rapid reaction between the produced ferrous ion and additional hydrogen peroxide (Kiwi et al., 1993):

$$Fe^{2+} + H_2O_2 \longrightarrow Fe^{3+} + {}^{\bullet}OH + OH^{-} \qquad (1)$$

$$Fe^{3+} + H_2O_2 \longrightarrow Fe^{2+} + HO_2^{\bullet} + H^{+} \qquad (2)$$

The hydroxyl radicals thus formed react rapidly and non-selectively with most organic compounds (Eq. 3), through three types of reactions: additions to double bonds, abstraction of a hydrogen atom, or electron transfer (Buxton et al., 1988; Haag and Yao, 1992). The consequence is the chemical decomposition of the organic substrate *via* the following general pathway:

$$^{\bullet}OH + \text{Organic compounds} \longrightarrow \text{Degradation products} \qquad (3)$$

Irgarol degradation in river water at pH 3 under simulated solar light was significantly faster than under dark conditions (Fig. 4). Irgarol was completely degraded by Fe^{2+}/H_2O_2/UV-Vis ($t_{1/2}$ = 15.1 min; k = 0.046 min^{-1}) and Fe^{3+}/H_2O_2/UV-Vis ($t_{1/2}$ = 8.32 min; k = 0.0833min^{-1}) in river water at pH 3 after 60 min. Conversely, Irgarol decomposition was found to be markedly slower under dark conditions, and it id not proceed to completion at the investigated time scale. Indeed, 14.5 and 32.2% of Irgarol remained in river water after 12-h treatment with Fe^{3+}/H_2O_2 ($t_{1/2}$ = 280 min; k = 0.0025 min^{-1}) and Fe^{2+}/H_2O_2 ($t_{1/2}$ = 408 min; k = 0.0017 min^{-1}), respectively.

An attempt to extend the optimum pH range for these processes toward neutral conditions was also made. The degradation of Irgarol by the photo-Fenton reactions in pure water was more efficient than in river water at pH 5 (Fig. 5). Specifically, Irgarol was completely degraded by Fe^{2+}/H_2O_2/UV-Vis ($t_{1/2}$ = 5.37 min; k = 0.129 min^{-1}) and Fe^{3+}/H_2O_2/UV-Vis ($t_{1/2}$ = 35.2 min; k = 0.0197 min^{-1}) in pure water at pH 5 after 45 and 90 min, respectively. Additionally, it disappeared after 180 min of irradiation in river water *via* the Fe^{2+}/H_2O_2/UV-Vis reaction ($t_{1/2}$ = 29.7 min; k = 0.0233 min^{-1}). However, it was not completely decomposed with Fe^{3+}/H_2O_2/UV-Vis ($t_{1/2}$ = 86.8 min; k = 0.00799 min^{-1}) after 360 min of irradiation in river water at pH 5.

The photo-Fenton degradation of Irgarol was slower in river water than in pure water. This may be attributed to the intense competition for $^{\bullet}OH$ between the degradable portion of dissolved organic matter in the water body and Irgarol itself (Amon and Benner, 1996; Sakkas et al., 2002). Similar results were reported in an investigation of linuron degradation by the photo-Fenton process conducted by Katsumata et al. (2005), who found that the degradation percentage of linuron increased rapidly as pH increased to 4, and then it decreased at higher pH. This occurred because the main species at pH 3, $Fe(OH)^{2+}(H_2O)_5$, has the largest light absorption coefficient and quantum yield for $^{\bullet}OH$ radical production, as well as for Fe(II) regeneration.

The photo-Fenton process is advantageous because iron ions are abundant, non-toxic, and easily removed from water (Safarzadeh-Amiri et al., 1996), and H_2O_2 is easy to handle and environmentally friendly (Benitez et al., 2007); however, the Fenton reaction is sensitive to pH. The efficiency of the photo-Fenton reactions at pH 5 was found to be lower than at pH 3 in this study. Similar findings were reported by Maezono et al. (2011), who indicated that the generation of $^{\bullet}OH$ radical in the photo-Fenton oxidation process was high at solution pH values of 3.0, while it decreased as the solution pH increased. The main reason for the lower reactivity at pH 5 than pH 3 would be the precipitation of Fe(III) as the hydrous oxyhydroxide, $Fe_2O_3 \cdot nH_2O$, which

inhibits the recycling of Fe(III)/Fe(II) (Georgi et al., 2007). As a result, the optimum pH for Fenton oxidations is usually around 3 (Pignatello et al., 2006). However, water may possess high buffer capacity and the need to acidify the reaction medium can limit the applicability of the Fenton process (Georgi et al., 2007). Consequently, this study examined the possibility to extend the optimum pH range for this process toward neutral conditions, to enhance its economical feasibility.

3.4. Hydroxyl radical formation rate

The results indicated that Fe^{3+}/H_2O_2/UV-Vis (photo-Fenton-like reaction) was likely to be the most important source of $^{\bullet}OH$ because of the higher rate of $^{\bullet}OH$ generation in this system (4150 and 3450 nM min^{-1} in pure and river water, respectively) compared to Fe^{2+}/H_2O_2/UV-Vis (3270 and 2870 nM min^{-1}, respectively) and Fe^{2+}/H_2O_2/Dark (61.7 and 272 nM min^{-1}, respectively). In the system Fe^{3+}/H_2O_2/Dark, it was observed 46.7 and 277 nM min^{-1} of $^{\bullet}OH$ formation in pure and river water, respectively. The measured $^{\bullet}OH$ photoformation rates in river water were lower than in pure water samples, probably because of the presence in the former of $^{\bullet}OH$ radical scavengers such as bicarbonate, carbonate and dissolved organic matter (DOM), which are common in river water samples. Indeed, DOM is known to play a major role as $^{\bullet}OH$ sink in freshwater (White et al., 2003).

Hydroxyl radicals ($^{\bullet}OH$) play an important role in the degradation of organic compounds in water (Andreozzi et al., 2003), because of their high reactivity with organic compounds in the aqueous phase (Buxton *et al*., 1988). The non-selective nature of hydroxyl radicals makes them useful for degrading a broad range of pollutants to give mineral end-products (Lindsey and Tarr,

2000). The effectiveness of $^{\bullet}OH$ in the degradation of organic compounds depends on its steady-state concentration (Nakatani et al., 2004).

3.5. Irgarol mineralization

To verify the mineralization (complete disappearance of the total organic carbon, TOC) of Irgarol in pure water using photo-Fenton reactions, the TOC time trend was assessed over 16 h of irradiation from an initial TOC concentration of 2.5 mgC L^{-1}. As shown in Fig. (6), the mineralization of Irgarol in the Fe^{3+}/H_2O_2/UV-Vis system was slightly faster than in the Fe^{2+}/H_2O_2/UV-Vis system, with 96.9 and 92.9% mineralization, respectively, occurring after 16 h of irradiation at pH 3. Additionally, mineralization was lower at pH 5, with values of 85.6 and 81.3% being observed following the aforementioned reactions, respectively. These results are consistent with the $^{\bullet}OH$ generation rate, suggesting an increasing contribution of the photo-Fenton-like reaction in Irgarol's mineralization due to the production of additional $^{\bullet}OH$ (4150 nM min^{-1}, compared to 3270 nM min^{-1} for Fe^{2+}/H_2O_2/UV-Vis). The total mineralization of Irgarol (i.e., complete disappearance of TOC) was a longer process than the disappearance of the substrate, which indicates that persistent intermediate products generated during the photo-Fenton processes are difficult to mineralize (Malato et al., 2003; Katsumata et al., 2005).

4. Conclusions

The photo-Fenton system is advantageous because it uses reagents that are environmentally friendly and relatively inexpensive. Moreover, the reaction can be initiated by application of a renewable source of energy such as sunlight, to overcome the relatively high costs of xenon

lamps and electrical energy, especially in areas where solar irradiation is readily available. Based on these findings, the system evaluated in this study has the potential for widespread application. However, further investigations should be conducted to confirm the present conclusions.

Acknowledgments

The authors are grateful to Dr. Kazuhiko Takeda, Dr. Nobutake Nakatani, and Hiroaki Kondo, Graduate School of Biosphere Science, Hiroshima University for their technical assistance during the course of this study. Thanks are also due to all lab mates for their kind help and many helpful discussions.

Acknowledgments

The authors are grateful to Dr. Kazuhiko Takeda, Graduate School of Biosphere Science, Hiroshima University for his technical assistance during the course of this study. Thanks are also due to all lab mates for their kind help and many helpful discussions.

References

Alzieu, C., 2000. Environmental impact of TBT: the French experience. Sci. Total Environ. 258, 99–102.

Amine-Khodja, A., Trubetskaya, O., Trubetskoj, O., Cavani, L., Ciavatta, C., Guyot, G., Richard, C., 2006. Humic-like substances extracted from composts can promote the photodegradation of Irgarol 1051 in solar light. Chemosphere 62, 1021–1027.

Amon, R.M.W., Benner, R., 1996. Photochemical and microbial consumption of dissolved organic carbon and dissolved oxygen in the Amazon River system. Geochim. Cosmochim. Acta 60, 1783–1792.

Andreozzi, R., Raffaele, M., Nicklas, P., 2003. Pharmaceuticals in STP effluents and their solar photodegradation in aquatic environment. Chemosphere 50, 1319-1330.

Arakaki, T., Faust, B.C., 1998. Sources, sinks, and mechanisms of hydroxyl radical (•OH) photoproduction and consumption in authentic acidic continental cloud waters from Whiteface Mountain, New York: The role of the Fe(r) (r = II, III) photochemical cycle. J. Geophys. Res. 103, 3487–3504.

Benitez, F.J., Real, F.J., Acero, J.L., Garcia, C., Llanos, E.M., 2007. Kinetics of phenylurea herbicides oxidation by Fenton and photo-Fenton processes. J. Chem. Technol. Biotechnol. 82, 65–73.

Buxton, G.V., Greestock, C.L., Helman, W.P., Ross, A.B., 1988. Critical review of rate constants for oxidation of hydrated electrons, hydrogen atoms and hydroxyl radicals ($^{\bullet}OH/ ^{\bullet}O^{-}$) in aqueous solutions. J. Phys. Chem. Ref. Data 17, 513-886.

Carbery, K., Owen, R., Frickers, T., Otero, E., Readman, J., 2006. Contamination of Caribbean coastal waters by the antifouling herbicide Irgarol 1051. Marine Poll. Bull. 52, 635–644.

Catastini, C., Sarakha, M., Mailhot, G., Bolte, M., 2002. Iron(III) aquacomplexes as effective photocatalysts for the degradation of pesticides in homogeneous aqueous solutions. Sci. Total Environ. 298, 219–228.

Dafforn, K.A., Lewis, J.A., Johnston, E.L., 2011. Antifouling strategies: history and regulation, ecological impacts and mitigation. Marine Poll. Bull. 62: 453–465.

Doria, F.C., Borges, A.C., Kim, J.K., Nathan, A., Joo, J.C., Campos, L.C., 2013. Removal of metaldehyde through photocatalytic reactions using nano-sized zinc oxide composites. Water Air Soil Poll. 224, 1434-1442.

Durand, G., Mansour, M., Barcelo, D., 1992. Identification and determination of fenitrothion photolysis products in water-methanol by gas chromatography-mass spectrometry. Anal. Chim. Acta 262, 167-178.

Durand, G., De Bertrand, N., Barcelo, D., 1991. Applications of thermospary liquid chromatography-mass spectrometry in photochemical studies of pesticides in water. J. Chromatogr. A. 554, 233–250.

El-Morsi, T.M., Emara, M.M., Abd El Bary, M.H.M., Abd-El-Aziz, A.S., Friesen, K.J., 2002. Homogeneous degradation of 1,2,9,10-tetrachlorodecane in aqueous solutions using hydrogen peroxide, iron and UV light. Chemosphere 47, 343–348.

Evans, S.M., Birchenough, A.C., Brancato, M.S., 2000. The TBT ban: out of the frying pan into the fire? Marine Poll. Bull. 40, 204–11.

Georgi, A., Schierz, A., Trommler, U., Horwitz, C.P., Collins, T.J., Kopinke, F.D., 2007. Humic acid modified Fenton reagent for enhancement of the working pH range. Appl. Catal. B-Environ. 7, 26–36.

Haag, W.R., Yao, D.C.C., 1992. Rate constants for reaction of hydroxyl radicals with several drinking water contaminants. Environ. Sci. Technol. 26, 1005-1013.

Hall Jr., L.W., Gardinali, P., 2004. Ecological risk assessment for Irgarol 1051 and its major metabolite in United States surface waters. Hum. Ecol. Risk Assess. 10, 525–542.

Huston, P.L., Pignatello, J.J., 1999. Degradation of selected pesticide active ingredients and commercial formulations in water by the photo-assisted Fenton reaction. Water Res. 33, 1238–1246.

IMO, 2001. International convention on the control of harmful antifouling systems on ships. International Maritime Organisation, London.

Katsumata, H., Kaneco, S., Suzuki, T., Ohta, K., Yobiko, Y., 2005. Degradation of linuron in aqueous solution by the photo-Fenton reaction. Chem. Eng. J. 108, 269–276.

Kim, N.S., Shim, W.J., Yim, U.H., Hong, S.H., Ha, S.Y., Han, G.M., Shin, K., 2014. Assessment of TBT and organic booster biocide contamination in seawater from coastal areas of South Korea. Marine Poll. Bull. 78, 201–208.

Kiwi, J., Pulgarin, C., Peringer, P., Gratzel, M., 1993. Beneficial effects of homogeneous photo-Fenton pretreatment upon the biodegradation of anthraquinone sulfonate in wastewater treatment. Appl. Catal. B: Environ. 3, 85-99.

Konstantinou, I.K., Albanis, T.A., 2004. World-wide occurrence and effects of antifouling paint booster biocides in the aquatic environment: a review. Environ. Int. 30, 235-248.

Koutsaftis, A., Aoyama, I., 2007. Toxicity of four antifouling biocides and their mixtures on the brine shrimp Artemia salina. Sci. Total Environ. 387, 166–174.

Kuhn, H.J., Braslavsky, S.E., Schmidt, R., 2004. Chemical actinometry (IUPAC Technical Report). Pure Appl. Chem. 76, 2105-2146.

Lindsey, M.E., Tarr, M.A., 2000. Inhibited hydroxyl radical degradation of aromatic hydrocarbons in the presence of dissolved fulvic acid. Water Res. 34, 2385-2389.

Liu, D., Pacepavicius, G.J., Maguire, R.J., Lau, Y.L., Okamura, H., Aoyama, I., 1999. Survey for the occurrence of the new antifouling compound Irgarol 1051® in the aquatic environment. Water Res. 33, 2833–2843.

Macounova, K., Krysova, H., Ludvik, J., Jirkovsky, J., 2003. Kinetics of photocatalytic degradation of diuron in aqueous colloidal solutions of Q-TiO_2 particles. J. Photochem. Photobiol. A. 156, 273–282.

Maezono, T., Tokumura, M., Sekine, M., Kawase, Y., 2011. Hydroxyl radical concentration profile in photo-Fenton oxidation process: Generation and consumption of hydroxyl radicals during the discoloration of azo-dye Orange II. Chemosphere 82, 1422–1430.

Malato, S., Caceres, J., Fernandez-Alba, A. R., Piedra, L., Hernando, M. D., Aguera, A., Vial, J., 2003. Photocatalytic treatment of diuron by solar photocatalysis: evaluation of main intermediates and toxicity. Environ. Sci. Technol. 37, 2516–2524.

Mohr, S., Schr◌der, H., Feibicke, M., Berghahn, R., Arp, W., Nicklisch, A., 2008. Long-term effects of the antifouling booster biocide Irgarol 1051 on periphyton, plankton and ecosystem function in freshwater pond mesocosms. Aquat. Toxicol. 90, 109–120.

Moye, H.A., Malagodi, M.H., Yoh, J., Leibee, G.L., Ku, C.C., Wislocki, P.G., 1987. Residues of avermectin B_{1a} on rotational crops and soils following soil treatment with C^{14} avermectin B_{1a}. J. Agric. Food Chem. 35, 859-864.

Nakatani, N., Hashimoto, N., Sakugawa, H., In: Hill, R.J., Leventhal, J., Aizenshtat, Z., Baedecker, M.J., Claypool, G., Eganhouse, R., Goldhaber, M., Peters, K. (Eds.) 2004. Geochemical Investigations in Earth and Space Science: A Tribute to Issac R. Kaplan, Elsevier B.V, The Netherlands, p. 233.

Okamura, H., Aoyama, I., Liu, D., Maguire, J., Pacepavicius, G.J., Lau, Y.L., 1999. Photodegradation of Irgarol 1051 in water. J. Environ. Sci. Health B. 34, 225–238.

Okamura, H., Nishida, T., Ono, Y., Shim, W.J., 2003. Phytotoxic effects of antifouling compounds on nontarget plant species. Bull. Environ. Contam. Tox. 71, 881–886.

Pignatello, J.J., Oliveros, E., MacKay, A., 2006. Advanced oxidation processes for organic contaminant destruction based on the Fenton reaction and related chemistry. Crit. Rev. Environ. Sci. Technol. 36, 1–84.

Pirkanniemi, K., Sillanpää, M., 2002. Heterogeneous water phase catalysis as an environmental application: a review. Chemosphere 48, 1047–1060.

Safarzadeh-Amiri, A., Bolton, J.R., Cater, S.R., 1996. The use of iron in advanced oxidation processes. J. Adv. Oxid. Technol. 1, 18–26.

Sakkas, V.A., Lambropoulou, D.A., Albanis, T.A., 2002. Photochemical degradation study of Irgarol 1051 in natural waters: influence of humic and fulvic substances on the reaction. J. Photochem. Photobiol. A. 147, 135–141.

Saleh, A., Fumani, N.S., Molaei, S., 2014. Microfunnel-supported liquid-phase microextraction: Application toextraction and determination of Irgarol 1051 and diuron in thePersian Gulf seawater samples. J. Chromatogr. A. 1356, 32–37.

Sapozhnikova, Y., Wirth, E., Schiff, K., Fulton, M., 2013. Antifouling biocides in water and sediments from California marinas. Marine Poll. Bull. 69, 189–194.

Schwarzenbach, R.P., Escher, B.I., Fenner, K., Hofstetter, T.B., Johnson, C.A., Von Gunten, U., Wehrli, B., 2006. The challenge of micropollutants in aquatic systems. Science 313, 1072–1077.

Takeda, K., Shindo, H., Nakatani, N., Sakugawa, H., 2005. Photochemical formation of hydroxyl radicals from chemical species dissolved in river water. J. Jpn. Soc. Wat. Environ. 28, 509-513.

Thomas, K.V., Brooks, S., 2010. The environmental fate and effects of antifouling paint biocides. Biofouling 26, 73–88.

Walling, C., 1975. Fenton's reagent revisited. Acc. Chem. Res. 8, 125-131.

White, E.M., Vaughan, P.P., Zepp, R.G., 2003. Role of the photo-Fenton reaction in the production of hydroxyl radicals and photobleaching of colored dissolved organic matter in a coastal river of the southeastern United States. Aquat. Sci. 65, 402-414.

Zamy, C., Mazellier, P., Legube, B., 2004. Phototransformation of selected organophosphorus pesticides in dilute aqueous solutions. Water Res. 38, 2305–2314.

Zhou, J.L., 2008. Occurrence and persistence of antifouling biocide Irgarol 1051 and its main metabolite in the coastal waters of Southern England. Sci. Total Environ. 406, 239–246.

Table 1: Chemical analysis of river water* collected for Irgarol degradation

Analytical item	Concentration ± S.D.
Cl^-	43.6±3.78 mg l^{-1}
NO_2^-	0.54±0.04 mg l^{-1}
NO_3^-	3.89±0.39 mg l^{-1}
SO_4^{2-}	70.0±6.68 mg l^{-1}
Na^+	35.5±3.41 mg l^{-1}
NH_4^+	3.28±0.24 mg l^{-1}
K^+	4.29±0.35 mg l^{-1}
Mg^{2+}	1.42±0.13 mg l^{-1}
Ca^{2+}	25.2±2.74 mg l^{-1}
Conductivity	355±11.5 µS cm^{-1}
DOC	3.49± 0.24 mg Cl^{-1}
pH	7.29±0.23

*Kurose River water, Hiroshima, Japan (Ochiai bridge sampling site).

Figures Captions

Figure 1. Influence of solution pH on the direct photolysis of Irgarol (0.1 mg L^{-1}) in pure and river water. C_0 is the initial concentration of Irgarol and C is its residual concentration at a specific time.

Figure 2. Degradation of Irgarol (initial concentration 0.1 mg L^{-1}) at pH 3 in pure water, under different concentrations of a) Fe^{2+} and H_2O_2 during photo-Fenton reaction, and b) Fe^{3+} and H_2O_2 during photo-Fenton-like reaction.

Figure 3. Effect of Fenton and photo-Fenton reactions on the degradation of Irgarol (0.1 mg L^{-1}) at pH 3 in pure water.

Figure 4. Effect of Fenton and photo-Fenton reactions on the degradation of Irgarol (0.1 mg L^{-1}) at pH 3 in river water.

Figure 5. Effect of photo-Fenton reactions on the degradation of Irgarol (0.1 mg L^{-1}) at pH 5 in pure and river water.

Figure 6. Mineralization of 2.5 mg C L^{-1} of Irgarol by photo-Fenton reactions at pH 3 in pure water.

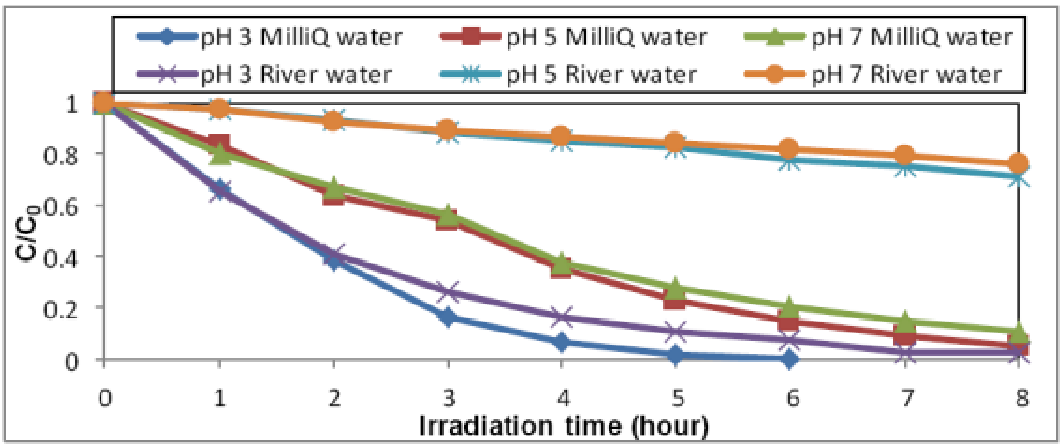

Figure 1

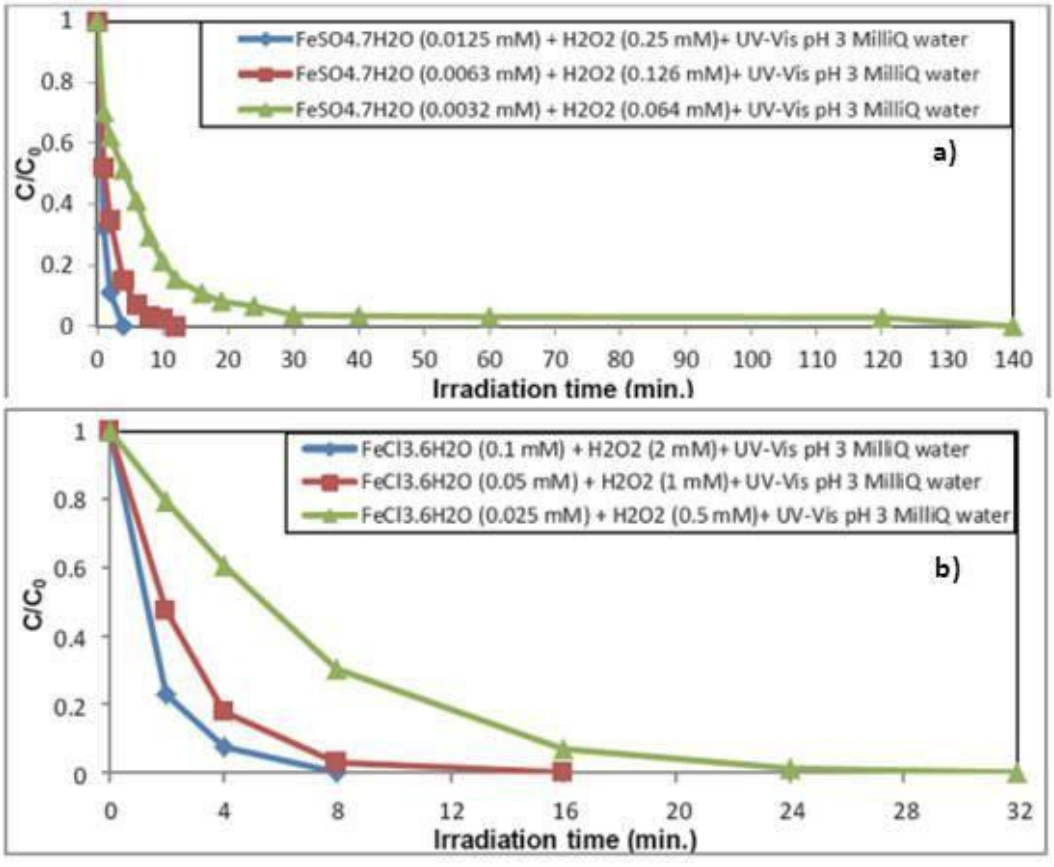

Figure 2

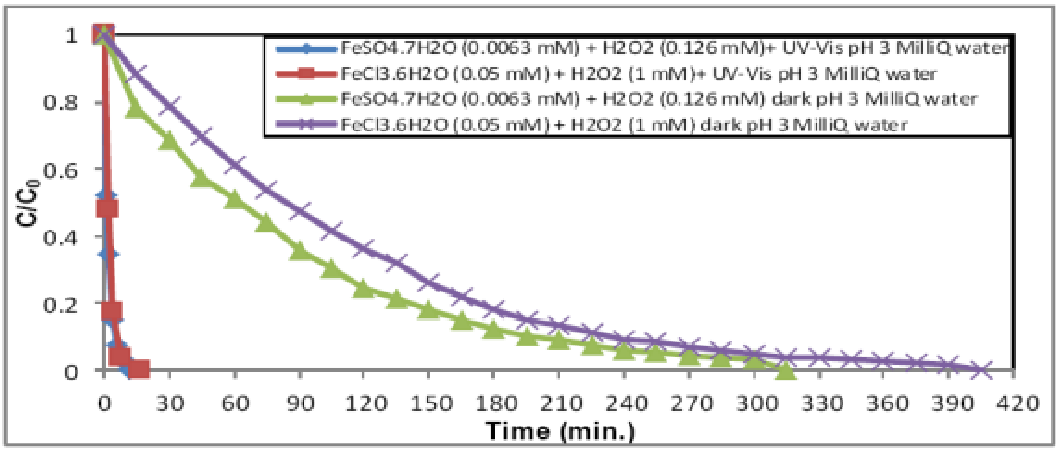

Figure 3

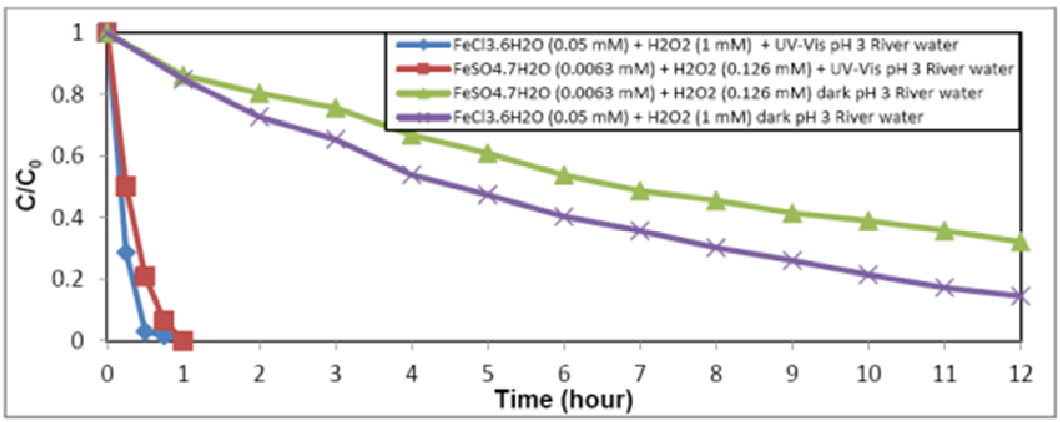

Figure 4

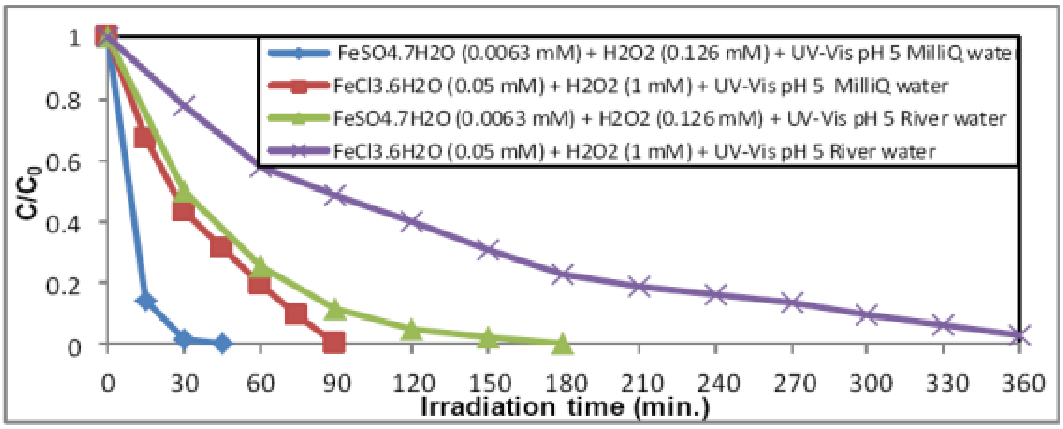

Figure 5

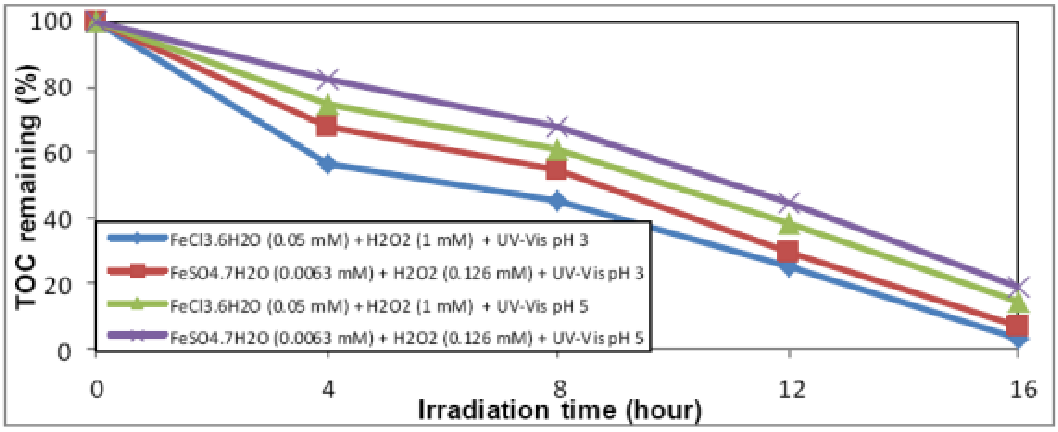

Figure 6